DOCTOR OF PHILOSOPHY

High power ultra-short pulse Quantum-dot lasers

Nikitichev, Daniil I.

Award date:
2012

DOCTOR OF PHILOSOPHY

High power ultra-short pulse Quantum-dot lasers

Daniil I. Nikitichev

2012

University of Dundee

High power ultra-short pulse Quantum-dot lasers

By

Daniil I. Nikitichev

A thesis submitted for the degree of

Doctor of Philosophy

To the School of Electronic Engineering, Physics and Mathematics,

University of Dundee

University of Dundee

January 2012

Declarations.

I, Daniil I. Nikitichev, hereby certify that this thesis, which is forty nine thousand and five hundred words in length, has been written by me, that it is the record of work carried out by me and that it has not been submitted in any previous application for a higher degree.

I was admitted as a research student and as a candidate for the degree of Doctor of Philosophy in October 2008; the higher study for which this is a record was carried out at the University of Dundee between 2008 and 2012.

In submitting this thesis to the University of Dundee I understand that I am giving permission for it to make available for use in accordance with the regulations of the University Library for the time being in force, subject to any copyright vested in the work not being affected thereby. I also understand that the title and abstract will be published, and that a copy of the work may be made and supplied to any *bona fide* library or research worker.

Signature of candidate. Date.

I hereby certify that the candidate has fulfilled the conditions of the Resolution and Regulations appropriate for the degree of Doctor of Philosophy in the University of Dundee and that the candidate is qualified to submit this thesis in application for that degree.

Signature of supervisor. Date.

Acknowledgements.

I am very grateful for all those who have provided me support, advice, direction over the past four years and made the completion of this work possible.

I would like to thank my supervisor Professor Edik Rafailov for this wonderful opportunity to work at the University of Dundee and for his constant support, insightful guidance and hard work in the proof-reading of this work and of many other manuscripts.

I am especially thankful for another supervisor Dr. Maria Ana Cataluna who has spent many hours of her time helping me to understand some deeper concepts behind the semiconductor laser. Her genuine friendship and involvement in this work are much appreciated.

Many thanks also go to Dr. Ying Ding with whom I have worked in the lab. His enthusiasm and support were very important for me.

Every member of the Photonics and Nanoscience research group in the school of Engineering, Physics and Mathematics, University of Dundee, both past and present, contributed one way or the other in the success of this work, especially I would like to pay credit to Prof. Mervin Rose, Prof. Grigorii Sokolovskii, Dr. Natalia Bazieva, Dr. Ksenia Fedorova, Dr. Sergei Sokolovski, Mantas Butkus, Ross Leyman and Tomacz Kruczek- my apologies if I left anyone out.

Moreover, I would like to express my deep appreciation for the excellent technical team who always help when the technical problems arouse. Many thanks go to Gary Callon, Grant Kydd and Callum Moore.

As I was involved in the international project I have had an opportunity to meet, to work with and to learn from the researchers from III-V lab, Innolume, University of Sheffield, Tampere University of Technology, Politecnico di Torino, Technische Universitut Darmstadt, ICFO- the Institute of Photonic Sciences, University of Athens and St. Andrews University. Particularly, I would like to mention Michel Krakowski, Mike Ruiz, Dr. Igor Krestnikov, Dr. Daniil Livshits, Dr. Richard Hogg, Prof. Oleg Okhotnikov, Prof. Ivo Montrosset, Dr. Mattia Rossetti, Prof. Dimitris Syvridis, Dr. Charis Mesaritakis, Dr., Prof. Wolfgang Elsaesser, Dr. Lukas Drzewietzki, Dr. Pablo Losa-Alvarez, Rodrigo Aviles-Espinosa and Prof. Wilson Sibbett.

I acknowledge the financial support of the EU FP7 “FAST-DOT” project Grant No. 224338.

On a personal note, I am very grateful for my mother Irina Aleksandrovna, my brothers Kirill and Evgeny, my sister Marina and the parents of my wife Valentina Ivanovna and Vyacheslav Anatolyevich for their support while being far away from home.

Most of all I appreciate the love of my wife, Anna, and my children, Matvey and Eva. Their constant support and sacrifices allowed me to finish this work successfully.

Спасибо тебе моя дорогая Анюта. Я тебя люблю.

List of publications.

Papers:

1. **D. I. Nikitichev**, Y. Ding, L. Drzewietzki, S.Breuer, W. Elsaβer, M. Ruiz, M. Tran, Y.Robert, M. Krakowski, M. Rossetti, P. Bardella, T. Xu, I. Montrosset, I. Krestnikov, D. Livshits, M. A. Cataluna and E. U. Rafailov, "High peak power and sub-picosecond Fourier-limited pulse generation from passively mode-locked monolithic two-section gain-guided tapered InGaAs quantum-dot lasers" accepted Laser Physics Journal, Nov 2011

2. Y. Ding, M. A. Cataluna, **D. I. Nikitichev**, I. Krestnikov, D. Livshits,and E. U. Rafailov "Broad repetition-rate continuously tunable quantum-dot external-cavity passively mode-locked laser with extremely narrow RF linewidth" accepted for publication in *Applied Physics Express*, 4(6), 062703, 2011

3. R. Leyman, **D. I. Nikitichev**, N. Bazieva, M. A. Cataluna, E. U. Rafailov, "Multimodal spectral control of a quantum-dot diode laser for THz difference frequency generation," *Applied Physics Letters,* 99, 171107, 2011

4. Maria Ana Cataluna, Ying Ding, Daniil I. Nikitichev, Ksenia A. Fedorova, and Edik U. Rafailov, "High-Power Versatile Picosecond Pulse Generation from Mode-Locked Quantum-Dot Laser Diodes" IEEE Journal of Selected Topics in Quantum Electronics, 17(5): p. 1302-1310, 2011.

5. **D. I. Nikitichev**, Y. Ding, M. Ruiz, M. Calligaro, N. Michel, M. Krakowski, I. Krestnikov, D. Livshits, M. A. Cataluna and E. U. Rafailov, "High-power passively mode-locked tapered InGaAs/GaAs quantum-dot lasers," *Applied Physics B, vol. 103, 3, 609-613, 2011*

6. Y. Ding, **Nikitichev D.I**, I. Krestnikov, D. Livshits, M. A. Cataluna and E. U. Rafailov., "Quantum-dot external-cavity passively modelocked laser with high peak power and pulse energy," *Electronics Letters,* vol. 46, pp. 1516-1518, 2010

7. M. A. Cataluna, **D. I. Nikitichev**, S. Mikroulis, H. Simos, C. Simos, C. Mesaritakis, D. Syvridis, I. Krestnikov, D. Livshits, E. U. Rafailov: "Dual-wavelength mode-locked quantum-dot laser, via ground and excited state transitions: experimental and theoretical investigation" Optics Express, Vol. 18, Issue 12, pp. 12832-12838, 2010

Conferences:

Invited talks:

1. M. A. Cataluna, Y. Ding, **D. I. Nikitichev**, E. U. Rafailov," High-power ultrafast quantum-dot edge-emitting lasers", *2nd EOS Topical Meeting on Lasers 2011(ETML'11)*, paper 4574, Capri, Italy
2. M. A. Cataluna, Y. Ding, **D.I. Nikitichev**, K. Fedorova and E. U. Rafailov,"Ultrafast InAs/GaAs quantum-dot laser diodes: unlocking spectral and temporal versatility", *European Materials Research Society (E-MRS) spring meeting 2011*, Symposium G, paper 21, Nice, France
3. **Nikitichev D. I.** ,"Record power from mode-locked two-section gain-guided tapered quantum-dot lasers", Scottish Universities Physics Alliance (SUPA) Annual General Meeting 2011, St. Andrews, UK http://www.supa.ac.uk/Graduate_School/AGM/2011/students_presentation

Other Conferences:

1. R. Aviles-Espinosa, Y. Ding, M. A. Cataluna, **D. Nikitichev**, P. Loza-Alvarez and E. Rafailov, "Ultrashort-pulsed chip-sized lasers for two-photon excited fluorescence imaging", submitted The Focus on Microscopy 2012
2. **D. I. Nikitichev**, K.A. Fedorova, Y. Ding, A. Alhazime, A. Able, W. Kaenders, I. Krestnikov, D. Livshits, E. U. Rafailov, "Broadly tunable picosecond pulses quantum-dot mode-locked laser", submitted CLEO 2012
3. Y. Ding, A. Alhazime, **D. Nikitichev**, K. Fedorova, M. Ruiz, M. Tran, Y. Robert, A. Kapsalis, H. Simos, C. Mesaritakis, T. Xu, P. Bardella, M. Rossetti, I. Krestnikov, D. Livshits, I. Montrosset, D. Syvridis, M. A. Cataluna, M. Krakowski, and E. Rafailov, "Tunable Master-Oscillator Power-Amplifier Using All Chirped Quantum-Dot Structures", submitted CLEO 2012
4. Y. Ding, A. Alhazime, **D. Nikitichev**, K. Fedorova, M. Ruiz, M. Tran, Y. Robert, A. Kapsalis, H. Simos, C. Mesaritakis, T. Xu, P. Bardella, M. Rossetti, I. Krestnikov, D. Livshits, I. Montrosset, D. Syvridis, M. A. Cataluna, M. Krakowski, and E. Rafailov, "30-W peak power generated from all-quantum-dot master-oscillator power-amplifier system for nonlinear bioimaging applications", submitted CLEO 2012
5. R. Aviles-Espinosa, Y. Ding, M. A. Cataluna, **D. Nikitichev**, P. Loza-Alvarez and E. Rafailov, "Nonlinear Bio-imaging with a High Peak Power All-Quantum-Dot Master-oscillator Power-amplified System", submitted CLEO 2012
6. **D. I. Nikitichev**, M. A. Cataluna, Y. Ding, I. Krestnikov, D. Livshits, E. U. Rafailov, "Tunable quantum-dot mode-locked monolithic laser", post deadline 4703, 2nd EOS Topical Meeting on Lasers (ETML'11), Italy

7. R. Leyman, **D. I. Nikitichev**, N. Bazieva, E. U. Rafailov, "Generation of Dual-Modes from a Quantum Dot Diode Laser for THz DFG", 4478, 2nd EOS Topical Meeting on Lasers (ETML'11), Italy

8. R. Leyman, **D. I. Nikitichev**, N. Bazieva, M.A. Cataluna, E. U. Rafailov, "Dual-Mode Control of a Quantum Dot Diode Laser for THz Difference Frequency Generation", B-O-9, UK Semiconductors, 2011, UK

9. **D. I. Nikitichev**, Y. Ding, M.Ruiz, M. Calligaro, N. Michel, M. Krakowski, I. Krestnikov, D. Livshits, M. A. Cataluna and E. U. Rafailov, "Passively mode-locked monolithic two-section gain-guided tapered quantum-dot lasers: II. Record 15 Watt peak power generation", *CB3.4 (847),* CLEO-EUROPE 2011, Germany.

10. **D. I. Nikitichev**, M. A. Cataluna, Y. Ding, K. A. Fedorova, I. Krestnikov, D. Livshits, E. U. Rafailov, "High-power spectral bistability in a multi-section quantum-dot laser under continuous-wave or mode-locked operation", CThG1, CLEO2011, USA.

11. M.Ruiz, N. Michel, M. Calligaro, Y.Robert, M. Krakowski, **D. I. Nikitichev**, M. A. Cataluna, D. Livshits and E. U. Rafailov: "New tapered quantum-dot mode-locked laser diode with high peak power, low divergence and good beam quality", *ISLC2010*, Japan

12. **D. I. Nikitichev**, M. A. Cataluna, M.Ruiz, M. Calligaro, N. Michel, M. Krakowski, D. Livshits, and E. U. Rafailov: 'High-power passively mode-locked tapered quantum-dot laser' , TuR3-09, *Laser Optics 2010*, Saint-Petersburg, Russia

13. **Nikitichev, D. I.,** Cataluna, M. A., Krestnikov, I., Livshits, D., Rafailov, E. U: : 'Investigation of the pulse dynamics in a modelocked quantum-dot laser involving the ground/excited state transitions', [2243], 1st EOS Topical Meeting on Lasers 2009, Capri, Italy

14. Cataluna, M. A., **Nikitichev, D. I.,** Krestnikov, I., Livshits, D.A., Kovsh, A. R., Rafailov, E. U.: 'Dual-wavelength mode-locked GaAs based quantum-dot laser", CB4.6 TUE, *CLEO Europe-EQEC 2009*, Munich, Germany

Posters:

1. Y. Ding, **D. I. Nikitichev**, I. Krestnikov, D. Livshits, M. A. Cataluna, and E. U. Rafailov "200-MHz Repetition Rate and Harmonics of up to 6.8 GHz Generated from a Quantum-dot External-cavity Passively Mode-locked Laser", CF.P.23 (817), CLEO-EUROPE 2011, Munich, Germany.

2. **Nikitichev D.I**, Y. Ding, M. A. Cataluna, E. U. Rafailov, "Mode-locked quantum-dot edge-emitting lasers", 66 th Scottish Universities Summer School in Physics (SUSSP 66) at Heriot-Watt University, 2 session, №17, 2010

Abstract.

In this thesis, novel multi-section laser diodes based on quantum-dot material are designed and investigated which exhibit a number of advantages such as low threshold current density; temperature-insensitivity and suppress carrier diffusion due to discrete nature of density of state of quantum-dots. The spectral versatility in the range of 1.1 μm – 1.3 μm wavelengths is demonstrated through novel mode-locking regimes such as dual-wavelength mode-locking, wavelength bistability and broad tunability. Moreover, broad pulse repetition rate tuning using an external cavity configuration is presented. A high peak power of 17.7 W was generated from the quantum-dot laser as a result of the tapered geometry of the gain section of the laser has led to successful application of such device for two-photon imaging.

Dual-wavelength mode-locking is demonstrated via ground (λ=1180 nm) and excited (λ=1263 nm) spectral bands with optical pulses from both states simultaneously in the 5-layer quantum-dot two-section diode laser. The widest spectral separation of 83 nm between the modes was achieved in a dual-wavelength mode-locked non-vibronic laser.

Power and wavelength bistability are achieved in a mode-locked multi-section laser which active region incorporates non-identical QD layers grown by molecular beam epitaxy. As a result the wavelength can be electronically controlled between 1245 nm and 1290 nm by applying different voltages to the saturable absorber. Mode-locked or continuous-wave regimes are observed for both wavelengths over a 260 mA – 330 mA current ranges with average power up to 28 mW and 31 mW, respectively. In mode-locked regime, a repetition rate of 10 GHz of optical pulses as short as 4 ps is observed. Noticeable hysteresis of average power for different bias conditions is also

demonstrated. The wavelength and power bistability in QD lasers are potentially suitable for flip-flop memory application. In addition, a unique mode-locked regime at expense of the reverse bias with 50 nm wavelength tuning range from 1245 nm to 1290 nm is also presented.

Broad repetition rate tunability is shown from quantum-dot external cavity mode-locked 1.27 μm laser. The repetition rate from record low of 191 MHz to 1 GHz from fundamental mode-locking was achieved. Harmonic mode-locking allows further to increase tuning up to 6.8 GHz (34th-order harmonic) from 200 MHz fundamental mode-locking. High peak power of 1.5 W can be generated directly from two-section 4 mm long laser with bent waveguide at angle of 7^{o} at 1.14 GHz repetition rate without the use of any pulse compression and optical amplifier. Stable mode-locking with an average power up to 60 mW, corresponding to 25 pJ pulse energy is also obtained at a repetition frequency of 2.4 GHz. The minimum time-bandwidth product of 1.01 is obtained with the pulse duration of 8.4 ps.

Novel tapered quantum-dot lasers with a gain-guided geometry operating in a passively mode-locked regime have been investigated, using structures that incorporated either 5 or 10 quantum dot layers. The peak power of 3.6 W is achieved with pulse duration of 3.2 ps. Furthermore, the record peak power of 17.7 W and transform limited pulses of 672 fs were achieved with optimized structure. The generation of picosecond pulses with high average power of up to 209 mW was demonstrated, corresponding to 14.2 pJ pulse energy.

The improved optical parameters of the tapered laser enable to achieve nonlinear images of fluorescent beads. Thus it is for the first time that QD based compact monolithic device enables to image biological samples using two-photon microscopy imaging technique.

Abbreviations.

AR- Anti reflective

AUT- Autocorrelator

CDMA-Code-division multiple access

DH- Double heterostructure

DOS- Density of State

ECDL- external cavity diode laser

ES- Excited state

ESCW- Excited state continuous wave

ESML- Excited state mode-locking

F- Fibre

FS- Fibre splitter

GaAs- Gallium Arsenide

GaInNaAsSb- Gallium Indium Sodium Arsenic Antimony

GS- Ground state

GSCW- Ground state continuous wave

GSML- Ground state mode-locking

GSS-Ground state splitting

HR- High reflective

HWP- Half wave plate

IF- Intermediate-frequency filter

InAs- Indium Arsenide

InGaAsP- Indium Gallium Arsenide Phosphorus

L- Lens

LED- light emitting diodes

LIDAR- Light Detection And Ranging

MBE- Molecular beam epitaxy

ML-mode-locked

MOCVD- Metal-organic chemical vapour deposition

N_L- Number of layers

OI- Optical isolator

OS- Optical spectrometer

OSC- Oscilloscope

OTDM- Optical time-domain multiplexing

PC- Personal computer

PD- Photo diode

PL- Photoluminescence

PM- Power meter

PMT- Photomultiplier tube

PS- Power supply

QD-quantum dot

QW- Quantum well

QWR- Quantum wire

RB- Resolution bandwidth

RFSA- RF spectrum analyzer

SESAM- Semiconductor saturable absorber mirror

SHG- Second harmonic generation

SiGe- Silicon Germanium

TBWP- Time bandwidth product

TC- Temperature controller

UV- Ultraviolet

VB- Video bandwidth

VCSELs- Vertical-cavity surface-emitting laser diodes

WDM- Wavelength-division multiplexing

$\mathbf{E_{abs}^{sat}}$ - The saturation energy of the absorber

$\boldsymbol{E_{gain}^{sat}}$**-** The saturation energy of the gain

$\mathbf{\partial a}/_{\mathbf{\partial n}}$- Differential loss

$\mathbf{\partial g}/_{\mathbf{\partial n}}$- Differential gain.

$\boldsymbol{\varphi_l}$- l-th longitudinal mode

µm- Micrometer

Å- Angstrom

A- Optical mode cross-sectional area

$\mathbf{A_a}$- Cross section of the absorber

$\mathbf{A_g}$- Cross section of the gain

c- Speed of light

D- The $1/e^2$ diameter of the collimated beam

d- The beam diameter at the focus

dBm- power ratio in decibels

$\mathbf{d_L}$- The length of the scanning mirror

$\mathbf{D_M}$- The distance between the parallel mirrors

E- Energy

E(t)- Amplitude of original replica

E(t+τ)- Amplitude of time delayed replica

$\mathbf{E_{b0}}$, $\mathbf{E_b}$- The barrier heights

$\mathbf{E_{diss}}$- Energy dissipated per cycle

$\mathbf{E_{g1}}$- Band gap energy of the material 1

$\mathbf{E_{g2}}$ - Band gap energy of the material 2

$\mathbf{E_{st}}$- Energy stored

F- Fermi level

f- Frequency

f- The lens focal length

$\mathbf{f_{3dB}}$- Frequency bandwidth at 3 dB

fs- Femtosecond

GHz- Gigahertz

$\mathbf{G_{th}}$- Gain corresponding to the total loss

h- Plank's constant

$\mathbf{I_{AC}}$- The intensity of autocorrelation

$\mathbf{I_{SH}}$- The intensity of second harmonic signal;

$\mathbf{J_{th}}$- Threshold current density

k- The factor of the two-photon absorption

kW- Kilowatt

L- The length of the cavity

$\mathbf{m^*}$**-** The electron effective mass

M1, M2, M3- Mirrors

meV- Milli-electron volt

MHz- Megahertz

mW- Milliwatt

N- Number of modes

n/a- Not applicable

nJ- Nanojoule

NL- figure of nonlinearity

nm- Nanometre

$\mathbf{N_{th}}$- Threshold carrier concentration

p- Momentum of a particle

$\mathbf{P_{AV}}$- Average power

pJ- Picojoule

$\mathbf{P_{loss}}$- Power loss per cycle

$\mathbf{P_{PEAK}}$- Peak power

ps- Picosecond

Q - Quality factor

rf- Radio frequency

Si- Silicon

T- Pulse period

T(1),(2)- Temperature

$\mathbf{T_0}$-Characteristic temperature

THz- Terahertz

$\mathbf{T_t}$- Total scan range

V- Volt

W- Watt

$\mathbf{\Delta E_c}$- Bandgap difference between material 1 and 2 in conduction band

$\mathbf{\Delta E_v}$- Bandgap difference between material 1 and 2 in valence band

$\mathbf{\Delta\lambda}$- Full width half maximum

$\mathbf{\Delta\nu_L}$- The total oscillating bandwidth

$\mathbf{\Delta\tau_P}$- Pulse width

$\boldsymbol{\lambda}$- Emission wavelength

$\boldsymbol{\lambda_B}$- Wavelength de Broglie

$\boldsymbol{\nu}$- Optical frequency

$\boldsymbol{\pi}$- Pi

$\boldsymbol{\tau}$- Pulse duration

$\boldsymbol{\tau_{MEASUREMENT}}$- The measured pulse duration

$\boldsymbol{\tau_{osc}}$- Rise time of the oscilloscope

$\boldsymbol{\tau_{photodiode}}$- Rise time of the photodiode

$\boldsymbol{\tau_{signal}}$- Actual pulse width

Γ- The saturation fluence

$\boldsymbol{\Delta\nu}$- The frequency difference between consecutive longitudinal modes

$\boldsymbol{\beta}$- Numerical factor

$\boldsymbol{\varphi}$- A constant

Figures.

Fig. 1.1 (a) Decreasing of the energy step under forward bias, allowing electrons and holes to cross the junction, **(b)** Increasing of the energy step with reverse bias, with very few carriers cross the junction.

Fig. 1.2 Diagram of behaviour in classical heterostructures: **(a)** One-side injection and superinjection; **(b)** diffusion in built-in quasi-electric field; **(c)** electron and optical confinement; **(d)** wide-gap window effect; **(e)** diagonal tunnelling through a heterostructure interface.

Fig. 1.3 Simplified energy band diagram for a double heterostructure (DH).

Fig. 1.4 (top) Schematic morphology and **(bottom)** the density of states of charge carriers for **(a)** bulk, **(b)** quantum well, **(c)** quantum wire, **(d)** quantum dot semiconductor structures.

Fig. 1.5 Single photon (left) and two-photon (middle) and three photon (right) excitation diagrams.

Fig. 1.6 One photon excitation **(left)** and multi-photon excitation **(right)** at a focal plane of the microscope objective.

Fig. 1.7 Absorption in tissue is dominated by protein and DNA in the UV, by water in the IR, and by haemoglobin and melanin in the visible light.

Fig. 1.8 Mapping of the state of the art at the beginning of this work and goal for the QD based mode-locked lasers used in my thesis.

Fig.2.1 Stranski-Krastanow growth of three-dimensional (3D) islands.

Fig. 2.2 Schematic of the geometry of InAs/GaAs QD.

Fig. 2.3 Cross-sectional schematic structure of several layers of quantum dots (QDs).

Fig. 2.4 The strain distribution in y-z plane in the middle of x axis at T=300 K**.**

Fig. 2.5 Dependence of photoluminescence spectra at 77 K of GaAs/InAs with effective thickness of deposited InAs**.**

Fig. 2.6 Schematic population of QD density of states (solid curves) **(a)** at threshold, and **(b)** evolution of the population with increasingthreshold gain and **(c)** temperature. DOS of the ground states and the first exited state are indicated by dotted curves**.**

Fig. 2.7 (top) Schematic Morphology and **(bottom)** the density of states for charge carriers in **(a)** an ideal quantum dot-based material and **(b)** a real quantum dot-based material with inhomogeneous broadening.

Fig. 3.1 Gain switching laser dynamics **a)** applied current, **b)** carrier density and **c)** optical power.

Fig. 3.2 Active Q-switching laser time evolution of **a)** loss, gain and **b)** optical power.

Fig. 3.3 Passive Q-switching laser time evolution of **a)** loss, gain and **b)** optical power.

Fig. 3.4 Cavity longitudinal mode formation.

Fig. 3.5 Active mode-locking laser dynamics of **a)** drive current, and **b)** optical power.

Fig. 3.6 Passive mode-locking laser dynamics of **a)** loss, gain **b)** carrier density and **c)** optical power.

Fig. 3.7 Gain/loss dynamics versus carrier concentration for successful mode-locking in laser diodes.

Fig. 3.8 Tunnelling electron's escape mechanism with applied electric field.

Fig. 4.1 Top view schematic of the autocorrelator. SHG- Second harmonic generation, PMT- Photomultiplier tube.

Fig. 4.2 Autocorrelation functions without (**top**) and without (**bottom**) background for various optical inputs.

Fig. 4.3 Relationship between time and frequency domain.

Fig. 4.4 The temporal relationship between selected Fourier components of **a)** a transform-limited pulse, **b)** a positively chirped pulse.

Fig. 4.5 The relation between peak power **(P_{PEAK})**, average power **(P_{AVR})**, pulse width **($\Delta\tau_P$)** and period **(T).**

Fig. 4.6 The schematic of the experimental setup: **QD -TS**: quantum dot - two section diode on the XYZ mount, **A**- absorber, **TC**: temperature controller, **PS**: power supply, **L**-lens, **PM**- Power meter, **OI**: optical isolator, **HWP**: half wave plate, **F**: fibre, **FS**: fibre splitter, **PD**: photo diode, **RFSA**: RF spectrum analyzer, **AUT**: autocorrelator, **OSC**: oscilloscope, **OS**: optical spectrometer, **PC**-personal computer.

Fig. 4.7 Schematic of the Faraday isolator.

Fig. 4.8 The effect of half-wave plate on light polarization.

Fig. 4.9 Ray trace for collimating and focusing using aspheric lens.

Fig. 4.10 Fibre coupler 1x3 40/40/20 split designed for 1310/1550nm.

Fig. 4.11 FC/APC (ferrule connector/angled physical contact) connector.

Fig. 4.12 Rotating parallel mirrors in the autocorrelator setup. D_M- the distance between parallel mirrors M1 and M2, f- the frequency of rotation, d_L-the length of the scanning mirror.

Fig. 4.13 Block diagram of a spectrum analyzer**.**

Fig. 4.14 A schematic of a grating spectrometer.

Fig. 5.1 Map of the different Mode-locking regimes with bias conditions: GSML – Ground state mode-locking; GSML ESCW- Ground state mode-locking in coexistence with excited state continuous wave emission; ESML – Excited state mode-locking.

Fig. 5.2 The dependence of an injected current of **(a)** pulse duration, **(b)** average output power for GS and ES mode-locking at 6.15 V reverse bias. GSML – Ground state

mode-locking; GSML ESCW- Ground state mode-locking in coexistence with excited state continuous wave emission; ESML – Excited state mode-locking.

Fig. 5.3 Dependence on reverse bias of **(a)** pulse duration **(b)** average output power for GS and ES mode-locking at I=300mA current. **Inset**: average power of ES band with reverse bias; GSML – Ground state mode-locking; ESML – Excited state mode-locking.

Fig. 5.4 (a) Mapping of the different operating regimes observed in 2 mm QD mode-locked laser. **(b)** Mapping of the dual-wavelength mode-locking regime here described (GSML+ESML). Legend: GSML – ground-state mode-locking; ESML – excited-state mode-locking; GSCW - ground-state continuous wave operation.

Fig. 5.5 (a) Optical spectrum and **(b)** RF spectrum characteristics of the dual-wavelength mode-locked regime, for an injection current of 425 mA and reverse bias of 6 V.

Fig. 5.6 Autocorrelation traces for (a) GS mode-locking and (b) ES mode-locking at 6 V reverse bias and 425 mA gain current.

Fig. 5.7 Pulse width dynamics with bias conditions for 2 mm laser with **(a)** 5, **(b)** 10 and **(c)** 15 QD layers. Number of measured points is ~ 1600.

Fig. 5.8 Peak Power dynamics with bias conditions for a 2 mm laser with **(a)** 5, **(b)** 10 and **(c)** 15 QD layers. Number of measured points is ~ 1600.

Fig. 5.9 Mapping of mode-locking regimes observed for a 1.3 mm long 5 QD layers device, under an operating temperature of **(a)** 20^{o}C and **(b)** 14^{o}C. GS/ES: ground-state/excited state. CW/ML: continuous-wave/mode-locked operation.

Fig. 5.10 The average power dynamics for a 1.3 mm long device having 5 QD layers with **(a)** 0 V, **(b)** 2 V and **(c)** 3.5 V reverse bias. GS/ES: ground-state/excited state. CW/ML: continuous-wave/mode-locked operation.

Fig. 5.11 (a) Pulse width and **(b)** Peak power evolution with bias conditions for a 1.3 mm long device having 5 QD layers. Number of measured points is ~ 400.

Fig. 6.1 Schematic of a multi-section quantum dot laser.

Fig. 6.2 (a) Dynamics for a fixed gain current of 260 mA with various values of ascending and descending reverse bias of the emission wavelength ; **(b)** pulse duration and **(c)** output power.

Fig. 6.3 Dynamics of the emission wavelength with various values of ascending (black line) and descending (red line) reverse bias for a fixed gain current of **a)** 300 mA and **b)** 330 mA in continuous wave (CW) and mode-locking (ML) regimes of operation.

Fig. 6.4 Dynamics of the pulse duration with ascending (black line) and descending (red line) direction of applied reverse bias for a fixed gain current of **(a)** 300 mA and **(b)** 330 mA.

Fig. 6.5 Dynamics of the average power with descending (black line) and descending (red line) direction of applied reverse bias for a fixed gain current of **(a)** 300 mA and **(b)** 330 mA.

Fig. 6.6 (a) Spectral tunability, **(b)** corresponding autoccorelations and **(c)** RF spectra in the ascending direction for a fixed gain current of 300 mA with applied reverse bias.

Fig. 6.7 Spectral tunability with high suppression ratio of more than 40 dB in descending direction for a fixed gain current of 330 mA with applied reverse bias.

Fig. 6.8 Dual-mode generation with 40 dB suppression ratio in both mode with similar power of 15 mW in descending direction at 0 V reverse bias for a fixed gain current of **a)** 300 mA and **b)** 330 mA.

Fig. 7.1 The experimental setup for an external cavity laser system (QD curve TS: quantum dot curved two-section diode; A- Absorber section, G- Gain section, L: lens,

OC: output coupler (T=53 % or 96 %), TS: motorized translation stage, OI: optical isolator, HWP: haft wave plate, F: fibre, FS: single mode fibre splitter, PD: photo diode, RFSA: RF spectrum analyzer, AUT: autocorrelator, OSC: oscilloscope, OSA/SA: Optical spectrum analyzer/ Spectrum analyzer, PC-personal computer).

Fig. 7.2 Light-current characteristics of the QD laser **(a)** without external feedback; and **(b)** the external-cavity laser for 0 V and 7.2 V of reverse-bias.

Fig. 7.3 (a) Autocorrelation trace, **(b)** optical spectrum, **(c)** RF spectrum with 500 MHz span and **(d)** 10-GHz span at a reverse bias of 7.2 V and forward current of 457 mA.

Fig. 7.4 (a) Peak power, average power and **(b)** pulse duration versus forward current with 7.2 V reverse bias.

Fig. 7.5 Representative RF spectra with 10 GHz span at a reverse bias of 8 V and forward current of 300 mA recorded for the variable repetition rate from 1 GHz to 191 MHz.

Fig. 7.6 A stable fundamental mode-locking regime with a repetition rate of 750 MHz.

Fig. 7.7 Dynamics of a peak power and average power at 8 V reverse bias for **(a)** different pulse repetition rate for a fixed forward current of 300 mA**, inset:** autocorrelation trace for 191 MHz corresponding to 10.2 ps pulse duration and **(b)** different driving forward current for a fixed repetition rate of 375 MHz.

Fig. 7.8 (a) RF spectrum with 10 GHz span corresponding to a fundamental pulse repetition rate 200 MHz measured under a reverse bias of 8 V and forward current of 300 mA. The resolution and video bandwidth for this acquisition were 30 Hz and 3 Hz, respectively. **(b)** A broad tunable harmonics repetition rate region up to 6.8 GHz – 34^{th} order harmonic of a 200 MHz fundamental frequency.

Fig. 7.9 (a) RF spectrum measured at a reverse bias of 8 V and forward current of 300 mA, at a 281 MHz pulse repetition rate. **(b)** RF spectrum with a 10 KHz span, with a

-3dB linewidth of ~30 Hz (obtained after Lorentzian fit). The resolution and video bandwidth for this acquisition were 30 Hz and 3 Hz, respectively.

Fig. 7.10 Dynamic of -3 dB RF linewidth with frequency from the QD-Based external cavity mode-locked laser at a reverse bias of 8 V and forward current of 300 mA.

Fig. 8.1 A schematic of the tapered **(a)** fully-index and **(b)** index- gain-guided lasers

Fig. 8.2 A schematic of the tapered fully gain guided laser.

Fig. 8.3 Light-current (L-I) characteristics for fully connected 5-layer and 10-layer quantum dot devices. **Upper left inset**: L-I characteristics obtained for an applied absorber bias of -4 V. **Lower right inset**: dependence between the threshold current and the absorber bias.

Fig. 8.4 Mapping of mode-locking regimes observed for **(a)** the 5-layer quantum dot laser, **(b)** the 10 layer quantum dot laser.

Fig. 8.5 (a) Pulse duration and **(b)** average power dynamics at a reverse bias -4 V for the 5-layer quantum dot laser.

Fig. 8.6 Far-fields **(a)** under uniform injection and **(b)** under -4 V reverse bias on the absorber section for the 5-layer quantum dot laser (characterized by III-V Lab, France).

Fig. 8.7 (a) Autocorrelation, **(b)** RF spectrum and **(c)** optical spectrum for an injection current of 950 mA and reverse bias of 5.1 V at a high peak power regime in the 5-layer quantum dot laser.

Fig. 8.8 (a) Autocorrelation, **(b)** RF spectrum and **(c)** optical spectrum for an injection current of 1044 mA and reverse bias of 4.9 V at high peak power regime in the 10-layer quantum dot laser.

Fig. 8.9 Simulated pulse width **(a)**, average power **(b)** and peak power **(c)** as a function of the SA voltage and current above threshold $I-I_{th}$, for a 4 mm device with a 2° full

angle tapered gain section and 17% SA section to gain section length ratio. Shaded region highlights unstable ML due to large leading edge (LE) instability (performed by the Politecnico di Torino, Italy).

Fig. 8.10 Pulse width **(a)**, average power **(b)** and peak power **(c)** as a function of the SA voltage and current above threshold $I\text{-}I_{th}$, for a 4 mm device with 2° full angle tapered gain section and 25% SA section to gain section length ratio. No leading edge instability to spontaneous emission noise perturbations has been observed in the investigated range of bias parameters (performed by the Politecnico di Torino, Italy).

Fig. 8.11 Dynamic characterization experimental setup: QD -TSD: quantum dot - two section diode, A- absorber section, G: gain section, TC: temperature controller, L: lens, OI: optical isolator, HWP: half wave plate, SMF: single-mode fiber, FS: fiber splitter, OSA: optical spectrum analyzer; PC: personal computer; Autoco: autocorrelator; Osc: oscilloscope; PD: photo detector; RFSA: RF spectrum analyzer.

Fig. 8.12 Light current characteristic for device A at a reverse bias of -6.0V. The shortest pulses are obtained at 570 mA and the highest peak power at 695 mA (Characterized at Technical University of Darmstadt, Germany).

Fig. 8.13 Autocorrelation signal of the shortest pulse width of laser A; inset left: an optical spectrum; inset right: RF spectrum at a gain current of 570 mA and reverse bias of -6.0 V. $Sech^2$ fit (Characterized at Technical University of Darmstadt, Germany).

Fig. 8.14 Pulse width in dependence of a gain current of laser A at a reverse bias of -6.0 V (Characterized at Technical University of Darmstadt, Germany).

Fig. 8.15 Dependence of peak power as a function of a gain current of laser A at a reverse bias of -6.0 V (Characterized at Technical University of Darmstadt, Germany).

Fig. 8.16 Far field slow-axis pattern measured on device A at 575 mA and 675 mA with a very low full width of 2.4° and 3.1° at $1/e^2$ of maximum, respectively (characterized by III-V Lab, France).

Fig. 8.17 a, b Light-current curves for a laser B at 20^o C **(a)** under uniform injection (red line) with a threshold current of 341 mA and **(b)** under an applied voltage of -4 V on the absorber section (black line) with a 720 mA threshold current.

Fig. 8.18 (a) Pulse duration and **(b)** peak power dynamics at a -4 V reverse bias for quantum-dot tapered laser B.

Fig. 8.19 (a) Autocorrelation (Inset: RF spectrum); **(b)** optical spectrum for an injection current of 1 A and reverse bias of -4 V for a short pulse regime for quantum-dot tapered laser B.

Fig. 8.20 (a) Autocorrelation (Inset: RF spectrum); **(b)** optical spectrum for an injection current of 1.5 A and reverse bias of -4 V for a record-high peak power regime for quantum-dot tapered laser B.

Fig. 8.21 Shows far field slow-axis pattern measured on device B at 1 A (shortest pulse width) and 1.5 A (highest peak power) with a very low full width of 3.3°and 2.2° at $1/e^2$ of maximum, respectively (characterized by III-V Lab, France).

Fig. 8.22 A phase noise and integrated timing jitter for an injection current of 955 mA and reverse bias of -4.17 V at 14˚C for laser B.

Fig. 8.23 Experimental setup for two-photon imaging with a tapered laser and nonlinear microscope.

Fig. 8.24 A two-photon image of fluorescent beads using QD tapered laser B.

Fig. 9.1 A map for a progress of QD based lasers: MML Laser- monolithic mode-locked laser, ECML- external cavity mode-locked laser, Tapered mode-locked (ML) laser toward biophotonics.

Tables.

Table 3.1 A performance summary of the main types of short pulse generation techniques for electrically pumped semiconductor lasers**.**

Table 3.2 Overview of mode-locked InGaAs quantum well lasers with the following characteristics: $\boldsymbol{\tau_p}$-pulse duration, **λ**-emission wavelength, **Δλ**- full width half maximum, $\mathbf{f_{rep}}$- pulse repetition rate, $\mathbf{P_{peak}}$–peak power, **TBWP**- Time bandwidth product, $\mathbf{N_L}$-number of layers, n/a- not applicable. The best performances are in bold.

Table 3.3 Overview of mode-locked InGaAsP quantum well lasers with the following characteristics: $\boldsymbol{\tau_p}$-pulse duration, **λ**-emission wavelength, **Δλ**- full width half maximum, $\mathbf{f_{rep}}$- pulse repetition rate, $\mathbf{P_{peak}}$–peak power, **TBWP**- Time bandwidth product, $\mathbf{N_L}$-number of layers, n/a- not applicable. The best performances are in bold.

Table 3.4 Overview of mode-locked InAs/GaAs Quantum Dot lasers with the following characteristics: $\boldsymbol{\tau_p}$-pulse duration, **λ**-emission wavelength, **Δλ**- full width half maximum, $\mathbf{f_{rep}}$- pulse repetition rate, $\mathbf{P_{peak}}$–peak power, **TBWP**- Time bandwidth product, $\mathbf{N_L}$-number of layers, n/a- not applicable. The results highlighted in green are shown in more detail in the thesis. In blue are the results which were achieved by our group in the past. The best performances are in bold.

Table 4.1 Second-order autocorrelation functions and bandwidth products for Gaussian, Hyperbolic Secant squared and Lorentzian pulse shapes. **TBWP**- Time-bandwidth product**.**

Table 5.1 Bias conditions: reverse voltage to the absorber (**V)** and forward current to the gain section **(I)**; pulse duration **(τ)**, Average power **(Pav)**, Peak Power **(Ppeak)**, Time bandwidth product **(TBWP)**, full width half maximum of optical spectra (**Δλ**), central

wavelength **(λ)**, GS –ground state (black) or ES-excited state (red) of dual-mode regime in QD-based mode-locked laser.

Table 9.1 Performance of QD-based devices presented in the thesis.

Equations.

1.1 $\lambda_{\mathrm{B}} = \frac{\mathrm{h}}{\mathrm{p}} = \frac{\mathrm{h}}{\sqrt{2\mathrm{m}^{*}\mathrm{E}}}$

1.2 $\mathrm{I} = \mathrm{k}\frac{\boldsymbol{\Delta\tau_{p}}}{\mathrm{T}}\mathrm{P}_{\mathrm{peak}}^{2}$

1.3 $\mathrm{I} = \mathrm{kP_{av}P_{peak}}$

3.1 $Q = 2\pi * \frac{E_{st}}{E_{diss}} = 2\pi f * \frac{E_{st}}{P_{loss}}$

3.2 $\varphi_{l} - \varphi_{l-1} = \varphi$

3.3 $\Delta\nu = \frac{c}{2Ln}$

3.4 $\Delta\tau_{P} = \frac{\beta}{\Delta\nu_{L}}$

3.5 $E_{abs}^{sat} \equiv \frac{h\nu A}{\partial a/\partial n} < \frac{h\nu A}{\partial g/\partial n} \equiv E_{gain}^{sat}$

3.6 $\Gamma_{gain}^{sat} = \frac{h\nu}{A_{g}}$

3.7 $\Gamma_{abs}^{sat} = \frac{h\nu}{2A_{a}}$

4.1 $\tau_{FWHM}=0.44/f_{3dB}$

4.2 $\tau_{MEASUREMENT} = \sqrt{\tau_{osc}{}^{2} + \tau_{photodiode}{}^{2} + \tau_{signal}{}^{2}}$

4.3 $I_{SH}(t+\tau) \sim [E(t) + E(t+\tau)]^{2}$

4.4 $I_{SH}(t+\tau) \sim E(t)^{2} + 2E(t)E(t+\tau) + E(t+\tau)^{2}$

4.5 $I_{SH}(t+\tau) \sim 2E(t)E(t+\tau)$

4.6 $I_{AC}(\tau) \sim \int [2E(t)E(t+\tau)]^{2}\, dt$

4.7 $I_{AC}(\tau) \sim \int I(t)I(t+\tau)\, dt$

4.8 $\Delta\nu^{*}\Delta\tau = c^{*}\Delta\lambda^{*}\, \Delta\tau/\lambda^{2}$

4.9 $P_{PEAK}=P_{AVR}{}^{*}T/\, \Delta\tau_{P}$

4.10 $f=dD\pi/4\lambda$

4.11 $\mathrm{T} = \frac{4\pi \mathrm{f} \mathrm{D_M}}{\mathrm{c}} \mathrm{t}$

4.12 $T_t = \frac{\sqrt{2} d_L}{c}$

4.13 $\mathrm{NL} = \frac{\mathrm{d_L}}{4\mathrm{D_M}}$

4.14 $\mathrm{X(dBm)} = 10\log_{10} P(\,mW)$

Contents

Declarations. ii

Acknowledgements. iii

List of publications. v

Abstract. viii

Abbreviations. x

Figures. xvi

Tables. xxv

Equations. xxvii

Contents xxix

Chapter 1. Introduction. 1

1.1 Ultrashort-pulse lasers. 1

1.2 The development of semiconductor lasers. 3

1.2.1 p-n Junction. 3

1.2.2 Double heterostructure. 5

1.2.3 Dimensionality of the semiconductor structures. 8

1.3 Diode lasers toward Biophotonics. 11

1.4 Goals and structure of the thesis. 16

1.5 References. 18

Chapter 2. Semiconductor Quantum Dot Devices. 24

2.1 Stranski-Krastanow material growth method. 24

2.2 Self-organized InGaAs quantum dots on a GaAs substrate. 26

2.2.1 Shape, size, and distribution of quantum dots. 26

2.2.2 Lattice mismatch and critical thickness. 28

2.2.3 Optical emission range. 30

2.3 Unique QDs properties for ultrafast generation. 32

2.3.1 Low threshold current density. 32

2.3.2 Inhomogeneous broadening. 33

2.3.3 Ultrafast carrier dynamics. 35

2.4 Conclusion 36

2.5 References. 37

Chapter 3. Ultrashort pulse generation. 43

3.1 Main techniques for ultrashort pulse generation. 43

3.1.1 Gain switching and Q-switching. 43

3.1.2 Mode-locking techniques in semiconductor lasers. 46

3.1.3 Saturable absorber for passive mode-locking. 50
3.2 State of the art of Mode-locking 52
3.2.1 Quantum well lasers. 52
3.2.2 Quantum dot lasers 55
3.3 Conclusion 59
3.4 References. 60
Chapter 4. Characterization of QD-based devices under mode-locking regime. 73
4.1 Characterization techniques 73
4.1.1 Pulse shape and duration. 73
4.1.2 RF spectra (good stable ML). 78
4.1.3 Optical spectra characteristics. 80
4.1.4 Power characteristics (duty cycle, FOM) 82
4.2 Experimental setup 84
4.2.1 Peltier cooler. 86
4.2.2 Optical isolator and half plate 87
4.2.3 Aspheric lenses. 89
4.2.4 Fibre splitter. 91
4.2.5 Autocorrelator. 92
4.2.6 RF spectrum analyzer and fast photodiode. 95
4.2.7 Optical spectrometer. 98
4.2.8 Power meter. 100
4.3 Conclusion 101
4.4 References. 102
Chapter 5. Different mode operations in monolithic quantum dot lasers. 104
5.1 State of the art: multi-wavelength ultrashort pulse generation. 104
5.2 Ultrashort pulse generation via ground and/or excited states. 107
5.2.1 Introduction 107
5.2.2 Device structures. 108
5.2.3 Experimental results and discussion. 109
5.2.4 Conclusion. 113
5.3 Dual-wavelength mode-locking via ground and excited states. 114
5.3.1 Introduction/State of the art. 114
5.3.2 Experimental results and discussion. 115
5.3.3 Conclusion. 120

5.4 Influence of the cavity length and number of QD layers on ultrashort pulse generation. 121
5.4.1 Introduction. 121
5.4.2 Device structures. 122
5.4.3 Experimental results and discussion. 123
5.4.4 Conclusion. 130
5.5 Summary. 131
5.6 References. 132
Chapter 6. Bistable quantum dot laser. 137
6.1 The concepts of bistability (polarization, power, wavelength) and tunability. 137
6.2 Device description. 140
6.3 Experimental results and discussion. 142
6.4 Conclusions. 148
6.5 References. 149
7. External cavity Quantum Dot lasers. 155
7.1 Introduction. 155
7.1.1 An external cavity configuration laser. 155
7.1.2 Experimental setup and device. 157
7.2 A high peak power laser 159
7.2.1 State of the art. 160
7.2.2 Experimental results and discussion. 161
7.2.3 Conclusions. 165
7.3 Fundamental and Harmonic Mode-locking. 166
7.3.1 State of the art. 167
7.3.2 Fundamental Mode-locking experimental results. 168
7.3.3 Harmonic Mode-locking experimental results. 173
7.3.4 Conclusion. 175
7.4 Narrow RF linewidth. 176
7.4.1 State of the art. 177
7.4.2 Experimental results and discussion. 178
7.4.3 Conclusion. 180
7.5 Summary. 181
7.6 References. 182
Chapter 8. Quantum-Dot tapered lasers 185
8.1 Introduction. 185

8.1.1 Basics of tapered lasers. 185
8.1.2 Different designs of tapered laser. 187
8.2 First iteration of tapered lasers. 189
8.2.1 Fully gain-guided high power tapered lasers. 190
8.2.2 Experiments and Discussion. 192
8.2.3 Conclusion. 197
8.3 Second iteration of tapered lasers. 198
8.3.1 Introduction. 198
8.3.2 Optimized fully gain-guided tapered lasers. 199
8.3.3 Simulation results. 201
8.3.4 Experiments and Discussion. 204
8.3.5 Conclusion. 213
8.4 Multiphoton imaging using tapered lasers. 214
8.4.1 Introduction. 214
8.4.2 Experimental setup. 215
8.4.3 Experiments and Discussion. 217
8.4.4 Conclusion. 219
8.5 Summary. 220
8.6 References. 221
Chapter 9. Conclusions. 226
9.1 Summary of the work. 226
9.2 Future work. 229
9.3 References. 230

Chapter 1. Introduction.

1.1 Ultrashort-pulse lasers.

Recent development and progress of the ultrafast optical sources enable them to be used for a variety of applications from medical treatment (dentistry, eye surgery, dermatology, tattoo removal, hair removal, photodynamic therapy) [1], displays [2], spectroscopy, Light Detection and Ranging (LIDAR)and photochemistry (cancer detection and treatment) [3-4], optical metrology (precise measurement, navigation, scanners, optical sampling, all-optical clock, fibre-optic sensors) [5] to material processing [6] and laser cooling [7].

New doors were opened with the generation of femtosecond optical pulses for areas such as material processing, biophotonics, and telecommunication. Due to the ultra short pulse the peak power can be very high despite low average power. It is very important for a variety of applications as the thermal stress is reduced, for example, micro-machining and photo-ablation of biological tissues. Nano surgery in a living cell is now possible without surface damage to the membrane. The high peak power of femtosecond laser is very useful for generating nonlinear optical response in biological samples. Several innovative nonlinear optical microscopy techniques involving multi-photon fluorescence and second harmonic generation have become widely used for biological and biomedical research providing 3D imaging of fine structures, even at a cellular level [8]. Femtosecond laser tweezers can now be used in near-field optics as well as for studying fundamental cell biology and cell mechanics [9-10]. In telecommunication, ultrafast optical technology is facing the challenge of increasing networks capacity. Ultra high speed data streams can be created by femtosecond pulses [11]. Code-division multiple accesses (CDMA) are possible due to broad-band

coherence of ultrashort optical pulses. As a result of the high peak power such lasers can be used for nonlinear processes such as frequency conversion, optical time-domain multiplexing (OTDM)/demultiplexing, wavelength-division multiplexing (WDM), and further spectral broadening [12]. Precise timing of the short pulses is used for all-optical clock recovery [13].

Crystal-based solid state lasers have shown great potential for a variety of applications due to the possibility of generating femtosecond pulses with high peak power [14-15]. Thin-disk Yb: YAG lasers can produce up to 60 W average power [16] and Kerr-lens-mode-locked Ti: Sapphire lasers allow directly generating the pulses as short as 5 fs [17]. Notwithstanding of all the advantages solid state lasers are very expensive, complex, and bulky as well as the overall wall plug efficiency is far from ideal [18]. They are not electrically pumped and thus a separate pump laser is often required with a cooling system. Also there is no direct control over the laser gain medium. The low gain of the crystals defines the required minimum crystal length which in turn limits the pulse repetition rate. Scientists are looking for alternative laser systems which will remove the above limitations. One of the ways is to use fibre laser systems. It was shown that short pulses 3.5 ps can be generated at 1075 nm wavelength with a repetition rate of 22 MHz [19]. High output power Yb doped fibre laser is now developed with output more than 100 W operating at 1080 nm as well [20]. Another way to do this is to use electrically pumped semiconductor femtosecond diode lasers that are very cheap, compact, integrated devices with high wall plug efficiency.

1.2 The development of semiconductor lasers.

1.2.1 p-n Junction.

Laser diodes are formed by doping a thin layer of the semiconductor crystal inhomogeneously. In the crystal p-doped (with an excess of holes) and n-doped (i.e., with an excess of electrons) regions are produced one above the other resulting in a heterojunction (p-n junction). In this area the diffusion process takes place ideally until the carrier concentrations become equal on both sides of the junction. The holes diffuse from the p-side leaving behind the ionized acceptor atoms while the electrons move from n-side and leave the ionized donor atoms. As the result the electric field appears in the direction of the n-side to p-side thus opposing diffusion of holes from the p-side and electrons from the n-side. Electrons' movement from n-side to p-side is corresponding to the diffusion current. The flow of the carriers in the opposite direction constitutes the drift current. As forward bias is applied to the junction (where p-side is connected to the positive end and n-side to the negative end of the voltage source) the electrons move more freely into the p-type region and the diffusion current exceeds the drift current (Fig. 1.1 (a)). Thus the direction of the net current is from p-side to n-side. If reverse bias is applied to the p-n junction then the energy step at this junction is increased as shown in Fig. 1.1 (b) and it becomes more difficult for electrons move from n-side to p-side. In such a scenario the drift current exceeds the diffusion current and the net current is directed from the n-side to the p-side [21]. In a two-section laser, the gain section is forward biased while the absorber section is reversed bias.

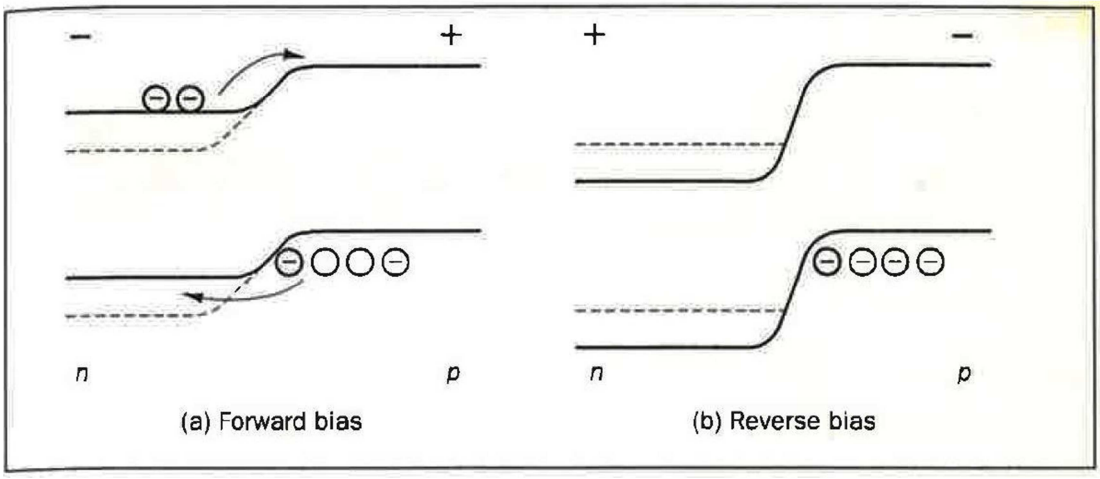

Fig. 1.1 (a) Decreasing of the energy step under forward bias, allowing electrons and holes to cross the junction, **(b)** Increasing of the energy step with reverse bias, and very few carriers cross the junction [21].

1.2.2 Double heterostructure.

Semiconductor lasers based on p-n junction were not very efficient until after the development of double heterostructure. B. I. Davydov's diffusion theory of p-n heterojunction rectification and W. Shockley's junction theory laid the foundations of semiconductor laser diodes [22-23]. Basov *et.al* [24-25] proposed semiconductors lasers and Nasledov [26] showed first indication of stimulated emission. *Hall et.al.* invented the first semiconductor injected laser converting electrical energy to coherent infrared radiation [27]. Shortly after, three other groups iterated the same discovery [28-30]. They observed sharp beam radiation patterns, abrupt increases of the light intensity above threshold, and narrowing of the spectral distribution of the emission beyond threshold current [28-30]. Semiconductor lasers exhibited very high optical and electrical losses as bulk material was used until after the revolutionary idea of using double heterostructure (DH) as active region of the lasers was proposed [31-32]. In 2000 Zhores I. Alferov and Herbert Kroemer were awarded the Nobel Prize in Physics for developing semiconductor heterostructures used in high-speed and opto-electronics [33]. Heterostructures are formed from multiple heterojunctions. In classical heterostructures several fundamental physical phenomena take place: superinjection of carriers, optical confinement as well as electron confinement, wide-gap window effect, and diffusion and tunnelling, as shown in Fig. 1.2 [31].

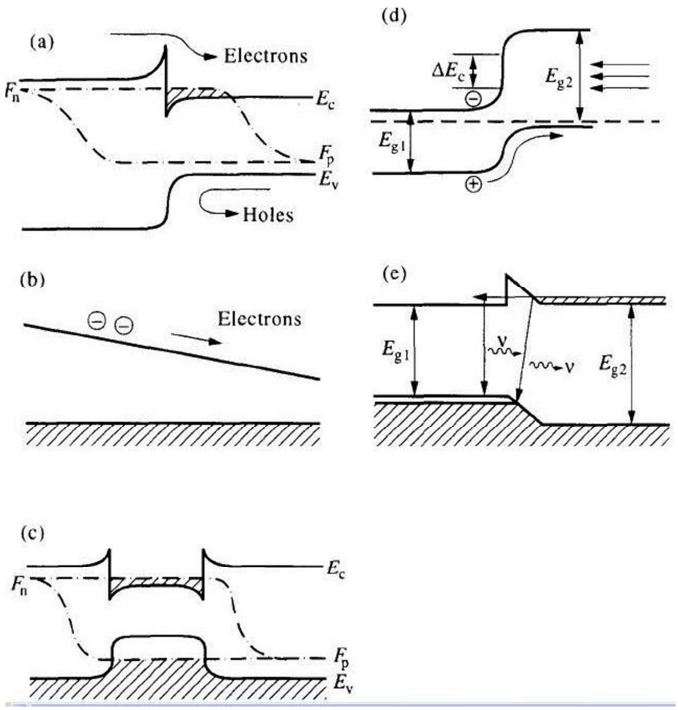

Fig.1.2 Main physical phenomena in classical heterostructures: **(a)** One-side injection and superinjection; **(b)** diffusion in built-in quasi-electric field; **(c)** electron and optical confinement; **(d)** wide-gap window effect; **(e)** diagonal tunnelling through a heterostructure interface [31].

DH is a sandwich of lattice-matched material (for example GaAs and AlGaAs) where the centre of the sandwich has a lower energy gap than the sides $E_{g2} < E_{g1}$, as shown in Fig. 1.3. Thus a fundamental advantage of DH is the effective confinement of both electrons and holes in the narrow gap region (ΔE_c and ΔE_v) enhancing the efficiency of the laser. In addition, the centre region, E_{g2}, with lower energy bandgap typically has a higher refractive index than the outer layers forming a slab waveguide and guiding the emitted light. Such advantages of DH have led to a decrease of the threshold current density (J_{th}) of the laser. If a centre region is sufficiently thin then quantum properties play an important role in the layer.

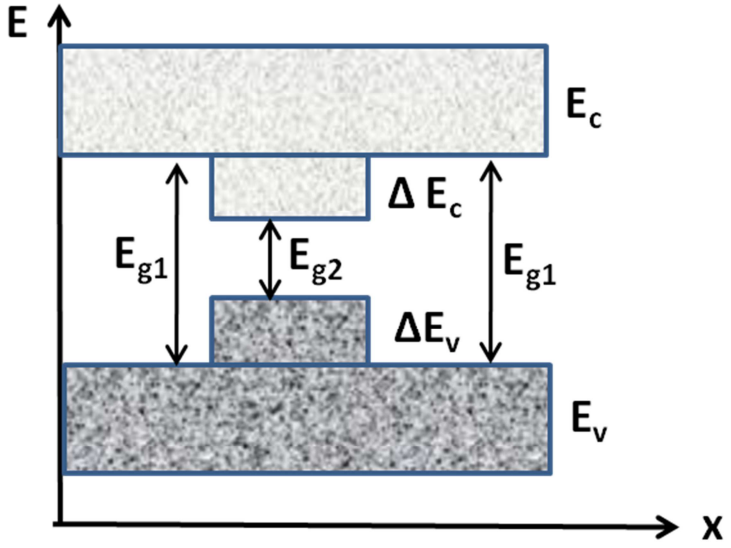

Fig. 1.3 Simplified energy band diagram for double heterostructure (DH).

1.2.3 Dimensionality of the semiconductor structures.

The dimensionality of a semiconductor structure has a strong influence on its optoelectronics properties. Quantum size effect takes place when the thickness of an active semiconductor region is reduced to a carrier de Broglie wavelength, as shown in Eq. 1:

$$\lambda_B = \frac{h}{p} = \frac{h}{\sqrt{2m^*E}} \quad \textbf{(1.1)},$$

where λ_B-wavelength, h-Planck's constant, p-momentum of a particle, m^*-the electron effective mass, and E-the energy [34].

Typical λ_B for AlGaAs is in order of 10-20 nanometres. Therefore, when the centre layer thickness is below 10-20 nm, the charge carriers are effectively confined in one dimension. Allowed electron/hole energies are no longer a continuum, as in bulk materials, but discrete as defined by solving the quantum mechanical problem of a particle in a potential well. Such thin DH, so-called "quantum-wells", exhibited better performance in term of recombination in a narrow linewidth or fixed wavelength as well as in terms of more efficient carrier thermalization due to the change of the density of state (DOS) of the carriers [35]. The DOS gives a measure of the maximum number of carriers that can occupy an energy range. The wavelength of the light emitted by a quantum well laser is determined by the width of the active region rather than just the bandgap of the material from which it is constructed. Much shorter wavelengths than a conventional laser diode can be achieved by this configuration. The confinement of electrons/holes in two dimensions and free movement in the third, has leads to a further change of the energy-momentum relationship and formation of quantum wire (QWR). For QWR, the DOS for certain energies becomes higher than the

DOS for QW or bulk semiconductors. Lastly, a zero-dimensional (meaning in all three dimensions confined) structure is called quantum dot (QD). QDs are clusters of semiconductor material, just a few nanometres size in all three dimensions. The DOS is changed as well and presents itself like a delta peak function, so the charge carriers take up only a specific set of energy levels like electrons in an atom. That is why QDs are often called "artificial atoms". The schematic morphology of different dimensionality semiconductor structures, with corresponding density of states of charge carriers, is shown in Fig. 1.4.

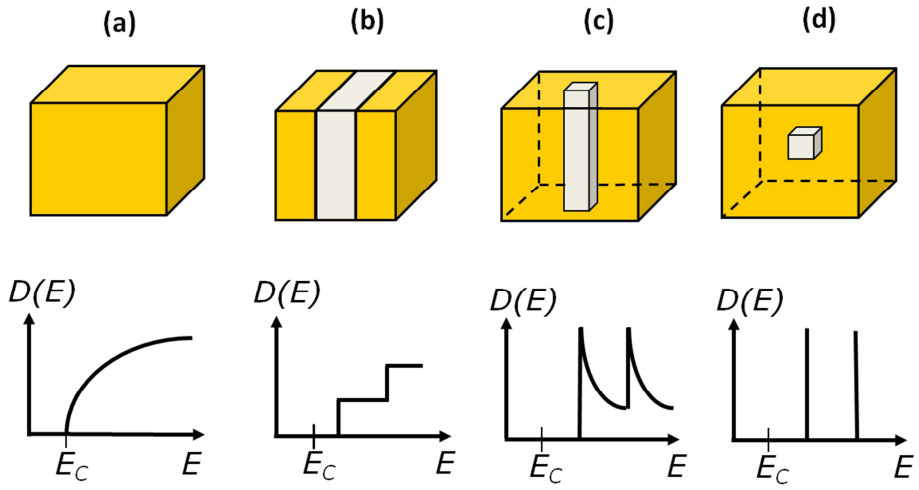

Fig. 1.4 (up) Schematic morphology and **(down)** the density of states of charge carriers for **(a)** bulk, **(b)** quantum well, **(c)** quantum wire, **(d)** quantum dot semiconductor structures.

The electronic characteristics of QDs are closely related to the size and shape of the individual crystal. The smaller the size of the crystal, the higher the band gap between the lowest conduction band and the highest valence band becomes, thus increasing the energy required to excite the dot. As a consequence more energy is released during relaxation. Thus QD based laser exhibits several advantages such as record-low threshold current density, suppressed carrier diffusion, resilience to temperature, ultra-fast carrier dynamics, and lower absorption saturation fluence. The technological

progress of semiconductor lasers have allowed the fabrication of compact, electrically pumped, quantum dot based devices, that generate picosecond and femtosecond pulses with high repetition rates. These can be used as photo detectors and for data transmission systems [36-38]. Consequently, QDs have become a very exciting area of scientific research.

1.3 Diode lasers toward Biophotonics.

In recent years, imaging techniques based on nonlinear optical effects have been greatly improved by the technological progress of mode-locked femtosecond lasers. When biological tissue interacts with an intense ultrashort pulse laser beam, a non-linear response to the applied field strength is observed, which can be used as the imaging contrast. Multi-photon microscopy can not only provide multicolour imaging of a surface but also reveal internal organs [39-44]. Compared to single-photon fluorescence microscopy, multi-photon fluorescence microscopy has a number of advantages (Fig. 1.5). As a result of using a long wavelength for excitation, the penetration depth is improved reducing the effect of unwanted Mie and Rayleigh scatterings [45]. Although, the axial resolution is greatly improved by use of a confocal mask [46]. Two-photon absorption occurs only at the focal plane of the microscope objective and fluorescence is confined in the focal volume (Fig. 1.6). Thus three-dimensional, high resolution, images can be produced without using a confocal pinhole mask [47-48]. In addition, some fluorophores are only efficiently excited with two photons.

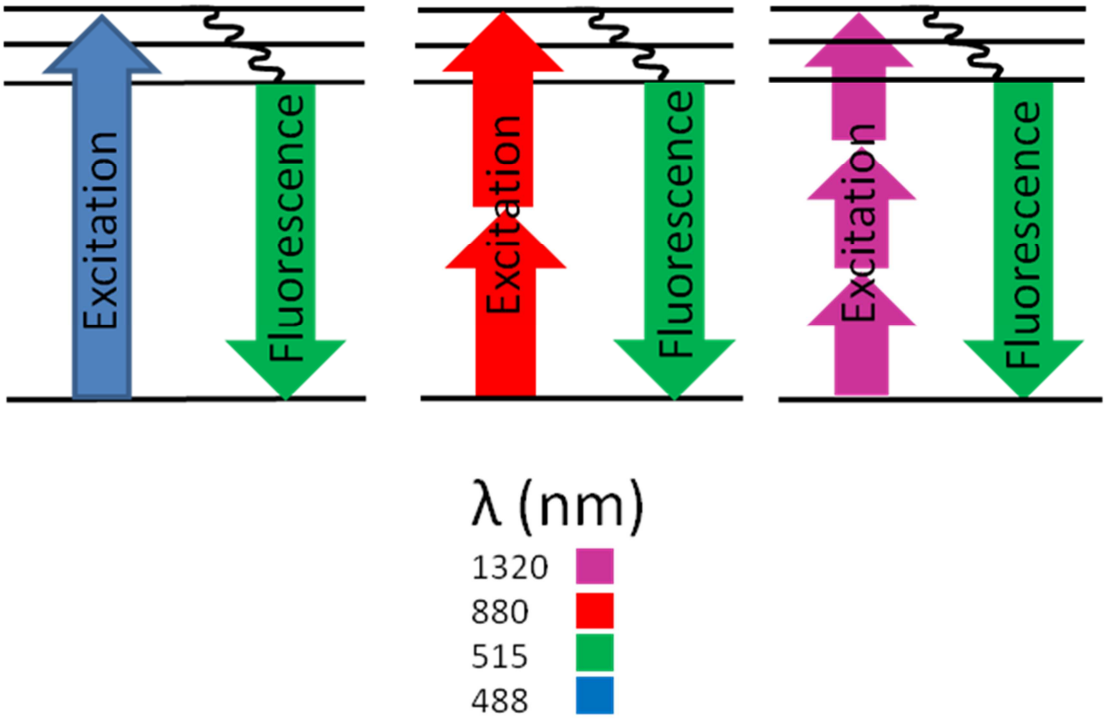

Fig. 1.5 Single photon (left) and two-photon (middle) and three photon (right) excitation diagrams.

Fig. 1.6 One photon excitation **(left)** and multi-photon excitation **(right)** at a focal plane of the microscope objective.

The idea of two-photon fluorescence scanning microscopy was proposed by Sheppard *et. al.*[49-50] Two-photon fluorescence microscopy was first demonstrated in 1990 by Denk *et. al.*[51]. Three-photon fluorescence was also generated when three incident photons were absorbed simultaneously in organic solutions, with the radiating photon triple the energy of the incident one [52]. Not long after, the first three-photon fluorescence microscopic image was recorded using a nonlinear crystal [53].

For successful multiphoton imaging laser should produce enough output power to have sufficient high fluorescent intensity (I) that increases with pulse duration (τ), the square of the peak power (P_{PEAK}), and with the reciprocal of optical pulse period (T) (Eq. 1.2.) [54]:

$$I = k\frac{\tau}{T}P_{peak}^2 \quad \textbf{(1.2),}$$

where the factor k depends on the two-photon absorption cross section of the fluorophore at the laser wavelength, and on the spatial energy distribution in the focus.

Knowing duty cycle relationship $P_{AV}/P_{PEAK}=\tau/T$, Eq. 1.2 can be rewritten as Eq.1.3:

$$I = kP_{av}P_{peak} \quad \textbf{(1.3)},$$

where Pav is the average power.

Given these relationships, how much output power do we need for successful multiphoton imaging? The average power should be high enough for excitation of the fluorophore, but at the same time it must not to destroy the biological samples. Temperature rises due to water absorption and beyond a certain threshold, cells and tissues may degrade because of protein denaturation. For imaging through biological tissue, a wavelength region between 600 nm and 1300 nm is desirable since this corresponds to a transmission window in the absorption profile as shown in Fig. 1.7. At wavelengths higher than 1300 nm light absorption by water molecules becomes substantial. Several groups have managed to achieve high peak power [55-56]. For example, Kim *et.al* managed to get 1.4 kW peak power at 974 nm from a master oscillator system based on eXtreme Chirped Pulse Amplification (X-CPA) involving a colliding pulse external cavity mode-locked semiconductor laser, significant pulse stretching, multiple amplification stages, and significant compression [55].

Schlauch *et.al* demonstrated 622 fs pulses with 513 mW output power from an ~830 nm passive mode-locked tapered laser resulting in a world-record peak power of 2.5 kW [56]. At the same time, another group has shown the possibility of two-photon fluorescence bioimaging of actin filaments in PtK2 cells using a second harmonics generation of 1.55 µm gain-switched distributed-feedback-Bragg laser diode generating 1 kW of peak power after several amplification stages [54].

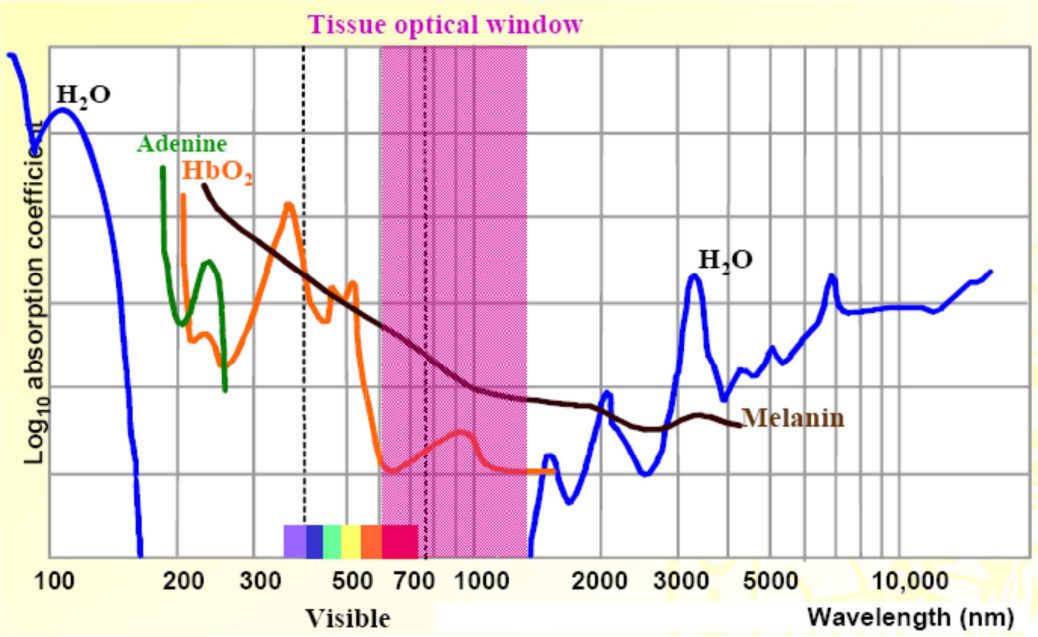

Fig. 1.7 Absorption in tissue is dominated by protein and DNA in the UV, by water in the IR, and by haemoglobin and melanin in the visible light [57].

It was shown that several tens of watts of peak power can be enough for multiphoton imaging [58-59]. For example, multiphoton imaging of a cell containing Coumarin and mouse kidney was achieved using an external-cavity mode-locked laser generating 5 ps pulses with a repetition rate of 500 MHz at 800 nm wavelength with 20 W and 32 W peak powers, respectively, at the sample plane. The active region of the laser consisted of 3 quantum well layers. In order to achieve high peak power, a two-stage amplifier configuration was also implemented [58].

QD based lasers emitting at 1100 nm to 1300 nm and generating short pulses with high output power can be effectively used for multiphoton imaging of biological samples due to higher penetration depth. This is one of the goals of this thesis (Fig. 1.8).

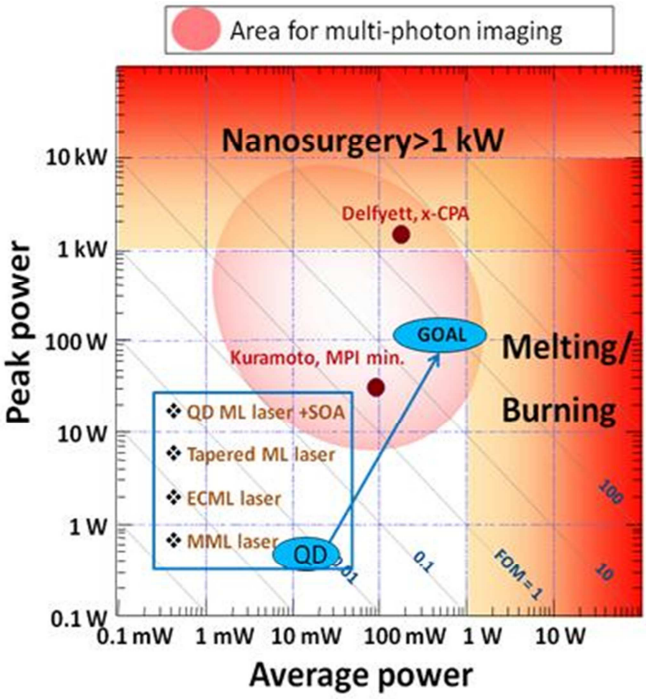

Fig. 1.8 Mapping of the initial state of art at the beginning of this work and goal for the QD based mode-locked lasers used in my thesis.

1.4 Goals and structure of the thesis.

The goal of this thesis is to utilize properties of quantum-dot (QD) based semiconductor materials and devices for the generation and amplification of ultrashort optical pulses using their broad gain/absorption bandwidth. Parallel work will also include on progress in the generation and amplification of ultrashort pulses in 1100 nm and 1300 nm window and the fabrication of compact, environmentally-stable and lower-cost ultrafast lasers and semiconductor optical amplifiers. In addition, electrically pumped quantum-dot mode-locked lasers in monolithic and extended cavity configurations are investigated as laser sources suitable for a range of biomedical applications.

Chapter 2 of the thesis describes, in detail, the Stranski-Krastanow method of quantum dot formation as well as the electronics and morphological properties of QDs, leading to an exploration several advantages of QD-based devices that make them favourable for ultrafast generation. An overview of the mode-locking techniques and state of the art quantum well (QW) and QD GaAs devices are presented in Chapter 3. The main equipment and method for characterizing of QD based lasers and devices in the experiments are discussed in Chapter 4. The influence of the structural parameters of the laser such as cavity length, number of QD layers on ground and/or excited state emissions are investigated in Chapter 5. The advanced growing technique makes possible tunable and bistable QD lasers. The wavelength and power bistability in QD lasers are described in Chapter 6, showing how such devices are suitable for flip-flop memory application. QD lasers in an external cavity configuration have exhibited a low repetition rate, narrow RF linewidth; fundamental and harmonic mode-locking (see Chapter 7). In order to increase output power a tapered geometry gain section of a QD

laser was designed, fabricated in III-V Labs in France, characterized at the University of Dundee and two-photon imaging tests were performed at the Institute of Photonics (ICFO) in Spain. Main results of these tests are shown in Chapter 8. Finally, concluding remarks and future work are presented in Chapter 9.

1.5 References.

[1] B. Wardle, *Principles and Applications of Photochemistry*: John Wiley and Sons, Ltd, 2009.

[2] M. S. Brennesholtz and E. H. Stupp, *Projection Displays*, 2nd ed.: John Wiley and Sons, Ltd, 2008.

[3] W. Demtröder, *Laser spectroscopy: basic concepts and instrumentation*, 3rd ed. New York: Springer-Verlag Berlin Heidelberg, 2003.

[4] H. H. Telle*, et al.*, *Laser Chemistry: Spectroscopy, Dynamics and Applications*. Chichester: John Wiley and Sons Ltd, 2007.

[5] A. Horn, *Ultra-fast Material Metrology*. Darmstadt: Wiley-VCH Verlag GmbH & Co. KGaA, Weinheim, 2009.

[6] W. M. Steen and J. Mazumder, *Laser Material Processing*, Fourth ed. New York: Springer-Verlag London Limited, 2010.

[7] H. J. Metcalf and P. Van der Straten, *Laser cooling and Trapping*. New York: Springer-Verlag New York, Inc, 1999.

[8] P. J. Campagnola and L. M. Loew, "Second-harmonic imaging microscopy for visualizing biomolecular arrays in cells, tissues and organisms," *Nat Biotech,* vol. 21, pp. 1356-1360, 2003.

[9] U. K. Tirlapur and K. Konig, "Cell biology: Targeted transfection by femtosecond laser," *Nature,* vol. 418, pp. 290-291, 2002.

[10] D. Day*, et al.*, "High-Speed Fluorescence Imaging and Intensity Profiling of Femtosecond-Induced Calcium Transients," *International Journal of Biomedical Imaging,* vol. 2006, pp. 1-6, 2006.

[11] M. Attygalle*, et al.*, "All-optical coding of mode-locked semiconductor laser pulse trains for high bit rate optical communications," *Optics Communications,* vol. 217, pp. 161-167, 2003.

[12] G. A. Keeler*, et al.*, "The benefits of ultrashort optical pulses in optically interconnected systems," *Selected Topics in Quantum Electronics, IEEE,* vol. 9, pp. 477-485, 2003.

[13] S. Arahira*, et al.*, "Polarization-, Wavelength-, and Filter-Free All-Optical Clock Recovery in a Passively Mode-Locked Laser Diode With Orthogonally Pumped Polarization-Diversity Configuration," *Quantum Electronics, IEEE,* vol. 45, pp. 476-487, 2009.

[14] D. E. Spence*, et al.*, "60-fsec pulse generation from a self-mode-locked Ti:sapphire laser," *Opt. Lett.,* vol. 16, pp. 42-44, 1991.

[15] U. Keller*, et al.*, "Solid-state low-loss intracavity saturable absorber for Nd:YLF lasers: an antiresonant semiconductor Fabry-Perot saturable absorber," *Opt. Lett.,* vol. 17, pp. 505-507, 1992.

[16] E. Innerhofer*, et al.*, "60-W average power in 810-fs pulses from a thin-disk Yb:YAG laser," *Opt. Lett.,* vol. 28, pp. 367-369, 2003.

[17] R. Ell*, et al.*, "Generation of 5-fs pulses and octave-spanning spectra directly from a Ti:sapphire laser," *Opt. Lett.,* vol. 26, pp. 373-375, 2001.

[18] C. T. A. Brown*, et al.*, "Compact laser-diode-based femtosecond sources," *New Journal of Physics,* vol. 6, 2004.

[19] S. V. Smirnov*, et al.*, "Mode-Locked Fibre Lasers with High-Energy Pulses," in *Laser Pulses*. vol. 1, D. K. Jakubczak, Ed., ed, 2011, pp. 39-58.

[20] B. Wang and A. Sanchez, "All-fiber passive coherent combining of high power lasers," *Optical Engineering,* vol. 50, pp. 111606-4, 2011.

[21] R. Turton, *The Quantum Dot: A journey into the Future of Microelectronics*. New York: W. H. Freeman Spektrum, 1995.

[22] W. Shockley, "Circuit Element Utilizing Semiconductive Material.," USA Patent, Filed June 26, 1948. Issued September 25, 1951.

[23] B. I. Davydov, "O kontaktnom soprotivlenii poluprovodnikov" ("On the contact resistance of semiconductors") " *Zh. Eksp. Teor. Fiz,* vol. 9, p. 451, 1939.

[24] N. G. Basov*, et al.*, "Quantum-mechanical semiconductor generators and amplifiers of electromagnetic oscillations," *Sov. Phys. JETP,* vol. 10, p. 416, 1960.

[25] N. G. Basov*, et al.*, "The possibility of use of indirect transitions to obtain negative temperature in semiconductors," *Sov. Phys. JETP,* vol. 12, p. 1033, 1961.

[26] Nasledov D. N.*, et al.*, "Recombination radiation of galium arsenic," *Fiz Tverd. Tela,* vol. 4, p. 1062, 1962.

[27] R. N. Hall*, et al.*, "Coherent Light Emission From GaAs Junctions," *Physical Review Letters,* vol. 9, p. 366, 1962.

[28] T. M. Quist*, et al.*, "Semiconductor maser of GaAs," *Applied Physics Letters,* vol. 1, pp. 91-92, 1962.

[29] M. I. Nathan*, et al.*, "Stimulated emission of radiation from GaAs p-n junctions," *Applied Physics Letters,* vol. 1, pp. 62-64, 1962.

[30] N. Holonyak, Jr. and S. F. Bevacqua, "Coherent (visible) light emission from Ga AsP junctions," *Applied Physics Letters,* vol. 1, pp. 82-83, 1962.

[31] Z. I. Alferov*, et al.*, "Investigation of the influence of the AlAs-GaAs heterostructure parameters on the laser threshold current and realization of

continuous emission at room temperature," *Sov. Phys. Semicond.,* vol. 4, pp. 1573-1575, 1971.

[32] I. Hayashi*, et al.*, "Junction lasers which operate continuously at room temperature," *Applied Physics Letters,* vol. 17, pp. 109-111, 1970.

[33] Available: http://nobelprize.org/nobel_prizes/physics/laureates/2000/

[34] V. N. Lutskii, "Quantum size effect-present state and perspectives of experimental investigations," *Physics Status Solidi (a),* vol. 1, pp. 199-220, 1970.

[35] V. Ahmadi and M. H. Yavari, "Analysis of carrier and photon dynamic effects on the modulation behaviour of self assembled quantum dot lasers," in *Transparent Optical Networks, 2008. ICTON 2008. 10th Anniversary International Conference on*, Athens, 2008, pp. 137-140.

[36] K. T. Tan*, et al.*, "High bit rate and elevated temperature data transmission using InGaAs quantum-dot lasers," *Photonics Technology Letters, IEEE,* vol. 16, pp. 1415-1417, 2004.

[37] H. Liu*, et al.*, "Quantum dot infrared photodetectors," *Applied Physics Letters,* vol. 78, 2001.

[38] P. J. Delfyett*, et al.*, "Modelocked diode lasers for ultra-wideband communications and signal processing," in *Lightwave Technologies in Instrumentation and Measurement Conference*, 2004, pp. 2-8.

[39] M. Gu*, et al.*, *Femtosecond Biophotonics: Core Technology and Applications*. Cambridge: Cambridge University Press, 2010.

[40] A. Zumbusch*, et al.*, "Three-Dimensional Vibrational Imaging by Coherent Anti-Stokes Raman Scattering," *Physical Review Letters,* vol. 82, p. 4142, 1999.

[41] A. Zoumi*, et al.*, "Imaging cells and extracellular matrix in vivo by using second-harmonic generation and two-photon excited fluorescence," *Proceedings of the National Academy of Sciences,* vol. 99, pp. 11014-11019, August 20, 2002 2002.

[42] K. König, "Multiphoton microscopy in life sciences," *Journal of Microscopy,* vol. 200, pp. 83-104, 2000.

[43] L. Moreaux*, et al.*, "Coherent Scattering in Multi-Harmonic Light Microscopy," *Biophysical Journal,* vol. 80, pp. 1568-1574, 2001.

[44] W. R. Zipfel*, et al.*, "Nonlinear magic: multiphoton microscopy in the biosciences," *Nat Biotech,* vol. 21, pp. 1369-1377, 2003.

[45] X. Deng and M. Gu, "Penetration Depth of Single-, Two-, and Three-Photon Fluorescence Microscopic Imaging through Human Cortex Structures: Monte Carlo Simulation," *Appl. Opt.,* vol. 42, pp. 3321-3329, 2003.

[46] M. Gu and X. S. Gan, "Effect of the detector size and the fluorescence wavelength on the resolution of three- and two-photon confocal microscopy," *Bioimaging,* vol. 4, pp. 129-137, 1996.

[47] M. Gu, "Resolution in three-photon fluorescence scanning microscopy," *Opt. Lett.,* vol. 21, pp. 988-990, 1996.

[48] C. J. R. Sheppard and M. Gu, "Image formation in two-photon fluorescence microscopy," *Optik,* vol. 86, pp. 104-106, 1990.

[49] C. Sheppard*, et al.*, "The scanning harmonic optical microscope," *Quantum Electronics, IEEE,* vol. 13, pp. 912-912, 1977.

[50] C. J. R. Sheppard and R. Kompfner, "Resonant scanning optical microscope," *Appl. Opt.,* vol. 17, pp. 2879-2882, 1978.

[51] W. Denk*, et al.*, "Two-photon laser scanning fluorescence microscopy," *Science,* vol. 248, pp. 73-76, April 6, 1990.

[52] G. S. He*, et al.*, "Three-photon-absorption-induced fluorescence and optical limiting effects in an organic compound," *Opt. Lett.,* vol. 20, pp. 1524-1526, 1995.

[53] S. Hell, "Three-photon excitation in fluorescence microscopy," *J. Biomed. Opt.,* vol. 1, p. 71, 1996.

[54] H. Yokoyama*, et al.*, "Two-photon bioimaging with picosecond optical pulses from a semiconductor laser," *Opt. Express,* vol. 14, pp. 3467-3471, 2006.

[55] K. Kim*, et al.*, "1.4kW high peak power generation from an all semiconductor mode-locked master oscillator power amplifier system based on eXtreme Chirped Pulse Amplification(X-CPA)," *Opt. Express,* vol. 13, pp. 4600-4606, 2005.

[56] T. Schlauch*, et al.*, "High peak power femtosecond pulses from modelocked semiconductor laser in external cavity," *Electronics Letters,* vol. 44, pp. 678-679, 2008.

[57] V. A. Serebryakov, "Lectures notes," *St. Petersburg State University of Information*

Technologies, Mechanics and Optics; Department of Laser Technologies and Applied Ecology, 2007.

[58] M. Kuramoto*, et al.*, "Two-photon fluorescence bioimaging with an all-semiconductor laser picosecond pulse source," *Opt. Lett.,* vol. 32, pp. 2726-2728, 2007.

[59] H. Yokoyama*, et al.*, "Nonlinear-microscopy optical-pulse sources based on mode-locked semiconductor lasers," *Opt. Express,* vol. 16, pp. 17752-17758, 2008.

Chapter 2. Semiconductor Quantum Dot Devices.

2.1 Stranski-Krastanow material growth method.

The first semiconductor lasers were fabricated by the inexpensive and relatively simple liquid phase epitaxy method, where the substrate wafer is immersed into a container of the molten material that is supposed to be deposited or has a molten zone passed over it [1-2]. However, at first such lasers were delivering only a few milliwatts of power because of the nonuniform thick-growth wafers that resulted in the limitation of the laser's aperture size to a few micrometers and the thickness of the active regions up to 0.5 μm [3-6]. Recently, the Al-free InGaAsP active-region lasers have been developed generating the output power up to 20 W in continuous wave [7-8]. Alternatively, metal-organic chemical vapour deposition (MOCVD) and molecular beam epitaxy (MBE) fabrication methods were developed [9-13]. These fabrication methods permitted the control of the crystal deposition in atomic layer accuracy. Thus, quantum dot (QD) and quantum well (QW) active layers can be fabricated with uniform material deposition. This enables the development of large aperture laser structures with improved output power, up to 16W for QD and up to 20 W for QW [14-21]. Currently, there are a number of ex situ and in situ methods for the formation of zero-dimensional quantum size objects [22-24]. One of the most promising in situ methods for the formation of quantum size object during the growth process is called the Stranski-Krastanow growth mode. Stranski-Krastanow growth is a particularly efficient, defect free, reproducible method of direct semiconductor nanostructure synthesis of typically 10 nm in size. The method uses spontaneous islands formation during strained-layer heteroepitaxy. The semiconductor material is grown epitaxially, meaning as a single crystal, one on the top of the other (substrate) that has several

percent lower lattice constant. The structure is grown layer by layer as shown in Fig. 2.1. In the beginning atoms form a planar layer called the wetting layer. As the process continues the formation of three-dimensional islands, QDs, occurs. Since the QDs appear spontaneously during growth, they are said to be self-assembling. As a result Stranski-Krastanow growth opened new doors for the formation of high quality extremely small QDs in a maskless and defectless process in one simple deposition step.

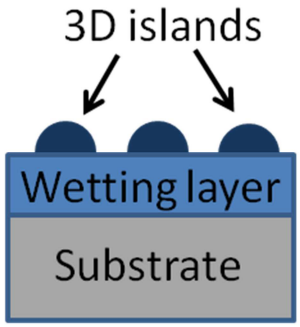

Fig.2.1 Stranski-Krastanow growth mode of formation three-dimensional (3D) islands.

2.2 Self-organized InGaAs quantum dots on a GaAs substrate.

2.2.1 Shape, size, and distribution of quantum dots.

The shape of the QD's are usually pyramidical with a base of 15-20 nm and a height in the order of 5 nm [25-27] (Fig. 2.2). The size of the islands can be manipulated within a certain range by changing the amount of deposited dot material. In order to fabricate an efficient laser, the level of gain and optical confinement should be high enough.

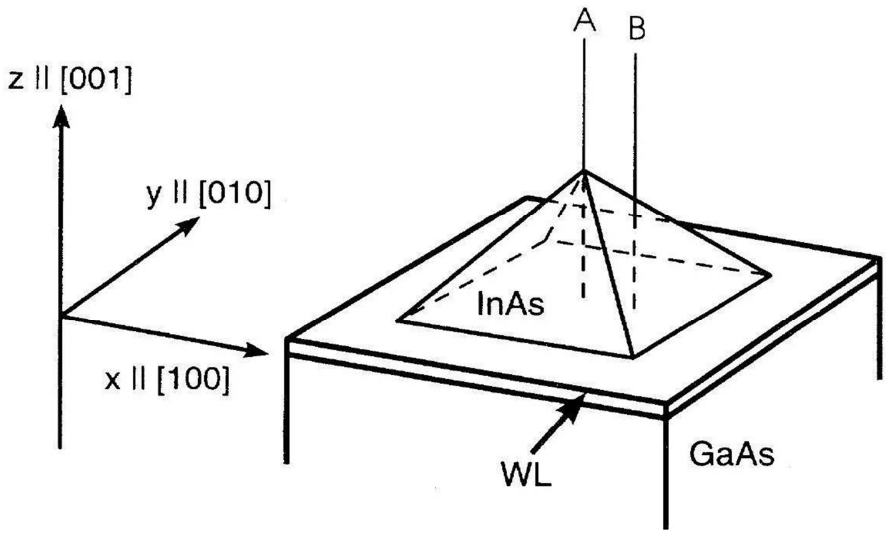

Fig.2.2 Schematic of the geometry of InAs/GaAs QD [22].

The densities of quantum dots lie in the range of 10^9 and 10^{12} cm^{-2}[28]. It means one single stack of QDs result in a low gain due to sparse distribution [29]. But there is a solution. Instead of using just one stack of QDs it was proposed growing many layers one by one, in order to achieve a desirable optical gain without increasing the internal optical loss [30]. For this reason GaAs spacer layers between InAs QD layers can be used for eliminating high strain accumulation in each Indium arsenic (InAs) QD layer which may lead to strain relaxation with the formation of misfit dislocations and degradation in optical properties (Fig.2.3) [31].

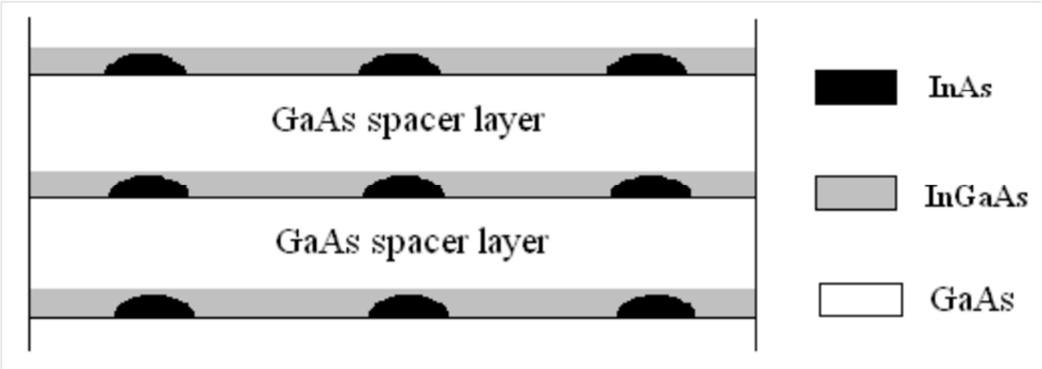

Fig.2.3 Schematic cross-sectional structure of several layers of quantum dots (QDs)[31].

2.2.2 Lattice mismatch and critical thickness.

InAs having a lattice constant of 6.06 Å can be grown on the GaAs substrate with a lattice constant of 5.64 Å due to small lattice mismatch which is one of the requirements for effective epitaxial growth. Too large a lattice mismatch could produce a dislocated epitaxial layer prior to the formation of the coherently strained islands [32]. Another requirement for successful QD formation is associated with critical layer thickness. Above the certain level of thickness, misfit dislocations appear causing a breakdown of coherence between the substrate and epitaxial layer.

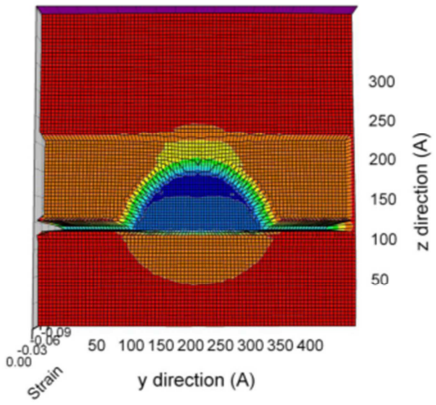

Fig. 2.4 The strain distribution in y-z plane in the middle of x axis at T=300 K [31].

After the formation of the wetting layer at critical thickness, the atoms of InAs tend to bunch up and form clusters or islands. Such formation is energetically favourable, as the increased strain energy can be reduced within the islands as shown in Fig. 2.4 [25, 31, 33-34]. The strain inside the QD region is compressive shown as the blue region. It was shown that the strain distribution depends on the shape of the QD but not on its size [25]. Above the wetting layer, the InGaAs layer can be used to cover the InAs QD, and the strain in this region is less compressive which works like a buffer between the InAs QD and the GaAs substrate. The lattice mismatch is the main

parameter defining the misfit dislocation formation between the epitaxial layer and the substrate according to the Matthew-Blakeslee (M-B) model [35-38] .

It was also shown that for weakly strained InGaAs layers (InAs mole fraction $\leq$0.2) result in a lattice mismatch by misfit dislocations, while highly strained InGaAs films (InAs mole fraction $\geq$0.5) grow in a three-dimensional mode prior to the dislocation formation [22, 34].

2.2.3 Optical emission range.

Grundmann *et al*. predicted the increase in the emission wavelength with the increase in the island base size [39]. Experimental study of the emission wavelength of the InAs/GaAs QDs dependence on a effective thickness of deposited InAs [40]. As shown in Fig. 2.5 the photoluminescence (PL) spectra at 77 K of QDs is shifted to longer wavelengths from 800 nm up to 1200 nm as the effective thickness of deposited InAs increased [40].

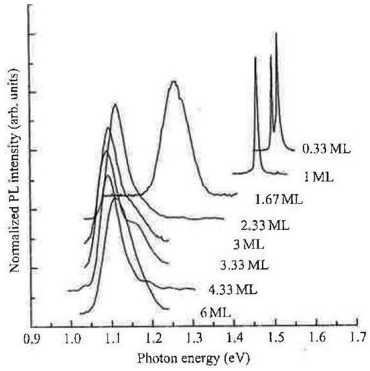

Fig. 2.5 Dependence of photoluminescence spectra at 77 K of GaAs/InAs with effective thickness of deposited InAs [40].

It can be used for growing a material with a very broad gain bandwidth. This can be exploited in a number of ways: developing a superluminescent diode, as well as bistable and broadly tunable lasers, as will be shown in chapter 6.

Moreover, the lasing can occur through either ground state or excited states depending on cavity length or bias conditions as will be described in detail in Chapter 5. Switching between the ground and excited states happens due to gain saturation. The maximum optical gain which can be attained is limited by the degeneracy and the surface density of QDs. As the gain of ground states is saturated and insufficient for lasing at some loss, the excited state emission occurs due to higher degeneracy and therefore higher saturated gain. As shown in Fig. 2.6 (a) ground state is mostly

populated when the total loss is relatively low ($G_{th}(1)$) and as the result the threshold carrier concentration is also small ($N_{th}(1)$), the Fermi level is also at a low position (F(1)). As the loss is increased ($G_{th}(2)>G_{th}(1)$), the Fermi level moves to F(2) to satisfy the necessary gain on the ground state and the excited state becomes higher populated. Thus, the excited state gain becomes higher than ground state and the lasing emission switches to the excited state (Fig. 2.6 b). As the temperature is increased the excited state also becomes more populated as well (Fig. 2.6 c) [22].

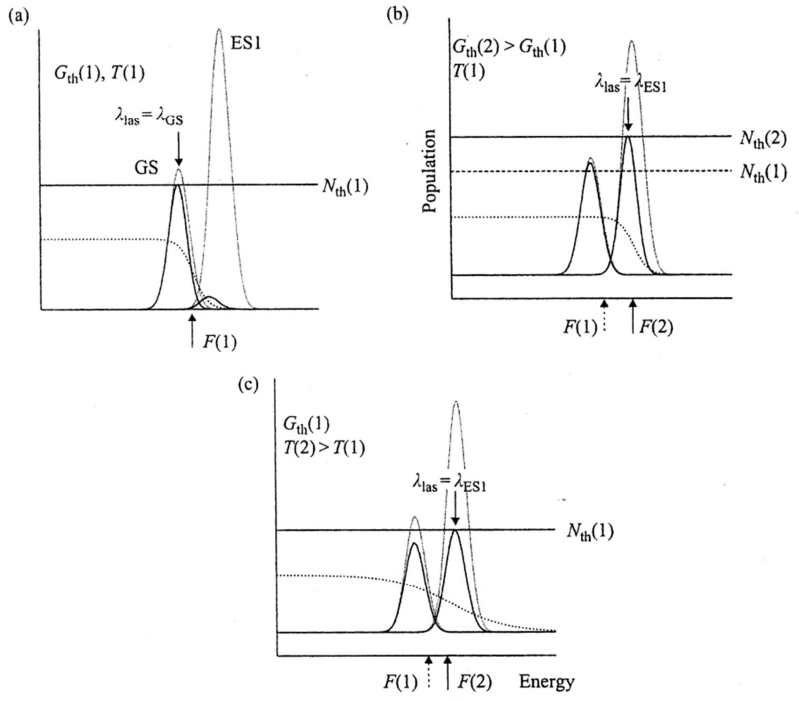

Fig. 2.6 Schematic population of QD density of states (solid curves) **(a)** at threshold, and **(b)** evolution of the population with increasing threshold gain and **(c)** temperature. DOS of the ground states and the first exited state are indicated by dotted curves [22].

2.3 Unique QDs properties for ultrafast generation.

2.3.1 Low threshold current density.

Strained-QW lasers have shown low threshold current densities of 50 A/cm^2 from 2.05 μm [41] and 0.98 μm [42] lasers. QD-based devices also exhibit extremely low threshold current densities of 11.5 A/cm^2 from 1.23 μm 5.1 mm-long QD laser, formed by atomic layer epitaxy due to low transparency current [28]. Single layer QD lasers formed by DWELL-designed active region, where InAs QDs are capped by InGaAs quantum well, exhibited threshold current densities of 26 A/cm^2 with uncoated facets and up to 11.7 A/cm^2 with HR-coated facets [43-45]. In addition, a 19.2 mm long oxide-confined laser with two InAs QDs layers, emitting at 1.28 μm, had a 24 A/cm^2 threshold current density [46]. As the compact QD-based structures do not require higher current injection, the carrier density is reduced as well as amplified spontaneous emission [47]. Spontaneous emission results in photon density, gain, and refraction index variations. Thus low spontaneous emission less affects the round-trip time and the timing of the pulses [48-49].

2.3.2 Inhomogeneous broadening.

An ideal QD-based laser would be temperature insensitive, generating single frequency emission with low threshold current density. But in reality lasers based on self-organized QDs are temperature-sensitive and exhibit broader spectral bandwidths (>200 nm) [50] than QW-based lasers (70 nm) [51]. The fundamental difference is associated with inhomogeneous broadening of energy levels because of QD size variations. The self-assembling of QDs that occurs during molecular beam epitaxy growth is one of the reasons for a Gaussian size distribution of QDs with a corresponding distribution of emission frequencies. This is also connected to variance of elastic strain in different parts of the wafer. The schematic morphology and density of states for charge carriers in an ideal quantum dot-based material compared to a real quantum dot-based material with inhomogeneous broadening effect are presented below in Fig. 2.7.

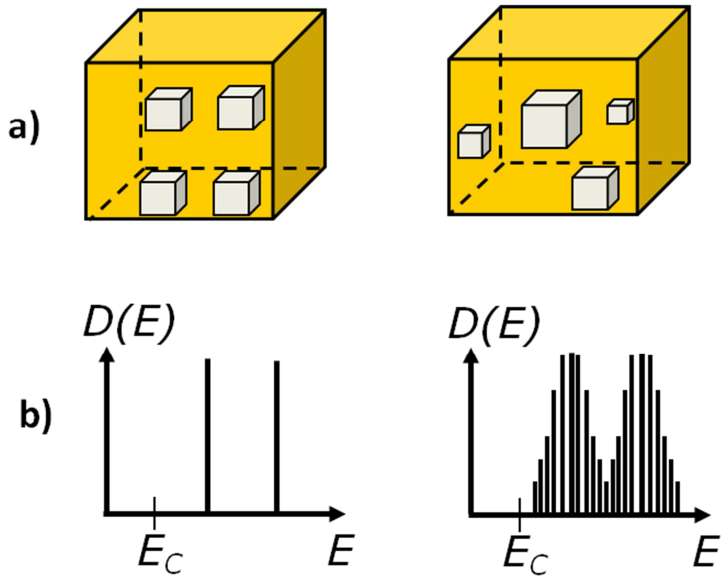

Fig. 2.7 (top) Schematic Morphology and **(bottom)** the density of states for charge carriers in **(a)** an ideal quantum dot-based material and **(b)** a real quantum dot-based material with inhomogeneous broadening.

The inhomogeneous broadening effect can be very effectively used for the development of the amplifiers and femtosecond lasers with broad tunable range due to their wide bandwidth. Furthermore, currently available QD growth technologies enable a high degree of control over broadening by selecting QD layers with desirable size distribution (as discussed in Chapter 6). It is also important to take into account some of the disadvantages of a high level of the inhomogeneous broadening gain: the density of states broadened, increased transparency current and reduced modal and differential gain. Moreover, QD-based optical sources are not using full potential by generating the ultra short pulses which are one or two orders of magnitude broader than the inverse width of the inhomogeneously broadened gain spectrum.

2.3.3 Ultrafast carrier dynamics.

It was predicted that by changing the geometry of the active region from QW to QD, the laser would suffer some limitations due to a phonon bottleneck effect - the effect of inefficient energy relaxation of charge carriers via phonon interaction [52-53]. The experimental results of QD-based lasers prove the assumption of low threshold current performance but at the same time disapproved an idea of a strong influence of the phonon bottleneck effect on its properties. Coulomb and exciton-phonon interaction studies have shown ultrafast carrier dynamics of QD structures both under gain and absorption conditions [54].

Fast recovery time in quantum dot saturable absorbers was confirmed by the pump-probe technique [55-56]. A fast recovery time of the absorption was found around 1 ps which can be effectively used for mode-locking at high frequencies where the absorption recovery time should be shorter than the round-trip period of the cavity [55].

Despite the above the following QD properties should also be emphasized: lower absorption saturation fluence than in QW [57], suppressed carrier diffusion [58], and low temperature sensitivity [59].

High characteristic temperature of the threshold current, T_0, is a key factor for semiconductor lasers. The high value of T_0 would make it possible to create heatsink-free transmitter modules and reduce the cost. QD-based lasers are characterized by very deep localization of carriers in the active region (~400-450 meV) with respect to GaAs band edges [22]. Therefore, these devices can provide a temperature-independent operation with T_0> 650 K [59].

2.4 Conclusion

The unique structural, electronic and optical properties of self-organized QDs described in this chapter enable the use of semiconductor QD-based materials for developing the next generation of lasers, amplifiers and absorbers for a number of applications from high speed telecommunication to multiphoton imaging.

2.5 References.

[1] A. Krier*, et al.*, "InAsSbP quantum dots grown by liquid phase epitaxy," *Journal of Physics D: Applied Physics,* vol. 32, p. 2587, 1999.

[2] D. Z. Garbuzov*, et al.*, "High-power 0.8 µm InGaAsP-GaAs SCH SQW lasers," *Quantum Electronics, IEEE Journal of,* vol. 27, pp. 1531-1536, 1991.

[3] T. P. Pearsall, *GaInAsP Alloy Semiconductor*. Chichester: John Wiley & Sons Ltd, 1982.

[4] G. H. B. Thompson, *Physics of semiconductor laser devices*. Chichester: Wiley-Interscience, 1980.

[5] H. Kressel*, et al.*, "Effect of Substrate Imperfections on GaAs Injection Lasers Prepared by Liquid Phase Epitaxy," *Journal of Applied Physics,* vol. 40, pp. 3587-3597, 1969.

[6] J. K. Butler, *Semiconductor injection lasers*. New York: IEEE Press, 1980.

[7] Z. Li*, et al.*, "High-power Al-free SCH-SQW lasers grown by LPE," Beijing, China, 2005, pp. 223-227.

[8] B. Baoxue*, et al.*, "InGaAsP/GaAs SCH SQW laser arrays grown by LPE," *Optics & Laser Technology,* vol. 32, pp. 335-338, 2000.

[9] M. J. Ludowise, "Metalorganic chemical vapor deposition of III-V semiconductors," *Journal of Applied Physics,* vol. 58, pp. R31-R55, 1985.

[10] M. A. Herman and H. Sitter, *Molecular Beam Epitaxy: Fundamentals and Current Status*, 2nd edition ed. Berlin: Springer-Verlag, 1996.

[11] D. F. Welch, "A brief history of high-power semiconductor lasers," *Selected Topics in Quantum Electronics, IEEE Journal of,* vol. 6, pp. 1470-1477, 2000.

[12] A. Y. Cho, "Film Deposition by Molecular-Beam Techniques," *Journal of Vacuum Science and Technology,* vol. 8, pp. S31-S38, 1971.

[13] R. D. Dupuis, "AlGaAs-GaAs lasers grown by metalorganic chemical vapor deposition - A review," *Journal of Crystal Growth,* vol. 55, pp. 213-222, 1981.

[14] M. Sakamoto*, et al.*, "High power, high brightness 2 W (200 µm) and 3 W (500 µm) CW AlGaAs laser diode arrays with long lifetimes," *Electronics Letters,* vol. 26, pp. 729-730, 1990.

[15] D. F. Welch*, et al.*, "High-power, 8 W CW, single-quantum-well laser diode array," *Electronics Letters,* vol. 24, pp. 113-115, 1988.

[16] P. Crump*, et al.*, "Extending the wavelength range of single-emitter diode lasers for medical and sensing applications: 12xx-nm quantum dots, 2000-nm wells, > 5000-nm cascade lasers," *SPIE,* vol. 6456, 2007.

[17] M. V. Maximov and et al., "A 1.33 µm InAs/GaAs quantum dot laser with a 46 cm −1 modal gain," *Semiconductor Science and Technology,* vol. 23, p. 105004, 2008.

[18] D. G. Deppe*, et al.*, "Quantum dot laser diode with low threshold and low internal loss," *Electronics Letters,* vol. 45, pp. 54-56, 2009.

[19] B. Sumpf*, et al.*, "High-Brightness Quantum Well Tapered Lasers," *Selected Topics in Quantum Electronics, IEEE,* vol. 15, pp. 1009-1020, 2009.

[20] Z. Li*, et al.*, "InGaAs Quantum Well Grown on High-Index Surfaces for Superluminescent Diode Applications," *Nanoscale Research Letters,* vol. 5, 2010.

[21] K. Paschke*, et al.*, "15-W reliable operation of 96-µm aperture broad-area diode lasers emitting at 980 nm," in *Lasers and Electro-Optics, 2008 and 2008*

Conference on Quantum Electronics and Laser Science. CLEO/QELS 2008. Conference on, 2008, pp. 1-2.

[22] V. M. Ustinov*, et al.*, *Quantum Dot Lasers*. New York: Oxford University Press, 2003.

[23] H. Liu*, et al.*, "Optimizing the growth of 1.3 μm InAs/InGaAs dots-in-a-well structure," *Journal of Applied Physics,* vol. 93, 2003.

[24] L. Goldstein*, et al.*, "Growth by molecular beam epitaxy and characterization of InAs/GaAs strained-layer superlattices," *Applied Physics Letters,* vol. 47, pp. 1099-1101, 1985.

[25] M. Grundmann*, et al.*, "InAs/GaAs pyramidal quantum dots: Strain distribution, optical phonons, and electronic structure," *Physical Review B,* vol. 52, p. 11969, 1995.

[26] D. Bimberg*, et al.*, "InAs-GaAs quantum dots: From growth to lasers," *physica status solidi (b),* vol. 194, pp. 159-173, 1996.

[27] N. Liu*, et al.*, "Nonuniform Composition Profile in $In_{0.5}Ga_{0.5}As$ Alloy Quantum Dots," *Physical Review Letters,* vol. 84, p. 334, 2000.

[28] D. Huffaker and D. Deppe, "Electroluminescence efficiency of 1.3 μm wavelength InGaAs/GaAs quantum dots," *Applied Physics Letters,* vol. 73, 1998.

[29] N. Kirstaedter*, et al.*, "Gain and differential gain of single layer InAs/GaAs quantum dot injection lasers," *Applied Physics Letters,* vol. 69, 1996.

[30] P. Smowton*, et al.*, "Optical mode loss and gain of multiple-layer quantum-dot lasers," *Applied Physics Letters,* vol. 78, 2001.

[31] J. Chen*, et al.*, "Nanostructure model and optical properties of InAs/GaAs quantum dot in vertical cavity surface emitting lasers," *Opto-electronics review,* vol. 19, 2011.

[32] P. M. Petroff and S. P. DenBaars, "MBE and MOCVD growth and properties of self-assembling quantum dot arrays in III-V semiconductor structures," *Superlattices and Microstructures,* vol. 15, pp. 15-15, 1994.

[33] J. Tersoff*, et al.*, "Self-Organization in Growth of Quantum Dot Superlattices," *Physical Review Letters,* vol. 76, p. 1675, 1996.

[34] D. Leonard*, et al.*, "Critical layer thickness for self-assembled InAs islands on GaAs," *Physical Review B,* vol. 50, p. 11687, 1994.

[35] J. W. Matthews and A. E. Blakeslee, "Defects in epitaxial multilayers: I. Misfit dislocations," *Journal of Crystal Growth,* vol. 27, pp. 118-125, 1974.

[36] J. Matthews*, et al.*, "Accommodation of Misfit Across the Interface Between Crystals of Semiconducting Elements or Compounds," *Journal of Applied Physics,* vol. 41, 1970.

[37] J. W. Matthews, "Defects associated with the accommodation of misfit between crystals," *Journal of Vacuum Science and Technology,* vol. 12, pp. 126-133, 1975.

[38] J. W. Matthews and A. E. Blakeslee, "Defects in epitaxial multilayers: III. Preparation of almost perfect multilayers," *Journal of Crystal Growth,* vol. 32, pp. 265-273, 1976.

[39] M. Grundmann*, et al.*, "Nature of optical transitions in self-organized InAs/GaAs quantum dots," *Physical Review B,* vol. 53, p. R10509, 1996.

[40] A. Y. Egorov*, et al.*, "Optical emission range of structures with strained InAs quantum dots in GaAs " *Semiconductors,* vol. 30, 1996.

[41] G. W. Turner*, et al.*, "Ultralow-threshold (50 A/cm^2) strained single-quantum-well GaInAsSb/AlGaAsSb lasers emitting at 2.05 μm," *Applied Physics Letters,* vol. 72, 1998.

[42] N. Chand*, et al.*, "Excellent uniformity and very low (<<50 A/cm^2) threshold current density strained InGaAs quantum well diode lasers on GaAs substrate," *Applied Physics Letters,* vol. 58, pp. 1704-1706, 1991.

[43] P. Eliseev*, et al.*, "Transition dipole moment of InAs/InGaAs quantum dots from experiments on ultralow-threshold laser diodes," *Applied Physics Letters,* vol. 77, 2000.

[44] G. Liu*, et al.*, "Extremely low room-temperature threshold current density diode lasers using InAs dots in $In_{0.15}Ga_{0.85}As$ quantum well," *Electronics Letters,* vol. 35, pp. 1163-1165, 1999.

[45] H. Y. Liu*, et al.*, "High-performance three-layer 1.3 μm InAs-GaAs quantum-dot lasers with very low continuous-wave room-temperature threshold currents," *Photonics Technology Letters, IEEE,* vol. 17, pp. 1139-1141, 2005.

[46] X. Huang*, et al.*, "Efficient high-temperature CW lasing operation of oxide-confined long-wavelength InAs quantum dot lasers," *Electronics Letters,* vol. 36, pp. 41-42, 2000.

[47] T. W. Berg and J. Mork, "Quantum dot amplifiers with high output power and low noise," *Applied Physics Letters,* vol. 82, pp. 3083-3085, 2003.

[48] E. U. Rafailov*, et al.*, *Ultrafast lasers based on quantum-dot structures: physics and devices*: Wiley-VCH, 2011.

[49] P. Vasil'ev, *Ultrafast Laser Diodes: Fundamentals and Applications*. London: Artch House, 1995.

[50] K. A. Fedorova*, et al.*, "Broadly tunable high-power InAs/GaAs quantum-dot external cavity diode lasers," *Opt. Express,* vol. 18, pp. 19438-19443, 2010.

[51] S. V. Nalivko*, et al.*, "Design and characteristics of widely tunable quantum-well heterostructure lasers in the Littman and Metcalf cavity configuration," in

Transparent Optical Networks, 1999. International Conference on, 1999, pp. 215-218.

[52] K. Mukai*, et al.*, "Phonon bottleneck in self-formed $In_xGa_{1-x}As$/GaAs quantum dots by electroluminescence and time-resolved photoluminescence," *Physical Review B,* vol. 54, p. R5243, 1996.

[53] H. Benisty*, et al.*, "Intrinsic mechanism for the poor luminescence properties of quantum-box systems," *Physical Review B,* vol. 44, p. 10945, 1991.

[54] P. Borri*, et al.*, "Ultrafast carrier dynamics in InGaAs quantum dot materials and devices," *Journal of Optics A: Pure and Applied Optics,* vol. 8, p. S33, 2006.

[55] E. U. Rafailov*, et al.*, "Fast quantum-dot saturable absorber for passive mode-locking of solid-state lasers," *IEEE Photonics Technology Letters,* vol. 16, pp. 2439-2441, 2004.

[56] P. Borri*, et al.*, "Spectral Hole-Burning and Carrier-Heating Dynamics in InGaAs Quantum-Dot Amplifiers," *IEEE Journal of Selected Topics in Quantum Electronics,* vol. 6, 2000.

[57] M. G. Thompson*, et al.*, "Properties of InGaAs quantum dot saturable absorbers in monolithic mode-locked lasers," in *Semiconductor Laser Conference, 2004. Conference Digest. 2004 IEEE 19th International*, 2004, pp. 53-54.

[58] S. A. Moore*, et al.*, "Reduced surface sidewall recombination and diffusion in quantum-dot lasers," *Photonics Technology Letters, IEEE,* vol. 18, pp. 1861-1863, 2006.

[59] S. S. Mikhrin*, et al.*, "High power temperature-insensitive 1.3 μm InAs/InGaAs/GaAs quantum dot lasers," *Semiconductor Science and Technology,* vol. 20, p. 340, 2005.

Chapter 3. Ultrashort pulse generation.

3.1 Main techniques for ultrashort pulse generation.

3.1.1 Gain switching and Q-switching.

There are several techniques for producing ultra-short pulses from semiconductors lasers such as: gain switching, Q-switching and mode-locking [1-2]. Gain switching (Fig. 3.1) is the easiest technique for generation of short pulses that doesn't involve any external cavity or sophisticated drive electronics [3-4]. The main idea consists of the injection of a large number of carriers (electrons) by electrical pulses, which increase in turn the carrier density above the threshold. As the result the carriers are quickly depleted by stimulation emission, generating optical pulses shorter than electrical ones at that [5]. The carrier density then decreases below the threshold density and the lasing process stops before the next electrical pulse is introduced.

Q-switching is achieved by changing the cavity loss actively using an external modulator (Fig. 3.2) or passively via a saturable absorber (Fig. 3.3) which switches the cavity *Q* factor from a low to a high value [6-7]. This technique allows the generation of pulses with high (gigawatt) peak power called giant pulses. The *Q* factor is a dimensionless parameter which describes how under-damped an oscillator or resonator is. The Q factor is defined by the ratio of the energy stored in the resonator to the energy supplied by a generator, per cycle, to keep signal amplitude constant, at a frequency *f*, where the stored energy is constant with time (Eq. 3.1) [8].

$$Q = 2\pi * \frac{E_{st}}{E_{diss}} = 2\pi f * \frac{E_{st}}{P_{loss}} \quad \textbf{(3.1)},$$

where Q – quality factor, E_{st}-energy stored, E_{diss}-energy dissipated per cycle, f-frequency, P_{loss}-power loss per cycle.

A higher *Q* indicates a lower rate of energy loss relative to the stored energy of the oscillator. In active Q-switching, the electric field is applied to the modulator section in order to vary the loss. For example, the quantum confined Stark effect can be used which causes the shift of the exciton absorption peak to lower energies. Commonly used methods for active Q-switching are based on electro-optical switches, rotating prisms or acousto-optic modulators by way of an external drive source (Pockel cell voltage power supply, rotating motor or RF oscillator). The passive Q-switching method of generating short pulses is based on the non-linear absorption behaviour of the absorber, a material which transmission increases after the intensity exceeds some threshold. Due to high losses in the absorber initially the laser doesn't emit any light. As the laser is further pumped, the amount of the energy stored in the laser cavity increases until the absorber is saturated. At that point the absorber rapidly reduces the cavity loss (bleaches) and the laser has a gain well in excess of the losses as shown in Fig. 3.3. As a result, all stored energy is extracted by a pulse called "giant".

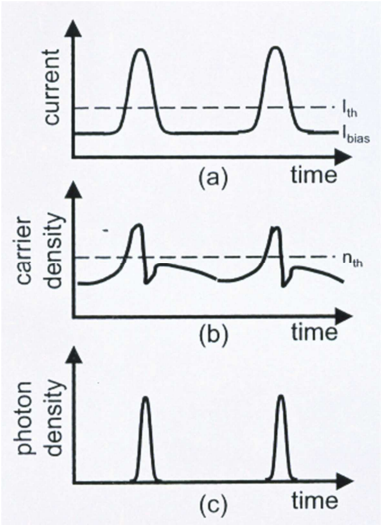

Fig.3.1 Gain switching laser dynamics **a)** applied current, **b)** carrier density and **c)** optical power [11].

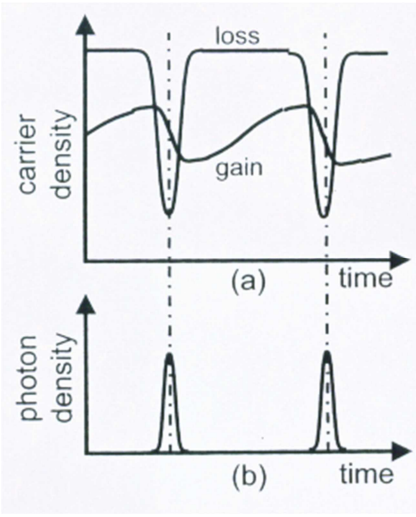

Fig.3.2 Active Q-switching laser time evolution of **a)** loss, gain and **b)** optical power [11].

After the pulse, the absorber recovers to its high-loss state, before the gain recovers, and next pulse is produced. Using this technique, the repetition rate can be controlled only indirectly by the pump rate and the mount of the absorber.

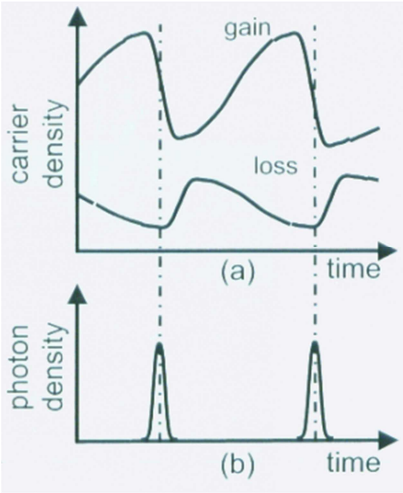

Fig.3.3 Passive Q-switching laser time evolution of **a)** loss, gain and **b)** optical power [11].

3.1.2 Mode-locking techniques in semiconductor lasers.

Alternatively, the mode-locking technique can be used by locking the longitudinal modes of the laser together allowing the generation of short pulses (Fig. 3.4). It is the most interesting technique for optical data/tele-communication and imaging of the biological samples as it is possible to generate much shorter pulses at much higher repetition rates and often with low timing jitter compared to gain-switching and Q-switching. Formation of the cavity longitudinal modes in the gain bandwidth enables the generation of pulses as short as 393 femtoseconds [9]. If instead of oscillating independently, each mode in the laser cavity operates with a fixed phase between it and the other modes (Eq. 3.2) all modes of the laser will constructively interfere with one another, producing an intense burst or pulse of light with a constant repetition rate $\Delta\nu$ (Eq. 3.3). In reality, not all the modes have the same phase and as a result not all laser gain bandwidth is effectively used for generating ultra-short pulses.

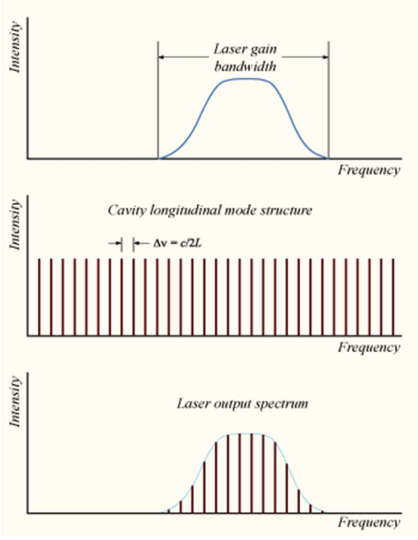

Fig.3.4 Cavity longitudinal mode formation.

$$\varphi_l - \varphi_{l-1} = \varphi \quad \textbf{(3.2)},$$

where φ is a constant, φ_l- l-th longitudinal mode.

$$\Delta\nu = \frac{c}{2Ln} \quad \textbf{(3.3)},$$

Where Δν- the frequency difference between consecutive longitudinal modes, c- speed of light, L-the length of the cavity, n- refractive index.

The total oscillating bandwidth $\Delta\nu_L$ ($\Delta\nu_L$=N*$\Delta\nu$, N-number of modes) is related to pulse width $\Delta\tau_P$ if the mode-locking phase relation condition is kept (Eq. 3.3) by the relation Eq. 3.4. Thus the more modes are in phase the shorter pulses can be produced.

$$\Delta\tau_P = \frac{\beta}{\Delta\nu_L} \quad \textbf{(3.4)},$$

where β is a numerical factor.

The numerical factor β depends on the shape of the spectral intensity distribution. For example, for Gaussian pulse shape β is 0.4413 while for Lorentzian is 0.2206. A pulse that satisfies this condition (Eq. 3.4) is said to be transformed-limited.

There are three main techniques for mode-locking: (1) Active mode-locking and (2) passive mode-locking (Fig. 3.5 and 3.6) which are possible when the laser resonator includes an optical modulator or saturable absorber accordingly [10-11], (3) hybrid mode-locking which is defined by gain/loss modulation applied to an external cavity or multiple section lasers in contrast to active mode-locking where it's applied to a single contact laser.

Active mode-locking can be induced by an amplitude modulator (AM mode-locking), by a phase modulator (FM mode-locking), or by a periodic modulation of laser gain at the fundamental cavity frequency (ML by synchronous pumping). The main idea is achieving locking of the modes by modulating the loss or gain of a laser at a frequency of the intermodal spacing $\Delta\nu$ so that each spectral mode is driven by the modulation

sidebands of its neighbours [12].The modulation of the gain can be achieved by external modulator or by modulating the driving current as shown in Fig. 3.5.

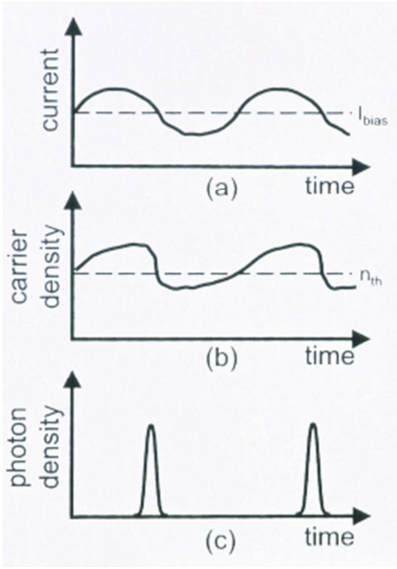

Fig.3.5 Active mode-locking laser dynamics of **a)** drive current, and **b)** optical power [11].

Passive mode-locking is achieved by inserting an element called a saturable absorber in the cavity which is then saturated quicker than the gain of the laser, and also has a recovery time faster than the gain, thus forming a narrow net gain window for formation of the pulses (Fig. 3.6).

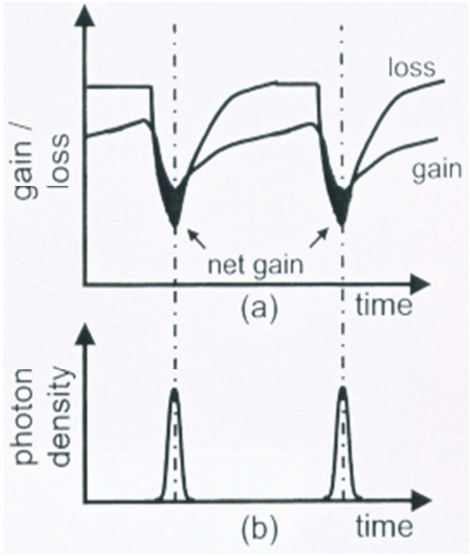

Fig.3.6 Passive mode-locking laser dynamics of **a)** loss, gain **b)** carrier density and **c)** optical power [11].

The pulse repetition rate in passive mode-locking is defined by the round-trip time of the laser cavity and does not depend on the pumping conditions; while in passive Q-switching the pulse repetition rate is set by the amplitude of the driving currents. A performance summary of the main techniques for ultrashort pulse generation is presented in table 3.1. Timing jitter is presented as well which relates to the fluctuations of the temporal positions of pulses from those in a perfectly periodic pulse train.

Table 3.1 A performance summary of the main types of short pulse generation techniques for electrically pumped semiconductor lasers.

Technique	**Pulse Width**	**Repetition Rates**	**Pulse Energy**	**Control of repetition rate/Jitter**	**References**
Gain Switching	<1.3 ps	250 MHz-20 GHz	5 nJ	Good control via electrical drive/ Jitter-160 fs	[13-19]
Passive Q-switching	1.6 ps	32.5 MHz-20 GHz	300 pJ	Limited control / Jitter- 800 fs	[20-26]
Active Q-switching	1.2 ps	<100 MHz- 10.5 GHz	470 pJ	Set by electrical drive/ Jitter- 250 fs	[27-34]
Passive Mode-Locking	240 fs	191 MHz-2.1 THz	60 pJ	Set by cavity length/ Jitter- 100 fs	[9, 35-44]
Active Mode-Locking	560 fs	660MHz-193 GHz	3 pJ	Set by cavity length/ Excellent jitter- 7.5 fs	[45-49]

3.1.3 Saturable absorber for passive mode-locking.

Saturable absorbers can be classified by their recovery time as either fast (ps) or slow (ns), depending on whether their recovery time is longer or shorter than the pulse duration, respectively. In semiconductors for short pulse generation a combination of a slow saturable absorber and gain saturation is used. In order to achieve stable mode-locking the saturation energy of the absorberE_{abs}^{sat} should be less than of the gain medium E_{gain}^{sat} (Eq. 3.5):

$$E_{abs}^{sat} \equiv \frac{h\nu A}{\partial a/\partial n} < \frac{h\nu A}{\partial g/\partial n} \equiv E_{gain}^{sat} \quad \textbf{(3.5)},$$

where *h*-Plank's constant, *ν*-optical frequency, *A*-optical mode cross-sectional area, $\partial a/\partial n$- differential loss, $\partial g/\partial n$- differential gain, a- absorber, g- gain.

In other words, differential loss $\partial a/\partial n$ should be higher than differential gain $\partial g/\partial n$- as shown in Fig. 3.7.

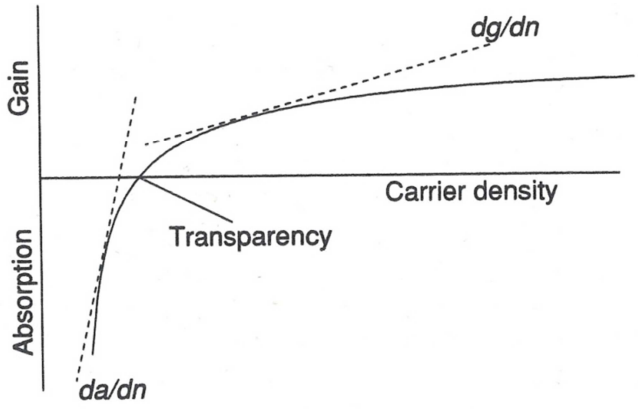

Fig. 3.7 Gain/loss dynamics versus carrier concentration for successful mode-locking in laser diodes [4].

The absorber's recovery time plays a crucial role in terms of ultrashort pulse generation in high repetition rate lasers. It is important for forming narrow net gain as shown in Fig. 3.6. If this requirement is met than the gain overcomes the loss only near the peak of the pulse and the spontaneous emission is not amplified between the

pulses. Looking at frequency domain description of mode-locking, the burst of noise is the result of an instantaneous phase locking occurring among a number of modes. The self-saturation at the saturable absorber then helps to sustain and strengthen self-starting mode-locking. The saturation fluence *Γ* of the gain (Eq. 3.6) and absorber (Eq. 3.7) must be low enough in order be saturated by the intracavity laser fluence.

$$\Gamma_{gain}^{sat} = \frac{h\nu}{A_g} \quad \textbf{(3.6)},$$

$$\Gamma_{abs}^{sat} = \frac{h\nu}{A_a} \quad \textbf{(3.7)},$$

where A_g and A_a-cross sections of the gain and absorber respectively.

The QD saturable absorber's recovery is associated primarily with thermionic emission and tunnelling mechanisms [50-52]. At low reverse bias applied to the absorber a recovery time of around 62 ps was observed. It was not governed by recombination processes but by the thermal activation of the electrons from the QD ground state into excited QD states with subsequent emission into the GaAs matrix. As higher reverse bias was applied, the decrease in the absorption recovery time down to 700 fs was observed. The tunnelling electron escape mechanism from the QD ground state into the GaAs barrier becomes dominant as the barrier height is lowered from E_{b0} to E_b by electric field and a triangular barrier is formed as shown in Fig. 3.8 [50].

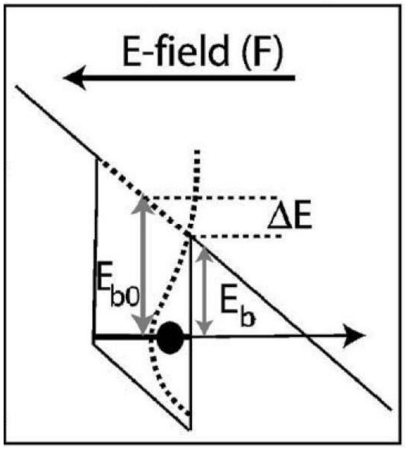

Fig. 3.8 Tunnelling electron's escape mechanism with applied electric field [53].

3.2 State of the art of Mode-locking.

3.2.1 Quantum well lasers.

GaAs based semiconductor quantum well mode-locked lasers have been developed over the past 20 years (see table 3.2). They can generate ultrashort transform-limited pulses [54-55]. For example, hybrid mode-locking 830 nm laser in external cavity configuration in order to get low 335 MHz repetition rate with amplification and compression stages generated 460 fs transform-limited pulses, resulting in a peak power of 72 W which can be improved up to 160 W by using a cubic compensator for the generation of 200 fs [54]. The highest repetition rate of 2.1 Thz was achieved by compound cavity mode locking 860 nm double QW laser with 2.2 mW average power and 0.24 ps pulses [36]. Furthermore, InGaAs and GaInAsP quantum well lasers were developed as shown in table 3.3.

Table 3.2 Overview of mode-locked InGaAs quantum well lasers with following characteristics: $\boldsymbol{\tau_p}$-pulse duration, **λ**-emission wavelength, **Δλ**- full width half maximum, $\mathbf{f_{rep}}$- pulse repetition rate, $\mathbf{P_{peak}}$–peak power, **TBWP**- Time bandwidth product, $\mathbf{N_L}$- number of layers, n/a-not applicable. The best performances are in bold.

N_L	ML regime	Setup	τ_p (ps)	λ (nm)	Δλ (nm)	f_{rep} (GHz)	P_{peak} (W)	TBWP	Ref	Year
4	Active/ Passive/ Hybrid	External	9/ 2.5/ 2.7	840	0.75/ 1.68/ 1.87	5.5	0.02/ 0.07/ 0.06	2.9/ 1.8/ 2.2	[56-57]	1991
4	Active/ Passive/ Hybrid	Monolithic	13/ 6.5/ 10	840	0.77/ 0.93/ 1.26	5.5	0.013/ 0.028/ 0.018	4.3/ 4.0/ 3.5	[56-57]	1991
4	Passive/ Hybrid	Monolithic	5.5/ 2.2	840/ 1580	1.29/ 4.16	11/ 21	0.096/ 0.013	3/ 1.1	[56]	1992
4	Colliding pulse	Monolithic	1.3	1580	4.99	41	0.015	0.78	[56, 58]	1992
n/a	Hybrid	External+SOA	5.1	830	2.5	0.335	72	5.44	[54]	1992

		compression	(0.46)		(3.2)			(**0.44**)		
n/a	Hybrid	External+SOA Compression	**0.2**	830	n/a	0.335	**165**	n/a	[54]	1992
3	Colliding pulse	Monolithic	0.26	1555	n/a	1540	0.04	n/a	[35, 42]	1994
3	Passive	Monolithic/ single contact	0.86	1024	n/a	116	0.06	n/a	[59]	1995
3	Passive	External	3.3	980	n/a	n/a	>2	n/a	[60]	1995
2	Passive	External	3.5	1550	n/a	9.32	n/a	n/a	[61]	1998
2	Passive	Monolithic	0.24	860	n/a	**2100**	0.004	n/a	[36]	2001
6	Passive	External	1.7	1300	n/a	25	~0.047	n/a	[62]	2004
1	Hybrid	External Compression	27.1 (3.4)	976	0.6	0.535	0.26	0.64	[63]	2005
1	Passive	External Compression	38.2 (8.8)	976	n/a	0.535	n/a	n/a	[63]	2005
1	Passive	Monolithic	8.3	1305	n/a	9.48	n/a	n/a	[64]	2007
n/a	Passive	Monolithic	0.7	1631	5.49	37.9	n/a	0.5	[65]	2009
n/a	Passive	Monolithic	1.8	1564	4.6	38	n/a	1	[66]	2009
2	Colliding-pulse	Monolithic	1.84/ 2	830	0.55/0. 5	19.75	0.46/0. 67	**0.44**	[55]	2011

Compared to InGaAs, InGaAsP laser showed the highest repetition rate of 860 GHz at 1265 nm using colliding pulse harmonic mode-locking technique [67]. For generating higher power slab coupled lasers were fabricated from the same material [41, 68]. A peak power of 5.8 W was delivered from a 4.3 GHz InGaAsP laser incorporating 5 quantum well layers with 10 ps pulses at 1544 nm wavelength [41]. Recently, up to 200 fs optical pulses were generated with high peak power of 52 W from an 830 nm QW laser at 266 MHz repetition rate in external cavity configuration with intracavity dispersion management and a grating compressor [69]. An alternative material growth such as GaInNAsSb can be used for the development of passively mode-locked laser emitting at 1583 nm [64, 70].

Table 3.3 Overview of mode-locked InGaAsP quantum well lasers lasers with following characteristics: τ_p-pulse duration, **λ**-emission wavelength, **Δλ**- full width half maximum, f_{rep}-pulse repetition rate, P_{peak}–peak power, **TBWP**- Time bandwidth product, N_L- number of layers, n/a- not applicable. The best performances are in bold.

N_L	ML regime	Setup	τ_p (ps)	λ (nm)	Δλ (nm)	f_{rep} (GHz)	P_{peak} (W)	TBWP	Ref	Year
6	Hybrid	Monolithic	1.4	1300	n/a	15.1	n/a	n/a	[71]	1989
5	Passive	Monolithic	1/0.83	1515/1545	2.68/2.89	156/80	n/a	0.34/0.31	[72]	1992
5	Passive	Monolithic	**0.64**	1560	4	350	n/a	0.32	[72]	1992
6	Colliding-pulse harmonics	Monolithic	n/a	~1265	n/a	**860**	n/a	n/a	[67]	1997
n/a	Passive	Monolithic	1.2	1584	12.6	~37	n/a	1.8	[73]	1999
8	Passive	Monolithic	0.41	1550	6.8	133	n/a	0.35	[74]	2002
1/2/3	Passive	Monolithic	2.8/4.5/4.9	1531/1556/1574	1.1/0.7/1.1	39.63/39.46/39.49	0.064 0.05**/** n/a	0.4/0.39/0.66	[75]	2004
5	Passive	Monolithic Slab coupled	10	1544	5.7	4.29	**5.8**	7.5	[41]	2006
1	Passive	Monolithic	0.86	1540	5	21.31	0.5	0.57	[76]	2008
5	Passive	Monolithic Slab coupled	5.8	1550	~6	4.6	~2	~4.3	[68]	2008
2	Passive	External (compression)	7.4 (**0.2**)	830	1.8 (6.48)	0.266	3.2 (**52**)	5.7 (0.58)	[69]	2010

3.2.2 Quantum dot lasers.

Unfortunately, traditional quantum well lasers based on GaAs operate in the range of 635-nm to 1100-nm while InP-based devices operate from 1280-nm to 2000-nm, as a result a region from 1100 to 1280-nm is not covered [77]. 1310 nm wavelength as the central O band is very important for data- and telecommunications. Moreover, wavelengths from 1240 nm to 1300 nm are transparent to Si waveguide and detectable by SiGe photodetectors, for intra-chip / inter-chip clocking and signalling applications. Thus InAs Quantum-Dot based devices on a GaAs substrate became very promising due to 1.1-1.3 μm emission wavelength, combined with ultrashort pulse generation using mode-locking techniques. The first passive mode-locked InAs QD based laser was built in 2001 by Huang *et. al.*[78]. In this report, 17 ps pulses were produced by 2-layer QD 1278 nm laser at 7.4 GHz frequency with highly chirped pulse with time bandwidth product of 3.1 [78]. The highest repetition rate of 238 GHz was achieved by a GaAs based quantum-dot laser in colliding-pulse mode-locking regime [79]. Here, transform-limited pulses of 1.3 ps duration are generated with 1.4 nm full-width half-maximum of optical spectra at 1280 nm wavelength. A great step forward was made when 3 Watt peak power was achieved by a 5 -layer QD-based 1.26 μm laser with 390 fs optical pulses [9, 80]. In 2006 a tapered design of the gain section was proposed and the first QD passive mode-locked tapered laser was realized [38]. Close to transform-limited pulses of 790 fs were generated at 1276 nm wavelength with a peak power of 500 mW. In this context, further development of tapered geometry QD lasers in term of power and ultrashort pulse generation was implemented [39, 44]. GaAs based 10-layer QD lasers, working in passive mode-locked regime, generated 360 fs pulses at 17 GHz frequency. The emission wavelength was centred at 1280 nm with

optical spectra of 5.56 nm resulting in TBWP of 0.36. A peak power up to 2.25 W was achieved [39, 44]. A high peak power up to 17.7 W was attained by our group and will be discussed, in detail, in Chapter 8 [40]. QD-based external-cavity configuration lasers are excellent candidates for systems where a reduced and broadly tunable repetition rate is required which is not achievable with monolithic mode-locked lasers [44, 49, 81-85]. It is particularly important for nonlinear multiphoton excitation fluorescence bioimaging [86-88]. A high peak power of 1.5 W in an external cavity configuration was demonstrated and a lowest repetition rate of 191 MHz was attained by our group as described in Chapter 7 [37, 89-90]. Very recently, InAs/GaAs QD-based lasers grown on Ge and Si substrates were reported although with just 26-28 mW output powers [91-92]. These may be very promising devices as the potential for mass production and creation of complex optoelectronic circuits for optical communications.

Table 3.4 Overview of mode-locked InAs/GaAs Quantum Dot lasers with following characteristics: τ_p-pulse duration, **λ**-emission wavelength, **Δλ**- full width half maximum, f_{rep}-pulse repetition rate, P_{peak}–peak power, **TBWP**- Time bandwidth product, N_L- number of layers, n/a- not applicable. The results highlighted in green are shown in more detail in the thesis. In blue the results which are achieved by group in the past. The best performances are in bold.

N_L	ML regime	Setup	τ_p (ps)	λ (nm)	Δλ (nm)	f_{rep} (GHz)	P_{peak} (W)	TBWP	Ref	Year
2	Passive	Monolithic	17	1278	1	7.4	~0.02	3.1	[78]	2001
3	Hybrid	Monolithic	14.2	1107	0.8	10	0.004	2.8	[93]	2003
3	Passive	Monolithic	5	1107	0.8	18.3	0.005	0.9	[94]	2003
5	Passive	Monolithic	1.7	1277	0.86	9.7	0.06	0.27	[95]	2004
5	Passive	Monolithic	7	1283	~0.4	35	0.006	~0.5	[96]	2004
5	Hybrid	Monolithic	11	1286	~0.22	20	n/a	0.44	[96]	2004
5	Passive	Monolithic	3	1281	0.8	50	0.006	0.44	[97]	2004
10	Passive	Monolithic	10	1291	0.2	18	0.0025	0.36	[98]	2004
10	Passive	Monolithic	3.2	1260	7.1	5	1.7	4.3	[99]	2005

n/a	Passive	Monolithic	5.7	1264	4.5	5.2	0.29	4.8	[100]	2005
5	Passive	Monolithic	**0.39**	1260	14	21	**3**	1	[9, 80]	2005
3	Colliding-pulse	Monolithic	7	1107	0.32	20	0.013	0.54	[101]	2005
10	Passive	External+SOA (Compression)	15 (1.2)	1268	3.1	4.95	1.22	6 (0.69)	[83]	2005
10	Passive	External+SOA (compression)	14 (0.97)	1275	6	2.7	n/a	15.5 (1.1)	[84]	2006
10	Passive	External+SOA (compression)	10.8 (1.2)	1193	4.25	2.7	n/a	9.7 (1.1)	[84]	2006
10	Active	External	24	1269	2	12.77	n/a	10	[49]	2006
5	Colliding-pulse/ harmonic	Monolithic	1.3	1280	1.4	**238**	0.01	0.33	[79]	2006
10	Hybrid	Monolithic	0.71	1280	n/a	20	n/a	n/a	[102]	2006
10	Passive	Monolithic	1.5	1280	6.18	80	n/a	1.7	[102]	2006
5	Passive	Monolithic	7	1190	5.5	21	0.156	8.1	[103]	2006
5	Passive	Monolithic (tapered waveguide)	0.79	1276	3.6	24	0.5	**~0.5**	[38]	2006
10	Passive	Monolithic	1.8	1300	~2.2	39.87	n/a	0.72	[104]	2006
10	Passive	Monolithic	1.5	1300	~6.4	80	n/a	1.7	[104]	2006
15	Hybrid	Monolithic (SOA)	0.7 (0.7)	1300	8.5	20	0.13	1.1	[105]	2006
15	Hybrid	Monolithic (SOA)	1.8 (1.9)	1300	2.2	40	0.014	0.7	[105]	2006
15	Passive	Monolithic (SOA)	1.9 (2.2)	1300	4.2	80	0.011	1.5	[105]	2006
9	Passive/ Hybrid	External	n/a	1205	n/a	0.35-1.5	n/a	n/a	[81]	2007
10	Passive	Monolithic	1.9	1300	n/a	19.46	0.07	n/a	[106]	2007
6	Passive	Monolithic	6.4	1216	2.6	7.2	0.224	3.4	[107]	2007
6	Passive/ harmonic	Monolithic	6	1216	2.6	50.7	0.07	3.2	[107]	2007
6	Passive/ harmonic	Monolithic	6.6	1216	1.7	42.4	0.234	2.3	[107]	2007
6	Passive	Monolithic	5.7	1240	~4.5	4.97	1.04	~0.5	[64]	2007
10	Passive/ harmonic	Monolithic (compression)	9.8 (0.96)	1260	5.5	5	>1	10 (1)	[108]	2008
10	Passive/ harmonic	Monolithic (compression)	8.6 (0.58)	1260	7.2	40	>1	12 (0.8)	[108]	2008
5	Passive	External	0.93	1300	2.3	1(0.31)	0.41	0.385	[82, 85]	2008(11)
10	Passive	Monolithic (tapered waveguide)	**0.36**	1280	5.56	17	2.25	0.36	[39, 44]	2008(9)
5	Passive	Monolithic	~1	1300	~5.6	40	~0.2	~1	[109]	2009

6	Passive	Monolithic	10	1209	2.8	10.2	~0.11	~5.7	[110]	2009
5	Passive	Monolithic	2	1300	n/a	10	n/a	n/a	[111]	2009
15	Passive/ Hybrid	Monolithic (compression)	1.6 (0.7)	1310	~1.2 (0.5)	40	n/a (0.006)	1.4 (0.8)	[112]	2010
6	Passive	Monolithic	5.7	1240	~5	4.97	1.04	~5.5	[113]	2010
8	Passive	Monolithic	5	1240	4.3	4.97	n/a	4.2	[113]	2010
6	Passive	Monolithic	6	1270	n/a	12.105	n/a	n/a	[114]	2010
6	Passive	Monolithic	3.3	1207	n/a	12.321	n/a	n/a	[114]	2010
10	Passive	External	13.6	1274	1.2	1.14	**1.5**	3.02	[89]	2010
5/ 10	Passive	Monolithic	3.2/ 3.3	1250/ 1260	7.3/ 8.4	14.65/ 14.57	3.6	4.4/ 5.2	[115]	2010
10	Passive	External	12	1268	4	0.281 (**0.191**)	0.5	~8.9	[37, 90]	2011
5	Passive	External	2.2	1300	5.3	1.1	0.16	2.1	[82]	2011
8	Passive	Monolithic	2.7	n/a	n/a	5	n/a	n/a	[116]	2011
15	Passive	Monolithic	1.2	1300	n/a	40	n/a	n/a	[117]	2011
10	Passive	Monolithic	1.26	1260	5.6	10	**17.7**	1.33	[40]	2011

3.3 Conclusion.

QW-based devices exhibited good performances such as: high repetition rate (up to 2.1 THz) [36], short pulse generation down to 200 fs using a pulse compression technique [69] and high pulse energy generation around 60 pJ [41] but the emission wavelength was 860 nm, 830 nm and 1.5µm respectively. The emission wavelengths of QD-based devices can be in the range of 1100 nm- 1300 nm which is important for a variety of applications including metro networking and multiphoton imaging. The QD-based lasers offer several advantages such as low threshold current density, temperature-insensitivity and single-frequency generation due to discrete nature of the density of state of QD materials. In addition, ultrafast carrier dynamics of the QD absorber are very useful for generating ultrashort pulses using the mode-locking technique. For example, it was shown in our group that it is possible to generate 393 fs pulses directly from a QD-based device [9]. In Chapters 5 through 8 the latest results achieved from QD-based lasers will be discussed, in more detail (see Table 3.4 highlighted in green), including the generation of a high peak power of 17.7 W directly from monolithic tapered gain-guided lasers without use of compression and amplification techniques [40]. In addition, the generation of optical pulses with a record-low repetition rate of 191 MHz [37, 90] and high peak power of 1.5 W and pulse energy of 25 pJ directly from the oscillator using an external cavity configuration [89].

3.4 References.

[1] P. Vasil'ev, P*., et al.*, "Fast phenomena in semiconductor lasers," *Reports on Progress in Physics,* vol. 63, p. 1997, 2000.

[2] O. Svelto, "Transient Laser Behavior," in *Principles of Lasers*, ed New York: Springer, 2010, pp. 319-370.

[3] K. Y. Lau, "Gain switching of semiconductor injection lasers," *Applied Physics Letters,* vol. 52, 1988.

[4] P. Vasil'ev, *Ultrafast Laser Diodes: Fundamentals and Applications*. London: Artch House, 1995.

[5] N. G. Basov*, et al.*, "Investigation of GaAs laser radiation pulsation," *Soviet Physics Semiconductors,* vol. 1, 1968.

[6] T. Nick, *LASER: The inventor, the Nobel laureate, and the thirty-year patent war.* New York: Simon and Schuster, 2000.

[7] F. J. McClung and R. W. Hellwarth, "Giant optical pulsations from ruby," *Journal of Applied Physics,* vol. 33, pp. 828-829, 1962.

[8] J. H. Harlow, *Electric power transformer engineering*: CRC Press, 2004.

[9] E. U. Rafailov*, et al.*, "High-power picosecond and femtosecond pulse generation from a two-section mode-locked quantum-dot laser," *Applied Physics Letters,* vol. 87, 2005.

[10] A. Weiner, *Ultrafast Optics*, 2009.

[11] R. Penty, "Short pulse generation using semiconductor lasers," in *Ultrafast Photonics*, P. Osborne, Ed., ed, 2002.

[12] K. Y. Lau, "Short-pulse and high-frequency signal generation in semiconductor lasers," *Lightwave Technology,* vol. 7, pp. 400-419, 1989.

[13] T. Sogawa*, et al.*, "Observation of a short optical pulse (< 1.3 ps) from a gain-switched quantum well laser," *Applied Physics Letters,* vol. 53, pp. 1580-1582, 1988.

[14] J. AuYeung, "Picosecond optical pulse generation at gigahertz rates by direct modulation of a semiconductor laser," *Applied Physics Letters,* vol. 38, pp. 308-310, 1981.

[15] J. Chung*, et al.*, "Generation of transform-limited optical pulses using a combination of a gain-switched diode laser and a semiconductor optical amplifier," *Photonics Technology Letters, IEEE,* vol. 7, pp. 860-862, 1995.

[16] Y. Sheng-Hui*, et al.*, "Generation of high-power picosecond pulses from a gain-switched two-section quantum-well laser with a laterally tapered energy-storing section," *Photonics Technology Letters, IEEE,* vol. 8, pp. 337-339, 1996.

[17] P. Anandarajah*, et al.*, "High frequency pulse generation using a gain-switched commercial semiconductor laser with strong external injection," in *High Frequency Postgraduate Student Colloquium, 2000*, 2000, pp. 121-126.

[18] N. Stelmakh*, et al.*, "100 W 50 ps gain-switched pulses from vertical-stack laser diode," *Electronics Letters,* vol. 36, pp. 1022-1024, 2000.

[19] S. Nogiwa*, et al.*, "Generation of gain-switched optical pulses with very low timing jitter by using external CW-light injection seeding," *Electronics Letters,* vol. 36, pp. 235-236, 2000.

[20] P. P. Vasil'ev and I. S. Goldobin, "New method for passive Q switching of an injection laser with an ultrashort absorber recovery time," *Soviet Journal of Quantum Electronics,* vol. 17, p. 835, 1987.

[21] B. Cakmak, "Passively Q-switched operation of a double contact tapered InGaAs/GaAs diode laser," *Microelectronic Engineering,* vol. 65, pp. 273-278, Mar 2003.

[22] P. Gavrilovic*, et al.*, "High energy CW Q-switched operation of multicontact semiconductor laser," *Electronics Letters,* vol. 31, pp. 1154-1155, 1995.

[23] M. J. R. Heck*, et al.*, "Observation of Q-switching and mode-locking in two-section InAs/InP (100) quantum dot lasers around 1.55 ?m," *Opt. Express,* vol. 15, pp. 16292-16301, 2007.

[24] P. P. Vasil'ev*, et al.*, "High power, low-jitter encoded picosecond pulse generation using an RF-locked self-Q-switched multicontact GaAs/GaAlAs diode laser," *Electronics Letters,* vol. 29, pp. 1593-1594, 1993.

[25] P. P. Vasil'ev*, et al.*, "Direct high bit rate encoding of a high power picosecond pulse train generated by a self-Q-switched multicontact laser," presented at the Conference on Lasers and Electro-Optics, Baltimore, 1993.

[26] A. Steinmetz*, et al.*, "Reduction of timing jitter in passively Q-switched microchip lasers using self-injection seeding," *Opt. Lett.,* vol. 35, pp. 2885-2887, 2010.

[27] A. Klehr*, et al.*, "High-peak-power pulse generation with GHz repetition rate using a Q-switched 1060nm DBR tapered laser," San Francisco, California, USA, 2010, pp. 76161J-12.

[28] I. Y. Khrushchev*, et al.*, "Picosecond Q-switched bow-tie laser diode array," *Electronics Letters,* vol. 33, pp. 426-428, 1997.

[29] B. J. Thedrez*, et al.*, "Experimental and theoretical investigation of large output power Q-switched AlGaAs semiconductor lasers," *Photonics Technology Letters, IEEE,* vol. 5, pp. 19-22, 1993.

[30] D. Z. Tsang*, et al.*, "Q switching of low-threshold buried-heterostructure diode lasers at 10 GHz," *Applied Physics Letters,* vol. 45, pp. 204-206, 1984.

[31] I. H. White*, et al.*, "Direct streak-camera observation of picosecond gain-switched optical pulses from a 1.5 µm semiconductor laser," *Electronics Letters,* vol. 21, pp. 197-199, 1985.

[32] T. L. Koch*, et al.*, "Picosecond carrier dynamics and laser action in optically pumped buried heterostructure lasers," *Applied Physics Letters,* vol. 41, pp. 6-8, 1982.

[33] Y. Arakawa*, et al.*, "Active Q switching in a GaAs/AlGaAs multiquantum well laser with an intracavity monolithic loss modulator," *Applied Physics Letters,* vol. 48, pp. 561-563, 1986.

[34] A. Shen*, et al.*, "Low timing jitter of gain- and Q-switched laser diodes for high bit rate OTDM applications," *Electronics Letters,* vol. 33, pp. 1875-1877, 1997.

[35] S. Arahira*, et al.*, "Mode-locking at very high repetition rates more than terahertz in passively mode-locked distributed-Bragg-reflector laser diodes," *Quantum Electronics, IEEE Journal of,* vol. 32, pp. 1211-1224, 1996.

[36] D. A. Yanson*, et al.*, "Terahertz repetition frequencies from harmonic mode-locked monolithic compound-cavity laser diodes," *Applied Physics Letters,* vol. 78, pp. 3571-3573, 2001.

[37] Y. Ding*, et al.*, "Broad Repetition-Rate Tunable Quantum-Dot External-Cavity Passively Mode-Locked Laser with Extremely Narrow Radio Frequency Linewidth," *Applied Physics Express,* vol. 4, 2011.

[38] M. G. Thompson*, et al.*, "Subpicosecond high-power mode locking using flared waveguide monolithic quantum-dot lasers," *Applied Physics Letters,* vol. 88, pp. 133119-3, 2006.

[39] M. G. Thompson*, et al.*, "Regimes of mode-locking in tapered quantum dot laser diodes," in *Semiconductor Laser Conference, 2008. ISLC 2008. IEEE 21st International*, 2008, pp. 27-28.

[40] D. Nikitichev*, et al.*, "High peak power and sub-picosecond Fourier-limited pulse generation from passively mode-locked monolitic two-section gain-guided tapered InGaAs quantum-dot lasers," *Journal of Laser Physics,* 2011.

[41] J. J. Plant*, et al.*, "250 mW, 1.5µm monolithic passively mode-locked slab-coupled optical waveguide laser," *Opt. Lett.,* vol. 31, pp. 223-225, 2006.

[42] S. Arahira*, et al.*, "Terahertz-rate optical pulse generation from a passively mode-locked semiconductor laser diode," *Opt. Lett.,* vol. 19, pp. 834-836, 1994.

[43] M. Haji*, et al.*, "A low jitter passively mode locked laser diode at 40 GHz using regenerative feedback via an optical fiber loop," in *Lasers and Electro-Optics Europe (CLEO EUROPE/EQEC), 2011 Conference on and 12th European Quantum Electronics Conference*, 2011, pp. 1-1.

[44] M. G. Thompson*, et al.*, "InGaAs Quantum-Dot Mode-Locked Laser Diodes," *Selected Topics in Quantum Electronics, IEEE,* vol. 15, pp. 661-672, 2009.

[45] R. S. Tucker*, et al.*, "40 GHz active mode-locking in a 1.5 µm monolithic extended-cavity laser," *Electronics Letters,* vol. 25, pp. 621-622, 1989.

[46] Y. L. Bessonov*, et al.*, "Generation of picosecond pulses in an injection laser with an external selective resonator," *Soviet Journal of Quantum Electronics,* vol. 12, p. 1510, 1982.

[47] J. E. Bowers*, et al.*, "Actively mode-locked semiconductor lasers," *Quantum Electronics, IEEE Journal of,* vol. 25, pp. 1426-1439, 1989.

[48] M. Teshima*, et al.*, "Experimental investigation of injection locking of fundamental and subharmonic frequency-modulated active mode-locked laser diodes," *Quantum Electronics, IEEE Journal of,* vol. 34, pp. 1588-1596, 1998.

[49] M.-T. Choi*, et al.*, "Ultralow noise optical pulse generation in an actively mode-locked quantum-dot semiconductor laser," *Applied Physics Letters,* vol. 88, pp. 131106-3, 2006.

[50] D. B. Malins*, et al.*, "Ultrafast electroabsorption dynamics in an InAs quantum dot saturable absorber at <equation>1.3 μm</equation>," *Applied Physics Letters,* vol. 89, pp. 171111-171111-3, 2006.

[51] C. M. A. Kapteyn*, et al.*, "Electron escape from InAs quantum dots," *Physical Review B,* vol. 60, pp. 14265-14268, 1999.

[52] P. W. Fry*, et al.*, "Electric-field-dependent carrier capture and escape in self-assembled InAs/GaAs quantum dots," *Applied Physics Letters,* vol. 77, pp. 4344-4346, 2000.

[53] R. Turton, *The Quantum Dot: A journey into the Future of Microelectronics*. New York: W. H. Freeman Spektrum, 1995.

[54] P. J. Delfyett*, et al.*, "High-power ultrafast laser diodes," *Quantum Electronics, IEEE,* vol. 28, pp. 2203-2219, 1992.

[55] G. Tandoi*, et al.*, "Nonabsorbing Mirrors for Quantum-Well Colliding Pulse Mode-Locked Lasers," *Photonics Technology Letters, IEEE,* vol. 23, pp. 293-295, 2011.

[56] D. J. Derickson*, et al.*, "Short pulse generation using multisegment mode-locked semiconductor lasers," *Quantum Electronics, IEEE Journal of,* vol. 28, pp. 2186-2202, 1992.

[57] D. J. Derickson*, et al.*, "Comparison of timing jitter in external and monolithic cavity mode-locked semiconductor lasers," *Applied Physics Letters,* vol. 59, pp. 3372-3374, 1991.

[58] D. J. Derickson*, et al.*, "Comparison of colliding pulse and self-colliding pulse monolithic cavity mode-locked semiconductor lasers," 1992, p. ThB3.

[59] K. A. Williams*, et al.*, "Monolithic passive mode-locking in single contact tapered lasers," in *Lasers and Electro-Optics Society Annual Meeting, 1995. 8th Annual Meeting Conference Proceedings, Volume 1., IEEE*, 1995, pp. 135-136 vol.2.

[60] A. Mar*, et al.*, "High-power mode-locked semiconductor lasers using flared waveguides," *Applied Physics Letters,* vol. 66, pp. 3558-3560, 1995.

[61] F. Camacho*, et al.*, "Passive modelocking in semiconductor lasers with monolithically integrated passive waveguides," *Optoelectronics, IEE Proceedings -,* vol. 145, pp. 43-46, 1998.

[62] F. Robert*, et al.*, "Passive mode locking of InAlGaAs 1.3 µm strained quantum wells extended cavity laser fabricated by quantum-well intermixing," *Photonics Technology Letters, IEEE,* vol. 16, pp. 374-376, 2004.

[63] S. Lee*, et al.*, "Picosecond pulse generation using a saturable absorber section of grating-coupled surface-emitting laser," *Photonics Technology Letters, IEEE,* vol. 17, pp. 2676-2678, 2005.

[64] Y. C. Xin*, et al.*, "Monolithic Passively Mode-Locked Lasers using Quantum Dot or Quantum Well Materials Grown on GaAs Substrates," *Proc. of SPIE,* vol. 6468, 2007.

[65] J. Javaloyes*, et al.*, "Wide range 40-GHz Passive Mode-Locking operation of an AlGaInAs 1.55 µm Strained Quantum Well laser," in *Lasers and Electro-Optics*

2009 and the European Quantum Electronics Conference. CLEO Europe - EQEC 2009. European Conference on, 2009, pp. 1-1.

[66] A. C. Bryce*, et al.*, "Passive mode-locking of AlGaInAs quantum well laser, modelling and experiment," in *LEOS Annual Meeting Conference Proceedings, 2009. LEOS '09. IEEE*, 2009, pp. 515-516.

[67] T. Shimizu*, et al.*, "860 GHz rate asymmetric colliding pulse modelocked diode lasers," *Electronics Letters,* vol. 33, pp. 1868-1869, 1997.

[68] F. R. Ahmad and F. Rana, "Passively Mode-Locked High-Power (210 mW) Semiconductor Lasers at 1.55 μm Wavelength," *Photonics Technology Letters, IEEE,* vol. 20, pp. 190-192, 2008.

[69] T. Schlauch*, et al.*, "Femtosecond passively modelocked diode laser with intracavity dispersion management," *Opt. Express,* vol. 18, pp. 24316-24324, 2010.

[70] Y. C. Xin*, et al.*, "Monolithic 1.55 μm GaInNAsSb Quantum Well Mode-Locked Lasers," in *Lasers and Electro-Optics, 2007. CLEO 2007. Conference on*, 2007, pp. 1-2.

[71] P. A. Morton*, et al.*, "Monolithic hybrid mode locked 1.3 μm semiconductor laser arrays," in *Electron Devices Meeting, 1989. IEDM '89. Technical Digest., International*, 1989, pp. 865-868.

[72] Y.-K. Chen and M. C. Wu, "Monolithic colliding-pulse mode-locked quantum-well lasers," *Quantum Electronics, IEEE Journal of,* vol. 28, pp. 2176-2185, 1992.

[73] D. Kunimatsu*, et al.*, "Passively mode-locked laser diodes with bandgap-wavelength detuned saturable absorbers," *Photonics Technology Letters, IEEE,* vol. 11, pp. 1363-1365, 1999.

[74] Y. Nomura*, et al.*, "Mode locking in Fabry-Perot semiconductor lasers," *Physical Review A,* vol. 65, p. 043807, 2002.

[75] K. Yvind*, et al.*, "Low-jitter and high-power 40-GHz all-active mode-locked lasers," *Photonics Technology Letters, IEEE,* vol. 16, pp. 975-977, 2004.

[76] K. Merghem*, et al.*, "Short pulse generation using a passively mode locked single InGaAsP/InP quantum well laser," *Opt. Express,* vol. 16, pp. 10675-10683, 2008.

[77] P. Crump*, et al.*, "Extending the wavelength range of single-emitter diode lasers for medical and sensing applications: 12xx-nm quantum dots, 2000-nm wells, > 5000-nm cascade lasers," *SPIE,* vol. 6456, 2007.

[78] X. Huang*, et al.*, "Passive mode-locking in 1.3 µm two-section InAs quantum dot lasers," *Applied Physics Letters,* vol. 78, pp. 2825-2827, 2001.

[79] A. R. Rae*, et al.*, "Harmonic Mode-Locking of a Quantum-Dot Laser Diode," in *Lasers and Electro-Optics Society, 2006. LEOS 2006. 19th Annual Meeting of the IEEE*, 2006, pp. 874-875.

[80] E. U. Rafailov*, et al.*, "Mode-locked quantum-dot lasers," *Nat Photon,* vol. 1, pp. 395-401, 2007.

[81] A. D. McRobbie*, et al.*, "High power all-quantum-dot-based external cavity modelocked laser," *Electronics Letters,* vol. 43, pp. 812-813, 2007.

[82] M. Xia*, et al.*, "External-Cavity Mode-Locked Quantum-Dot Laser Diodes for Low Repetition Rate, Sub-Picosecond Pulse Generation," *Selected Topics in Quantum Electronics, IEEE,* vol. PP, pp. 1-1, 2011.

[83] M. T. Choi*, et al.*, "Ultrashort, high-power pulse generation from a master oscillator power amplifier based on external cavity mode locking of a quantum-

dot two-section diode laser," *Applied Physics Letters,* vol. 87, pp. 221107-3, Nov 2005.

[84] J. Kim*, et al.*, "Pulse generation and compression via ground and excited states from a grating coupled passively mode-locked quantum dot two-section diode laser," *Applied Physics Letters,* vol. 89, Dec 2006.

[85] M. Xia*, et al.*, "External-cavity mode-locked quantum-dot lasers for low repetition rate, sub-picosecond pulse generation," in *Lasers and Electro-Optics, 2008 and 2008 Conference on Quantum Electronics and Laser Science. CLEO/QELS 2008. Conference on*, 2008, pp. 1-2.

[86] M. Kuramoto*, et al.*, "Two-photon fluorescence bioimaging with an all-semiconductor laser picosecond pulse source," *Opt. Lett.,* vol. 32, pp. 2726-2728, 2007.

[87] H. Yokoyama*, et al.*, "Nonlinear-microscopy optical-pulse sources based on mode-locked semiconductor lasers," *Opt. Express,* vol. 16, pp. 17752-17758, 2008.

[88] S.-W. Chu*, et al.*, "Real-time second-harmonic-generation microscopy based on a 2-GHz repetition rate Ti:sapphire laser," *Opt. Express,* vol. 11, pp. 933-938, 2003.

[89] Y. Ding*, et al.*, "Quantum-dot external-cavity passively modelocked laser with high peak power and pulse energy," *Electronics Letters,* vol. 46, pp. 1516-1518, 2010.

[90] M. A. Cataluna*, et al.*, "High-Power Versatile Picosecond Pulse Generation from Mode-Locked Quantum-Dot Laser Diodes," *Selected Topics in Quantum Electronics, IEEE,* vol. 17, pp. 1302-1310, 2011.

[91] H. Liu*, et al.*, "Long-wavelength InAs/GaAs quantum-dot laser diode monolithically grown on Ge substrate," *Nat Photon,* vol. 5, pp. 416-419, 2011.

[92] T. Wang*, et al.*, "1.3 μm InAs/GaAs quantum-dot lasers monolithically grown on Si substrates," *Opt. Express,* vol. 19, pp. 11381-11386, 2011.

[93] M. G. Thompson*, et al.*, "10 GHz hybrid modelocking of monolithic InGaAs quantum dot lasers," *Electronics Letters,* vol. 39, pp. 1121-1122, 2003.

[94] K. T. Tan*, et al.*, "Investigation of high repetition rate mode-locked quantum dot lasers," in *Lasers and Electro-Optics Society, 2003. LEOS 2003. The 16th Annual Meeting of the IEEE*, 2003, pp. 826-827 vol.2.

[95] A. E. Gubenko*, et al.*, "Mode-locking at 9.7 GHz repetition rate with 1.7 ps pulse duration in two-section QD lasers," in *Semiconductor Laser Conference, 2004. Conference Digest. 2004 IEEE 19th International*, 2004, pp. 51-52.

[96] M. Kuntz*, et al.*, "35 GHz mode-locking of 1.3 μm quantum dot lasers," *Applied Physics Letters,* vol. 85, pp. 843-845, 2004.

[97] M. Kuntz and et al., "Direct modulation and mode locking of 1.3 μm quantum dot lasers," *New Journal of Physics,* vol. 6, p. 181, 2004.

[98] M. G. Thompson*, et al.*, "Transform-limited optical pulses from 18 GHz monolithic modelocked quantum dot lasers operating at ~ 1.3 μm," *Electronics Letters,* vol. 40, pp. 346-347, 2004.

[99] A. Gubenko*, et al.*, "High-power monolithic passively modelocked quantum-dot laser," *Electronics Letters,* vol. 41, pp. 1124-1125, 2005.

[100] L. Zhang*, et al.*, "Low Timing Jitter, 5 GHz Optical Pulses from a Monolithic Two-Section Passively Mode-Locked 1250/1310 nm Quantum Dot Laser for High Speed Optical Interconnets," 2005, p. OWM4.

[101] M. G. Thompson*, et al.*, "Colliding-pulse modelocked quantum dot lasers," *Electronics Letters,* vol. 41, pp. 248-250, 2005.

[102] D. Bimberg*, et al.*, "High speed nanophotonic devices based on quantum dots," *Physica Status Solidi (a),* vol. 203, pp. 3523-3532, 2006.

[103] M. A. Cataluna*, et al.*, "Stable mode locking via ground- or excited-state transitions in a two-section quantum-dot laser," *Applied Physics Letters,* vol. 89, pp. 081124-3, 2006.

[104] M. Laemmlin*, et al.*, "Quantum dot based photonic devices at 1.3 µm: Direct modulation, mode-locking, SOAs and VCSELs," *physica status solidi (c),* vol. 3, pp. 391-394, 2006.

[105] M. Laemmlin*, et al.*, "Distortion-free optical amplification of 20-80 GHz modelocked laser pulses at 1.3 µm using quantum dots," *Electronics Letters,* vol. 42, pp. 697-699, 2006.

[106] F. Kefelian*, et al.*, "High Repetition Rate Monolithic Passively Mode-Locked Semiconductor Quantum-Dot Laser: Investigation of the Locking Regimes and the RF Linewidth," in *Lasers and Electro-Optics, 2007. CLEO 2007. Conference on*, 2007, pp. 1-2.

[107] Y. C. Xin*, et al.*, "Reconfigurable quantum dot monolithic multisectionpassive mode-locked lasers," *Opt. Express,* vol. 15, pp. 7623-7633, 2007.

[108] A. Gubenko*, et al.*, "Frequency up-chirping in monolithic passively mode-locked InGaAs quantum dot lasers," in *IEEE Lasers and Electro-Optics Society, 2008. LEOS 2008. 21st Annual Meeting of the*, 2008, pp. 469-470.

[109] G. Fiol*, et al.*, "Quantum-Dot Semiconductor Mode-Locked Lasers and Amplifiers at 40 GHz," *Quantum Electronics, IEEE Journal of,* vol. 45, pp. 1429-1435, 2009.

[110] C. Y. Lin*, et al.*, "Compact Optical Generation of Microwave Signals Using a Monolithic Quantum Dot Passively Mode-Locked Laser," *Photonics Journal, IEEE,* vol. 1, pp. 236-244, 2009.

[111] G. Carpintero*, et al.*, "Low Noise Performance of Passively Mode-Locked 10-GHz Quantum-Dot Laser Diode," *Photonics Technology Letters, IEEE,* vol. 21, pp. 389-391, 2009.

[112] H. Schmeckebier*, et al.*, "Complete pulse characterization of quantum dot mode-locked lasers suitable for optical communication up to 160 Gbit/s," *Opt. Express,* vol. 18, pp. 3415-3425, 2010.

[113] L. Lester*, et al.*, "Pulse characteristics of passively mode-locked quantum dot lasers," *Proceedings of SPIE,* vol. 7616, 2010.

[114] S. Breuer*, et al.*, "Reverse-emission-state-transition mode locking of a two-section InAs/InGaAs quantum dot laser," *Applied Physics Letters,* vol. 97, pp. 071118-3, 2010.

[115] D. Nikitichev*, et al.*, "High-power passively mode-locked tapered InAs/GaAs quantum-dot lasers," *Applied Physics B: Lasers and Optics,* vol. 103, pp. 609-613, 2011.

[116] Y. Li*, et al.*, "Pulse characterization of a passively mode-locked quantum dot semiconductor laser using FROG and autocorrelation," 2011, p. JWA89.

[117] M. Radziunas*, et al.*, "Pulse Broadening in Quantum-Dot Mode-Locked Semiconductor Lasers: Simulation, Analysis, and Experiments," *Quantum Electronics, IEEE Journal of,* vol. 47, pp. 935-943, 2011.

Chapter 4. Characterization of QD-based devices under mode-locking regime.

The description of the technique and the experimental setups which were used during the experiments for characterising different type's lasers are presented.

4.1 Characterization techniques.

4.1.1 Pulse shape and duration.

Direct measurement of laser pulses can be realised by digital sampling oscilloscopes in which the bandwidth is limited to 60 GHz [1]. As the frequency domain is related to the time domain (Eq. 4.1) the full-width half-maximum of the pulse (τ_{FWHM}) for 60 GHz digital sampling oscilloscope would be 7.3 ps assuming a Gaussian pulse shape of the signal.

$$\tau_{FWHM}=0.44/f_{3dB} \qquad \textbf{(4.1)}$$

where f_{3dB}- frequency bandwidth at 3 dB.

However, it is important to understand that the minimum possible measured pulse should be longer than 7.3 ps. The observed pulse duration depends on the bandwidths/rise times of the signal, photodiode and the oscilloscope. The rise time is the time different between the 10% point and the 90% point of the peak amplitude output on the leading edge of the pulse. Thus the measured pulse duration is calculated by the root of the sum of the squares of the rise times of the equipment involved and the signal (Eq. 4.2).

$$\tau_{MEASUREMENT} = \sqrt{\tau_{osc}{}^2 + \tau_{photodiode}{}^2 + \tau_{signal}{}^2} \qquad \textbf{(4.2),}$$

where τ_{osc}-rise time of the oscilloscope, $\tau_{photodiode}$-rise time of the photodiode, τ_{signal}- actual pulse width.

In order to keep the error of observation between the actual and observed rise times to less than 3 %, the ratio of signal risetime to scope rise time should be greater than 4:1. In addition, considering that the rise time of the 29 GHz photodiode is ~15 ps, only ~20ps optical pulses can be measured with a large bandwidth digital sampling oscilloscope [2-3]. Alternatively, streak cameras can be used for direct measurement of the pulses as short as 200 fs but only for wavelengths from 280 nm up to 850 nm [4-5]. The time resolution of streak cameras in the infrared range is only few picoseconds [6]. In order to measure pulses with good resolution up to 1 fs in the infrared range, indirect methods of pulse measurement have been developed [7-8]. The most simple and relatively chip technique is autocorrelation when information of phase of the pulse is not required. In Fig. 4.1 the general setup of autocorrelation is depicted. The principle of operation is based on a Michelson Interferometer which is used for recording the second order correlation function. An incident pulse with electric field E(t) is split into two branches by a beam splitter. The two replicas are used for generation of a time delay τ between them by means of two independent delay lines (fix and variable). After that those replicas E(t) and E(t+τ) are recombined in a nonlinear crystal for generation second harmonic signal I_{SH}. The intensity of this signal is proportional to square of the sum of the electrical signals (Eq.4.3).

$$I_{SH}(t+\tau) \sim [E(t) + E(t+\tau)]^2 \qquad \textbf{(4.3)},$$

where I_{SH}- intensity of second harmonic signal; E(t), E(t+τ)- Amplitude of original and time delayed replicas

When the square in equation 4.3 is expanded the component of the second harmonic is present (Eq. 4.4) due to the temporal overlap of the two pulses. So, the

second harmonic signal will be generated only when two pulses are overlapping in time.

$$I_{SH}(t+\tau) \sim E(t)^2 + 2E(t)E(t+\tau) + E(t+\tau)^2 \quad \textbf{(4.4)}$$

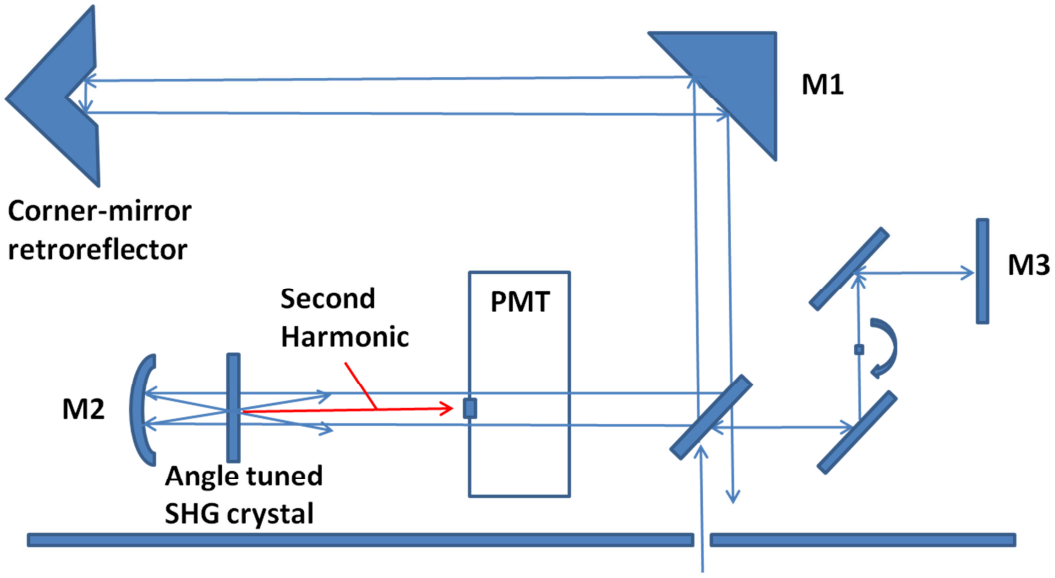

Fig. 4.1 Top view schematic of the autocorrelator. SHG- Second harmonic generation, PMT-Photomultiplier tube.

As can be seen from Fig. 4.1, two beams enter the crystal noncollinearly and when phase matching conditions are satisfied, equation (4.4) is simplified to (eq. 4.5).

$$I_{SH}(t+\tau) \sim 2E(t)E(t+\tau) \quad \textbf{(4.5)}$$

The iris positioned after the doubling crystal blocks the two initial replica beams, and the middle second harmonic beam is sent to a detector which converts the second harmonic to an electrical signal, squares the incident field and integrates over the duration of the pulse, t. Now, the amplitude of the photo detector signal I_{AC} is proportional to (Eq. 4.6) that can be written as (Eq. 4.7) due to the fact that square of

the electric field amplitude is intensity. This is the intensity of autocorrelation of the laser pulse proportional to two replicas.

$$I_{AC}(\tau) \sim \int [2E(t)E(t+\tau)]^2 \, dt \quad \textbf{(4.6),}$$

I_{AC}-The intensity of autocorrelation

$$I_{AC}(\tau) \sim \int I(t)I(t+\tau) \, dt \quad \textbf{(4.7)}$$

Eq. 4.7 is called a correlation integral. It shows that the autocorrelation is not measuring the pulse but a correlation function of pulses of the two replicas. If two pulses are identical Eq. 4.7 can be easily solved analytically by multiplying the autocorrelation signal width by a constant factor that depends on the shape of the pulse [9]. For example, for Gaussian pulse the constant ($\Delta t/\Delta \tau$) is 0.7071 for hyperbolic $sech^2$ is 0.6482 and Lorentzian is 0.5 see table 4.1 [10-11]. Time-bandwidth product ($\Delta t * \Delta \nu$) is 0.4413 and 0.2206 for Gaussian and Lorentzian pulse shapes respectively. Autocorrelation function I_{AC} for optical signals with different intensity profiles is depicted in Fig. 4.2.

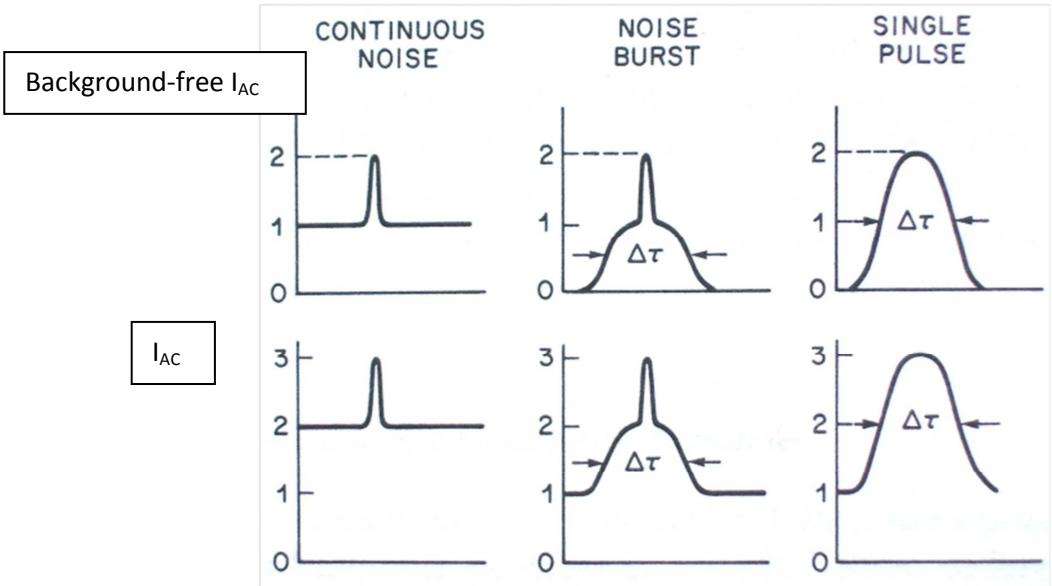

Fig. 4.2 Autocorrelation functions without (**top**) and without (**bottom**) background for various optical inputs [12].

Table 4.1 Second-order autocorrelation functions and bandwidth products for Gaussian, Hyperbolic Secant squared and Lorentzian pulse shapes. **TBWP**- Time-bandwidth product**.**

Pulse Shape	**$I_{AC}(\tau)$=**	**I(t)**	**Δt/Δτ**	**Pulsewidth FWHM)Δt**	**TBWP ΔtΔv**
Gaussian	$Exp[-ln(2)*(2\tau/\Delta\tau)^2]$	$Exp[-ln(2)*(2t/\Delta t)^2]$	0.7071	1.665	0.4413
Hyperbolic $sech^2$	$3[(c\tau/\Delta\tau)*coth(c\tau/\Delta\tau)-1]/[sinh^2(c\tau/\Delta\tau)]$,c=2.71	$sech^2(1.7625t/\Delta t)$	0.6482	1.763	0.3148
Lorentzian	$1/(1+(2\tau/\Delta\tau)^2$	$1/(1+(2t/\Delta t)^2)$	0.5	2	0.2206

Thus by analyzing the shape of the autocorrelation function it can be concluded whether it is noise or optical pulse. As the information of the phase of the pulse is absent, there is some degree of uncertainty in fitting a pulse shape to the autocorrelation trace. Using this technique, it is very difficult to detect weak background noise that may associate with an optical pulse as well [9, 13]. But overall, the intensity autocorrelation technique is a very effective and cost efficient solution for estimation of optical pulses less than 100 ps.

4.1.2 RF spectra (good stable ML).

According to Fourier theory, any time-domain electrical phenomenon is made up of one or more sine waves of appropriate frequency, amplitude, and phase [14]. In other words, a time-domain signal can be transformed into its frequency domain equivalent as shown in Fig. 4.3. A spectrum is a collection of sine waves, producing complex signal which can be represented in time domain or frequency domain forms.

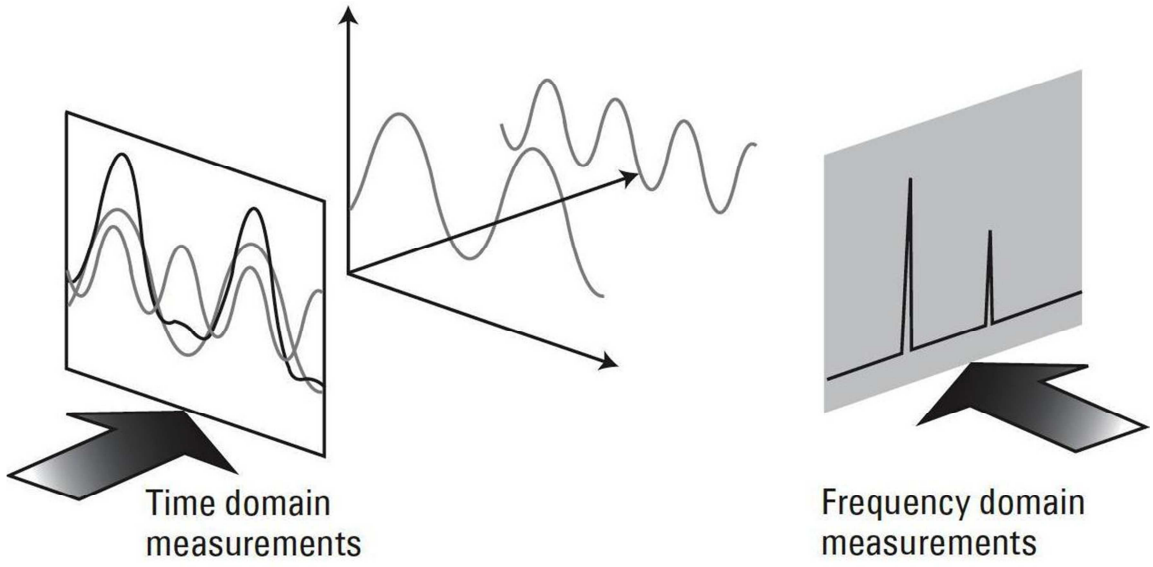

Fig. 4.3 Relationship between time and frequency domain [15].

On one hand, the time domain is very useful for measuring pulse rise and fall times, overshoot, and ringing. On the other hand, the frequency domain is more useful in determining the harmonic content of a signal, out-of-band and spurious emission and electromagnetic interference (unwanted emissions). So the repetition rate of the pulse can be accurately obtained by frequency domain measurements. An electrical spectrum analyzer, after converting the optical signal into an RF signal by a photodiode with a suitable bandwidth, is used for this purpose. It can be concluded from the RF signal-to-noise ratio of the fundamental and harmonics, as well as the -3dB bandwidth whether mode-locking is stable or not. For instance, the quality of pulse frequency

oscillation depends on the pedestal of the RF signal. If it's broadened then the jitter is higher and there is some noise around the carrier. Mode locking was considered to be stable when the pedestal was narrow and the signal-to-noise ratio was 15dB or more. Thus the RF spectrum can provide information not only about the repetition rate of the pulse but also about the stability of mode-locking.

4.1.3 Optical spectra characteristics.

An optical spectrum analyzer gives us information about the central emission wavelength(s) and full width half maximum (FWHM) of the optical spectrum. It is used for calculating the time-bandwidth product (Eq. 4.8).

$$\Delta\nu*\Delta\tau=c*\Delta\lambda*\Delta\tau/\lambda^2 \qquad \textbf{(4.8)},$$

where c-speed of light, λ-wavelength, Δλ- FWHM of optical spectrum and Δτ- pulse width.

Ultrashort laser pulses carry significant bandwidth as a result of the time-bandwidth relationship. The pulse is said to be at its transform limit if the spectral components that fall under the bandwidth of the laser pulse are time coincident (Fig. 4.4 a). The phase of the several frequencies that make up the pulse can be different in time due to material properties (dispersion) (Fig. 4.4 b). As a result of this effect, called “chirp”, the pulse is broadened [16]. Thus the time-bandwidth product estimates whether measured optical pulses are transform-limited or chirped pulses. As can be seen in Table 4.1 transform-limited pulses for Gaussian pulse shape have TBWP of 0.4413 which is higher than TBWP of 0.2206 for Lorentzian pulse shape.

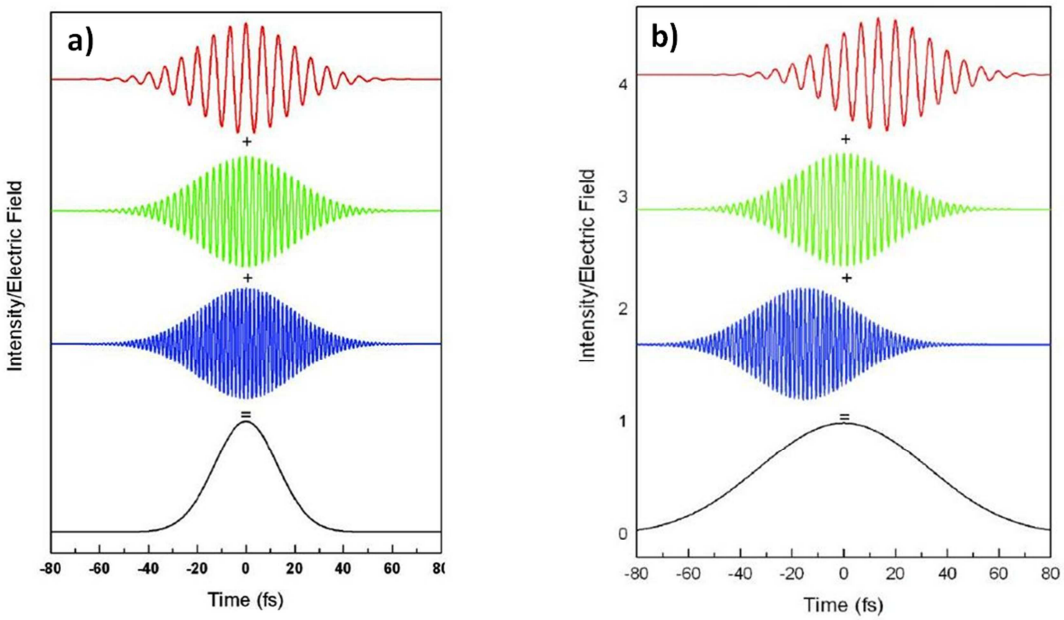

Fig. 4.4 The temporal relationship between selected Fourier components of **a)** a transform-limited pulse, **b)** a positively chirped pulse [16].

4.1.4 Power characteristics (duty cycle, FOM).

It is quite important to understand the difference and relation between average power and peak power. The energy content of the pulse is equal to the peak power of the pulse multiplied by the pulse width. However, power meters measure the power over a period of time that is longer than the pulse width – they measure the so-called average power. The ratio of the pulse width ($\Delta\tau_P$) and pulse period (T) is called the duty cycle of a system (Fig. 4.5). Duty cycle is the fraction of time that a system is in an "active" state. In particular, duty cycle is the proportion of time during which a component, device, or system is operated. Peak power is calculated knowing the average power, repetition rate of the pulse and the pulse width (Eq. 4.9).

$$P_{PEAK}=P_{AVR}*T/\Delta\tau_P \qquad \textbf{(4.9)},$$

Where P_{PEAK}- Peak Power, P_{AVR}-Average Power, T- Pulse period, $\Delta\tau_P$ -Pulse width.

High average power in the laser is not always desirable as in the case of micro-machining and photo-ablation due to thermal damage to the surrounding areas of processing. As shown in Fig. 4.5 the peak power of the pulse can be high while the average power is low.

It is also important to remember that equation 4.9 can be used for defining of the peak power of the laser when the amplified spontaneous emission is negligible. In general, spontaneous emission should be subtracted from average power for correct pulse energy estimation.

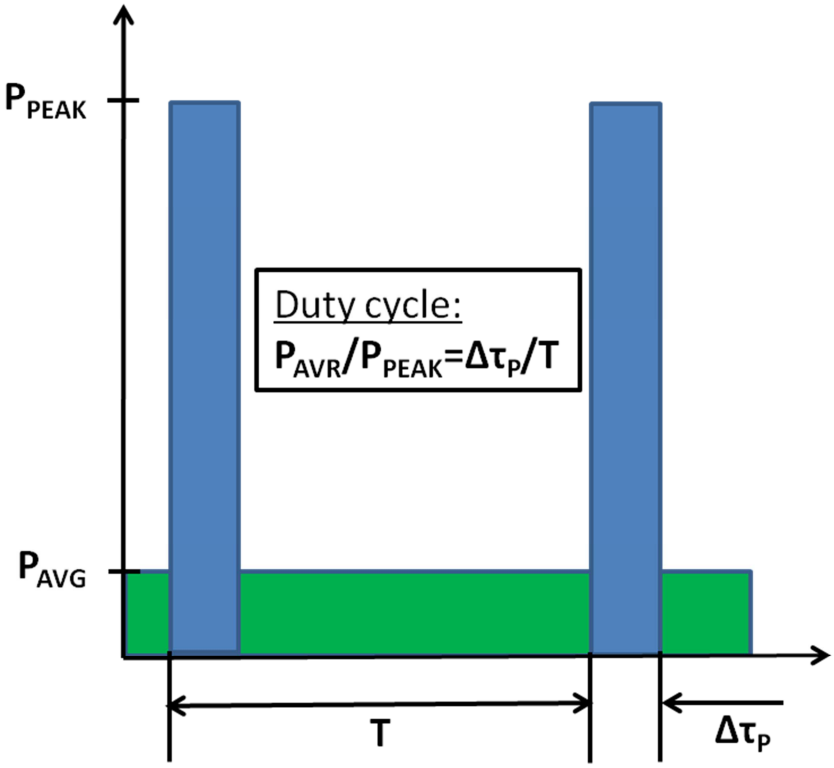

Fig. 4.5 The relation between peak power **(P_{PEAK})**, average power **(P_{AVR})**, pulse width **(τ)** and period **(T).**

In this context, as explained in chapter 1 the Figure of merit (FOM) can be used for estimating whether the laser produces enough energy for applying it in multi-photon imaging (FOM=P_{AVR}*P_{PEAK}).

4.2 Experimental setup.

The experimental setup shown in Fig. 4.6 was used in all experiments with a slight modification for the external cavity configuration, where an output coupler is added. During the measurement of the tapered lasers, several cylindrical lenses were also used to collimate the beam due to astigmatism.

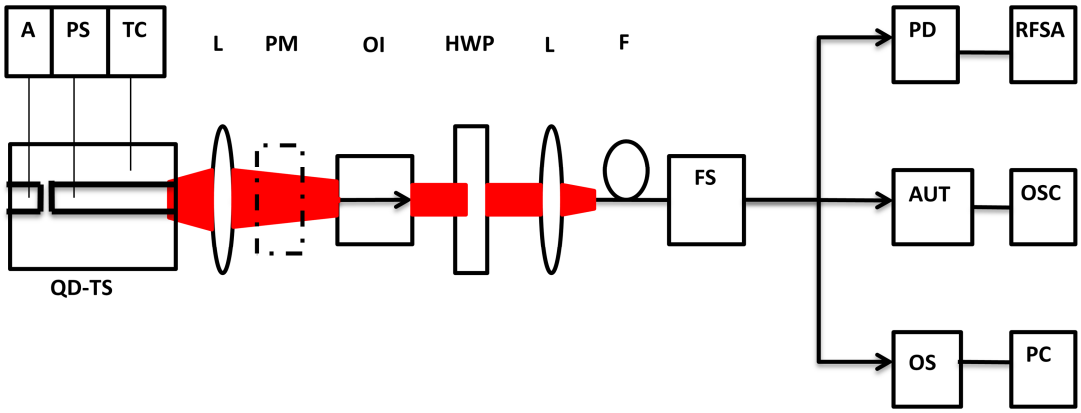

Fig. 4.6 The schematic of the experimental setup: **QD -TS**: quantum dot - two section diode on the XYZ mount, **A**- absorber, **TC**: temperature controller, **PS**: power supply, **L**, **PM**- Power meter, **OI**: optical isolator, **HWP**: half wave plate, **F**: fibre, **FS**: fibre splitter, **PD**: photo diode, **RFSA**: RF spectrum analyzer, **AUT**: autocorrelator, **OSC**: oscilloscope, **OS**: optical spectrometer, **PC**-personal computer.

The laser is mounted on the Peltier cooler in order to maintain a constant temperature. Multi-section diode lasers are electrically pumped devices which consist of a gain section and an absorber section. The former one is forward bias while the latter one is reverse bias using a Thurlby PL 320 (30V-2A) power supply. Aspheric lenses are used for collimating/focussing the light to the testing equipment. An optical isolator protects the laser from feedback and a half wave plate helps to achieve the correct polarization. A fibre optical coupler splits the beam into three different outputs

and enables monitoring of different parameters of the laser at the same time. A power meter helps determine the output average power, an autocorrelator with oscilloscope allows the measurement of ultrashort pulses, an RF spectrum analyzer combined with a fast photo diode shows the operating frequency and the quality of mode-locking and an optical spectrum displays the central emission wavelength(s).

All straight waveguide lasers were fabricated by Innolume GmbH, Germany while the tapered lasers were fabricated by III-V Lab, France on the wafer provided by Innolume GmbH, Germany. As soon as the devices were tested and characterized the feedback of the performance with comments on possible way of optimisation the devices was given to Innolume and III-V Lab. In addition, some simulations were performed by the Politecnico di Torino, Italy as well as the University of Athens. Not all the devices worked very well. For example, it was found that 8 mm long 5, 10 and 15 QD layers with 900 µm absorber didn't mode-locked due to high an absorber-to-gain ratio as will be explained in section 5.4.

4.2.1 Peltier cooler.

The investigated semiconductor lasers were mounted p-side up on the mount with the Peltier cooler connected to the temperature controller/Power Supply (TC/PS) Model SE 5010 Marlow industries. TC/PS is designed for the precision temperature control (between -99.9^{o}C to 150^{o}C) of all types of thermoelectric cooling devices. With an adjustable DC output power of 192 Watts, the TC/PS can be used for a variety of applications, including: temperature control of laser diodes, infrared detectors, CCDs and thermoelectric heat exchangers. Thermoelectric cooling is based on the Peltier effect (discovered by Jean-Charles Peltier), or the effect of generating heat at an electrified junction between two different metals. A Peltier cooler, heater, or thermoelectric heat pump is a solid-state active heat pump which transfers heat from one side of the device to the other side against the temperature gradient (from cold to hot), with the consumption of electrical energy. When direct current runs through the Peltier device, heat is moved from one side to the other. Therefore it can be used either for heating or for cooling, although in practice the main application is cooling. The mount was covered with a thin layer of heat sink compound for better heat transfer from the laser.

4.2.2 Optical isolator and half plate.

Faraday optical isolators are composed of three elements: entrance and exit polarizers and Faraday rotator (Fig. 4.7) [17]. The rotator consists of a strong permanent magnet containing a Terbium Gallium Garnet (TGG) crystal. The magnetic field and the length of the crystal are adjusted so that the input light's polarization rotates by 45^{o} on exiting the crystal. In the reverse direction, the Faraday rotator continues to rotate the light's polarization in the same direction that it did in the forward direction so that the polarization of the light is now rotated 90^{o} with respect to the input signal. So the light travels in only one direction and it helps to protect the laser from optical elements' feedback which causes instabilities in the operation of the laser. A custom designed optical isolator was used in the experiments with the following parameters: IO-4-1180 nm/1260 nm -VLP, Aperture: 4.0mm, Isolation @ 1180 & 1260nm: 23dB, Isolation @ 1220nm: 35dB, Transmission @ 1180nm: 88%, Transmission @ 1260nm: 88-91% (OFR-Thorlab).

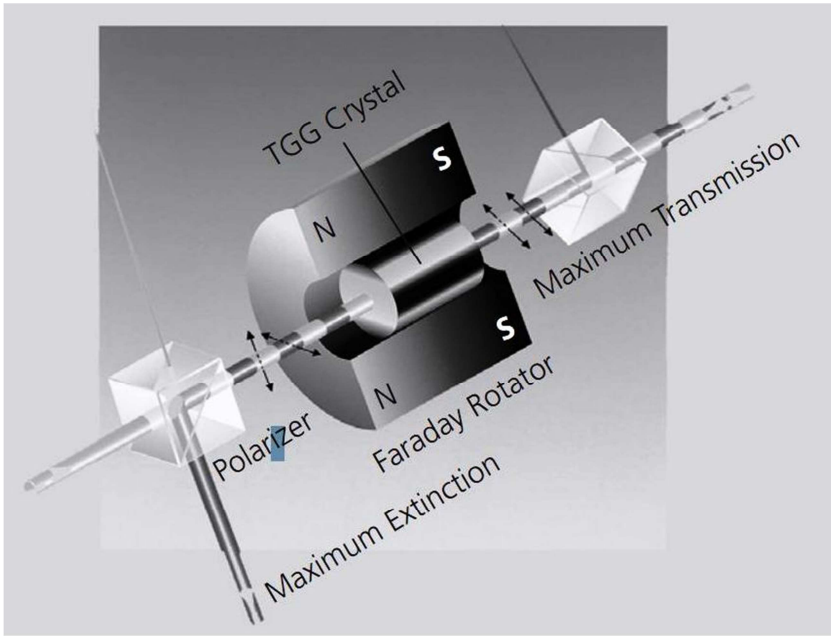

Fig. 4.7 Schematic of the Faraday isolator [17].

A mounted Achromatic Half-Wave Plate, 1100 - 2000 nm AHWP05M-1600 Thorlab is used in the experiment. Half wave plate is used for rotating the plane of plane polarized light as shown in Fig. 4.8 [18].

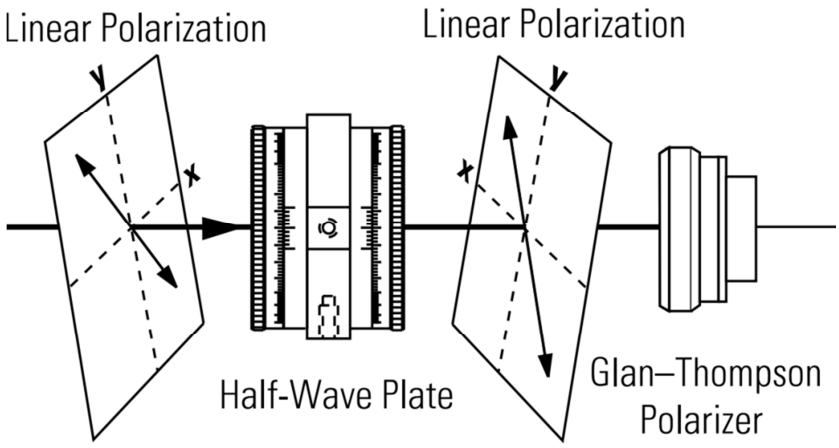

Fig. 4.8 The effect of half-wave plate on light polarization [18].

It is very important for autocorrelator that the polarization has to be in the right direction in order to generate any second harmonic signal.

4.2.3 Aspheric lenses.

The compact aspheric Lenses (Model 5722-HC New Focus) with a broadband antireflection coating (1000-1600 nm) made of Corning C0550 glass provide a convenient, high-quality alternative to microscope objectives. Aspheric lenses are very good for refracting the light at large angles as they don't introduce any significant spherical aberration compared to conventional spherical lenses. This allows a single aspheric lens to perform the same function as a compound lens system. They are useful for coupling light into and out of optical fibers or collimating diode lasers because the aspheric surface minimizes the aberrations experienced by rays travelling through the outer circumference of the lens. Each asphere is made from laser-quality glass to provide optimum performance and has extremely low wavefront distortion over a wide wavelength range. Each lens is mounted in a threaded lens holder marked with the focal length and equivalent microscope-objective power. In order to choose the best lens for the experiment its focal length can be estimated by using this formula (Eq. 4.10):

$$f = dD\pi/4\lambda \qquad \textbf{(4.10),}$$

where **f** is the lens focal length, **d** is the beam diameter at the focus, **D** is the $1/e^2$ diameter of the collimated beam, and **λ** is the wavelength.

The main parameters of the plano-convex aspherical lenses used in the experiments are: diameter of 6.3mm with focal length of 4.51 mm (tolerance +-1%), working distance 2.91 mm, housing dimension 10.6 mm, clear aperture 4.96 mm, and numerical aperture (NA) 0.55. The aspheres are less lossy, less bulky, and have fewer components. It is also important while collimating the beam to make sure the NA of

the lens is larger than that of the fibre or diode so that all the available light is captured. On the other hand, when focusing into a fibre, it is crucial that the NA of the focused beam is smaller than the NA of the fibre to maximize coupling efficiency (Fig.4.9).

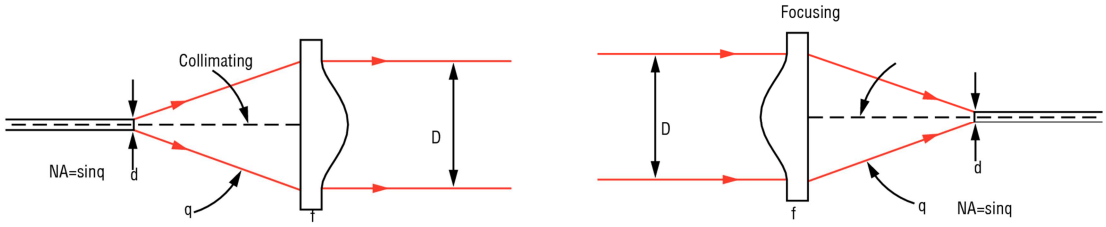

Fig.4.9 Ray trace for collimating and focusing using aspheric lens.

4.2.4 Fibre splitter.

A single mode optical coupler designed for 1310/1550nm wavelengths splits the input light into a 40/40/20 ratio with a fibre diameter of 900µm (Fig. 4.10). All legs were terminated with FC/APC (ferrule connector/angled physical contact) connectors to provide non-optical disconnect performance (Fig. 4.11). The fibre endface is polished at 8^{o} degree angle to prevent reflected light from interface travelling back up the fibre core, but instead leaks out into the cladding.

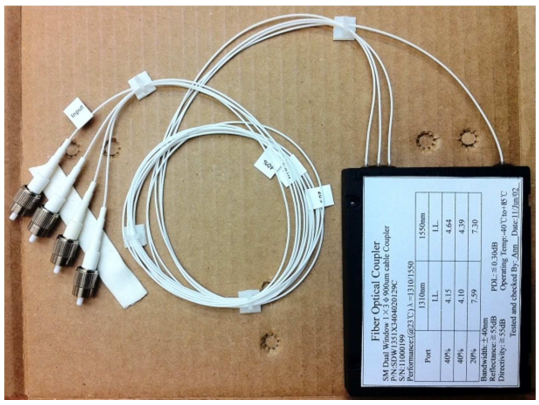

Fig. 4.10 Fibre coupler 1x3 40/40/20 split designed for 1310/1550nm.

Fig. 4.11 FC/APC (ferrule connector/angled physical contact) connector.

4.2.5 Autocorrelator.

In all experiments, a Femtochrome FR103XL/IR autocorrelator was used operating in the wavelength range λ=700 nm -1800 nm with a $LiIO_3$ crystal (1 mm/24^o) and fundamental filter λ=1100-1300nm inside. This high resolution instrument was designed for continuous monitoring and display of femtosecond and picosecond laser pulses. The autocorrelator provides a dispersion free scan range of 200 ps with high linearity. High reflecting metallic coated mirrors are used for eliminating the dispersion. The focus in the nonlinear crystal is obtained by means of a curved mirror M2 (Fig. 4.1). The standard FR-103XL is based on background-free (noncollinear) second harmonic generation and measures the autocorrelation function of repetitive ultrashort laser pulses as explained in section 4.1.1. Repetitive linear delay generation in one arm of the Michelson arrangement is introduced by a pair of parallel mirrors centred about a rotating axis (Fig. 4.12). The rotating parallel mirrors changes the optical path of the beam. This way the transmitted pulse train is delayed (or advanced) about the reference (zero delay) position. For small angular changes, the delay as a function of time is linear (Eq. 4.11) [19].

$$T = \frac{4\pi f D_M}{c} t \qquad \textbf{(4.11)},$$

where T is delay, D_M is the distance between parallel mirrors, f is the frequency of rotation, c is the speed of light.

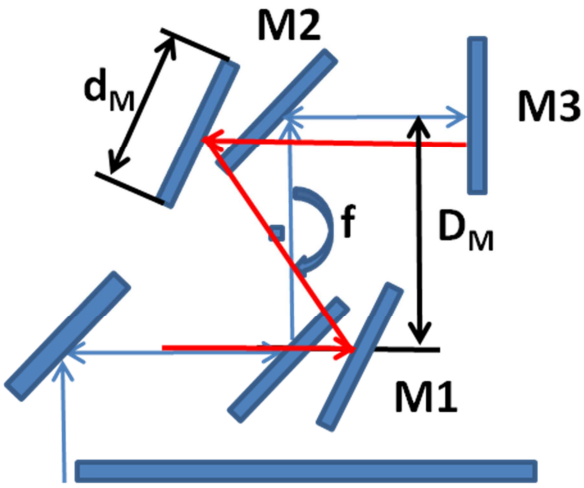

Fig. 4.12 Rotating parallel mirrors in the autocorrelator setup. D_M- the distance between parallel mirrors M1 and M2, f- the frequency of rotation, d_L-the length of the scanning mirror.

Thus the rotating mirrors provide repetitive generation of linear delay which is used for SHG and for a continuous display of the autocorrelation function of the pulses on an oscilloscope synchronized to this rotation. In the experiments, a Textronix TDS 2022B two channel digital storage oscilloscope 200MHz, 2GS/s was used. The total scan range is given by Eq.4.12.

$$T_t = \frac{\sqrt{2}d_L}{c} \qquad \textbf{(4.12)},$$

where T_t-total scan range, d_L-the length of the scanning mirror, c –speed of light.

A figure of nonlinearity over the full scan range is Eq. 4.13.

$$\mathrm{NL} = \frac{\mathrm{d_L}}{4\mathrm{D_M}} \qquad \textbf{(4.13)},$$

where NL- figure of nonlinearity, d_L-the length of the mirror, D_M-the distance between the parallel mirrors.

The delay range of the autocorrelator is proportional to the mirror size used. For long pulse widths, the effect of scan nonlinearity needs to be taken into account.

The scan mirror has a size of d=1.7'' and the distance between the mirrors D=3'', the rotating frequency is f=10 Hz. This means from the Eq. (4.11)-(4.13):

T/t=31 ps/ms;

T_t=200 ps;

NL=7%/100 ps

The T/t value is an important delay calibration factor. Once the autocorrelation is obtained the full width half maximum of the trace is multiplied by calibration factor and by factor associated with pulse shape (discussed in 4.1.1) in order to get the true value of the pulse width. In other words, the calibration factor suggests that a 31 ps pulse autocorrelation width would produce a 1 ms FWHM trace when viewed on an oscilloscope. Resolution is limited only by the SHG crystal thickness, which is typically 0.3 mm, giving a resolution of ~15 fs. Using a thinner (<0.05 mm) crystal, a resolution of <5 fs can be achieved. Figure of nonlinearity (NL) shows that for a pulsewidth as long as 100 ps, the pulsewidth measurement error due to scan nonlinearity is 7%. The sensitivity of the autocorrelator depends on the operation wavelength and the characteristics of the nonlinear crystal, an average input power (Pav) of a few mW is typically sufficient. Thus minimum detectable signal level can be as low as Ppeak*Pav= $(mW)^2$, where Ppeak is the peak power.

The precision of pulse width measurements is a bit difficult to estimate precisely. The "hardware" precision is related with the spatial calibration of the autocorrelator, but the major source of error will come from the fact that to estimate pulse duration, one has to fit a certain pulse shape to the autocorrelation function, which may not necessarily be the "actual" pulse shape. We could only "see" the actual pulse shape if a completely different type of autocorrelation is used, such as FROG. Roughly, there is a 10% error for both pulse duration and peak power.

4.2.6 RF spectrum analyzer and fast photodiode.

Rohde and Schwarz RSP Spectrum analyzer FSP-40 used in the experiment is based on a narrow band receiver for measuring high frequency signals (Fig.4.13) [15]. The frequency of a receiver is swept repetitively over the desired range of frequencies. The input signal passes through an attenuator, then through a low-pass filter, where high frequency signals are blocked, to a mixer, where it mixes with a signal from a local oscillator. The outputs of the non-linear mixer include not just two original signals but also their harmonics and the sums and differences of the original frequencies and their harmonics. Only those signals are processed further to a logarithmitic amplifier which fall within the passband of the intermediate-frequency (IF) filter. The bandwidth of the IF filter defines the frequency difference resolution called the resolution bandwidth (RB). For higher resolution, a narrower bandwidth is required but the sweep rate is decreased (or sweep time is increased) as the response time of IF filter becomes slower.

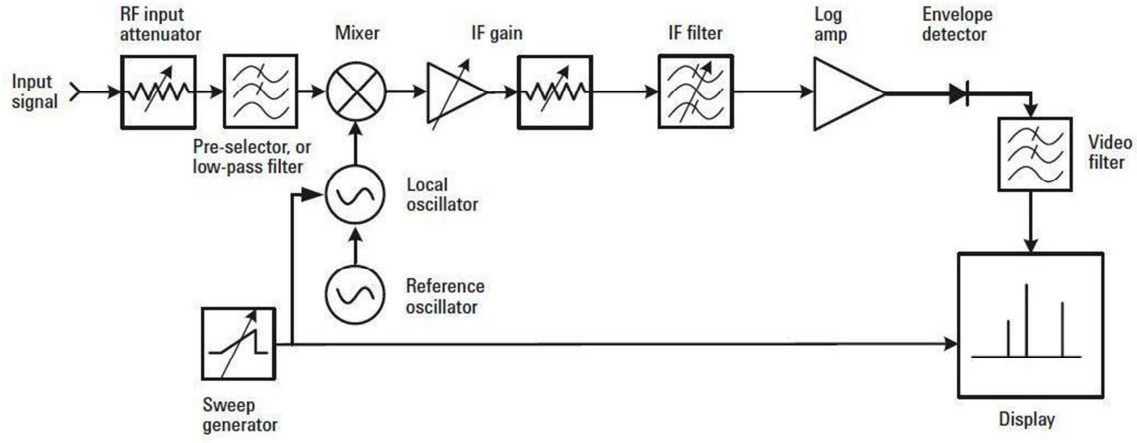

Fig. 4.13 Block diagram of a spectrum analyzer [15].

The envelope detector converts the signal voltage from the IF into power measurements (video signals). Following the power detector there is a low pass smoothing filter for providing a “clean” display of amplitude. The bandwidth of this filter is called video bandwidth (VB). If a narrow video bandwidth is chosen the sweep rate reduces as in the case of the IF filter. The ratio RB/VB determines the “noisiness” of the displayed signals. A ramp/sweep generator creates the horizontal movement across the display from left to right at the same time tunes the local oscillator so that its frequency change is in proportion to the ramp voltage. The horizontal axis of the display is linearly calibrated in frequency that increases from left to right. Setting the frequency consists of a two-step process. First the central frequency is adjusted with the central frequency control, then the frequency range (span) across the mapped display. The vertical axis is calibrated in amplitude. Logarithmic scale is used more often than the linear scale as it has a much wider dynamic range display. The top of the screen (reference level) displays the maximum power with the current settings and is usually measured in dBm. Power is converted from dBm to mW using Eq. 4.14.

$$\mathrm{X(dBm)} = 10\log_{10} P(mW) \qquad \textbf{(4.14),}$$

This means that 0 dBm corresponds to 1 mW power and 3 dBm difference corresponds to half reduction of the power. The frequency range of the spectrum analyzer is from 9 kHz (20 Hz) to 40 GHz. The speed of the RF analyzer is 2.5 ms sweep time in the frequency domain and 1 μs in the time domain. The accuracy is 0.5 dB total level uncertainty up to 3.6 GHz and <0.2 dB linearity error down to -70 dB.

In order to convert the optical signal into an electrical RF signal, a fast 29 GHz photodiode (model D-15 Newport) was used. The photodetector element is an

interdigitated metal-semiconductor-metal (MSM) structure fabricated on an InGaAs semiconductor structure. Light absorbed between the MSM fingers generates electron-hole pairs that are swept through the active region to their respective electrodes in picoseconds.

4.2.7 Optical spectrometer.

The laser spectrometer WaveScan APE (Angevandte Physik und Elektronik GmbH) RS232 version was designed for measuring the spectrum of continuous wave or high pulse repetition rate (> 4MHz) laser systems. This spectrometer is equipped with an FC/PC type connector for fibre input and consists of the spectrometer optics with a power adaptor. The optics unit is controlled by a personal computer (PC) via the RS232 serial port using the control software LasScan. This software manages the data transfer between the spectrometer and the PC and allows quasi real-time graphical monitoring of the spectra as well as data storage and processing. The wavelength range is from 800 nm to 1600 nm, bandpass < 0.2 nm, wavelength accuracy $\pm$0.2 nm and measuring rate of approximately 6 spectra per second. The WaveScan is a grating spectrometer in the Littrow configuration with a focal length of 200 mm (Fig. 4.14) [20]. The diffraction grating rotates with a rate of about 6 rounds per second and separates the several spectral components of the spectrum from the incident beam. The Si photodiode measures the intensity of the light in various regions of the spectrum every round trip.

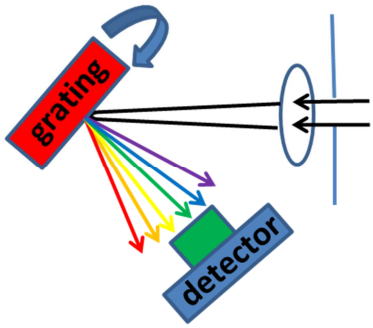

Fig. 4.14 Schematic of grating spectrometer.

At a distinct angular position of the grating a high precision trigger starts the measurement. Following that a fixed number of data points (exactly 32768) are taken with a sampling rate of about 1.3 MHz. A subset of these data is transferred to the control PC on request.

4.2.8 Power meter.

A power meter of model 2936C Newport was used for measuring average power with high power thermopile detector 818P-001-12 (with IRF1 filter). Thermopile detectors have become a popular choice for power measurements primarily due to the higher power measurement capability as well as the broadband nature of the detectors. The responsivity values for thermopiles are relatively flat across the operating wavelength range of the detector which makes it ideal for broadband applications such as solar measurements [21]. This detector can measure between 1 μW and 1 W of average power. The effective aperture diameter was 12 mm, wavelength range from 280 nm to 1.36 μm, power noise level of $\pm$ 0.5 μW, typical sensitivity of 180 mV/W, calibration uncertainty of $\pm$2.5 % and power resolution of $\pm$0.5 %.

4.3 Conclusion.

In this chapter, characterisation techniques were presented in detail. The autocorrelation technique for pulse measurement as well as the relationship between time domain and frequency domain representation of a spectrum were explained. Optical spectra measurement gives information about the central emission wavelength as well as whether the pulse is chirped or transform-limited. The experimental setup used for characterising the lasers was presented in Fig. 4.6. Optical elements such as an optical isolator, half plate, aspheric lenses, fibre splitter involved in the setup are explained. In addition, the basic parameters of the autocorrelator, RF spectrum analyzer, optical spectrometer and power meter are discussed.

4.4 References.

1. LeCroy. *LabMaster 10 Zi Oscilloscopes*. Available from: http://www.lecroy.com/labmaster/labmaster10zi/.
2. Andrews, J.R., *Comparison of Sampling Oscilloscopes with ~35 ps Transition Durations*, in *Picosecond Electronics and Optoelectronics II*, F.G. Leonberger, et al., Editors. 1987, Springer: New York. p. 64-66.
3. Picosecond_Pulse_Labs. *Comparison of Ultra-Fast Rise Sampling Oscilloscopes. Application Note AN-2a*. Available from: http://www.picosecond.com/objects/AN-2A.pdf.
4. Hamamatsu. *Femtosecond streak camera C6138 (Fesca-200)*. Available from: http://sales.hamamatsu.com/assets/pdf/hpspdf/e_c6138.pdf.
5. Koda, R., et al., *100 W peak-power 1 GHz repetition picoseconds optical pulse generation using blue-violet GaInN diode laser mode-locked oscillator and optical amplifier.* Applied Physics Letters, 2010. **97**(2): p. 021101-3.
6. Jaanimagi, P.A. *Breaking the 100-fs barrier with a streak camera*. 2004. San Diego, CA, USA: SPIE.
7. Diels, J.C. and W. Rudolph, *Ultrashort Laser Pulse Phenomena*. 1995, New York: Academic Press.
8. Trebino, R., *Frequency-Resolved Optical Gating: The measurement of Ultrashort Laser Pulses*. 2002, Boston: Kluwer Academic Publishers.
9. Ippen, E.P. and C.V. Shank, *Techniques for Measurements*, in *Ultrashort Light Pulses*, S.L. Shapiro, Editor. 1977, Springer: New York.

10. Sala, K., G. Kenney-Wallace, and G. Hall, *CW autocorrelation measurements of picosecond laser pulses.* Quantum Electronics, IEEE Journal of, 1980. **16**(9): p. 990-996.

11. Diels, J.-C.M., et al., *Control and measurement of ultrashort pulse shapes (in amplitude and phase) with femtosecond accuracy.* Appl. Opt., 1985. **24**(9): p. 1270-1282.

12. Vasil'ev, P., *Ultrafast Laser Diodes: Fundamentals and Applications*. 1995, London: Artch House.

13. Bradley, D.J. and G.H.C. New, *Ultrashort pulse measurements.* IEEE Proceedings, 1974. **62**.

14. Fourier, J.B.J., *The Analytical Theory of Heat*. 1822.

15. Agilent_Technologies *Agilent Spectrum Analysis Basics: Application Note 150*.

16. Newport *Application Note 33: Amplitude and Phase Characterization of Ultrashort Laser Pulses*.

17. QIOPTIQ *The LINOS Faraday Isolators*.

18. Newport *Application Note 3: Polarization and Polarization Control*.

19. Yasa, Z.A. and N.M. Amer, *A rapid-scanning autocorrelation scheme for continuous monitoring of picosecond laser pulses.* Optics Communications, 1981. **36**(5): p. 406-408.

20. Demtroder, W., *Laser spectroscopy: Basic Concepts and Instrumentation*. Third edition ed. 2003, New York: Springer. 989.

21. Newport *Photonics Technical Note N 11: Power meters and Detectors*.

Chapter 5. Different mode operations in monolithic quantum dot lasers.

5.1 State of the art: multi-wavelength ultrashort pulse generation.

The development of multi-wavelength ultrashort-pulse laser systems is required for a variety of applications such as time-domain spectroscopy, nonlinear optical frequency conversion, optic sensing and wavelength division multiplexing communication systems. Solid state based two-color mode-locked lasers systems have been very well developed using different materials such as Ti:Sapphire [1-2], Erbium-doped fiber [3], and ceramic lasers [4]. For example, two perfectly synchronized pulse trains that are independently tunable over a 100 nm wavelength range and with pulse durations below 30 fs were demonstrated [1]. A passively mode-locked erbium-doped fibre ring laser also exhibited the possibility of dual-wavelength short pulse generation with a 43.4 nm wavelength tuning range [3]. Recently, a two-wavelength mode-locked Yb:YAG ceramic laser simultaneously generating 380 fs pulses at 1033 nm and 1047 nm was demonstrated [4]. As solid state laser systems are not cheap and bulky, new technologies that are based on diode lasers are developed due to compactness and low cost of these devices. A single quantum well mode-locked laser in an external cavity configuration generates picosecond pulses in the order of 100 ps and 70 ps involving different transition states GS or ES respectively [5]. Monolithic QD based mode-locked edge-emitting lasers have also shown a great potential as compact high power ultrashort pulse versatile optical sources [6-8] due to the quantum confinement of the carriers in all three dimensions which leads to the properties discussed in

section 2.3. The discrete energy levels displayed by QD materials can also be exploited to access distinct spectral bands in the same device, adding an extra level of functionality to these ultrafast lasers. For instance, it is possible to achieve two-state lasing using the ground state (GS) and excited state (ES) transitions in a QD laser [9]. Alternatively, femtosecond pulses were generated from a Cr4+: forsterite mode-locked laser incorporated within a cavity a QD-based semiconductor saturable absorber mirror (SESAM) involving not only GS but ES as well [10]. First, an optically gain switched quantum-dot edge-emitting laser generating picosecond pulses from GS and ES states was demonstrated [11]. In this context, stable mode-locked operation involving either GS or ES in a two-section QD laser diode was shown for the first time, by controlling the injection current and reverse bias to force laser emission to switch from the GS to the ES transition [12-13]. Self-pulsation regimes in two-state QD laser operating simultaneously on the GS and ES were reported [14-15]. Furthermore, reverse GS/ES transitions were observed by Breuer et.al [16-18]. Such versatility of the QD mode-locked diode laser could enable its use as a two-band clock recovery source [19-20]. Moreover, dual-GS-wavelength mode-locking or continuous wave operation was reported by a number of groups, and variously attributed to Rabi-oscillations, AC-Stark effect, state filling effect, spectral hole burning or homogeneous and inhomogeneous broadenings, as the physical mechanism of operation is not yet fully understood [21-24] (more details in section 6.1.2). In addition, by changing structural parameters (the cavity length and number of QDs in the active region) of the laser GS or ES emission can be achieved [9, 25]. In this context, compact cheap electrically pumped QD-based mode-locked lasers are very promising candidates as versatile next generation optical sources which can be successfully applied to time-domain spectroscopy, wavelength-division multiplexing and ultrafast optical processing.

In section 5.2, the investigation of the influence of bias conditions on the pulse characteristics generated via ES in a two-section InAs/GaAs QD laser is presented [26]. In section 5.3, a dual-wavelength mode-locking regime is demonstrated, involving both the ground and excited-state transitions with a spectral separation of 83nm [27], which is the widest spectral separation ever to be observed in a non-vibronic dual-wavelength mode-locked laser. In section 5.4 the influence of the cavity length and number of QD layers in the device on pulse duration, and peak power along with achieving ES emission is outlined.

5.2 Ultrashort pulse generation via ground and/or excited states.

5.2.1 Introduction.

A thorough investigation of the dependence of the pulses generated via ES transition on the driving conditions has not been performed before. Indeed, the bias conditions for obtaining mode locking via only the ES transition were narrow and the transition between regimes displayed hysteresis [12-13], which inhibited a systematic characterization of the mode-locking regime involving solely ES. The understanding of bias factors influencing the pulse duration is important in order to establish the optimal bias condition rules for ultrashort pulse generation as the ES shows significant tolerance to optical feedback, compared to the GS mode-locking regime [28]. This is of importance for applications, as the use of an optical isolator can be avoided. The numerical analysis of the frequency chirp showed that a QD laser emitting from the GS gives a chirp considerably higher than from the ES, due to a large refractive index variation at the GS lasing wavelength caused by the accumulated carriers in the ES [29]. Moreover, the use of the ES transition can effectively extend the spectral range of laser emission towards shorter wavelengths.

5.2.2 Device structures.

A two-section QD laser diode was grown by molecular beam expitaxy on a GaAs substrate. The active region incorporated 5 layers of InAs QDs. The laser diode length was 2 mm, with an absorber section of 300 μm and the ridge width was 6 μm. The laser was tested at 20^{o}C controlled by a Peltier cooler. The front and back facets of the laser diode were anti-reflection (~3%) /high-reflection (~95%) coated respectively. The setup used in this experiment is almost the same as shown in Fig.4.6 and described in section 4.2. The only difference is related to power measurements of both GS and ES transitions which were performed with the grating as the light from GS and ES are reflected at different angles due to variance of refractive index between the bands. Initially the ratio of the powers of incident light to reflected light from the grating was obtained for each band when the other band is absent. Then at the regime of the simultaneous presence of both bands the power of the reflected light is measured of each band separately and recalculated using obtained ratios in order to achieve real values for the output powers. The pulse durations in both GS and ES spectral bands were measured by a non-collinear autocorrelator based on second-harmonic generation as explained in section 4.2.1. The spectral characteristics were measured by a spectrometer and mode-locking performance was further investigated with an RF spectrum analyzer in combination with a high-speed 29GHz photodiode. Mode-locking was achieved in a two-section laser by applying forward current to the gain section and reverse bias to the absorber, which is closer to the back facet of the laser and acts as the discriminator of the cavity loss for ultrashort pulse generation as explained in chapter 2.

5.2.3 Experimental results and discussion.

By varying the bias conditions, different mode-locking regimes were observed involving ground and excited states (Fig. 5.1). Ground state mode-locking (GSML) was observed at a wavelength λ=1250 nm and repetition rate of 20.1 GHz, while for excited-state mode-locking (ESML), λ=1177 nm and the repetition rate was 19.8 GHz. In order to better compare the dependence of the pulse duration and average power with increasing current between the GSML and ESML regimes, a fixed reverse bias of 6.15 V was applied to the saturable absorber, which allowed the observation of three different mode-locked regimes, as depicted in Fig.5.1.

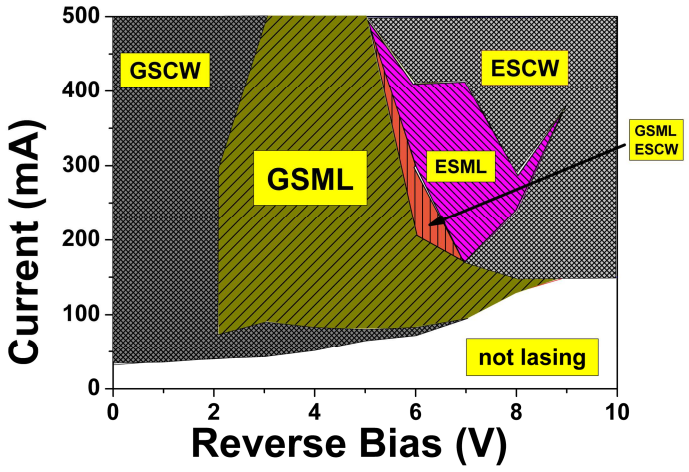

Fig. 5.1 Map of the different Mode-locking regimes with bias conditions: GSML – Ground state mode-locking; GSML ESCW- Ground state mode-locking in coexistence with excited state continuous wave emission; ESML – Excited state mode-locking.

The threshold current density under such reverse bias was 715 A/cm^2. For a bias current of up to 200 mA, it was observed (Fig. 5.2 a) that the pulse duration of GSML increased with current, which is mostly due to the well-known effect resulting from the increase in self-phase modulation effects with optical power, which in combination

with the group velocity dispersion in the semiconductor laser leads to a pulse broadening with increasing current [30].

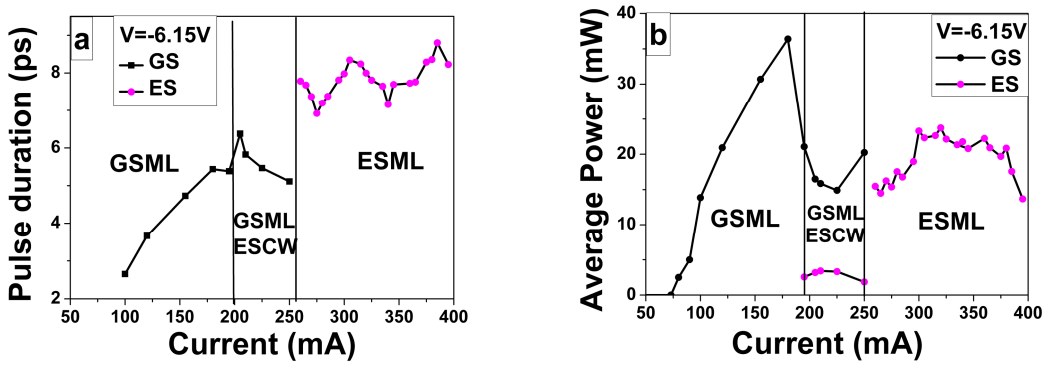

Fig. 5.2 Dependence on injected current of **(a)** pulse duration, **(b)** average output power for GS and ES mode-locking at 6.15 V reverse bias. GSML – Ground state mode-locking; GSML ESCW- Ground state mode-locking in coexistence with excited state continuous wave emission; ESML – Excited state mode-locking.

Between 200 mA and 250 mA we also observed a particular regime of GSML, where the coexistence with ES (CW) has the effect of reducing the pulse duration with increasing current. A similar mode-locking regime has been investigated and reported [31]. By increasing the current further, only ESML is observed, due to the gain saturation across the GS transition and the higher saturated gain that characterizes the ES. As evidenced in Fig. 5.2 a, the pulse duration in the ESML regime varies between 7 ps and 9 ps, thus exhibiting wider pulse durations than what was obtained for GSML (it is important to stress that ESML was only achieved at the expense of injecting high drive currents, which usually is associated with longer pulse durations). The corresponding average power was lower compared to that of the GS due to the increased non-saturated losses (Fig. 5.2 b). The output power changed between 15 mW and 25 mW with increasing current. The dependence of the pulse duration and

average power were also investigated with a fixed injection current (300mA) applied to the gain section, while the reverse bias applied to the saturable absorber was increased, resulting in the observation of the GSML and ESML regimes in succession (Fig. 5.3). As expected, the pulse duration of GSML was observed to decrease from 15.5 ps to 6 ps with reverse bias due to the fact that the absorption recovery becomes increasingly faster [8, 32-33]. Pulses are almost twice shorter compared to Kim.*et.al*. , where pulse duration changed from 25 ps to 14 ps with reverse bias [19]. For a higher value of reverse bias, the GSML regime is switched to an ESML regime, and whereby the duration of the pulses generated via ESML are in the range of 9.3 ps and 10.3 ps with increasing reverse bias up to 8 V while the average power continues to decrease with reverse bias as is also observed in the GSML regime. It is interesting that in a previous report [19], the ESML was achieved at lower reverse bias between 0-2 V with the pulse decreasing from 18 ps to 10.8 ps. ES lasing was observed only at low reverse bias, but not at the higher reverse bias due to the higher gain saturation required across the GS transition as explained in section 2.3.3. From this investigation, it can be concluded that such device can be very promising for the generation of ultrashort pulses using compression techniques, not only in GS but in ES transitions as well.

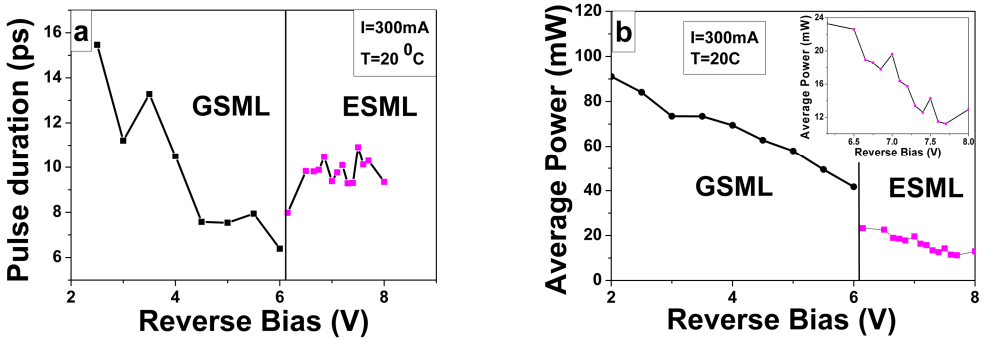

Fig. 5.3 Dependence on reverse bias of **(a)** pulse duration **(b)** average output power for GS and ES mode-locking at I=300mA current. **Inset**: average power of ES band with reverse bias; GSML– Ground state mode-locking; ESML – Excited state mode-locking.

The differences in pulse dynamics of GSML and ESML can be partially explained by the different intradot relaxation dynamics of the absorber for GS or ES transitions. As recently reported by Piwonski *et al.* [32], the absorption recovery via the GS is mediated mostly by phonon-assisted processes, while the ES absorption recovery is dominated by Auger-type processes. It was also shown [32] that the absorption recovery time reduced most significantly with increasing reverse bias for the GS, while the absorption recovery time for the ES was shown to be somewhat less sensitive to the reverse bias applied – and particularly so for higher values of reverse bias (5-9 V), which indeed encompasses the range of reverse bias values required to achieve stable pulse generation via ESML [26].

5.2.4 Conclusion.

The influence of the bias conditions (current and reverse bias) on the characteristics of the pulses generated via ESML in a monolithic two-section QD laser has been investigated. It is shown that the pulse duration of ESML does not exhibit as strong a dependence on the driving conditions as in the GSML regime, where the pulse duration is highly dependent on the applied gain current and absorber reverse bias. The reverse bias was not observed to produce a significant effect on the pulse duration, and as such it should be kept as low as possible in order to maximise the average power and consequently the peak power generated.

5.3 Dual-wavelength mode-locking via ground and excited states.

5.3.1 Introduction/State of the art.

In the previous section three different regimes of mode-locking: GSML or GSML with ESCW and ESML were demonstrated. Nevertheless, simultaneous generation of picosecond pulses from the GS and ES was not achieved so far from QD based mode-locked lasers but only the pulses from one of the states, GS or ES, were observed by changing bias conditions (gain current and absorber reverse bias). In this section a simultaneous dual-wavelength passive mode-locking regime is presented from a QD two-section monolithic laser with picosecond pulses generated from both GS (λ=1263 nm) and ES (λ=1180 nm) transitions simultaneously with the widest spectral separation of 83 nm ever observed in a non-vibronic ultrafast laser [27], which is slightly lower than previous results from a solid-state based laser [1]. The experimental setup described in section 4.2 is used for characterization of 2 mm two-section QD-based mode-locked devices. The structure of the device is the same as in the previous section (5.2.2) but emitting at a different wavelength as the result of formation of different size QDs during the growth process.

5.3.2 Experimental results and discussion.

The regime of simultaneous mode-locking in GS and ES was attained for current levels in the gain section between 330 and 430mA, and values of reverse bias between 6 and 10V in the saturable absorber section. A map depicting the different mode-locking regimes is represented in Fig. 5.4. It is interesting that ESML was observed both before and after the dual-wavelength mode-locking regime which can be attributed to interplay between the modes due to nonlinear absorption.

As can be seen from the table 5.1 the central emission wavelengths were ~1180 nm and ~1263 nm for ES and GS, respectively. The pulses during the simultaneous dual-wavelength mode-locking regime can be as short as 5.9 ps and 7 ps for GS and ES respectively depending on bias conditions. As an example, optical and RF spectra for a current of 425 mA applied to the gain section and a reverse bias of 6V applied to the absorber section are presented (Fig. 5.5 a) resulting in the spectral separation between GS and ES of 83 nm. As refractive index varies with wavelength, the pulse repetition rates for ES and GS were 0.5 GHz different, which were 19.6 GHz and 20.1 GHz respectively (Fig. 5.5 b). The autocorrelation traces obtained for the ES and GS were fitted using a Gaussian function and resulted in pulse durations of 5.9 ps for the GS and 8.6 ps for the ES bands, obtained for a reverse bias of 6 V and an injection current of 425 mA. Knowing the pulse duration, central emission wavelength and full width half maximum of optical spectra, the time-bandwidth product (TBWP) was estimated for the GS as 6.7 and for the ES as 9.

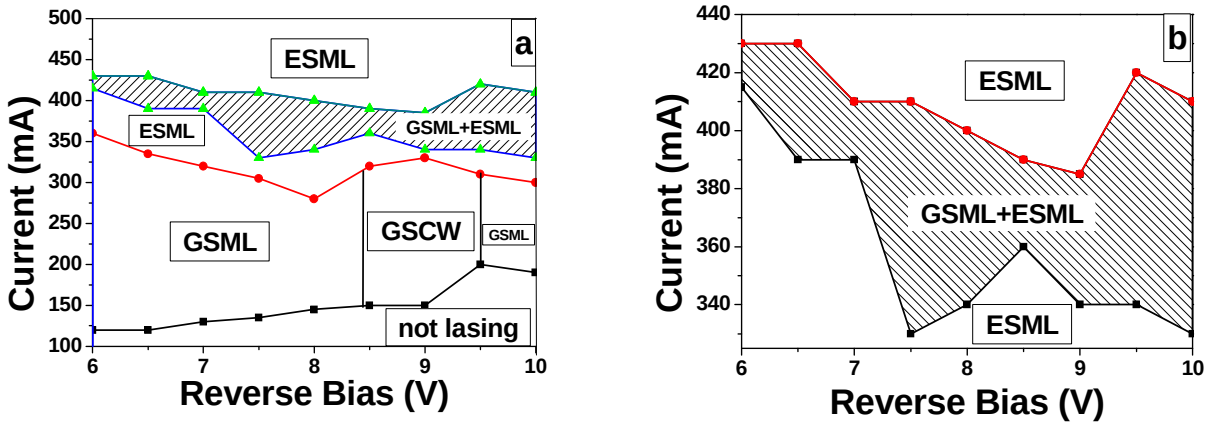

Fig. 5.4 (a) Mapping of the different operating regimes observed in 2 mm QD mode-locked laser. **(b)** Mapping of the dual-wavelength mode-locking regime here described (GSML+ESML). Legend: GSML– ground-state mode-locking; ESML– excited-state mode-locking; GSCW-ground-state continuous wave operation.

These pulse durations and TBWPs are similar to those previously observed in separate GS/ES mode-locking [13, 19]. The average power measured for the GS was 21.3 mW and for ES 32.1 mW, resulting in peak powers of 261 mW and 128 mW respectively (see table 5.1).

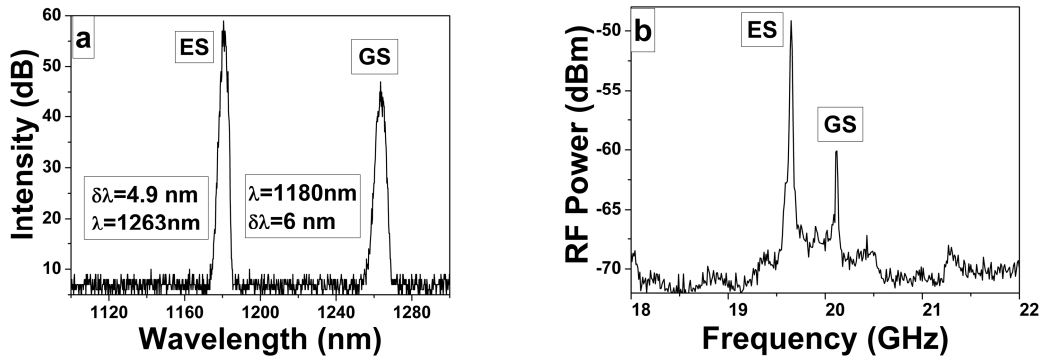

Fig. 5.5 (a) Optical spectrum and **(b)** RF spectrum characteristic of the dual-wavelength mode-locked regime, for an injection current of 425 mA and reverse bias of 6 V.

The difference in RF spectrum between GS and ES of 10 dB (shown in fig. 5.5b) is attributed to the different level of average power and pulse durations. As the pulse duration becomes broader according to the Fourier analysis, the amplitude of the Fourier transform of a Gaussian pulse train becomes higher.

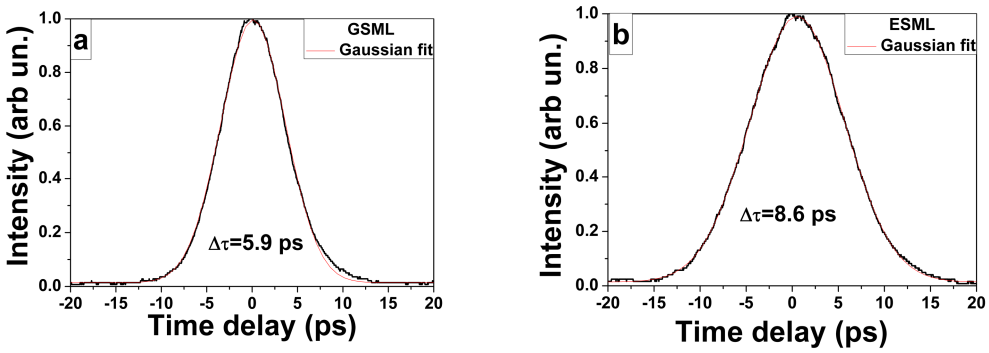

Fig. 5.6 Autocorrelation traces for (a) GS mode-locking and (b) ES mode-locking at 6 V reverse bias and 425 mA gain current.

The power ratio and pulse duration ratio of ES/GS for this bias condition (6 V, 425 mA) are 1.5 and 1.46 respectively. As a result, the amplitude of the Fourier transform for the ES will be 2.2 times higher (3.5 dB difference) than for the GS. Fourier transform amplitude is a double of amplitude in the electrical power spectrum. In other words, the RF peak for ES will be higher than for GS in the range of 7 dB. The remaining difference between the experimental observation of 10 dB and the above calculated 7 dB is attributed to the experimental conditions: variation in the average power, the RF spectrum settings and frequency response (flatness). The dual-wavelength regime of operation from a QD-based mode-locked two-section laser was proved by the numerical model based on the delay differential equation approximation [34] taking into account the dynamics of the quantum dot material [35]

and described in detail ref. [27]. Dual-wavelength emission is possible for reverse biases higher than 6 V due to the decrease of the absorber recovery time assisted by the tunnelling carrier escape mechanism [33].

Table 5.1 Bias conditions: reverse voltage to the absorber (**V)** and forward current to the gain section **(I)**; pulse duration **(τ)**, Average power **(Pav)**, Peak Power **(Ppeak)**, Time bandwidth product **(TBWP)**, full width half maximum of optical spectra (**Δλ**), central wavelength **(λ)**, GS – ground state (black) or ES-excited state (red) of dual-mode regime in QD-based mode-locked laser.

V (V)	I (mA)	τ (ps)	Pav (mW)	Ppeak (mW)	TBWP	Δλ (nm)	λ (nm)	State
6	425	5.9	32.1	261.6	6.7	6.0	1263.40	GS
6	430	7.1	35.5	249.7	9.5	7.1	1263.74	GS
6.7	400	5.9	17.1	144.1	7.0	6.2	1263.03	GS
7	394	6.6	11.8	89.9	7.6	6.2	1263.38	GS
8	375	9.3	12.1	65.2	8.0	4.6	1263.52	GS
8	390	7.1	12.5	87.9	6.9	5.2	1265.00	GS
9.2	380	7.3	10.5	71.6	7.3	5.3	1264.18	GS
9.3	344	9.4	8.3	44.0	8.4	4.7	1263.28	GS
6	425	8.6	21.4	128.4	9.0	4.9	1180.55	ES
6	430	8.8	11.8	67.6	9.8	5.2	1180.70	ES
6.7	400	7.9	21.7	136.7	8.2	4.8	1180.16	ES
7	394	8.7	24.5	140.9	9.0	4.8	1179.87	ES
8	375	8.5	29.2	171.9	8.1	4.4	1179.07	ES
8	390	8.6	33.7	196.6	8.4	4.5	1179.07	ES
9.2	380	8.6	11.6	67.0	8.0	4.3	1179.14	ES
9.3	344	7.0	34.8	250.2	6.7	4.5	1178.49	ES

The relatively narrow region of dual-wavelength regime is connected with the dynamics between the two states (GS, ES) which gives rise to instabilities due to the carrier intraband capture and escape processes between states. As a continuation of the presented results, stable two-state mode-locking was recently achieved from a

two-section mode-locked laser incorporating two repeats of three chirped QD layers [16-17]. It is interesting that reverse-emission-state-transition was observed where mode-locking starts at the ES emission as 0 V reverse bias was applied. Dual-state mode-locking was achieved at lower gain current between 130 mA- 170 mA compared to the above results (330 mA- 430 mA) because loss in the absorber is increased with voltage applied. The higher absorber-to-gain ratio 1:10, compared to 1:7, leads to the different the gain and absorber dynamics in the gain and the saturable absorber. The effect of the fast relaxation of ES carriers in the GS, so-called photon pumping or photon recycling process, results in the reduction of the absorption at the GS wavelength at the saturable absorber allowing the coexistence of GS and ES mode-locking [16-17].

5.3.3 Conclusion.

A dual-wavelength passive mode-locking regime of operation was investigated and presented for the first time where picosecond pulses are generated from both GS (λ=1263 nm) and ES (λ=1180 nm) in a two-section GaAs-based QD laser. Measured optical spectra showed a spectral separation of 83 nm which is the widest ever observed in a dual-wavelength mode-locked non-vibronic laser.

5.4 Influence of the cavity length and number of QD layers on ultrashort pulse generation.

5.4.1 Introduction.

The importance of a reliable saturable absorber for short pulse generation in passively mode-locked lasers was understood more than 20 years ago [36]. It was found that in multi-section monolithic devices pulse width and peak power show better results for mode-locked lasers with a longer passive section [37]. Sub-picosecond pulses (796 fs) were generated in a 20 GHz passive mode-locked quantum-dot laser diode incorporating 5 layers of QD in the active region with an absorber-to-gain ratio of 1:4 [38]. The ratio between the gain section and absorber plays a vital role in ultrashort pulse generation. As explained in [8] an absorber-to-gain ratio in QD lasers less than 1:3 is not desirable as there is not enough gain to overcome the losses in the absorber section, while an absorber-to-gain ratio more than 1:14 is not favourable for mode-locking due to insufficient saturable absorption. In this context, the influence of nonlinear absorption saturation and the Quantum Confined Stark effect in a QD laser on bias conditions were studied [39]. The understanding of ultrafast QD absorber dynamics gives further insight into pulse broadening/shortening mechanisms [40].The interrelation of the structural parameters (cavity length, number of QD layers) with optical characteristics (threshold current density, regime of operation GS/ES) of the laser working in continuous wave (cw) mode have been reported in the past [25, 41-43]. In this section**,** the dependence of pulse duration, average power, peak power on the number of QD layers incorporated in the two-section QD based mode-locked laser is presented. In addition, the interplay between GS and ES regimes of operation for a 1.3 mm cavity length is demonstrated.

5.4.2 Device structures.

The experimental setup described in section 4.2 is used for characterization of the two-section QD-based mode-locked lasers.

Investigated lasers had 2 mm and 1.3 mm total cavity length with the absorber of 300 μm resulting in the gain-to-absorber ratios of 1:6 and 1:4 respectively, which is very favourable for stable mode-locking as discussed above [8]. All lasers had a ridge waveguide width of 6 μm, the active region incorporated 5, 10 or 15 layers of QDs grown by the Stranski-Krastanow method as described in section 2.2. All lasers were maintained at 20^{o}C by Peltier cooler.

5.4.3 Experimental results and discussion.

Pulse duration dynamics with bias conditions for 2 mm devices with different number of QD layers (5, 10, 15) are presented in Fig. 5.7. Pulse duration changes from 1ps to 10 ps depending on applied forward current and reverse bias to the absorber. Pulse broadening with increasing gain current for all devices is attributed to a self-phase modulation effect [30]. The shortest pulse duration of 1 ps from a 10 QD layer laser was observed just above the lasing threshold with 6 V reverse bias and 122 mA forward current. The central emission wavelength for such bias conditions was around 1253 nm with a full-width half-maximum of 3.67 nm resulting in a TBWP of 0.7, which indicates that the pulse is not transform limited. The exponential decrease of pulse duration was observed for all devices and explained by exponential dependence of the absorber recovery time on the applied reverse bias [44-45]. The range of mode-locking for a 5 QD layer laser is between 4 V and 9 V with current range from 140 mA to 400 mA (Fig. 5.7 a). As the number of QD layers is increased to 10, the range of mode-locking is broadened and shorter pulses can be generated (Fig. 5.7 b). A 15 QD layer laser showed the widest range of mode-locking from 2 V to 10 V and driving current from 160 mA to 500 mA. The threshold current is higher for this laser as more gain is required to overcome optical losses. In Fig. 5.8 peak power dynamics are shown. The variation of peak power with reverse bias does not exhibit a clear trend as the increase in average power is somewhat compensated by the pulse broadening. The highest peak power of about 600 mW is achieved for the low current region of a 10 QD layer laser due to a higher average power than for the 5 QD layer laser and shorter pulse generation. As can be seen in Fig. 5.8 b) and c) peak power with increased number of

layers doesn't change much as broadening of the pulse balances the increased average power.

Furthermore, laser emission involving the ES transition was observed only for 5 layer devices as the lower number of layers allowed for an early saturation of the GS and achievement of the ES laser emission. ES mode-locking was observed for a gain current higher than 300 mA and reverse bias higher than 6 V in the absorber for the 2 mm long laser. In order to induce a transition from GS to ES emission, it is important to saturate the gain associated with the GS transition. This can be achieved by either increasing the forward current in the gain section, and/or by increasing the reverse bias in the saturable absorber, which leads to an increase of the GS non-saturated losses and consequently to an earlier saturation of the GS gain. Another way of enabling an easier access to ES emission is by decreasing the length of the laser resulting in a lower GS gain which is unable to compensate the total loss in the cavity [9, 25]. As an example, it was shown that ES emission from a 1.24 μm laser incorporating a single InAs quantum-dot layer appears for a laser cavity less than or equal to 1.5 mm [25]. In addition, a 3 QD layer-laser exhibited only ES lasing for a short cavity in the range of 1 mm to 2 mm long [9]. However, the higher the number QD layers the smaller the effect of gain saturation appears to be [46]. For example, a 10 QD layer InGaAs laser provides enough gain for GS lasing in a broad-area 1 mm long stripe laser [47].

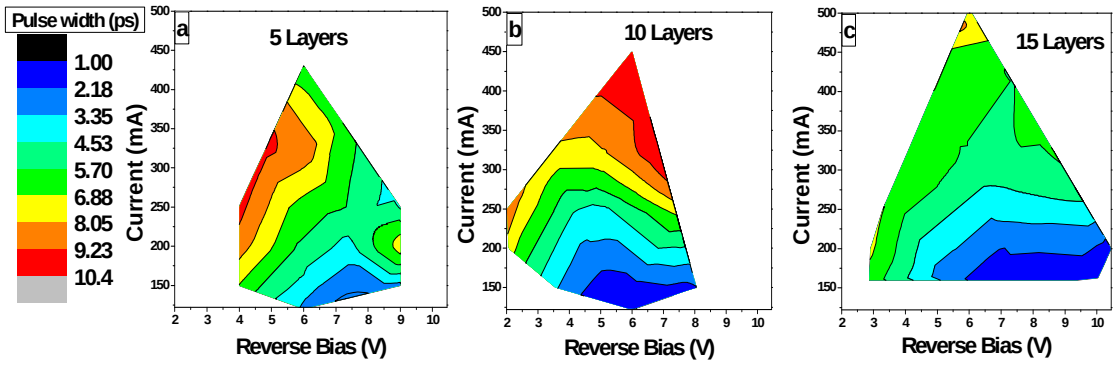

Fig. 5.7 Pulse width dynamics with bias conditions for 2 mm laser with **(a)** 5, **(b)** 10 and **(c)** 15 QD layers. Number of measured points is ~ 1600.

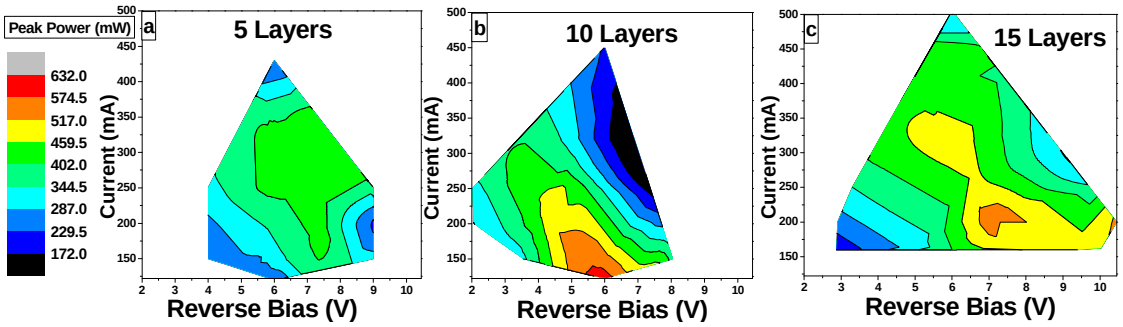

Fig. 5.8 Peak Power dynamics with bias conditions for a 2 mm laser with **(a)** 5, **(b)** 10 and **(c)** 15 QD layers. Number of measured points is ~ 1600.

In this context, a shorter device of 1.3 mm long with a 300 µm absorber and 5 QD layers in the active region was investigated. As the result, mode-locking from ES at ~1188 nm with or without coexistence of CW emission from GS at ~1274 nm was observed as depicted in Fig. 5.9 a), b) for operating temperatures of 20 and 14 ^{o}C respectively.

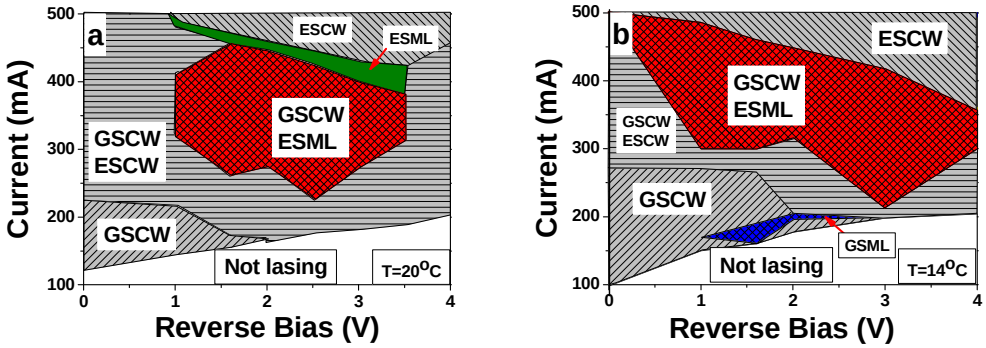

Fig.5.9 Mapping of mode-locking regimes observed for a 1.3mm long 5QD layers device, under an operating temperature of **(a)** 20°C and **(b)** 14°C. GS/ES: ground-state/excited state. CW/ML: continuous-wave/mode-locked operation.

ESML without the coexistence of GSCW was observed only for currents higher than 400 mA at 20°C operating temperature of the laser (Fig. 5.9 a). As the operating temperature was lowered to 14 °C a small region of GSML was noticed (Fig. 5.9 b) due to the fact that the GS intensity increases dramatically with decreasing temperature, but at the same time the ES intensity doesn't change significantly with temperature [48]. The region of ES mode-locking with GS-CW also becomes slightly broader as the temperature decreases. Output power for different states was measured at 0 V, 2 V and 3.5 V reverse bias (Fig. 5.10 a, b, c). As can be seen, in a short cavity laser at 0 V reverse bias both states exist in CW but when reverse bias is applied (2 V, 3.5 V) to the absorber section the ES power is increased whilst GS power decreases and ESML can be achieved due to the saturation of the GS emission. With applied voltage the range of existence of GS continuous-wave (CW) emission decreases from almost 400 mA (from 125 mA to 500 mA for V=0V) to less than 200 mA (from 188 mA to 380 mA for V=3.5 V). This is explained by the fact that the losses in the saturable absorber are

increased with reverse bias and due to the finite number of QDs, GS gain is more quickly saturated with increasing current. As a result the ES emission plays a more dominant role. As shown in Fig. 5.10 b) and c) ES mode-locking is achieved with the coexistence of GS, and even without GS at high voltage, and at the expense of the gain current. Average power of GS for 2 mm long devices increases with current then drops with coexistence of ES. In the case of the shorter 1.3 mm cavity GS average power for a reverse bias of 0 V behaves similarly as can be seen in Fig. 5.2(b) to the 2 mm device and increases in the first place up to 47 mW for current from 125 mA to 240 mA and then the power drops to 28 mW as ES appears. With further increased current GS power, along with ES power, increases. At a current of 420 mA the power level of GS and ES is the same at around 45 mW. Higher applied gain current results in lower GS power and higher ES power. As the reverse bias increases up to 3.5 V the power level of GS reaches a maximum 8.6 mW as ES emission becomes more favourable due to GS saturation. The highest average power of 84.5 mW can be attained in the ES mode-locking regime at 2 V reverse bias and 450 mA gain current. The average power for ES increases as applied voltage increases up to 2 V and then decreases with voltage while for 2 mm devices the average power always decreases with reverse bias for both GS and ES bands as shown in Fig. 5.3 (b). The increase of average power of ES is associated with gain saturation of GS while the following decrease of average power can be explained by an increase of the total loss at the expense of reverse bias.

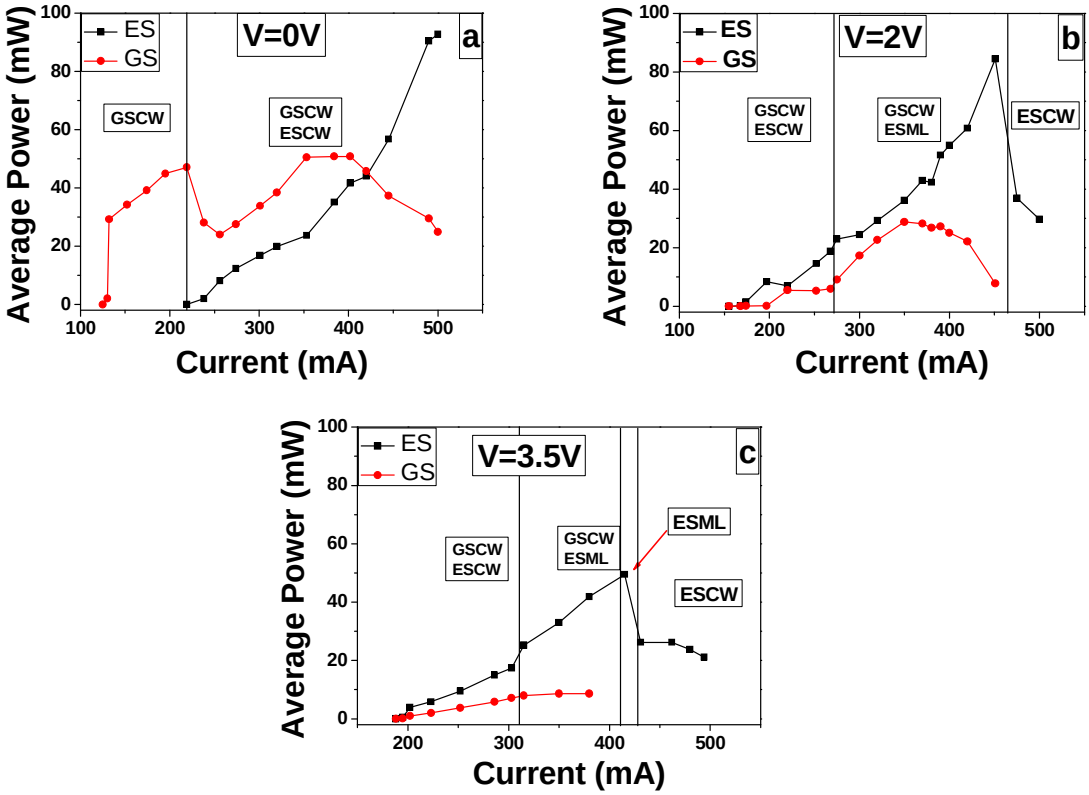

Fig. 5.10 Average power dynamics for a 1.3 mm long device having 5 QD layers with **(a)** 0 V, **(b)** 2 V and **(c)** 3.5 V reverse bias. GS/ES: ground-state/excited state. CW/ML: continuous-wave/mode-locked operation.

The shortest pulse duration obtained for ES the spectral band is 4.6 ps at 2.5 V reverse bias and 230 mA gain current with 16.6 mW average power (Fig. 5.11 a). The full width half maximum of the optical spectra for ES (1188 nm) was 2.9 nm giving a time bandwidth product of 2.83 suggesting that the pulses are not transform limited. Shorter pulses for ES are demonstrated for lower current and the same is observed for GS 2 mm devices. The peak power of ES increases with gain current from 77 mW up to 350 mW (Fig. 5.11 b). The highest peak power of 350 mW is achieved for a reverse bias of 2.5 V and driving current of 400 mA. The power level is similar to that which was achieved for the GS ML regime in a 2 mm laser.

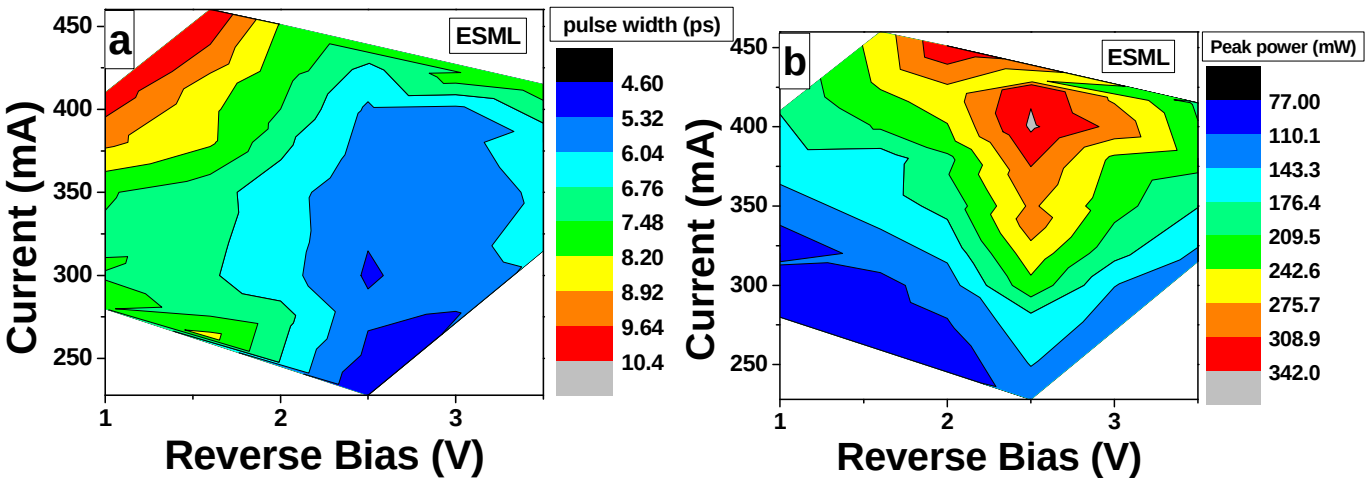

Fig. 5.11 (a) Pulse width and **(b)** Peak power evolution with bias conditions for a 1.3mm long device having 5 QD layers. Number of measured points is ~ 400.

5.4.4 Conclusion.

The dependence of the characteristics of the mode-locking regime upon the number of QD layers embedded in the active region of the lasers was studied. The highest peak power of 600 mW is achieved for 10 QD-layer lasers. The higher number of QD layers laser did show the improvement in peak power as increment in average power is accompanied by broader pulses, but the 15 layer QD lasers showed the widest range of mode-locking from 2 V to 10 V and driving current from 160 mA to 500 mA.

Additionally, it was shown that the emission switching between the GS and ES bands can be achieved by changing the bias conditions, thus adding an extra level of freedom that can be effectively used for multi-wavelength ultrafast sources. It was also demonstrated that the cavity length also plays an important role in the achievement of a variety of mode-locking regimes involving both GS and ES. ES ML can be achieved either by decreasing the laser cavity's number of layers (less than 10) up to 1 mm or increasing the applied current high enough in order to saturate GS. The average power for ES at shorter cavity length can be increased by reverse bias which is not possible in the case of GS for longer devices. Thus similar peak power level can be obtained for the ES band (1188nm).

5.5 Summary.

Different operating regimes of QD-based monolithic two-section devices were investigated. The interplay between GS and ES transitions was studied in great detail. It was shown that ESML can be achieved at the expense of the current applied to the gain section. The dependence on bias conditions of several of the GSML and ESML characteristics was presented. Dual-wavelength mode-locking was demonstrated with 83 nm spectral separation between the modes. Careful control of the structural parameters of the lasers can be effectively used for obtaining one or other emission mode. For example, the lasers with shorter cavity length (1.3 mm) allow achieving ESML even at low current, which cannot be observed for longer devices.

5.6 References.

[1] A. Leitenstorfer*, et al.*, "Widely tunable two-color mode-locked Ti:sapphire laser with pulse jitter of less than 2 fs," *Opt. Lett.,* vol. 20, pp. 916-918, 1995.

[2] C. W. Luo*, et al.*, "A widely tunable dual-wavelength CWTi:sapphire laser with collinear output," *Opt. Express,* vol. 16, pp. 3305-3309, 2008.

[3] C. Song*, et al.*, "Switchable and tunable dual-wavelength ultrashort pulse generation in a passively mode-locked erbium-doped fiber ring laser," *Optics Communications,* vol. 282, pp. 4408-4412, 2009.

[4] H. Yoshioka*, et al.*, "Dual-wavelength mode-locked Yb:YAGceramic laser in single cavity," *Opt. Express,* vol. 18, pp. 1479-1486, 2010.

[5] W. Elsasser*, et al.*, "Picosecond pulse generation in a GaAs/GaAlAs single-quantum-well laser at the first and second subband transition," *Photonics Technology Letters, IEEE,* vol. 4, pp. 966-969, 1992.

[6] M. A. Cataluna*, et al.*, "High-Power Versatile Picosecond Pulse Generation from Mode-Locked Quantum-Dot Laser Diodes," *IEEE Journal of Selected Topics in Quantum Electronics,* 2011.

[7] E. U. Rafailov*, et al.*, "Mode-locked quantum-dot lasers," *Nat Photon,* vol. 1, pp. 395-401, 2007.

[8] M. G. Thompson*, et al.*, "InGaAs Quantum-Dot Mode-Locked Laser Diodes," *Selected Topics in Quantum Electronics, IEEE Journal of,* vol. 15, pp. 661-672, 2009.

[9] A. Markus*, et al.*, "Simultaneous two-state lasing in quantum-dot lasers," *Applied Physics Letters,* vol. 82, pp. 1818-1820, 2003.

[10] C. G. Leburn*, et al.*, "Femtosecond Pulse Generation Using Ground-State and Excited-State Transitions in Quantum-Dot SESAMs," 2009, p. MB18.

[11] E. U. Rafailov*, et al.*, "Investigation of transition dynamics in a quantum-dot laser optically pumped by femtosecond pulses," *Applied Physics Letters,* vol. 88, 2006.

[12] M. A. Cataluna*, et al.*, "Ground and excited-state modelocking in a two-section quantum-dot laser," in *2005 IEEE LEOS Annual Meeting Conference Proceedings*, ed New York: Ieee, 2005, pp. 870-871.

[13] M. A. Cataluna*, et al.*, "Stable mode locking via ground- or excited-state transitions in a two-section quantum-dot laser," *Applied Physics Letters,* vol. 89, pp. 081124-3, 2006.

[14] E. A. Viktorov*, et al.*, "Dynamics of a two-state quantum dot laser with saturable absorber," *Applied Physics Letters,* vol. 90, 2007.

[15] A. Markus*, et al.*, "Two-state switching and dynamics in quantum dot two-section lasers," *Journal of Applied Physics,* vol. 100, 2006.

[16] S. Breuer*, et al.*, "Reverse-emission-state-transition mode locking of a two-section InAs/InGaAs quantum dot laser," *Applied Physics Letters,* vol. 97, pp. 071118-3, 2010.

[17] S. Breuer*, et al.*, "Reverse ground-state excited-state transition dynamics in two-section quantum dot semiconductor lasers: mode-locking and state-switching," *Proceedings of SPIE,* vol. 7720, 2010.

[18] S. Breuer*, et al.*, "State-switched modelocking of two-segment quantum dot laser via self-electro-optical quantum dot absorber," *Electronics Letters,* vol. 46, pp. 161-162, 2010.

[19] J. Kim*, et al.*, "Pulse generation and compression via ground and excited states from a grating coupled passively mode-locked quantum dot two-section diode laser," *Applied Physics Letters,* vol. 89, Dec 2006.

[20] J. Kim and P. J. Delfyett, "Interband optical pulse injection locking of quantum dot mode-locked semiconductor laser," *Optics Express,* vol. 16, pp. 11153-11161, 2008.

[21] J. Liu*, et al.*, "Dual-wavelength 92.5 GHz self-mode-locked InP-based quantum dot laser," *Opt. Lett.,* vol. 33, pp. 1702-1704, 2008.

[22] M. G. Thompson*, et al.*, "Regimes of mode-locking in tapered quantum dot laser diodes," in *Semiconductor Laser Conference, 2008. ISLC 2008. IEEE 21st International*, 2008, pp. 27-28.

[23] S. G. Li*, et al.*, "Two-color quantum dot laser with tunable wavelength gap," *Applied Physics Letters,* vol. 95, 2009.

[24] C. Mesaritakis*, et al.*, "Pulse width narrowing due to dual ground state emission in quantum dot passively mode locked lasers," *Applied Physics Letters,* vol. 96, 2010.

[25] L. F. Lester*, et al.*, "Optical characteristics of 1.24-μm InAs quantum-dot laser diodes," *Photonics Technology Letters, IEEE,* vol. 11, pp. 931-933, 1999.

[26] D. I. Nikitichev*, et al.*, "Investigation of the pulse dynamics in a mode-locked quantum-dot laser, involving the ground/excited state transitions," presented at the 1st EOS Topical Meeting on Lasers 2009, Capri, Italy, 2009.

[27] M. A. Cataluna*, et al.*, "Dual-wavelength mode-locked quantum-dot laser, via ground and excited state transitions: experimental and theoretical investigation," *Opt. Express,* vol. 18, pp. 12832-12838, 2010.

[28] C. Mesaritakis*, et al.*, "Effect of optical feedback to the ground and excited state emission of a passively mode locked quantum dot laser," *Applied Physics Letters,* vol. 97, pp. 061114-061114-3, 2010.

[29] M. Gioannini and I. Montrosset, "Numerical Analysis of the Frequency Chirp in Quantum-Dot Semiconductor Lasers," *Quantum Electronics, IEEE Journal of,* vol. 43, pp. 941-949, 2007.

[30] R. G. M. P. Koumans and R. Van Roijen, "Theory for passive mode-locking in semiconductor laser structures including the effects of self-phase modulation, dispersion, and pulse collisions," *Quantum Electronics, IEEE Journal of,* vol. 32, pp. 478-492, 1996.

[31] M. A. Cataluna*, et al.*, "New Mode Locking Regime in A Quantum-Dot Laser: Enhancement by Simultaneous CW Excited-State Emission," 2006, p. CThH3.

[32] T. Piwonski*, et al.*, "Refractive index dynamics of quantum dot based waveguide electroabsorbers," *Applied Physics Letters,* vol. 97, pp. 051107-3, 2010.

[33] D. B. Malins, *et al.*, "Ultrafast electroabsorption dynamics in an InAs quantum dot saturable absorber at 1.3 μm," *Applied Physics Letters,* vol. 89, pp. 171111-171111-3, 2006.

[34] E. A. Viktorov, *et al.*, "Model for mode locking in quantum dot lasers," *Applied Physics Letters,* vol. 88, pp. 201102-3, 2006.

[35] M. Sugawara, *et al.*, "Modeling room-temperature lasing spectra of 1.3-μm self-assembled InAs/GaAs quantum-dot lasers: Homogeneous broadening of optical gain under current injection," *Journal of Applied Physics,* vol. 97, 2005.

[36] K. Y. Lau, "Short-pulse and high-frequency signal generation in semiconductor lasers," *Lightwave Technology, Journal of,* vol. 7, pp. 400-419, 1989.

[37] Y. C. Xin, *et al.*, "Reconfigurable quantum dot monolithic multisectionpassive mode-locked lasers," *Opt. Express,* vol. 15, pp. 7623-7633, 2007.

[38] M. G. Thompson, *et al.*, "Absorber Length Optimisation for Sub-Picosecond Pulse Generation and Ultra-Low Jitter Performance in Passively Mode-Locked 1.3μm Quantum-Dot Laser Diodes," 2006, p. OThG3.

[39] X. Huang, *et al.*, "Bistable operation of a two-section 1.3 μm InAs quantum dot laser-absorption saturation and the quantum confined Stark effect," *Quantum Electronics, IEEE,* vol. 37, pp. 414-417, 2001.

[40] E. U. Rafailov, *et al.*, "Fast quantum-dot saturable absorber for passive mode-locking of solid-state lasers," *IEEE Photonics Technology Letters,* vol. 16, pp. 2439-2441, 2004.

[41] G. S. Solomon, *et al.*, "Vertically Aligned and Electronically Coupled Growth Induced InAs Islands in GaAs," *Physical Review Letters,* vol. 76, p. 952, 1996.

[42] H. Ishikawa, *et al.*, "Self-organized quantum dots and quantum dot lasers (invited)," *Journal of Vacuum Science & Technology A: Vacuum, Surfaces, and Films,* vol. 16, pp. 794-800, 1998.

[43] M. K. Zundel, *et al.*, "Structural and optical properties of vertically aligned InP quantum dots," *Applied Physics Letters,* vol. 71, pp. 2972-2974, 1997.

[44] M. G. Thompson*, et al.*, "Properties of InGaAs quantum dot saturable absorbers in monolithic mode-locked lasers," in *Semiconductor Laser Conference, 2004. Conference Digest. 2004 IEEE 19th International*, 2004, pp. 53-54.

[45] K. A. Williams*, et al.*, "Long-wavelength monolithic mode-locked diode lasers," *New Journal of Physics,* vol. 6, p. 179, 2004.

[46] S. V. Zaitsev*, et al.*, "Radiation characteristics of injection lasers based on vertically coupled quantum dots," *Superlattices and Microstructures,* vol. 21, pp. 559-564, 1997.

[47] V. M. Ustinov*, et al.*, *Quantum Dot Lasers*. New York: Oxford University Press, 2003.

[48] J. Chen*, et al.*, "Nanostructure model and optical properties of InAs/GaAs quantum dot in vertical cavity surface emitting lasers," *Opto-electronics review,* vol. 19, 2011.

Chapter 6. Bistable quantum dot laser.

6.1 The concepts of bistability (polarization, power, wavelength) and tunability.

In 1964 Lasher proposed the first bistable Fabry-Perot injection laser emitting coherent or spontaneous light switched by electrical pulses or incident light [1]. Double–heterostructure (DH) semiconductor lasers demonstrated the optical bistability as well [2-3] which is associated with the existence of two stable outputs depending on one parameter. It is a well known effect in many types of semiconductor lasers now such as disk lasers [4], ring lasers [5-6], Fabry-Perot injection locked lasers [7-8], photonic crystal lasers [9], vertical-cavity surface-emitting laser diodes (VCSELs) [10-14]. There are different types of optical bistability such as polarization switching, power-bistability, current-bistability and wavelength-bistability which can be used for the development of the next generation of low cost and compact optical communication systems and all-optical processing components such as flip-flop memory switches and wavelength converters [15-18]. For example, in VCSELs polarization switching was observed depending on the injected current, temperature or wavelength [10-12]. From a distributed feedback semiconductor laser power-bistability and switch on/off dynamic characteristics were reported [19-20]. In this context, bistability and hysteretic behavior of a quantum well laser with a saturable absorber due to bleaching of the saturable absorption with increasing pump power was explored in details [13-14, 21-23]. Recent progress of compact quantum-dot (QD) mode-locked lasers in generating high repetition rate ultrashort pulses along with low-noise makes such lasers great candidates for high speed application system [24-26]. Moreover, power-bistability was also demonstrated with applied reverse bias to the

absorber in two-section QD lasers due to the quantum-confined Stark effect in absorber and saturation properties in gain and absorber [27-31]. In the previous chapter it has been shown the possibility of wavelength-bistability in QD based mode-locked two-section lasers associated with the generating the pulses from GS or ES transitions controlled by the bias conditions of gain and absorber [32-38]. In this context, two-color lasing was reported from GS and ES simultaneously in CW [39-40] and pulse regimes [41]. On the other hand, simultaneous dual-wavelength ground state splitting (GSS) under CW was attributed to state filling effect [42]. Moreover, GSS in the mode-locked regime using the same mode was explained by Rabi oscillations in combination with the ac Stark effect [43] or homogenous and inhomogeneous broadening [31, 44-45]. Recently, it has been reported in two-section passively mode-locked QD lasers with a 7.9 GHz pulse repetition rate, using a device with an active region which comprised of a tenfold stack of InGaAs QDs layers. Bistability between 1166 nm and 1174 nm was achieved with power suppression ratios of 30 dB. However, the level of output power achieved in the latter work was rather low, ranging between 0.2-0.8 mW for an operating temperature of 12^{o}C [27-28]. Recently, we demonstrated robust, high power wavelength-bistability between 1245 nm and 1295 nm attributed to two different modes for monolithic two-section laser operating at 10 GHz frequency with average powers up to 25 mW for CW and 17 mW for mode-locking regimes. A suppression ratio higher than 40 dB was demonstrated [46-47].

Furthermore, currently-available QD growth technology enables a high degree of control over the emission spectrum of QD devices, which can be tailored for different applications, such as a broadly-tunable laser [48-52]. For instance, chirped multiple QD external-cavity diode lasers demonstrated impressive 208 nm tunability with near 200 mW maximum output power [50]. Monolithic multi-section devices have only

shown continuous sweeping region between 1029.1 nm to 1017.4 nm (11.7 nm) and extending to 1004.3 nm (with a total 24.8 nm sweep range) by applying different current to the sections [52].

In this chapter, further improvement of a new approach is presented in order to achieve wavelength bistability and tunability in a monolithic multi-section QD laser, by using an active region which incorporates non-identical InAs QD layers which emit at distinct wavelengths. The widest range of wavelength bistability of 54 nm - the largest spectral range which is ever achieved, controllable via the reverse bias applied to the saturable absorber has been demonstrated. Wide wavelength tunability between 1245 nm and 1290 nm under mode-locking regime with a 40 dB suppression ratio is demonstrated. Depending on the range of reverse bias applied, continuous wave (CW) or mode-locked regimes are obtained, with average powers up to 31 mW and 28 mW, respectively. This output power performance represents further improvement of magnitude when compared with previous results [27-28, 41, 47]. Moreover, electronically-controlled 45 nm tunability range is demonstrated from a monolithic multi-section mode-locked QD laser, allowing for the generation of picosecond pulses electronically tunable between 1245 nm and 1290 nm, with a pulse repetition rate of around 10 GHz [53]. This represents a completely new regime of operation of mode-locked laser diodes, which significantly enhances their spectral versatility, while offering the potential for high-speed electronic tuning.

6.2 Device description.

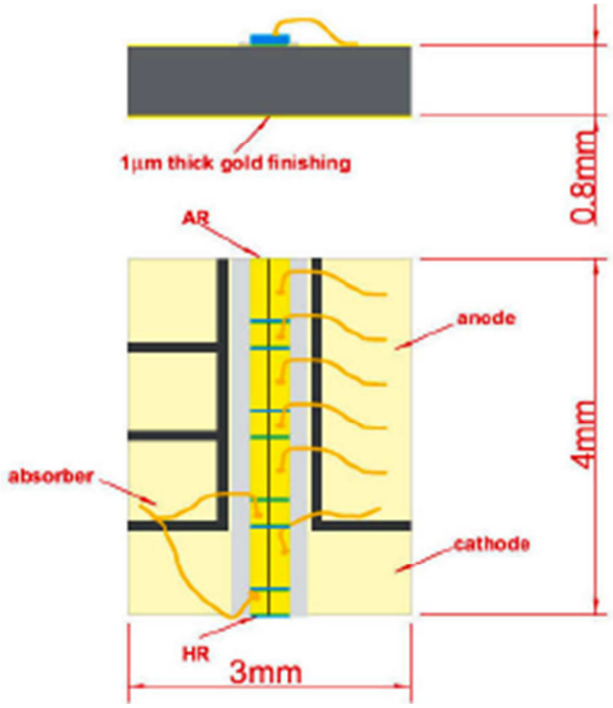

Fig.6.1 Schematic of a multi-section quantum dot laser.

The investigated multi-section laser has a ridge waveguide width of 6 µm and a total length of 4 mm, resulting in a pulse repetition rate of 10 GHz when mode-locked, as defined by the cavity round trip time. The device consists of multiple 1-mm-long electrically-insulated sections; each of these further divided into 300 µm and 700 µm sub-sections. A reverse bias is applied to the two 300 µm sections placed nearer the back facet, thus forming a distributed saturable absorber with a total length of 600 µm. The gain section is formed by the remaining sections which are forward biased (Fig.6.1). The output facet was deep-anti-reflection coated (on the gain section side), while the back facet was high-reflection coated (on the absorber side), with reflectivities of approximately 0.1% and 95%, respectively. The QD structure was grown on a GaAs substrate by molecular beam epitaxy. Its active region consists of 10 InAs QD layers covered by non-identical InGaAs capping layers, incorporated into

$Al_{0.35}Ga_{0.65}As$ cladding layers. The size of the QDs is related to the wavelength emission and can be control to some extent by manipulating the thickness of capping layers which leads to variance of the indium segregation into the QDs. As a result, the larger size of the QDs, the longer the emission wavelength. This structure consists of 3 QD layers with central wavelength emission at 1211 nm, 3 QD layers at 1243 nm and finally 4 QD layers at 1285 nm. The higher number of layers for larger QDs is used to keep the gain spectrum flat as the density of dots is decreased with the increasing QD size as explained in ref. [48]. The laser was kept at 20 ^{o}C by a Peltier cooler. The gain section was pumped with a low-noise current source and the absorber section was connected to a voltage source. The pulse durations were measured by a non-collinear autocorrelator based on second-harmonic generation. The spectral characteristics were measured by a spectrometer and mode-locking performance was further investigated with an RF spectrum analyzer in combination with a high-speed 29 GHz photodiode.

6.3 Experimental results and discussion.

The QD laser demonstrated wavelength bistability for fixed currents of 260 mA, 300 mA, and 330 mA applied to the gain section and the reverse bias between 0 V and 10 V, in both ascending and descending directions. Threshold current density was 370 A/cm^2 under 0 V reverse bias. For a fixed current of 260 mA as depicted in Fig. 6.2 a, the widest spectral separation of 54 nm was obtained between 1296 nm and 1242 nm at -4.6 V reverse bias. Pulse duration is changing from 24 ps to 4 ps with reverse bias changing from -2.6 V to -7 V (Fig. 6.2 b). At a gain current of 260 mA the pulse duration depends on the direction of applied voltage which is explained by different operating wavelengths (Fig.6.2 b).

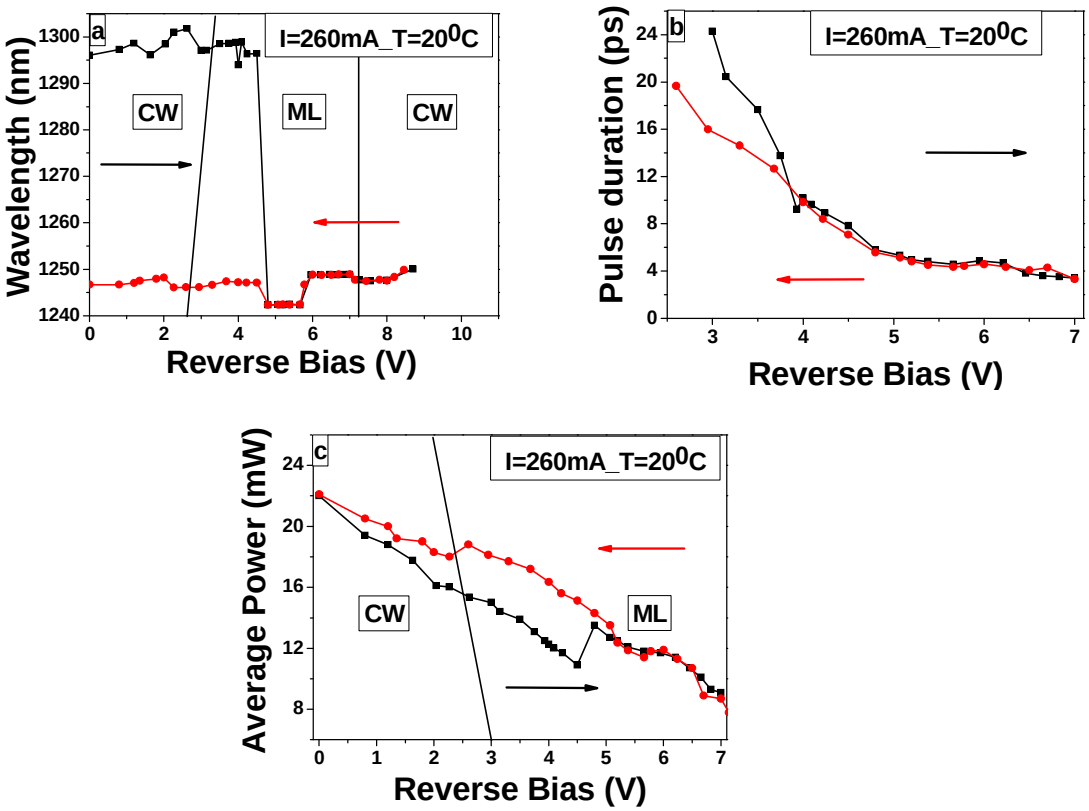

Fig. 6.2 (a) Dynamics for a fixed gain current of 260 mA with various values of ascending and descending reverse bias of the emission wavelength ; **(b)** pulse duration and **(c)** output power.

Shorter pulse durations were measured for the 1245 nm wavelength.

A transition in the laser operation mode – between CW and mode-locking – was found for a reverse bias of ~3 V for ascending and 2.6 V for descending directions for fixed current of 260 mA. Mode-locking wavelength switching was observed at ~4.8 V. The output power hysteresis occurs between 0-6 V reverse biases shown in Fig. 6.2 (c) due to nonlinear saturation of the QD absorption and quantum confined Stark effect in the absorber [27, 29-30].

When applying a higher fixed current of 300 mA and 330 mA, wavelength switching behaviour was observed, similar to what had been observed at 260 mA fixed current. However, at higher reverse bias values, a different regime of operation was obtained. (Fig.6.3 a, b). The region of mode-locking in descending direction for 330 mA current is slightly wider then ascending direction.

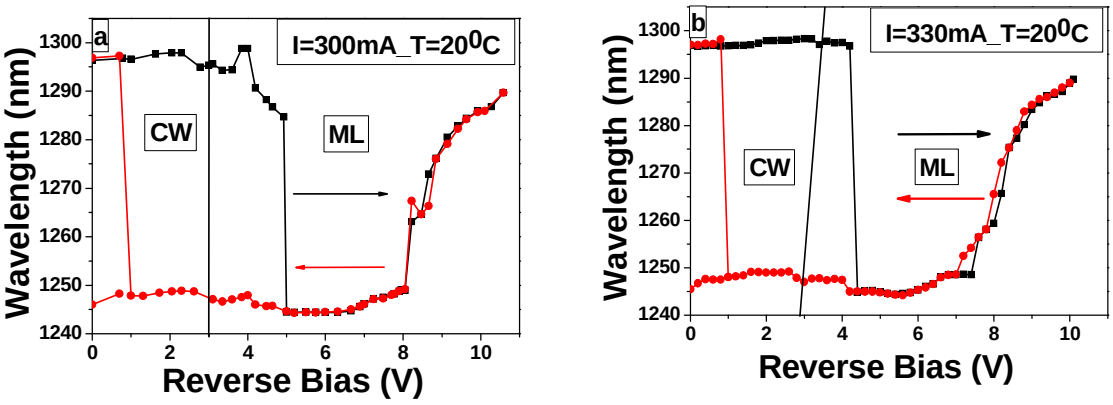

Fig.6.3 Dynamics of the emission wavelength with various values of ascending (black line) and descending (red line) reverse bias for a fixed gain current of **a)** 300 mA and **b)** 330 mA in continuous wave (CW) and mode-locking (ML) regimes of operation.

Pulse duration varies from 28 ps to 4 ps for -3 V and -10.6 V applied voltage, respectively (Fig. 6.4a, b). Pulse duration is slightly higheras the current increases which is well known due to the increase in self-phase modulation effect [54]. Pulse duration at low reverse bias at 300 mA gain current for ~1285 nm wavelength this time is shorter than for ~1245 nm wavelength, while for a higher gain current of 330 mA the pulse duration is about the same for both wavelengths as the result of interplay between gain current and nonlinear absorption in the absorber for the different spectral band.

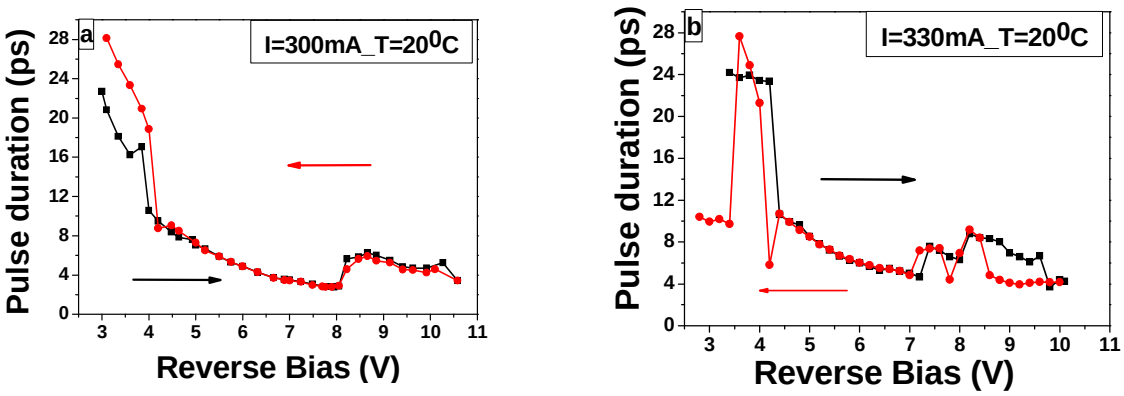

Fig. 6.4 Dynamics of the pulse duration with ascending (black line) and descending (red line) direction of applied reverse bias for a fixed gain current of **(a)** 300 mA and **(b)** 330 mA.

Noticeable hysteresis of average power is demonstrated in Fig.6.5 a, b for a fixed current of 300 mA and 330 mA with applied reverse bias associated with switching the laser operation from one wavelength to another.

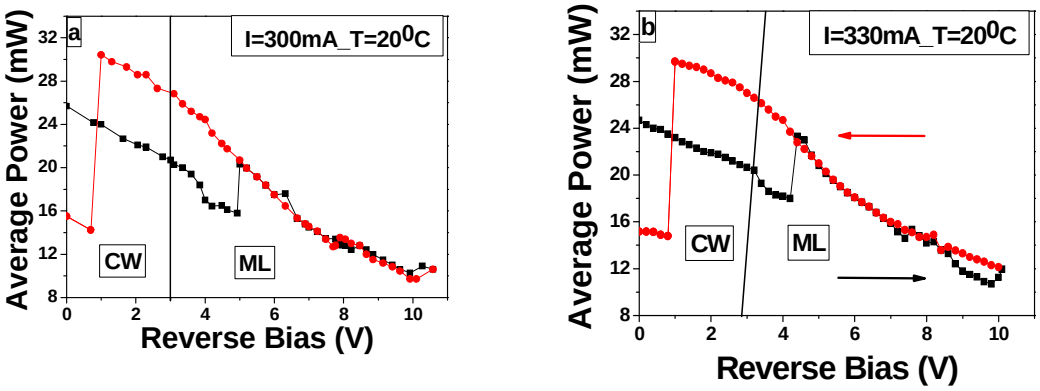

Fig. 6.5 Dynamics of the average power with descending (black line) and descending (red line) direction of applied reverse bias for a fixed gain current of **(a)** 300 mA and **(b)** 330 mA.

The highest output powers measured for 300 mA fixed current were 30.4 mW (25.7 mW) and 27 mW (20.7 mW) for CW and mode-locking regimes at ~1245 nm (~1295 nm), respectively. Wavelength tunability region between -7 V and -10.6 V applied voltage is observed for 300 mA as well as for 330 mA. At that unique mode-locking region, the wavelength can be tuned from 1245 nm to 1290 nm by applying a reverse bias to the absorber. It can be explained by the increased absorption which leads to a reduction of the laser power and the absorber current. As a result, a red shift of the absorption peak of the QD occurs with increasing reverse bias [30, 55]. It was shown that absorption spectra shifts to lower photon energies with increasing electric field up to 21% at 1.32 µm at 18 Volt bias for 3 QD layers InAs waveguides [55]. Such changes would favor mode-locked operation towards increasingly longer wavelengths, within the available broadband gain.

As evidence of this tuning regime for 300 mA fixed current in the ascending direction, the corresponding optical spectra are depicted in Fig.6.6 (a) along with autocorrelations and RF spectra (shown in Fig.6.6 b, c).

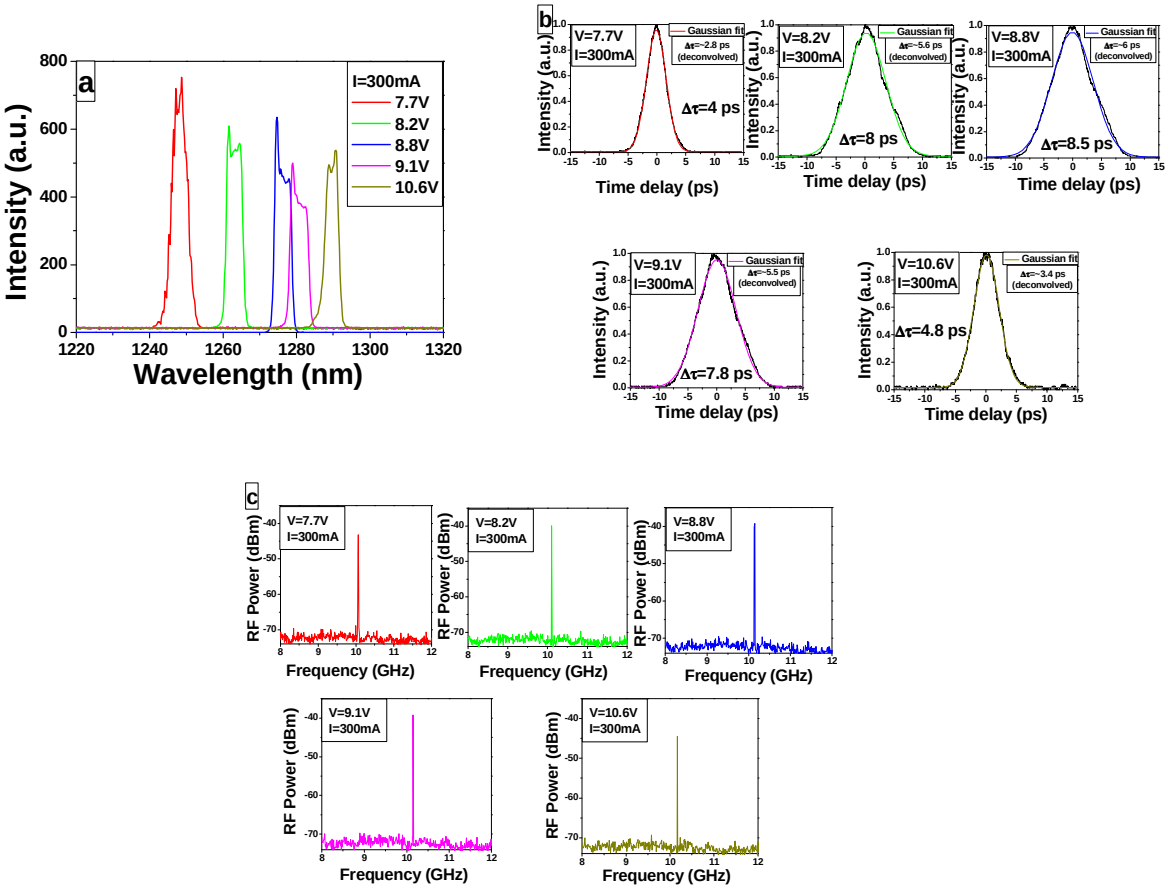

Fig 6.6 (a) Spectral tunability,**(b)** corresponding autoccorelations and **(c)** RF spectra in the ascending direction for a fixed gain current of 300 mA with applied reverse bias.

A suppression ratio higher than 40dB suggests the effectiveness of using novel QD material for building tunable electrically controlled optical source (Fig. 6.7).

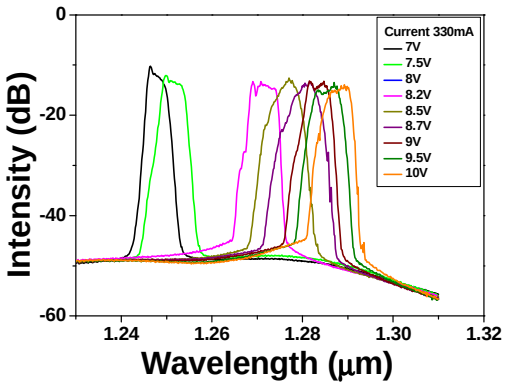

Fig. 6.7 Spectral tunability with high suppression ratio of more than 40 dB in descending direction for a fixed gain current of 330 mA with applied reverse bias.

Moreover, dual-mode CW regime is observed for descending direction at low reverse bias between 0 and -1 V for gain current between 300 mA and 330 mA with a high suppression ratio and with similar output power of ~15 mW in each spectral mode (Fig.6.8 a, b).

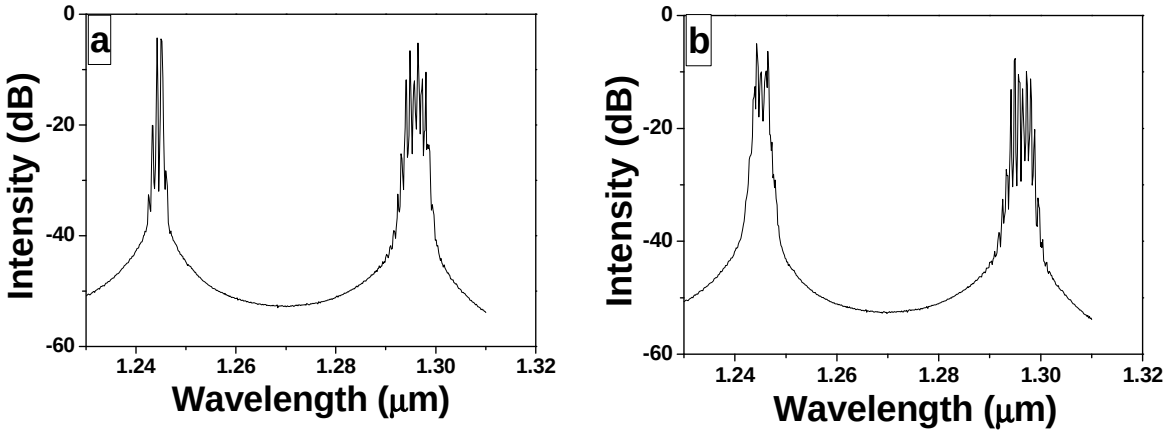

Fig. 6.8 Dual-mode generation with 40 dB suppression ratio in both mode with similar power of 15 mW in descending direction at 0 V reverse bias for a fixed gain current of **a)** 300 mA and **b)** 330 mA.

6.4 Conclusions.

In conclusion, robust wavelength bistability and tunability was demonstrated in a multi-section monolithic laser diode incorporating chirped QD layers. The highest achieved spectral bistability range was 54 nm, generating picosecond pulses at 10 GHz at 1245 nm or 1295 nm. The unique mode-locking regime of operating with a broad wavelength tunability range (45 nm) was shown as well where the wavelength was electronically controlled by applied reverse bias to the absorber section. It is important to stress that the spectral range reported here is important for all-optical processing and optical communications applications, due to the minimum dispersion that optical fibres exhibit in that range.

6.5 References.

[1] G. J. Lasher, "Analysis of a proposed bistable injection laser," *Solid-State Electronics,* vol. 7, pp. 707-716, 1964.

[2] S. Kobayashi and T. Kimura, "Injection locking in AlGaAs semiconductor laser," *Quantum Electronics, IEEE,* vol. 17, pp. 681-689, 1981.

[3] H. Kawaguchi, "Bistable operation of semiconductor lasers by optical injection," *Electronics Letters,* vol. 17, pp. 741-742, 1981.

[4] E. J. Saarinen*, et al.*, "Bistable mode-locking in a semiconductor disk laser," in *Lasers and Electro-Optics, 2008 and 2008 Conference on Quantum Electronics and Laser Science. CLEO/QELS 2008. Conference on*, 2008, pp. 1-2.

[5] M. Sorel*, et al.*, "Unidirectional bistability in semiconductor waveguide ring lasers," *Applied Physics Letters,* vol. 80, pp. 3051-3053, 2002.

[6] S. Sunada*, et al.*, "Random optical pulse generation with bistable semiconductor ring lasers," *Opt. Express,* vol. 19, pp. 7439-7450, 2011.

[7] S. Osborne*, et al.*, "All-optical memory based on the injection locking bistability of a two-color laser diode," *Opt. Express,* vol. 17, pp. 6293-6300, 2009.

[8] P. Heinricht*, et al.*, "Bistability in an injection locked two color laser with dual injection," *Applied Physics Letters,* vol. 99, pp. 011104-011104-3, 2011.

[9] L.-D. Haret*, et al.*, "Extremely low power optical bistability in silicon demonstrated using 1D photonic crystal nanocavity," *Opt. Express,* vol. 17, pp. 21108-21117, 2009.

[10] S.-H. Lee*, et al.*, "All-optical Flip-flop Operation Based on Polarization Bistability of Conventional-type 1.55-μm Wavelength Single-mode VCSELs," *J. Opt. Soc. Korea,* vol. 14, pp. 137-141, 2010.

[11] M. S. Torre*, et al.*, "Wavelength-induced polarization bistability in 1550 nm VCSELs subject to orthogonal optical injection," *J. Opt. Soc. Am. B,* vol. 27, pp. 2542-2548, 2010.

[12] H. Kawaguchi and I. S. Hidayat, "Gigahertz all-optical flip-flop operation of polarisation-bistable vertical-cavity surface emitting lasers," *Electronics Letters,* vol. 31, pp. 1150-1151, 1995.

[13] V. I. Klimov and D. W. McBranch, "Ultrafast energy relaxation and carrier trapping dynamics in semiconductor nanocrystals," in *Lasers and Electro-Optics Society Annual Meeting, 1997. LEOS '97 10th Annual Meeting. Conference Proceedings., IEEE*, 1997, pp. 439-440 vol.2.

[14] J. A. Hudgings*, et al.*, "Self-pulsations, bistability, and intracavity quantum well absorber modulation of VCSELs," *Proceedings of SPIE,* vol. 3290, 1997.

[15] D. Gallagher*, et al.*, "Gigabit pulse position bistability in semiconductor lasers," *Lightwave Technology,* vol. 5, pp. 1391-1398, 1987.

[16] H. Kawaguchi, "Bistable laser diodes and their applications: state of the art," *Selected Topics in Quantum Electronics, IEEE,* vol. 3, pp. 1254-1270, 1997.

[17] L. Linlin, "Optical bistability in semiconductor lasers under intermodal light injection," *Quantum Electronics, IEEE,* vol. 32, pp. 248-256, 1996.

[18] I. White*, et al.*, "Wavelength switching components for future photonic networks," *Communications Magazine, IEEE,* vol. 40, pp. 74-81, 2002.

[19] L. Wang*, et al.*, "Current-driven state-bistability and power-bistability in a DFB semiconductor laser subject to optical injection," *Laser Physics,* vol. 20, pp. 1957-1960, 2010.

[20] J. Zhou*, et al.*, "All-optical bistable switching dynamics in 1.55-µm two-segment strained multiquantum-well distributed-feedback lasers," *Lightwave Technology,* vol. 15, pp. 342-355, 1997.

[21] S. Tarucha and H. Okamoto, "Voltage-controlled optical bistability associated with two-dimensional exciton in GaAs-AlGaAs multiple quantum well lasers," *Applied Physics Letters,* vol. 49, pp. 543-545, 1986.

[22] H. Uenohara*, et al.*, "Static and dynamic response of multiple-quantum-well voltage-controlled bistable laser diodes," *Quantum Electronics, IEEE,* vol. 32, pp. 873-883, 1996.

[23] S. Sanders*, et al.*, "Passive mode locking of a two-section multiple quantum well laser at harmonics of the cavity round-trip frequency," *Applied Physics Letters,* vol. 58, pp. 681-683, 1991.

[24] E. U. Rafailov*, et al.*, "Mode-locked quantum-dot lasers," *Nat Photon,* vol. 1, pp. 395-401, 2007.

[25] M. T. Todaro*, et al.*, "Simultaneous achievement of narrow pulse width and low pulse-to-pulse timing jitter in 1.3 µm passively mode-locked quantum-dot lasers," *Opt. Lett.,* vol. 31, pp. 3107-3109, 2006.

[26] H. Schmeckebier*, et al.*, "Complete pulse characterization of quantum dot mode-locked lasers suitable for optical communication up to 160 Gbit/s," *Opt. Express,* vol. 18, pp. 3415-3425, 2010.

[27] M. Feng*, et al.*, "Wavelength Bistability and Switching in Two-Section Quantum-Dot Diode Lasers," *Quantum Electronics, IEEE,* vol. 46, pp. 951-958, 2010.

[28] M. Feng*, et al.*, "Wavelength Bistability in Two-Section Mode-Locked Quantum-Dot Diode Lasers," *Photonics Technology Letters, IEEE,* vol. 19, pp. 804-806, 2007.

[29] X. Huang*, et al.*, "Bistable operation of a two-section 1.3 μm InAs quantum dot laser-absorption saturation and the quantum confined Stark effect," *Quantum Electronics, IEEE,* vol. 37, pp. 414-417, 2001.

[30] O. Qasaimeh*, et al.*, "Bistability and self-pulsation in quantum-dot lasers with intracavity quantum-dot saturable absorbers," *Applied Physics Letters,* vol. 74, pp. 1654-1656, 1999.

[31] M. G. Thompson*, et al.*, "InGaAs Quantum-Dot Mode-Locked Laser Diodes," *Selected Topics in Quantum Electronics, IEEE,* vol. 15, pp. 661-672, 2009.

[32] D. I. Nikitichev*, et al.*, "Investigation of the pulse dynamics in a mode-locked quantum-dot laser, involving the ground/excited state transitions," presented at the 1st EOS Topical Meeting on Lasers 2009, Capri, Italy, 2009.

[33] M. A. Cataluna*, et al.*, "Ground and excited-state modelocking in a two-section quantum-dot laser," in *2005 IEEE LEOS Annual Meeting Conference Proceedings*, ed New York: Ieee, 2005, pp. 870-871.

[34] M. A. Cataluna*, et al.*, "Stable mode locking via ground- or excited-state transitions in a two-section quantum-dot laser," *Applied Physics Letters,* vol. 89, pp. 081124-3, 2006.

[35] S. Breuer*, et al.*, "Reverse ground-state excited-state transition dynamics in two-section quantum dot semiconductor lasers: mode-locking and state-switching," *Proceedings of SPIE,* vol. 7720, 2010.

[36] S. Breuer*, et al.*, "Reverse-emission-state-transition mode locking of a two-section InAs/InGaAs quantum dot laser," *Applied Physics Letters,* vol. 97, pp. 071118-3, 2010.

[37] W. Zhou, *et al.*, "Bias-controlled wavelength switching in coupled-cavity $In_{0.4}Ga_{0.6}As$/GaAs self-organized quantum dot lasers," *Applied Physics Letters,* vol. 74, pp. 783-785, 1999.

[38] M. Sugawara, *et al.*, "Modeling room-temperature lasing spectra of 1.3-μm self-assembled InAs/GaAs quantum-dot lasers: Homogeneous broadening of optical gain under current injection," *Journal of Applied Physics,* vol. 97, 2005.

[39] A. Markus, *et al.*, "Simultaneous two-state lasing in quantum-dot lasers," *Applied Physics Letters,* vol. 82, pp. 1818-1820, 2003.

[40] A. Markus, *et al.*, "Two-state switching and dynamics in quantum dot two-section lasers," *Journal of Applied Physics,* vol. 100, 2006.

[41] M. A. Cataluna, *et al.*, "Dual-wavelength mode-locked quantum-dot laser, via ground and excited state transitions: experimental and theoretical investigation," *Opt. Express,* vol. 18, pp. 12832-12838, 2010.

[42] S. G. Li, *et al.*, "Two-color quantum dot laser with tunable wavelength gap," *Applied Physics Letters,* vol. 95, 2009.

[43] J. Liu, *et al.*, "Dual-wavelength 92.5 GHz self-mode-locked InP-based quantum dot laser," *Opt. Lett.,* vol. 33, pp. 1702-1704, 2008.

[44] M. G. Thompson, *et al.*, "Regimes of mode-locking in tapered quantum dot laser diodes," in *Semiconductor Laser Conference, 2008. ISLC 2008. IEEE 21st International*, 2008, pp. 27-28.

[45] C. Mesaritakis, *et al.*, "Pulse width narrowing due to dual ground state emission in quantum dot passively mode locked lasers," *Applied Physics Letters,* vol. 96, 2010.

[46] M. A. Cataluna, *et al.*, "High-Power Versatile Picosecond Pulse Generation from Mode-Locked Quantum-Dot Laser Diodes," *IEEE Journal of Selected Topics in Quantum Electronics,* 2011.

[47] D. I. Nikitichev*, et al.*, "High-power spectral bistability in a multi-section quantum dot laser under continuous-wave or mode-locked operation," in *CLEO2011*, USA, 2011.

[48] K. A. Fedorova*, et al.*, "Broadly tunable high-power InAs/GaAs quantum-dot external cavity diode lasers," *Opt. Express,* vol. 18, pp. 19438-19443, 2010.

[49] X. Q. Lv*, et al.*, "Broadband external cavity tunable quantum dot lasers with low injection current density," *Opt. Express,* vol. 18, pp. 8916-8922, 2010.

[50] X. Q. Lv*, et al.*, "Broadly Tunable Grating-Coupled External Cavity Laser With Quantum-Dot Active Region," *Photonics Technology Letters, IEEE,* vol. 22, pp. 1799-1801, 2010.

[51] G. Ortner*, et al.*, "External cavity InAs/InP quantum dot laser with a tuning range of 166 nm," *Applied Physics Letters,* vol. 88, pp. 121119-121119-3, 2006.

[52] B. J. Stevens*, et al.*, "All semiconductor swept laser source utilizing quantum dots," *Applied Physics Letters,* vol. 91, 2007.

[53] D. I. Nikitichev*, et al.*, "Tunable quantum-dot mode-locked monolithic laser," presented at the 2nd EOS Topical Meeting on Lasers (ETML'11), Italy, 2011.

[54] R. G. M. P. Koumans and R. Van Roijen, "Theory for passive mode-locking in semiconductor laser structures including the effects of self-phase modulation, dispersion, and pulse collisions," *Quantum Electronics, IEEE,* vol. 32, pp. 478-492, 1996.

[55] I. B. Akca*, et al.*, "Electro-optic and electro-absorption characterization of InAs quantum dot waveguides," *Opt. Express,* vol. 16, pp. 3439-3444, 2008.

7. External cavity Quantum Dot lasers.

7.1 Introduction.

7.1.1 An external cavity configuration laser.

High-power, electrically-pumped mode-locked semiconductor lasers generating picosecond/femtosecond pulse trains have been regarded as potentially suitable for a wide variety of applications as mentioned in 1.3. Unique properties of QD semiconductor material such as low threshold current density, low optical losses, and low noise characteristics (discussed in 2.3) enable the fabrication of long-cavity and extremely high wall-plug efficiency lasers [1-3]. Quantum-dot based external-cavity configurations lasers are excellent candidates for systems where the reduced and broadly tunable repetition rate is required, which is not achievable with monolithic mode-locked lasers [4-7]. It is particularly important for the nonlinear multiphoton ex citation fluorescence bioimaging [8-10]. In addition, an extra level of versatility is possible through the introduction of appropriate optical elements (prism or grating) for tunability regime operation [11-12] or appropriate dispersion compensation [4, 7]. Moreover, the QD mode-locked lasers exhibited low timing jitter due to the reduced values of amplified spontaneous emission coupled to the wavelength of operation, when compared with QW or bulk material [13]. Indeed, spontaneous fluctuations in the number of photons represent one of the major sources of timing jitter, as it imparts random fluctuations in the index of refraction, thereby affecting the round-trip time and thus the timing of the pulses. In addition, the thermal and mechanical instabilities take place in the case of external-cavity mode-locked lasers which contribute to timing jitter. But if these instabilities are overcome, an improvement in the phase noise and timing jitter is expected in a stable external-cavity laser as the

active waveguide occupies only a fraction of the optical cavity [14]. In this chapter the latest results achieved with a QD-external cavity passively mode-locked laser are presented [15-18].

7.1.2 Experimental setup and device.

The QD chip was grown by molecular beam expitaxy (MBE) on an n+-GaAs (100) substrate which contained 10 layers of self-assembled InAs/GaAs QDs. The waveguide in gain section is bent and terminated at an angle of 7° relative to the cleaved facet, in combination with antireflection (AR) coating (R~10-5), while the back facet was high-reflection (HR) coated (R~95%). The total chip length is 4 mm, with a 600-µm-long saturable absorber section placed near the back facet resulting in absorber-to-length ratio of 15%. The temperature of the chip was maintained at 20°C by thermoelectric cooler control. A collimating aspherical lens with a numerical aperture of 0.55 was used to couple light to and from the chip. The output beam was focused onto a single-mode fibre splitter and input autocorrelator, radio-frequency (RF) spectrum analyzer and optical spectrum analyser for measurements. . An output coupler of variable transmissivity used for the external cavity facet was mounted on motorized translation stage with a 0.1 µm step motion. QD-external cavity mode-locked laser with an output coupler of 96% transmissivity showed the possibility of delivering high peak power (see section 7.2) while a laser with an output coupler of 53% exhibited the performance of fundamental and harmonic mode-locking along with low timing jitter (see section 7.3 and 7.4). A simplified schematic of the experimental setup for a QD-external cavity passively mode-locked laser is depicted in Fig.7.1.

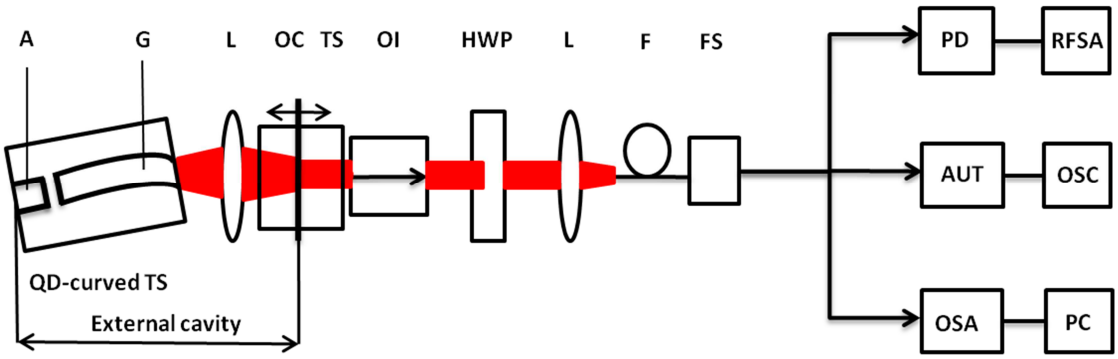

Fig. 7.1 The experimental setup for an external cavity laser system (QD curve TS: quantum dot curved two-section diode; A- Absorber section, G- Gain section, L: lens, OC: output coupler (T=53 % or 96 %), TS: motorized translation stage,, OI: optical isolator, HWP: haft wave plate, F: fibre, FS: single mode fibre splitter, PD: photo diode, RFSA: RF spectrum analyzer, AUT: autocorrelator, OSC: oscilloscope, OSA/SA: Optical spectrum analyzer/ Spectrum analyzer, PC- personal computer).

7.2 A high peak power laser.

In this section an InAs quantum-dot external-cavity passively mode-locked laser with an operation wavelength of 1.27 μm is demonstrated, based on a two section quantum-dot superluminescent diode with bending ridge waveguide and a 96 % output coupler. Stable mode-locking with an average power up to 60 mW was obtained at a repetition frequency of 2.4 GHz. This performance corresponds to a 25 pJ pulse energy obtained directly from the oscillator, which represents a 55-fold increase in pulse energy when compared to the current state-of-the-art for semiconductor lasers. At a repetition frequency of 1.14 GHz, optical pulses of 13.6 ps with an average power of 23.2 mW resulting in 1.5 W peak power are also demonstrated, representing the highest peak power achieved from an external-cavity laser at the 1.3 μm waveband, without the use of any pulse compression or optical amplification [15-16].

7.2.1 State of the art.

For the first time a QD external-cavity mode-locked laser at 1.27 µm was demonstrated in [5]. The QD laser with a repetition frequency of 5 GHz generated optical pulses of 15 ps which were sent to the grating compressor, resulting in 1.2 ps pulses. The amplified average power after compression was 7.2 mW resulting in 1.22 W peak power and 1.46 pJ pulse energy [5]. In another report [6], the repetition rates from 350 MHz to 1.5 GHz, with average output power of up to 27 mW (860 MHz) at 1.2 µm, were achieved by external-cavity quantum-dot lasers incorporating separate quantum-dot semiconductor saturable absorber mirrors (SESAMs).

The inclusion of an intra-waveguide saturable absorber opposed to the SESAM configuration previously demonstrated imparts more robustness and ease of alignment to the laser cavity. In a more recent investigation [7], a QD-external cavity mode-locked laser is demonstrated with record-low repetition rates of 310 MHz, albeit with a modest pulse energy around 0.45 pJ which was shown to be independent of the repetition rate. The highest peak power achieved after intra-cavity pulse compression was 0.41 W [7]. Furthermore, the improvement in peak power without the use of any optical amplification and pulse compression from the QD-external cavity mode-locked laser is presented in the next section.

7.2.2 Experimental results and discussion.

Light-current (L-I) characteristics of the QD based laser without external feedback and of the external-cavity laser using 96 % output coupler with reverse-bias of 0 V and 7.2 V on the absorber are shown in Fig. 7.2.

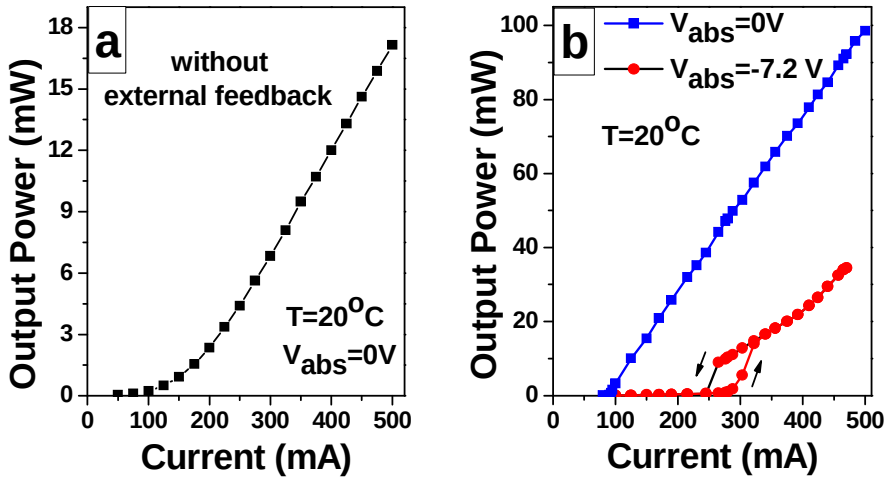

Fig. 7.2 Light-current characteristics of the QD laser **(a)** without external feedback; and **(b)** the external-cavity laser for 0 V and 7.2 V reverse bias.

Output power of 17.2 mW was obtained at a forward current of 500 mA applied to the gain section. The secondary-derivation curve of the laser shows a negligible peak, which hints an effective suppression of back reflection. When 7.2 V reverse bias is applied to the QD absorber a hysteresis loop of 45 mA width is observed as depicted in the figure 7.2 b. Such behaviour can be explained by the non-linearity of saturation in the absorber section. A continuous wave (CW) output power of nearly 100 mW can be achieved with an applied reverse bias of 0 V and forward bias current of 500 mA, while for the mode-locked operation regime an average power reaches up to 35 mW under a 7.2 V reverse bias. A mixture of fundamental mode-locking and high-order harmonic mode-locking may exist as the higher current is applied to gain section due to an

earlier and more complete gain recovery time, which in combination with the relatively long pulse roundtrip time in the long cavity, could lead to the appearance of multiple pulses in a wider net gain window. In fact, the superlinear behaviour of the L-I curve for 7.2 V reverse bias above 375 mA in Fig. 7.2 (b) is indicative of the increasing proportion of higher-order harmonic modes. As a result the external cavity laser alignment should be optimised for each operating point in order to achieve robust fundamental mode-locking at a higher current losing only a few mW in power. For gain current values equal and above 330 mA, robust fundamental mode-locking was achieved after optical feedback adjustment, with the corresponding RF peak exhibiting a signal-to-noise-ratio in excess of 50 dB.

In Figure 7.3, the autocorrelation, optical and RF spectra are represented for 7.2 V reverse bias and 457 mA forward current. Under these operating conditions, the FWHM of the autocorrelation trace is 19.2 ps (Δt) using Gaussing fit which results in deconvolved pulse duration of 13.6 ps ($\Delta \tau$). RF spectra with a dynamic range of 50 dB are indicating about very stable mode-locking. The average power of 23.2 mW at a 1.14 GHz repetition frequency results in the highest peak power of 1.5 W and 20.4 pJ pulse energy. Knowing the mode-locking lasing wavelength of 1274 nm with 1.2 nm full-width at half maximum, the time-bandwidth product of 3.02 can be calculated. Remarkably, a minimum time-bandwidth product of 1.01, only 2.3 times the Fourier limit, was obtained under 7.2 V reverse bias and 330 mA forward current with a pulse duration of 8.4 ps.

As depicted in Figure 7.4, the average power and pulse duration increased with forward current for a fixed reverse bias of 7.2 V and under the fundamental mode-locking conditions, as a result the peak power varies little even under a high drive current.

As is well known with the reduction of the reverse bias, the average power increases. Stable mode-locking with an output average power up to 60 mW was achieved with low reverse bias of 1.4 V corresponding to 25 pJ pulse energy was obtained at a repetition frequency of 2.4 GHz and 375 mA forward current - however, for these operating conditions, a broad pulse with 44 ps duration was generated.

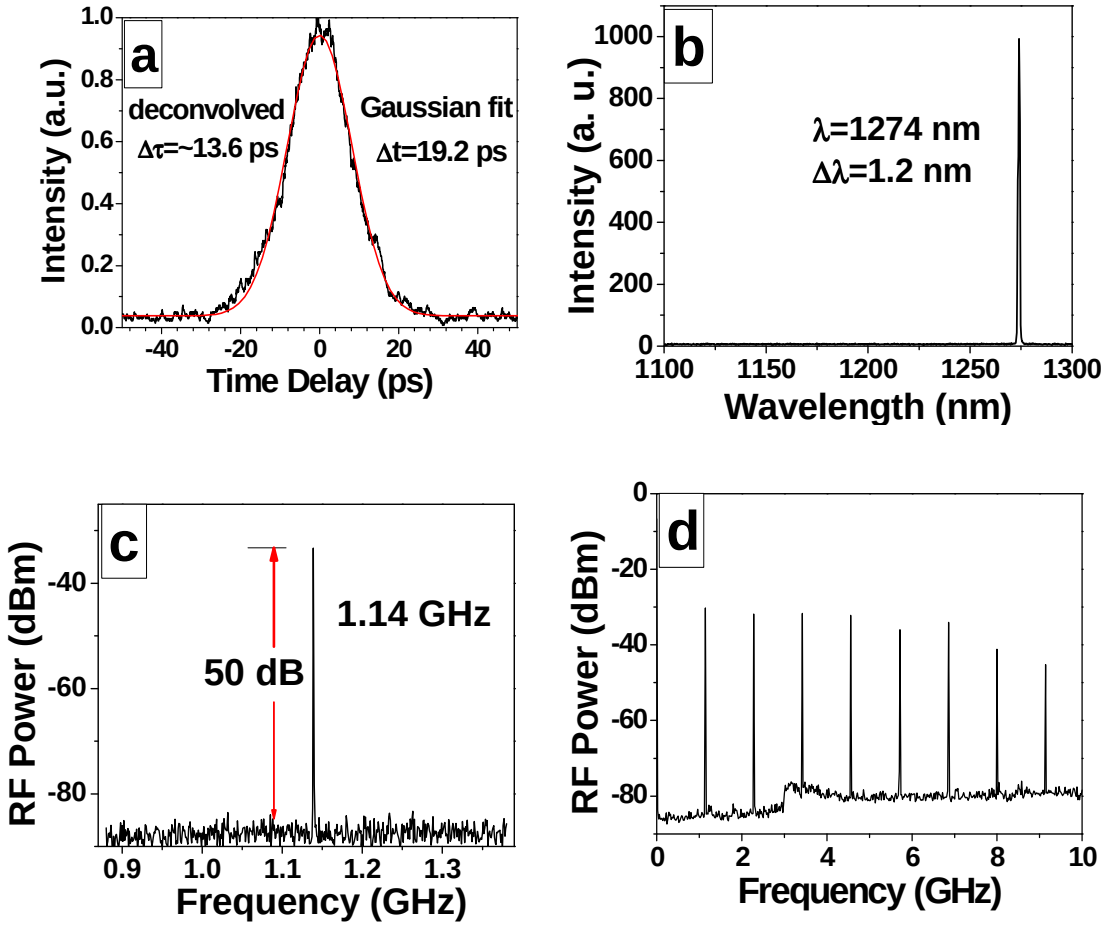

Fig. 7.3 (a) Autocorrelation trace, **(b)** optical spectrum, **(c)** RF spectrum with 500 MHz span and **(d)** 10-GHz span at a reverse bias of 7.2 V and forward current of 457 mA.

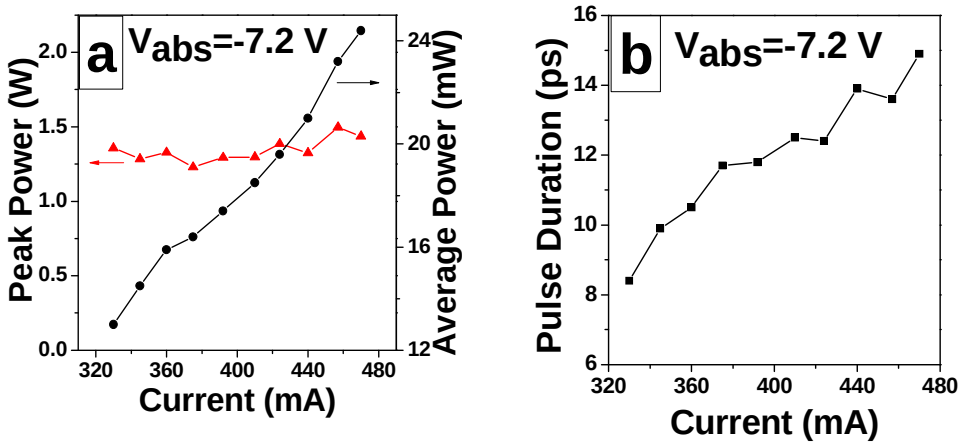

Fig. 7.4 (a) Peak power, average power and **(b)** pulse duration versus forward current with 7.2-V reverse bias.

7.2.3 Conclusions.

Electrically pumped 1.27 μm QD-ECMLLs with peak power of 1.5 W and average power of 23.2 mW with a repetition frequency of 1.14 GHz are achieved without the use of any pulse compression or optical amplifier. Stable mode-locking with an average power up to 60 mW, corresponding to 25 pJ pulse energy was also obtained at a repetition frequency of 2.4 GHz. The minimum time-bandwidth product of 1.01 was obtained with the pulse duration of 8.4 ps.

7.3 Fundamental and Harmonic Mode-locking.

A systematic investigation of a repetition-rate-tunable quantum-dot external-cavity passively mode-locked laser with a quasi-continuous fundamental frequency tuning range from 1 GHz to a record-low value of 191 MHz is demonstrated [16, 18]. A nearly constant pulse peak power at the different pulse repetition rates is revealed in the continuous frequency tuning range. The trend and optimization of the stable fundamental mode-locking are presented and interpreted. Furthermore, a very broad harmonic repetition rate tunable range with picosecond pulses up to 6.8 GHz corresponding to 34^{th}order harmonic of 200 MHz fundamental frequency is shown [17].

7.3.1 State of the art.

The versatility that QD based external-cavity lasers can offer for broad tunability of the pulse repetition rate in the range of MHz to GHz is very useful for non-linear imaging techniques [8-10]. As mentioned in 7.2.1 a fundamental repetition rate tunable range from 1.5 GHz to 350MHz can be achieved from a QD-external cavity mode-locked laser by changing the position of the QD SESAM [6]. The tunability of the fundamental repetition rate from 310 MHz to 1.1 GHz and harmonic repetition rate up to 4.4 GHz corresponding to 4^{th} order harmonic of 1.1 GHz fundamental frequency was demonstrated [7]. High-peak-power QD-external cavity laser performance with repetition frequency from 2.4 GHz to 1.14GHz using an output coupler of 96% transmissivity were demonstrated in the previous section 7.2 as well as in [7, 15-16]. Further investigations of fundamental and harmonic mode-locking from QD-external cavity mode-locked laser (shown in Fig. 7.1) are demonstrated in next two sections only using this time a 53% output coupler, which generally lead to lower output power, but also lower threshold current than with the 96% output coupler. It was found that such higher feedback strength was instrumental for achieving stable fundamental mode-locked operation with pulse repetition rates lower than 1GHz. A broad continuous fundamental frequency tuning range from 1 GHz to 191 MHz along with a very broad harmonic repetition rate tuning range up to 6.8 GHz corresponding to 34^{th} order harmonic of 200 MHz fundamental frequency are presented and discussed.

7.3.2 Fundamental Mode-locking experimental results.

The RF spectra with a 10-GHz span for a variable fundamental mode-locking repetition rate from 1 GHz to 191 MHz at reverse bias of 8 V and forward current of 300 mA is shown in Fig. 7.5. The corresponding total optical cavity length varies from 15 cm to 78.5 cm. The output coupler of 53 % transmissivity was mounted on the translation stage with a 0.1 μm step motion. As a result, the level of continuity of tuning the repetition rate depends on the control precision of the frequency which can be up to 700 Hz and 30 Hz at the repetition rate of 1 GHz and 200 MHz, respectively. The large number of harmonics in the RF spectra indicates the high quality of mode-locking for all cases, as depicted in Fig. 7.5.

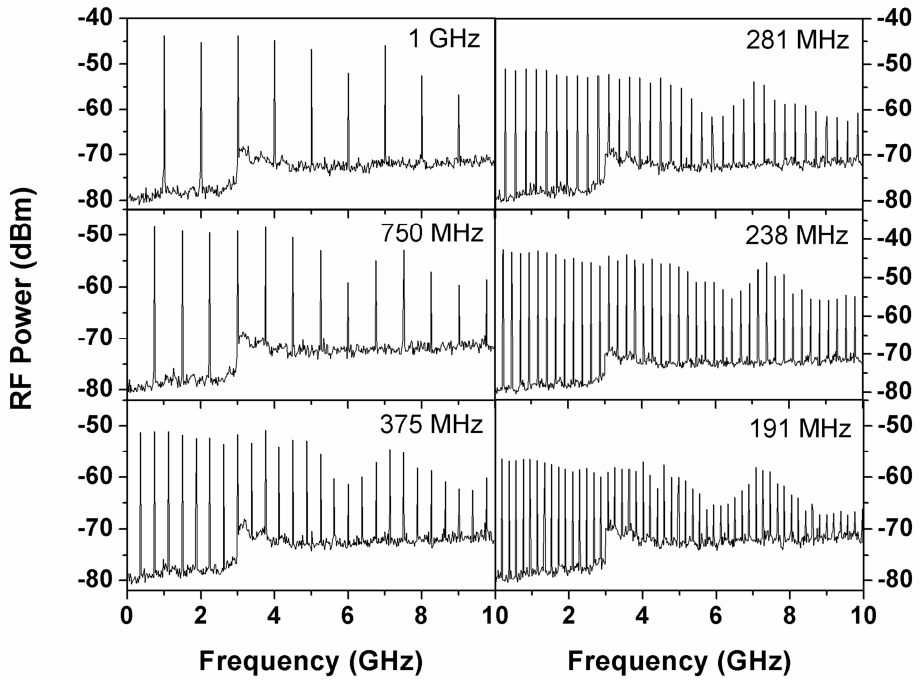

Fig. 7.5 Representative RF spectra with 10 GHz span at a reverse bias of 8 V and forward current of 300 mA recorded for the variable repetition rate from 1 GHz to 191 MHz.

Further investigations of the mode-locking performance were carried out for the

different repetition rates. The region of stable fundamental mode-locking regime for the repetition rate of 750 MHz is achievable between 3 V and 8 V reverse bias and forward current between 250 mA and 480 mA as plotted in Fig. 7.6.

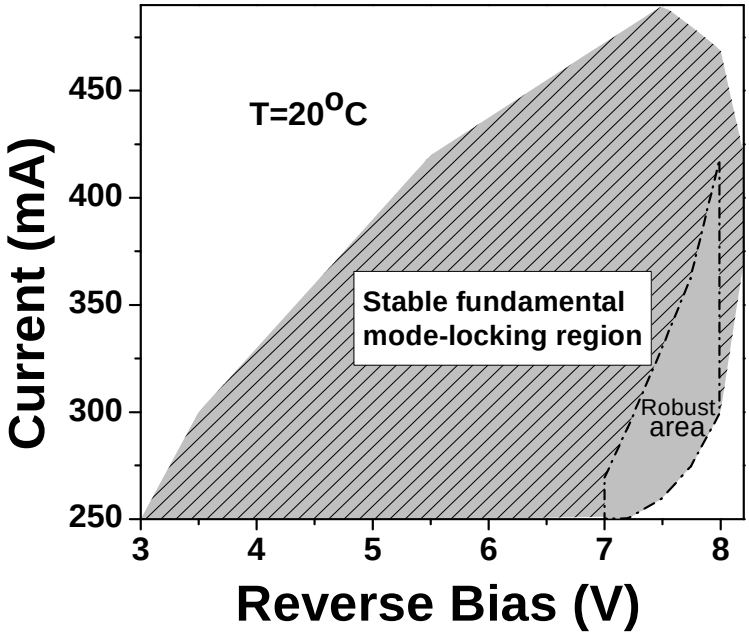

Fig. 7.6 A stable fundamental mode-locking regime with a repetition rate of 750 MHz.

As mentioned in section 7.2.2, the external cavity optical feedback from the output coupler should be optimized for each operating point in order to achieve stable fundamental mode-locking. In the robust operation area highlighted in Fig. 7.6, stable fundamental mode-locking can be obtained more easily and the setup has a high anti-jumping ability, e.g. resilience to vibration which is indicative of great application prospect. The region of robust fundamental mode-locking became narrower with higher values of current applied to the gain section due to the increasing tendency of the propagation of multiple pulses within the cavity which is favorable for operating in a harmonic mode-locking regime and a well-known phenomenon observed in monolithic mode-locked lasers [7, 19-20]. For the other pulse repetition rates, similar

mode-locking operation trends can be observed.

The peak power under 8 V reverse bias was found to remain nearly constant at about 0.5 W with increasing repetition rate from 191 MHz to 1 GHz at fix 300 mA forward current (Fig. 7.7 a) and with increasing current from 300 mA to 420 mA at a fixed 375 MHz repetition rate (Fig. 7.7 b). The average power increasing from 1 mW to 4.5 mW is linearly proportional to the repetition rate changing from 191 MHz to 1 GHz (Fig. 7.7 a) which implies that the constant pulse energy required to saturate the absorber is independent of repetition rate under certain operation conditions. This result is in principle in keeping with the conclusion reported in Ref. [21], where there is mention of constant pulse energy irrespective of pulse duration, repetition rate, reverse bias or drive current, for optimum mode-locking conditions. However, the fact of gradual increasing of average power and somewhat peak power with the increasing gain current for a certain reverse bias at a certain repetition rate (as in fig. 7.7 b) reveals an important issue for the employed external cavity setup (Fig. 7.1). The pulse duration slightly increases from 9.3 ps to 12 ps from 1 GHz to 281 MHz and then slightly decreases from 12 ps to 10.2 ps as repetition rate is further decreased up to 191 MHz (see fig. 7.7a). For the lowest 191 MHz fundamental repetition rate at 8V reverse bias and 300 mA forward current the pulse duration was 10.2 ps (fitted to a Gaussian pulse shape) as presented in the inset of fig.7.7a. The central wavelength was 1268 nm, with a full-width half-maximum of 5 nm, resulting in a time-bandwidth product of 9.5.

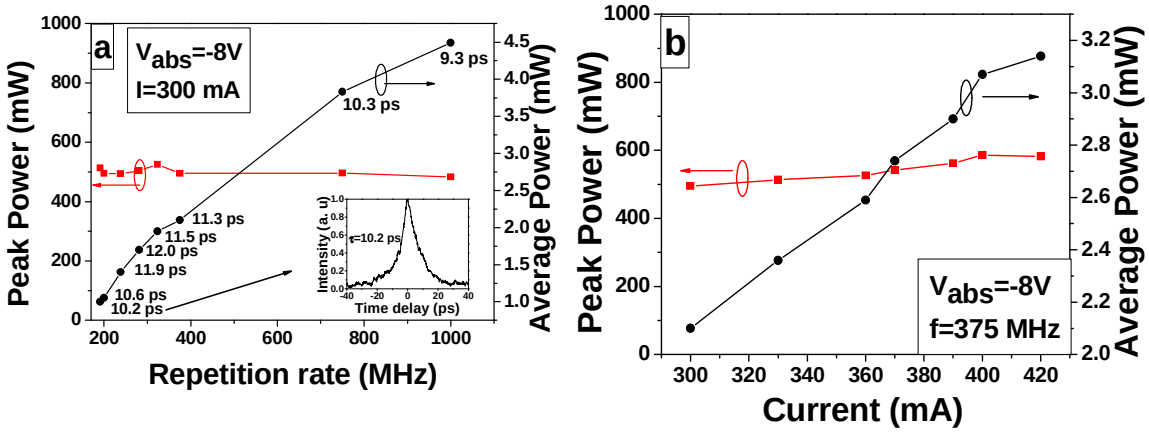

Fig. 7.7 Dynamics of a peak power and average power at 8 V reverse bias for **(a)** different pulse repetition rate for a fixed forward current of 300mA**, inset:** autocorrelation trace for 191 MHz corresponding to 10.2 ps pulse duration and **(b)** different driving forward current for a fixed repetition rate of 375 MHz.

For sustaining stable fundamental mode-locking, in one hand, the net gain should be low enough in a wide time window in order to suppress the high-order harmonic mode-locking, so the optimization of the feedback plays an important role. On the other hand, the pulse round trip time should not be much longer than spontaneous recombination time (for QD material in order of 1ns) otherwise stable mode-locking is overcome by spontaneous emission as noticed in [4, 6]. In order to keep the optical feedback at the appropriate level for stable fundamental mode-locking, it was noted that the photocurrent in the absorber should be kept at 6 mA-8 mA for optimal absorption saturation, independently of how much current was applied to the gain section. Consequently, the average output power (pulse energy) of stable fundamental mode-locking can be increased with increasing gain current due to the fixed transmissivity of the output coupler and the adjustable optical feedback. Obviously, for a higher gain current, a lower optical feedback is required to keep the balance of gain

and loss to achieve a stable fundamental mode-locking. Accordingly, as shown in previous section (7.2) a QD-based external cavity laser with an output coupler with higher transmissivity of 96 % will produce a higher output power, although the resonance formation and optical feedback adjustment are more challenging at a low frequency operation.

7.3.3 Harmonic Mode-locking experimental results.

An output coupler of 53 % transmissivity was placed 74 cm away from the external cavity two-section QD laser. The gain section of the laser was forward biased with 300 mA and reverse bias of 8V was applied to the absorber section. Fundamental mode-locking was achieved at 200 MHz frequency (corresponding to 5 ns pulse period). RF spectra with 10 GHz span was recorded as shown in Fig. 7.8 a), exhibiting a large number of harmonics indicating stable mode-locking. As discussed above, harmonic mode-locking can be achieved by increasing driving current to the absorber but at the same it is well known that pulse duration increases with current due to an increase in self-phase modulation effects with optical power, which in combination with the group velocity dispersion in the semiconductor laser leads to a pulse broadening with increasing current [22]. Wonderfully, harmonic mode-locking at fixed low gain current of 300 mA, reverse bias of 8V and cavity length corresponding to 200 MHz fundamental frequency was achieved by simply adjusting the collimating lens. A very broad harmonic repetition rate tunable range with picoseconds pulses from 800 MHz (4^{th}-order harmonic) up to 6.8 GHz corresponding to 34^{th}order harmonic of 200 MHz fundamental frequency was observed as shown in Fig. 7.8 b.

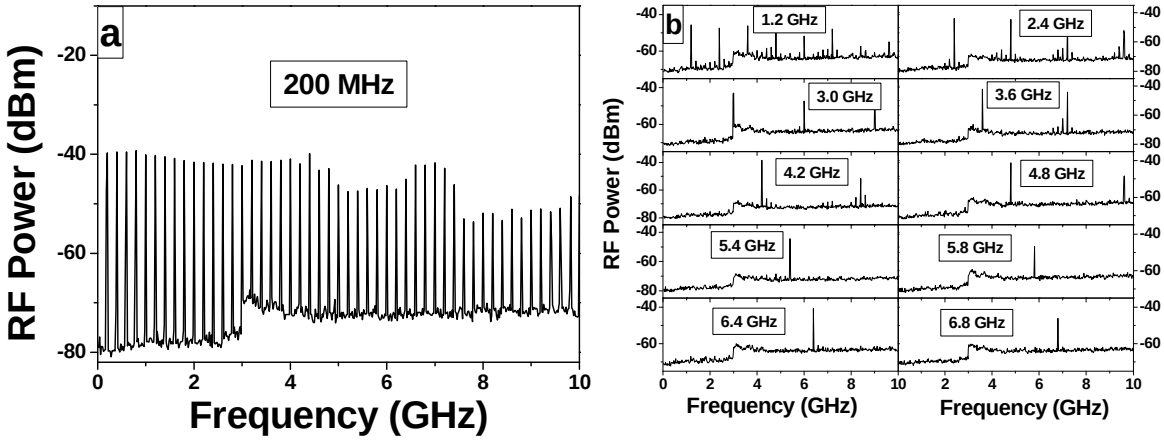

Fig. 7.8 (a) RF spectrum with 10 GHz span corresponding to a fundamental pulse repetition rate 200 MHz measured under a reverse bias of 8 V and forward current of 300 mA. The resolution and video bandwidth for this acquisition were 30 Hz and 3 Hz, respectively. **(b)** A broad tunable harmonics repetition rate region up to 6.8 GHz – 34^{th} order harmonic of a 200 MHz fundamental frequency.

7.3.4 Conclusion.

To conclude, the QD-based external cavity mode-locked laser offers broad repetition-rate tunability not only in fundamental but as well in harmonic regime of operations from a record low 191 MHz (fundamental) frequency to 6.8 GHz (harmonic) which can be very useful for ultrafast applications.

7.4 Narrow RF linewidth.

A record-low -3dB RF linewidth of ~30 Hz from the QD-based external- cavity passively mode-locked laser is illustrated for fundamental frequency of 281.3 MHz, which indicates the low noise and high stability operation of the device. The U dependence of -3dB RF linewidth with different fundamental repetition rates is measured and depicted [16, 18].

7.4.1 State of the art.

QD monolithic passively mode-locked lasers have shown very low noise performance, exhibiting a record-low RF linewidth of 500 Hz at 10 GHz repetition rates [23]. In a similar manner, a 1.58 μm quantum-dash-based passively mode-locked laser at 17 GHz has shown a RF linewidth of 500 Hz by using external optical feedback [24]. Lately, an RF linewidth narrowed up to 350 Hz by used of the external optical feedback was achieved from 5 GHz QD passively mode-locked laser [25]. Record-low noise performance from 12.8 GHz QD-based active harmonic mode-locked laser was made possible due to the external cavity configuration and electrical synchronization resulting in very low residual integrated timing jitter of 7.5 fs (in the range of 1Hz and 10 MHz) limited only by the driving synthesizer noise [26]. Such performance of mode-locked semiconductor lasers confirms the importance of QD materials in the pursuit of low-noise pulsed laser sources. In this section the lowest RF linewidth of ~30 Hz is presented from QD-based external cavity mode-locked laser. In addition, the dependence of RF linewidth on different repetition rates is studied.

7.4.2 Experimental results and discussion.

The experimental setup used for this experiment is the same as described in section 7.1.2 with an output coupler of 53 % transmissivity mounted on translation stage. A stable QD-based external cavity passively mode-locked laser operating regime was observed at 8V reverse bias and 300 mA for different repetition rates and RF spectra with 10 KHz span were measured with high resolution and video bandwidth (30Hz and 3Hz respectively) in order to determine the -3 dB RF linewidth by using a Lorentzian lineshape fitting. An extremely narrow -3 dB RF linewidth of ~30 Hz was attained at 281.3 MHz fundamental frequency due to the fact that the active waveguide occupies only a small fraction of the optical cavity (Fig. 7.9 a, b).

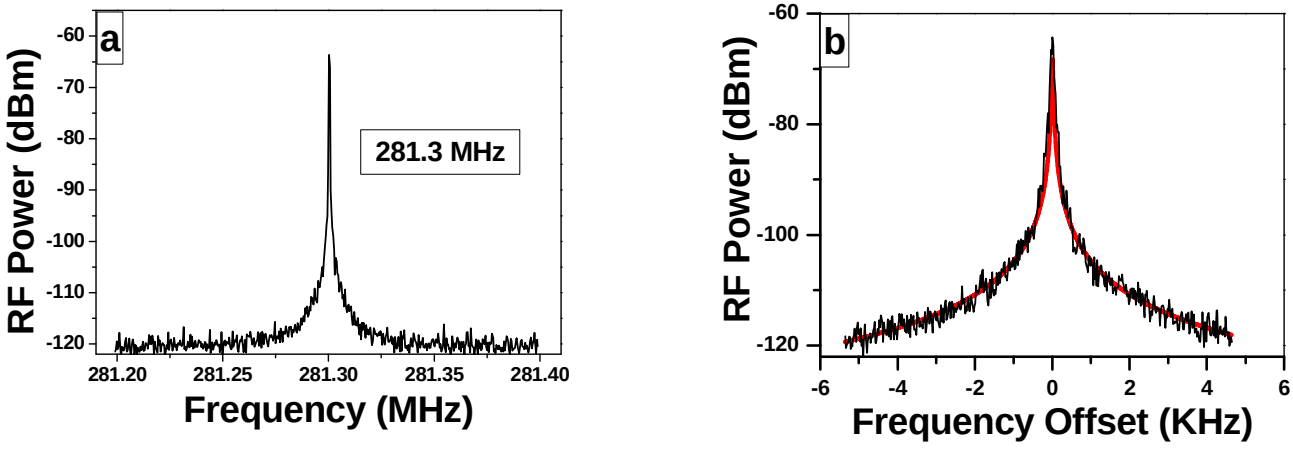

Fig. 7.9 (a) RF spectrum measured at a reverse bias of 8 V and forward current of 300 mA, at a 281 MHz pulse repetition rate. **(b)** RF spectrum with a 10 KHz span, with a -3dB linewidth of ~30 Hz (obtained after Lorentzian fit). The resolution and video bandwidth for this acquisition were 30 Hz and 3 Hz, respectively.

Moreover, the investigation of the influence of the repetition rate on RF linewidth

was carried out for the same bias conditions (8 V, 300 mA). It was found that as the repetition rate decreases from 332 MHz to 191 MHz the RF linewidth decreases from 300 Hz to 30 Hz as well, as shown in Fig. 7.10, after which the RF linewidth changes the trend in the opposite direction and increases up to 100 Hz. It is quite easily explained by two factors. In the first place, the cavity length which is longer for shorter repetition rates as the air occupies a higher fraction of the optical cavity, has less influences on the linewidth. Secondly, after a certain point mechanical instabilities along with spontaneous emission and perhaps some other factors play major role in defining the RF linewidth.

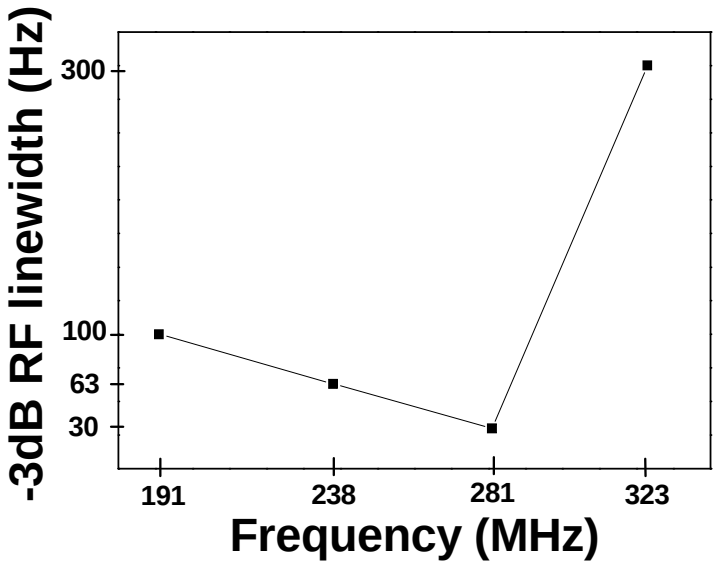

Fig. 7.10 Dynamic of -3 dB RF linewidth with frequency from the QD-Based external cavity mode-locked laser at a reverse bias of 8 V and forward current of 300 mA.

7.4.3 Conclusion.

QD based external cavity passively mode-locked lasers with ultra narrow RF linewidth of ~30 Hz have shown great potential as low-noise ultra-fast optical devices which can be used for varieties of applications including telecommunications.

7.5 Summary.

Electrically-pumped 1.3 µm QD mode-locked laser has shown great potential as a high power low noise optical source with tunable repetition rate. An average power of 60 mW at a repetition rate of 2.4 GHz corresponding to 25 pJ pulse energy was demonstrated. A high peak power of 1.5 W was achieved at a repetition rate of 1.14 GHz with optical pulses of 13.6 ps and an average power of 23.3 mW. The possibility of harmonic and fundamental mode-locking adds an extra level of versatility to the device which was achieved by using external cavity configuration. A fundamental frequency tuning range from 1 GHz to a record-low value of 191 MHz along with a harmonic repetition rate up to 6.8 GHz corresponding to 34^{th}order harmonic of 200 MHz fundamental frequency were presented. A low noise and high stability operation of the QD-based external-cavity passively mode-locked laser was illustrated by a record-low -3dB RF spectra of ~30 Hz for a fundamental frequency of 281.3 MHz.

7.6 References.

[1] E. U. Rafailov*, et al.*, "Mode-locked quantum-dot lasers," *Nature Photonics,* vol. 1, pp. 395-401, 2007.

[2] X. Huang*, et al.*, "Passive mode-locking in 1.3 μm two-section InAs quantum dot lasers," *Applied Physics Letters,* vol. 78, pp. 2825-2827, 2001.

[3] A. Gubenko*, et al.*, "High-power monolithic passively modelocked quantum-dot laser," *Electronics Letters,* vol. 41, pp. 1124-1125, 2005.

[4] M. G. Thompson*, et al.*, "InGaAs Quantum-Dot Mode-Locked Laser Diodes," *Selected Topics in Quantum Electronics, IEEE,* vol. 15, pp. 661-672, 2009.

[5] M. T. Choi*, et al.*, "Ultrashort, high-power pulse generation from a master oscillator power amplifier based on external cavity mode locking of a quantum-dot two-section diode laser," *Applied Physics Letters,* vol. 87, pp. 221107-3, Nov 2005.

[6] A. D. McRobbie*, et al.*, "High power all-quantum-dot-based external cavity modelocked laser," *Electronics Letters,* vol. 43, pp. 812-813, 2007.

[7] M. Xia*, et al.*, "External-Cavity Mode-Locked Quantum-Dot Laser Diodes for Low Repetition Rate, Sub-Picosecond Pulse Generation," *Selected Topics in Quantum Electronics, IEEE,* vol. PP, pp. 1-1, 2011.

[8] M. Kuramoto*, et al.*, "Two-photon fluorescence bioimaging with an all-semiconductor laser picosecond pulse source," *Opt. Lett.,* vol. 32, pp. 2726-2728, 2007.

[9] H. Yokoyama*, et al.*, "Nonlinear-microscopy optical-pulse sources based on mode-locked semiconductor lasers," *Opt. Express,* vol. 16, pp. 17752-17758, 2008.

[10] S.-W. Chu*, et al.*, "Real-time second-harmonic-generation microscopy based on a 2-GHz repetition rate Ti:sapphire laser," *Opt. Express,* vol. 11, pp. 933-938, 2003.

[11] J. Kim*, et al.*, "Pulse generation and compression via ground and excited states from a grating coupled passively mode-locked quantum dot two-section diode laser," *Applied Physics Letters,* vol. 89, Dec 2006.

[12] X. Q. Lv*, et al.*, "Broadband external cavity tunable quantum dot lasers with low injection current density," *Opt. Express,* vol. 18, pp. 8916-8922, 2010.

[13] T. W. Berg and J. Mork, "Quantum dot amplifiers with high output power and low noise," *Applied Physics Letters,* vol. 82, pp. 3083-3085, 2003.

[14] P. Vasil'ev, *Ultrafast Laser Diodes: Fundamentals and Applications*. London: Artch House, 1995.

[15] Y. Ding*, et al.*, "Quantum-dot external-cavity passively modelocked laser with high peak power and pulse energy," *Electronics Letters,* vol. 46, pp. 1516-1518, 2010.

[16] M. A. Cataluna*, et al.*, "High-Power Versatile Picosecond Pulse Generation from Mode-Locked Quantum-Dot Laser Diodes," *Selected Topics in Quantum Electronics, IEEE,* vol. PP, pp. 1-9, 2011.

[17] Y. Ding*, et al.*, "Fundamental and harmonic mode-locking with pulse repetition rate between 200 MHz and 6.8 GHz in a quantum-dot external-cavity laser," in *Lasers and Electro-Optics Europe (CLEO EUROPE/EQEC), 2011 Conference on and 12th European Quantum Electronics Conference*, 2011, pp. 1-1.

[18] Y. Ding*, et al.*, "Broad Repetition-Rate Tunable Quantum-Dot External-Cavity Passively Mode-Locked Laser with Extremely Narrow Radio Frequency Linewidth," *Applied Physics Express,* vol. 4, 2011.

[19] S. Arahira*, et al.*, "Terahertz-rate optical pulse generation from a passively mode-locked semiconductor laser diode," *Opt. Lett.,* vol. 19, pp. 834-836, 1994.

[20] E. A. Viktorov*, et al.*, "Stability of the mode-locked regime in quantum dot lasers," *Applied Physics Letters,* vol. 91, pp. 231116-231116-3, 2007.

[21] M. Xia*, et al.*, "External-cavity mode-locked quantum-dot lasers for low repetition rate, sub-picosecond pulse generation," in *Lasers and Electro-Optics, 2008 and 2008 Conference on Quantum Electronics and Laser Science. CLEO/QELS 2008. Conference on*, 2008, pp. 1-2.

[22] R. G. M. P. Koumans and R. Van Roijen, "Theory for passive mode-locking in semiconductor laser structures including the effects of self-phase modulation, dispersion, and pulse collisions," *Quantum Electronics, IEEE,* vol. 32, pp. 478-492, 1996.

[23] G. Carpintero*, et al.*, "Low Noise Performance of Passively Mode-Locked 10-GHz Quantum-Dot Laser Diode," *Photonics Technology Letters, IEEE,* vol. 21, pp. 389-391, 2009.

[24] K. Merghem*, et al.*, "Low noise performance of passively mode locked quantum-dash-based lasers under external optical feedback," *Applied Physics Letters,* vol. 95, pp. 131111-131111-3, 2009.

[25] C. Y. Lin*, et al.*, "rf linewidth reduction in a quantum dot passively mode-locked laser subject to external optical feedback," *Applied Physics Letters,* vol. 96, pp. 051118-051118-3, 2010.

[26] M.-T. Choi*, et al.*, "Ultralow noise optical pulse generation in an actively mode-locked quantum-dot semiconductor laser," *Applied Physics Letters,* vol. 88, pp. 131106-3, 2006.

Chapter 8. Quantum-Dot tapered lasers.

8.1 Introduction.

8.1.1 Basics of tapered lasers.

Low-cost, miniature semiconductor diode lasers are highly efficient light sources which have been widely used in a range of applications, most notably in optical fibre communications and biomedical applications. The improvement in their performance in terms of ultrashort pulse generation, good beam quality, high peak power as well as high average power will transform such devices into extraordinarily interesting and promising candidates for an extended variety of applications in industry and science, ranging from nonlinear biomedical imaging, nano-surgery, materials processing through to laser projector displays and free space optical communications [1-5]. Edge-emitting mode-locked semiconductor lasers with flared (tapered) waveguides are well-known for their capability to deliver high output power as well as ultrashort pulses [6-13]. For example, a single contact tapered mode-locked laser incorporating 3 layers of InGaAs quantum wells can generate pulses as short as 850 fs at 116 GHz resulting in 60 mW peak power [14]. But typically tapered lasers consist of a straight ridge-waveguide section coupled to a tapered section [7-10, 13]. Quantum-well tapered lasers with index-guided straight ridge waveguide section coupled to a gain-guided tapered section were effectively realized, generating high output power (more than 14 W at 980 nm) with good beam quality (M^2 <2) [8-10]. While the straight waveguide acts as a spatial filter in the cavity, the tapered section of increasing width delivers high power. As a result, tapered lasers show a great potential for providing single spatial mode, good quality beams with high power, as demonstrated by Mar *et. al.* [15]. In this paper, mode locking was achieved in an external cavity configuration, while using a

quantum well $In_{0.2}Ga_{0.8}As$ tapered laser – resulting in the generation of 3.3 ps pulses with 2 W peak power in the waveband of 980 nm [15]. Alternative technology based on high power passively mode-locked slab-coupled optical waveguide lasers (SCOWLs) has been demonstrated by several groups [16-17]. For instance, a 1.5 μm InGaAsP multi-quantum well mode-locked semiconductor SCOWL produced 10 ps pulses with energies of 58 pJ and average powers of 250 mW at a repetition rate of 4.29 GHz achieving 5.8 W peak power [16]. Moreover, in external-cavity configurations, record-high peak power pulses have been generated from edge-emitting external-cavity lasers with additional amplification and compression stages (and thus unavoidably larger footprint), resulting in pulses with 2.5 kW peak power [18]. VECSELs have also demonstrated their usefulness for ultrafast applications which require high peak power, such as multi-photon imaging [19].

8.1.2 Different designs of tapered laser.

Passively mode-locked quantum-dot (QD) lasers have attracted much attention of late as efficient compact ultrafast and high-power light sources due to their unique properties as discussed above in section 2.3 [20-22]. The combination of tapered waveguide laser design for higher power and passively mode-locking technique for short pulse duration has been successfully shown [23]. Tapered lasers can be designed in different ways: fully index-guided, index-gain guided designs (Fig.8.1 a, b). The latter, as it was mentioned above, can generate high continuous wave (CW) output power. Quantum-dot fully index-guided tapered lasers were able to generate transform-limited pulses with pulse durations of 360 fs, average power up to 15.6 mW, resulting in only 2.25 W peak power (under 12^{o}C operating temperature), although the mechanisms for the generation of transform- limited pulses from such a device without any additional dispersion compensation are not fully understood [24]. A new laser structure was proposed and processed by III-V Lab using fully gain-guided design (Fig. 8.2). More details about the new design will be given in the next section.

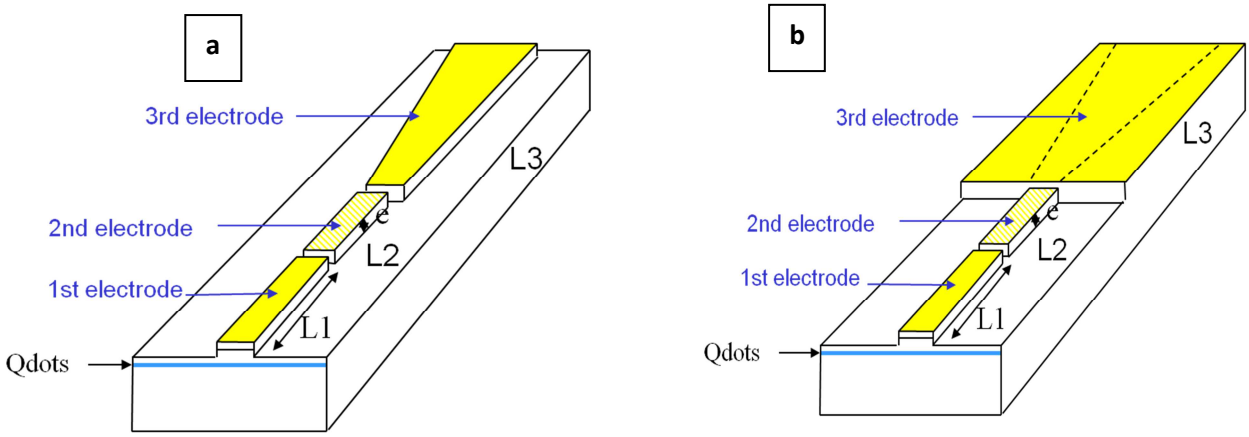

Fig. 8.1 A schematic of the tapered **(a)** fully-index and **(b)** index- gain-guided lasers.

In addition, fully gain-guided tapered lasers have the advantage of simpler, lower cost and rapid fabrication process compared to other tapered laser designs as it does not require any etching of a ridge.

8.2 First iteration of tapered lasers.

In the first iteration devices, the highest peak power of 3.6 W was achieved from a monolithic passively mode-locked quantum-dot tapered laser by using fully gain-guided tapered laser geometry [25].

The fabricated and investigated tapered lasers incorporated either 5 or 10 layers of InGaAs/GaAs quantum dots. Picosecond pulse generation with a high average power of 209 mW corresponding to 14.2 pJ pulse energy with 14.65 GHz repetition rate is demonstrated, which is more than one order of magnitude higher than previous results [24].

8.2.1 Fully gain-guided high power tapered lasers.

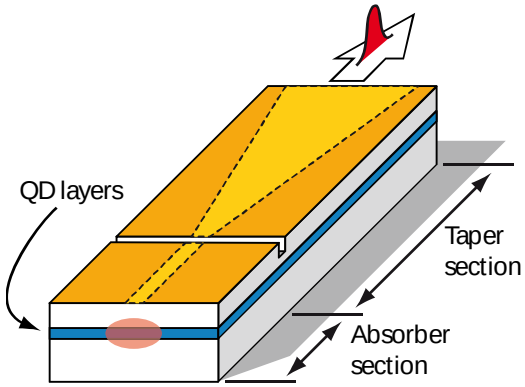

Fig. 8.2 A schematic of the tapered fully gain guided laser.

The QD epitaxial structures used in the tapered lasers were grown on a GaAs substrate using Molecular Beam Epitaxy (MBE). Two different structures were used, where the active region consisted of either 5 or 10 identical layers of InAs quantum dots separated by 33 nm GaAs barriers and incorporated in a AlGaAs waveguide with 35% Al content. The tapered lasers were fabricated with planar gain-guided tapered and straight waveguide section defined only by ion implantation, resulting in a gain-guided geometry (Fig. 8.3). The spontaneous emission coupling factor (β) in gain-guided lasers is larger than that in lasers with a comparable active layer volume and with a built-in index waveguide [26]. Owing to the large β, the spectral width of gain-guided lasers is significantly broader compared to lasers with a built-in index waveguide [26-27]. Accordingly, broad spectra of gain-guided lasers could afford potential for narrow pulses compared to index-guided lasers provided all of the bandwidth can be engaged coherently. The tapered sections are 2370 µm and 2380 µm long for the 5 layers and 10 layers devices respectively, with 2° taper angle, while the single spatial mode straight sections for mode filtering have a 400-µm length in both devices resulting in an absorber-to-gain length ratio of 1:6. A reverse bias was

applied to the straight waveguide section, which acted as a saturable absorber. The total lengths of the devices were therefore 2.77 mm (2.78 mm), resulting in a pulse repetition rate of 14.65 GHz (14.57 GHz). The anti-reflection coating (TiO_2/SiO_2) on the tapered section side and the high-reflection coating (Al_2O_3/Si)*3 on the ridge side were 3% and 95%, respectively. The central operating wavelengths are around 1250 nm (1260 nm) for the 5- and 10-layer devices, respectively. The lasers were mounted on a Peltier cooler and their operating temperatures were stabilized at 20^{o}C.

8.2.2 Experiments and Discussion.

By changing the driving conditions of the tapered and absorber sections (to which forward and reverse bias were applied respectively), stable mode-locking was achieved for a broad range of current and reverse voltage conditions. The light-current characteristics of the tapered lasers with 5 and 10 QD layers were measured at room temperature, and are shown in Figure 8.3. The highest output power exceeds 890 mW at 1800 mA, with a threshold current of 179 mA for a 5-layer QD structure under uniform current injection into both the gain and absorber sections. The slope efficiency of about 0.6 W/A with a lasing wavelength of ~1252 nm can be obtained.

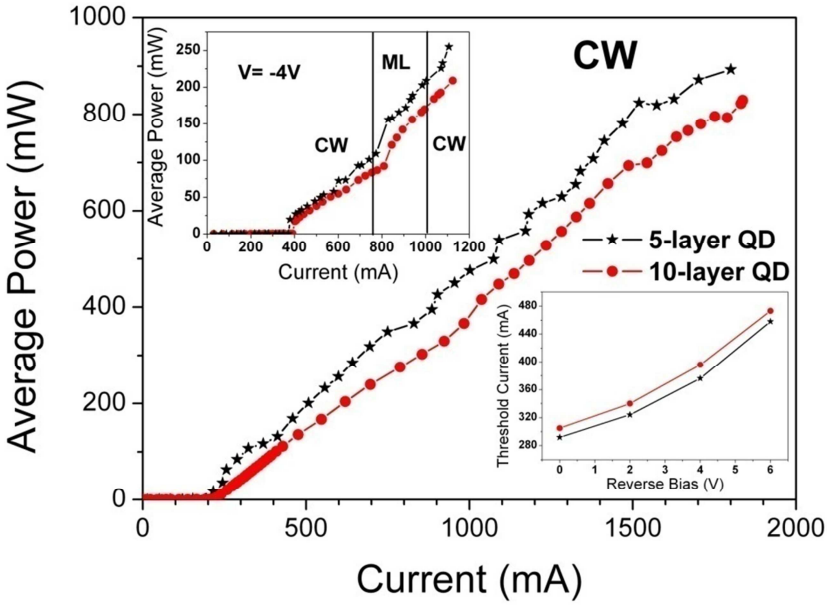

Fig. 8.3 Light-current (L-I) characteristics for fully connected 5-layer and 10-layer quantum dot devices. **Upper left inset**: L-I characteristics obtained for an applied absorber bias of -4 V. **Lower right inset**: dependence between the threshold current and the absorber bias.

On the contrary, the 10-layer QD laser has slightly lower output power (822 mW at 1830 mA) and larger threshold current (211 mA) under uniform injection. The range of

driving conditions over which stable mode-locking occurs at -4 V reverse bias for the 5-layer QD laser is illustrated in the upper left inset of Figure 8.3. The slope efficiency is estimated at 0.55 W/A with lasing wavelength located at ~1260 nm. We would like to point out that the difference in emission wavelength between the 5- and the 10-layer tapered lasers is not due to temperature variations, as the same bias conditions were applied and the same Peltier cooler was used to stabilise the operating temperature of both lasers. The most probable causes for this difference could be the result of a QD structure discrepancy. In fact, as is well known, an increase in QD size can lead to slightly red-shift of the QD transition wavelength, whereas a minute increase of In content in the capping layer of InGaAs may also produce a red-shift of QD transition wavelength.

The occurrence of stable mode-locking was examined as a function of the bias conditions – as represented in Figure 8.4, the 10-layer QD laser showed a wider mode-locking region compared to the 5-layer QD laser. For the 10-layer QD laser a narrow region of an unstable mode-locking regime was observed. In this regime, a combination of fundamental and harmonic mode-locking was observed, as was evident in the RF spectra and in the autocorrelation measurements. For the 5 QD-layer laser, the pulse duration and average power were measured as a function of an applied gain current, for a reverse bias of -4 V, as shown in Figure 8.5. A maximum high average power of 209 mW corresponding to 14.2 pJ pulse energy with 6-ps pulse duration is observed at -4 V reverse bias and 1 A current for this tapered laser.

The spatial beam characteristics of the 10-layer quantum-dot laser were also investigated in great detail. Far field and near field in the slow axis have been measured with a rotating photodiode and a vidicon camera. The fully gain-guided structure allows obtaining a stable far field with a low divergence. Indeed, under

uniform injection (Figure 8.6 a), the far field full width at half maximum (FWHM) varies from 1.7° to 1.1° when the current increases from 400 mA up to 800 mA. The corresponding far-field FWHM values at $1/e^2$ vary from 3.4° to 2.6°, and the near field ones from 28 µm to 65 µm. Single-lateral mode with a low divergence was therefore achieved with the beam quality parameter M^2 varies between 1.1 and 1.4. The method of measuring M^2 at $1/e^2$ that was used here is fast and easy one but it doesn't take all the beam profile into account. According to the International Standards Organization (ISO 11146) M^2 should be defined through the hyperbolic curve of real beam which is time consuming but gives more accurate value of M^2.

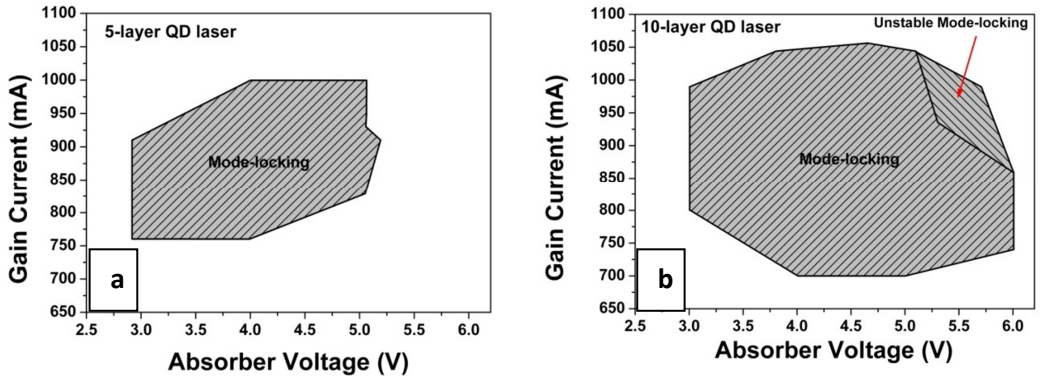

Fig. 8.4 Mapping of mode-locking regimes observed for **(a)** the 5-layer quantum dot laser, **(b)** the 10 layer quantum dot laser.

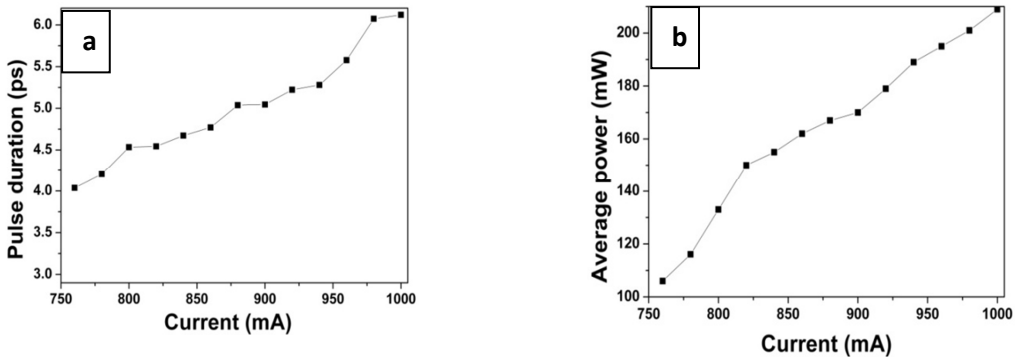

Fig. 8.5 (a) Pulse duration and **(b)** average power dynamics at a reverse bias -4 V for the 5-layer quantum dot laser.

Far field FWHM and M^2 remain below 2.7°and 3 respectively, for currents less than 1.2 A. Under -4 V reverse bias on the absorber section (Fig.8.6 b), the FWHM varies between 1.3° and 1.8°, while the $1/e^2$ values range between 2.3° and 3.6°. The M^2 varies between 1.1 and 1.8 [28]. Both tapered lasers - with either 5 or 10 layers of quantum dots - have demonstrated high peak power pulse generation. The highest peak power of 3.6 W is measured for a driving current of 950 mA (1044 mA) and 5.1 V (4.9 V) reverse bias for 5 (10) layers lasers respectively. The corresponding autocorrelation, RF and optical spectra are shown in Figure 8.7 and Figure 8.8. Gaussian shapes have been assumed to calculate the pulse width. The combination of a pulse duration of 3.2 ps (3.3 ps), and an optical spectrum FWHM of 7.3 nm (8.4 nm) results in a time-bandwidth product (TBWP) of 4.4 (5.2) measured from the 5- and 10-layer devices accordingly.

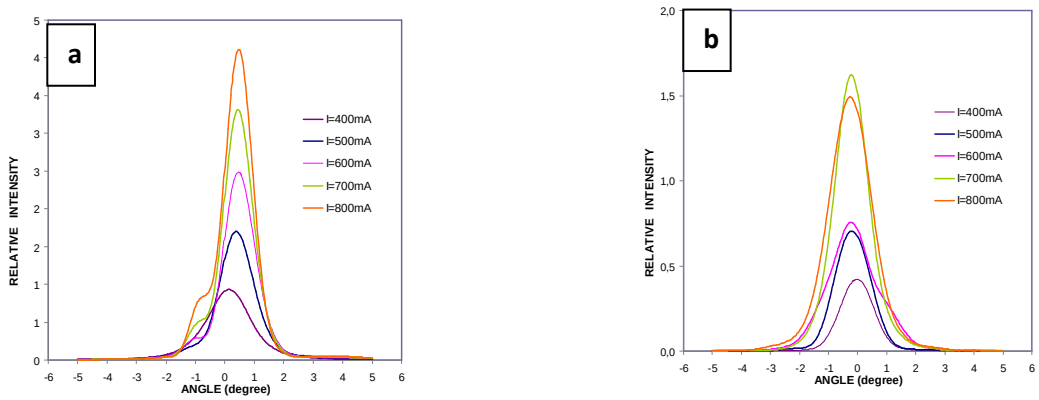

Fig. 8.6 Far-fields **(a)** under uniform injection and **(b)** under -4 V reverse bias on the absorber section for the 5-layer quantum dot laser (characterized by III-V Lab, France).

The generated pulse is therefore not transform-limited, which opens the possibility for significant pulse post-compression, which allows the potential to boost the peak power up to ~20 W by theoretical estimation. Further investigation work presented in next section was pursued by fabricating lasers with a smaller gain-to-absorber length

ratio, for instance from 6:1 (as in the present work) to 4:1, in order to generate shorter pulses as described in ref. [24].

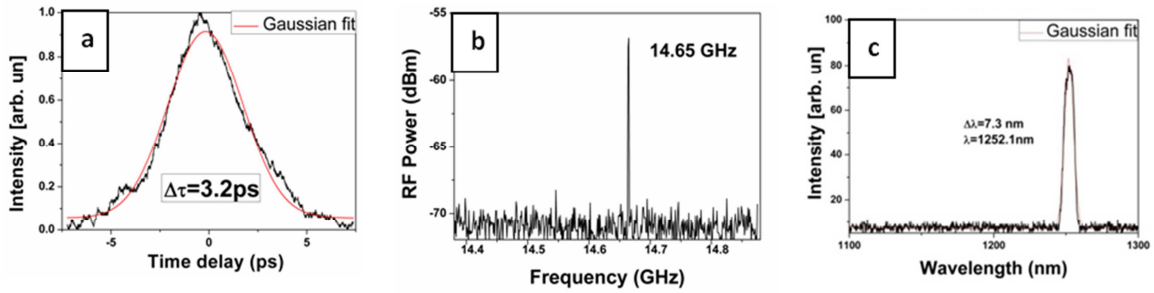

Fig. 8.7 (a) Autocorrelation, **(b)** RF spectrum and **(c)** optical spectrum for an injection current of 950 mA and reverse bias of 5.1 V at a high peak power regime in the 5-layer quantum dot laser.

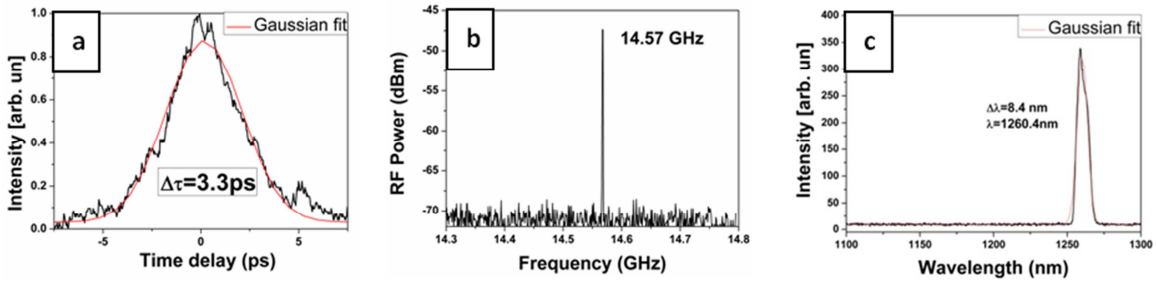

Fig. 8.8 (a) Autocorrelation, **(b)** RF spectrum and **(c)** optical spectrum for an injection current of 1044 mA and reverse bias of 4.9 V at high peak power regime in the 10-layer quantum dot laser.

8.2.3 Conclusion.

Novel tapered quantum-dot lasers with a gain-guided geometry operating in a passively mode-locked regime have been fabricated and investigated, using structures that incorporated either 5 or 10 QD layers. The generation of picosecond pulses with high average power of up to 209 mW was demonstrated, corresponding to 14.2 pJ pulse energy. A low slow axis far-field was demonstrated, which remains stable even under a high-current injection. Furthermore, a highest peak power of 3.6 W is achieved for a tapered quantum-dot laser (corresponding to a pulse duration of 3.2 ps), with a time-bandwidth product that offers the potential of further pulse post-compression for boosting the peak power up to 10 times – and thus forming the basis of an extremely compact ultrafast laser system**.**

8.3 Second iteration of tapered lasers.

8.3.1 Introduction.

It was previously shown that a reduction of the pulse duration from 2.3 ps to 800 fs can be achieved by changing the absorber-to-gain length ratio from 14:1 to 3:1 in straight QD waveguide lasers [29] and a similar approach has been successfully undertaken for two-section QD mode-locked index-guided tapered lasers [23-24]. A great improvement in output average power and peak power was shown in the previous section [25].

In this section, the generation of 6 ps pulses with a high average power of 209 mW corresponding to pulse energy of 14.2 pJ was achieved. Furthermore, by using an absorber-to-gain length ratio of 1:6, a high peak power of 3.6 W was directly generated from monolithic tapered fully gain-guided 5-layer and 10-layer quantum-dot lasers with optical pulses of 3.2 ps and 3.3 ps, respectively [25]. Here the record-high 17.7 W peak power is reported from monolithic two-section quantum-dot tapered laser with 1.26 ps pulse duration. A high average power of 287.7 mW with 2.2 ps pulses, corresponding to 28.7 pJ pulse energy is achieved. Phase noise and integration timing jitter of 2.6 ps is also demonstrated. Moreover, the generation of ultrashort Fourier-limited 672 fs pulses width with peak power of 3.4 W was achieved with another optimized structure where the absorber-to-gain length ratio was 5:1 [30].

8.3.2 Optimized fully gain-guided tapered lasers.

The QD wafer was grown on a n+-GaAs substrate by Molecular Beam Epitaxy (MBE), incorporating 10 identical layers of undoped InAs QDs separated by 35 nm GaAs barriers, which are used for eliminating high strain accumulation in each QD layer, and integrated in an AlGaAs waveguide. The investigated fully gain-guided tapered lasers were processed by III-V Lab the same way as the first iteration consisting of two separate and electrically-insulated sections: a narrow straight section near the back facet, which acts as a cavity spatial filter, extended by a tapered part which acts as an amplifier. Proton implantation has been performed outside the electrode area to achieve lateral gain guiding and to improve the electrical isolation between the two sections, resulting in fully gain-guided two-section geometry. For mode-locked operation, a reverse bias and forward current are applied to the straight and tapered sections, which act as saturable absorber (SA) and gain sections, respectively. The two lasers with different designs are denoted with A and B characterized at the Technical University of Darmstadt and the University of Dundee, respectively. The lengths of the straight and tapered sections are 0.4 mm (0.8 mm) and 2.14 mm (3.2 mm) for device A (B), respectively resulting in a total cavity length of 2.54 mm (4.00 mm), thus corresponding to a repetition rate of 16 GHz (10 GHz). The full taper angle was 2^{o} for both devices with linear flares from 14 µm (14 µm) to 88 µm (124 µm). A schematic of the tapered fully gain-guided laser was presented previously in Fig. 8.2. Anti-(TiO_2/SiO_2) and high-reflective (Al_2O_3/Si)*3 coatings of 3 % and 95 % were deposited on the front/back facets respectively. The lasers were mounted on a Peltier cooler to maintain the operating temperature of 20 ^{o}C. The central emission wavelength was around 1260 nm. The described designs have been derived from numerical simulations

[31-33] of the mode-locking regimes and their dependence on the particular structure layout. In the following section, a brief description of the major findings from the design procedure is outlined.

8.3.3 Simulation results.

The design of the optimized structures was obtained by performing preliminary beam propagation method simulations to verify the adiabatic transformation of the field in the tapered gain section, and by subsequently investigating the mode-locking regimes via both a delayed differential equation (DDE) numerical model [31] and a one-dimensional time-domain travelling-wave (TDTW) model [32], phenomenologically including the effect of the tapered gain section through a dependence of the active region volume and transverse field profile on the longitudinal position of the cavity.

Starting from the experimental results presented in section 8.2 [25], the possibility to further optimize the gain guided device was investigated at the Politecnico di Torino, Italy.

Tapered long cavities lasers operating in CW regime have shown the ability to generate a high output power [8-10]. However, in the mode-locking regime tapered long cavity lasers are exhibiting a large leading edge instability with increasing current induced by the spontaneous emission noise as dynamic simulations show in [34], resulting in low average and peak power from the devices. In order to overcome this obstacle, two different approaches have been therefore implemented:

I. A short cavity length (2.5 mm) is used with respect to the devices described in previous section (8.2) [25] but with the absorber-to-gain length ratio changed from 1:6 to 1:5. The simulations showed the possibility of generating shorter pulses from mode-locked lasers as already pointed out in [24]. The interplay between pulse shortening and pulse broadening mechanisms takes place within the device. Due to the small available density of states in the gain, the differential gain in the absorber is higher. The ratio between the differential gain in the absorber and gain is increased due to the

discrete nature of DOS as described in chapter 2. The increased absorber-to-gain length ratio enhances the losses in the absorber; this ensures a very small differential gain that highly reduces the gain saturation due to total carrier density depletion. In addition, the larger area of the tapered section with full angle of 2° was considered allowing a further increase in the gain saturation energy [24]. In this condition, gain saturation balancing the absorption bleaching in the SA is mainly due to spectral hole burning non-linearities enabling the generation of ultrashort mode-locked pulses.

II.A device with higher than in [25] total length (4 mm) and with highly enhanced the absorber-to-gain length ratio in order to avoid the onset of large leading edge instabilities with increasing current is considered. The simulations identified the ratio 1:4 as the optimum ratio. Furthermore the same full angle of 2° characterizing the tapered gain section was considered. As shown in Fig. 8.9 and Fig. 8.10, changing the absorber-to-gain length ratio from 1:6 [25] to 1:4 allows the full Elimination of the onset of leading edge instabilities in the ML regime, enabling large average power and, as for the case I, to significantly shorten the achieved mode-locked pulses. In addition, the reduced pulse repetition rate also contributes to the achievement of higher energy pulses.

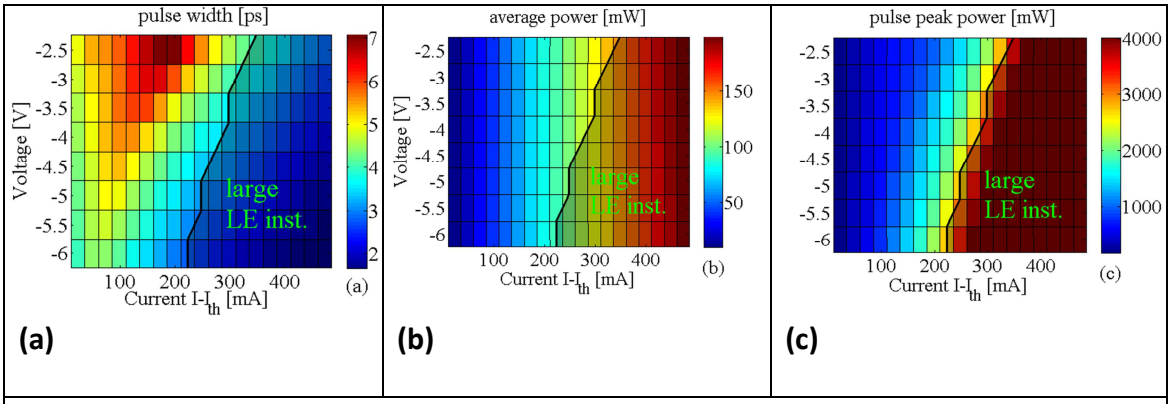

Fig. 8.9 Simulated pulse width **(a)**, average power **(b)** and peak power **(c)** as a function of the SA voltage and current above threshold I-I_{th}, for a 4 mm device with a 2° full angle tapered gain section and 17% SA section to gain section length ratio. Shaded region highlights unstable ML due to large leading edge (LE) instability (performed by the Politecnico di Torino, Italy).

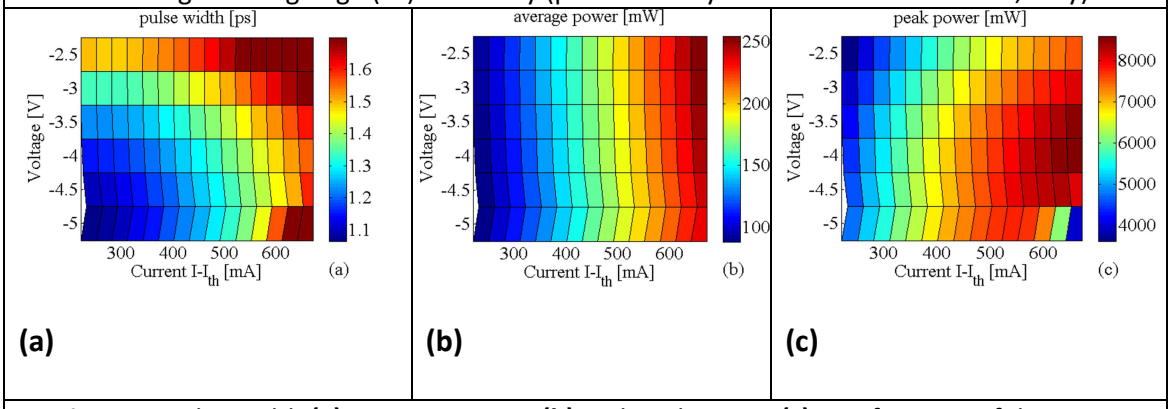

Fig. 8.10 Pulse width **(a)**, average power **(b)** and peak power **(c)** as a function of the SA voltage and current above threshold I-I_{th}, for a 4 mm device with 2° full angle tapered gain section and 25% SA section to gain section length ratio. No leading edge instability to spontaneous emission noise perturbations has been observed in the investigated range of bias parameters (performed by the Politecnico di Torino, Italy).

8.3.4 Experiments and Discussion.

Pulse measurements were carried out with an autocorrelator using second harmonic generation. Optical and RF spectra were recorded by respective analyzers. The experimental setup is shown in Fig. 8.11.

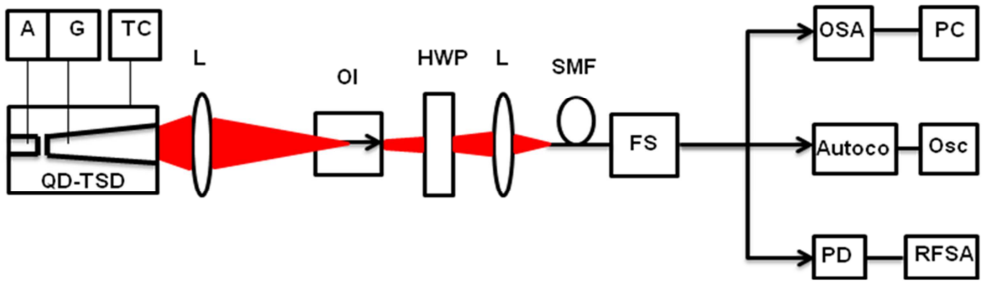

Fig. 8.11 Dynamic characterization experimental setup: QD -TSD: quantum dot - two section diode, A- absorber section, G: gain section, TC: temperature controller, L: lens, OI: optical isolator, HWP: half wave plate, SMF: single-mode fiber, FS: fiber splitter, OSA: optical spectrum analyzer; PC: personal computer; Autoco: autocorrelator; Osc: oscilloscope; PD: photo detector; RFSA: RF spectrum analyzer.

It was identified that the optimum reverse voltage for generation of the shortest pulses in the mode locking regime for device A is -6.0 V. A region of mode locking was from 570 mA to 625 mA and from 675 mA to 720 mA. Below 570 mA incomplete mode-locking occurs, above 720 mA strong modulation at a frequency of 560 MHz is existent and in the intermediate non mode-locking region a progressive repetition rate transition takes place [35]. The light-current characteristic at -6.0 V reverse bias is shown in Fig. 8.12. The lasing threshold amounts to 500 mA at -6.0 V and the total output power at a gain current of 720 mA amounts to 72 mW. This current corresponds to the upper border of the ML regime and thus provides the highest average power. Mode locking starts at 570 mA which is close to lasing threshold. The shortest pulse width of 672 fs is observed at 570 mA and the corresponding pulse trace

is depicted in Fig. 8.13. The calculated time-bandwidth-product amounts to 0.35 using a sech² fit for the autocorrelation.

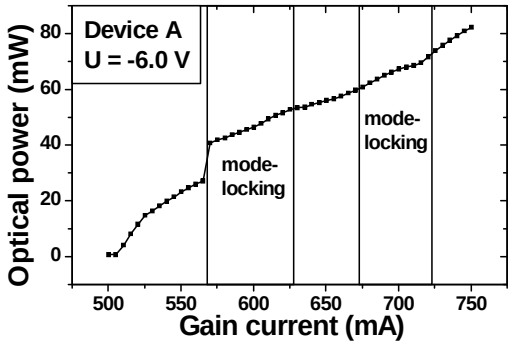

Fig.8.12 Light current characteristic for device A at a reverse bias of -6.0V. The shortest pulses are obtained at 570 mA and the highest peak power at 695 mA (Characterized at Technical University of Darmstadt, Germany).

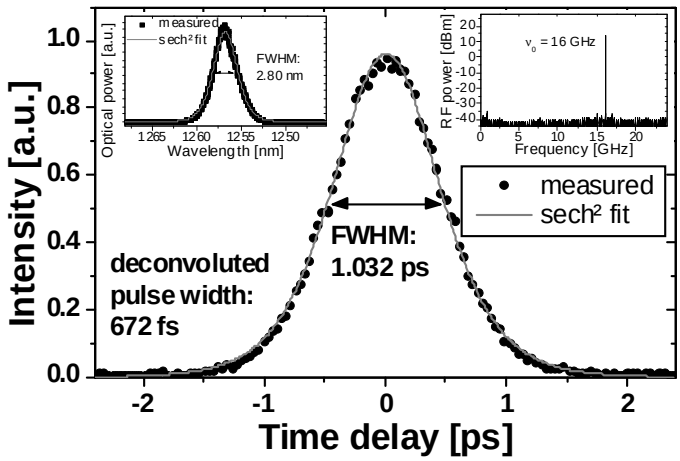

Fig. 8.13 Autocorrelation signal of the shortest pulse width of laser A; inset left: an optical spectrum; inset right: RF spectrum at a gain current of 570 mA and reverse bias of -6.0 V. Sech^2 fit. (Characterized at Technical University of Darmstadt, Germany).

Within the complete mode-locking regime a time-bandwidth product below 0.77 is measured and from 570 mA to 600 mA Fourier-limited pulses are obtained. The influence of the gain current on the pulse width is shown in Fig. 8.14. The pulse width increases from 672 fs at 570 mA to 938 fs at 720 mA.

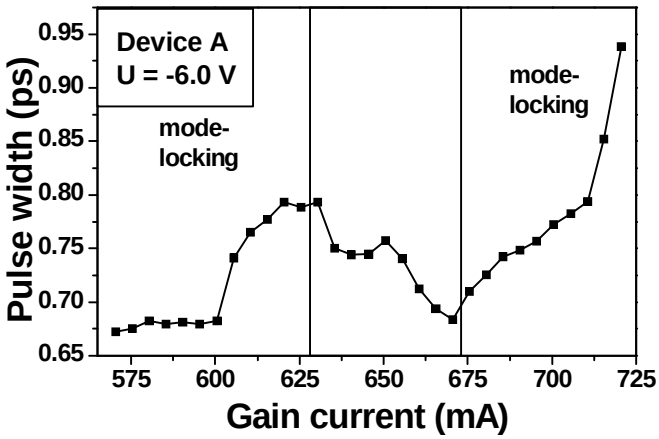

Fig. 8.14 Pulse width in dependence of a gain current of laser A at a reverse bias of -6.0 V (Characterized at Technical University of Darmstadt, Germany).

The peak power from the measured pulse width, average power and the repetition rate were estimated. The peak power evolution in dependence of gain current is depicted in Fig. 8.15. Peak power increases from 3.8 W at 570 mA to 4.78 W at 720 mA with a maximum peak power of 5.48 W together with a pulse width of 757 fs at a gain current of 695 mA. This achieved peak power is the highest reported peak power for a tapered gain-guided mode-locked quantum-dot two-section laser with repetition rate of 16 GHz.

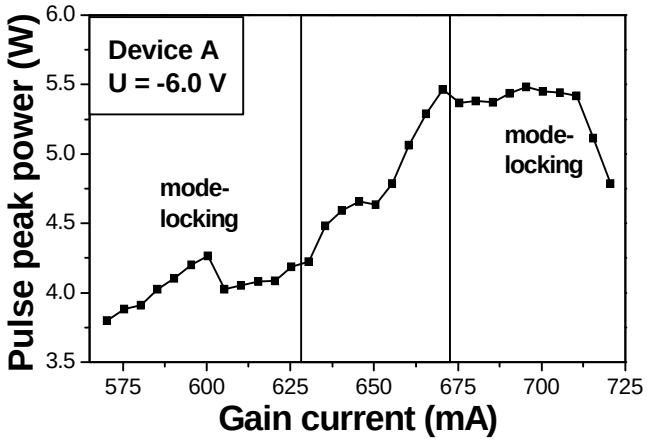

Fig. 8.15 Dependence of peak power as a function of a gain current of laser A at a reverse bias of -6.0 V (Characterized at Technical University of Darmstadt, Germany).

The measurements of the far field pattern on device A presented in Fig. 8.16 are performed by III-V Lab at 575 mA and 675 mA currents. We observe the single mode behaviour together with a very low full width of 2.4° and 3.1° at 1/e² of maximum respectively. M² values are 1.3 and 1.7, for the gain current values of 575 mA and 675 mA, respectively (reverse bias of -6 V).

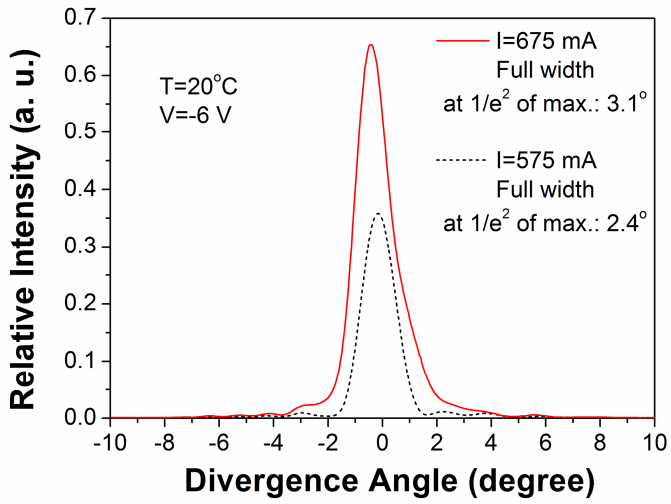

Fig. 8.16 Far field slow-axis pattern measured on device A at 575 mA and 675 mA with a very low full width of 2.4° and 3.1° at 1/e² of maximum respectively (characterized by III-V Lab, France).

As indicated by numerical simulations, an alternative way to even further increase peak power is by increasing the overall laser length and the absorber-to-gain-length-ratio as realized in device B where stable mode-locking was achieved for reverse bias between 3V and 6 V applied to the absorber and gain current between 800 mA and 1800 mA.. Indeed, the optimum mode locking regime for device B is found at a reverse bias of -4.0 V, attributed to the change in absorber-to-gain-length-ratio. In analogy to Fig. 8.12 the average power dependence of gain current under uniform injection and under an applied reverse bias of -4.0 V are shown in Fig. 8.17 a, b. Under uniform

injection a threshold current of 341 mA and differential efficiency of 0.38 W/A were observed. When a reverse bias of -4 V is applied on the absorber, laser emission takes place at 720 mA with a hysteresis loop. A self starting mode-locking regime was observed from current of 830 mA up to 1.7 A. Compared to laser A, the threshold is shifted from 500 mA to 720 mA and the start of the mode locking region is shifted from 575 mA to 830 mA. Both changes confirm our assumption of the determining influence of the ratio of gain-to-absorber lengths. The maximum output average power achieved was 287.7 mW, for a reverse bias of -4 V and current 1.8 A at 20 ^{o}C, corresponding to 28.7 pJ pulse energy with2.2 ps pulse duration (Fig. 8.17 b).

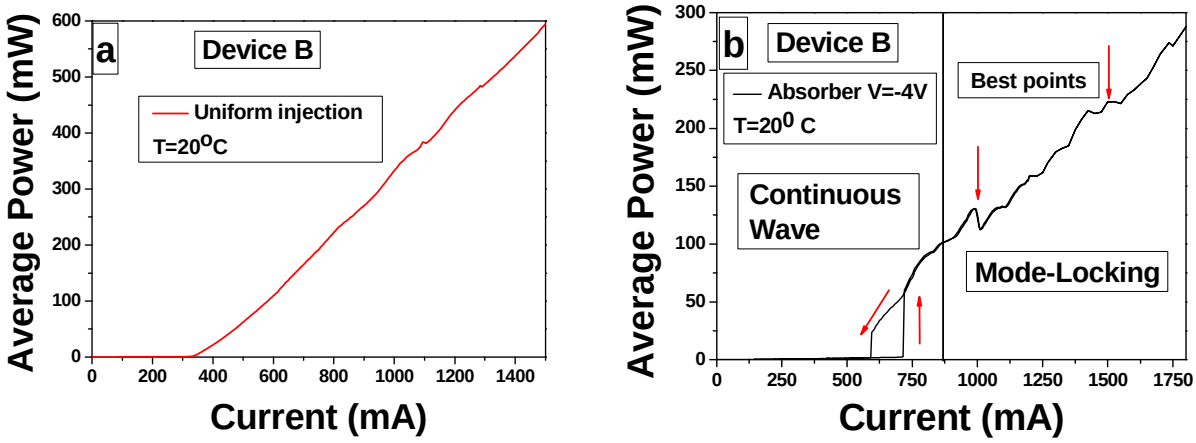

Fig. 8.17 a, b Light-current curves for a laser B at 20^{o} C **(a)** under uniform injection (red line) with a threshold current of 341 mA and **(b)** under an applied voltage of -4 V on the absorber section (black line) with a 720 mA threshold current.

This corresponds to an increase in average power by a factor of 4.5 as compared to laser A as reflected directly as one contribution to the peak power. Pulse duration increases from 820 fs to 2.2 ps with increasing current and is only slightly higher than

compared to the pulse observed with laser A, as shown in Fig.8.18 a. Peak power varies between 9 W and 17.7 W depending on the bias conditions (Fig. 8.18 b).

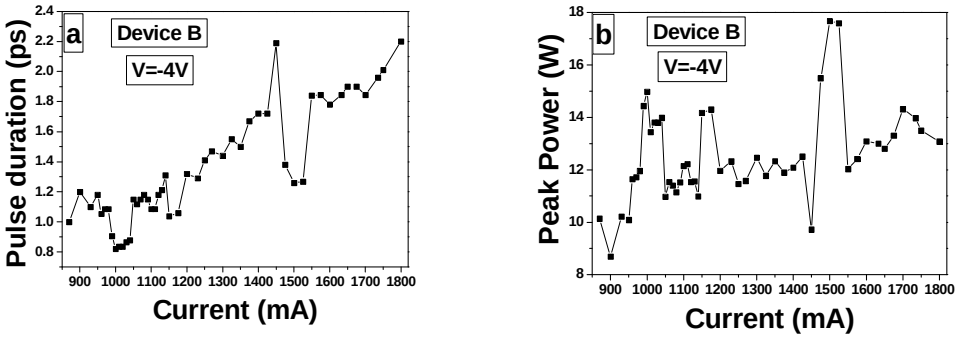

Fig. 8.18 (a) Pulse duration and **(b)** peak power dynamics at a -4 V reverse bias for a quantum-dot tapered laser B.

The shortest pulse width of 820 fs for a reverse bias of -4 V and injected current of 1 A was obtained associated at the same time with high peak power of 15 W and a high average power of 123 mW and, which is made possible due to the increasing length of the tapered section and the reduction of the repetition rate by a factor of 0.62 (Fig 8.19 a, b). The optical spectrum was centred at 1259.5 nm with a full-width half-maximum of 5.36 nm, resulting in a time-bandwidth product of 0.83.

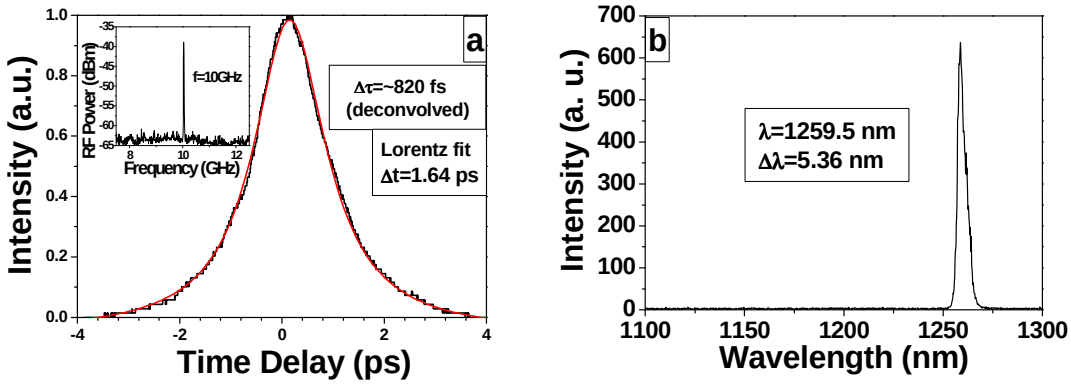

Fig. 8.19 (a) Autocorrelation (Inset: RF spectrum); **(b)** optical spectrum for an injection current of 1 A and reverse bias of -4 V for a short pulse regime for quantum-dot tapered laser B.

A record-high peak power of 17.7 W with 1.26 ps pulse duration and 222.7 mW average power was attained for -4 V and 1.5 A bias condition (Fig. 8.20 a, b). This represents the highest reported peak power to be generated from mode-locked monolithic semiconductor lasers. It is noteworthy to mention that the central wavelength suffered a nearly negligible shift to 1260.4 nm for such a high current of 1.5 A (resulting in current density of only 671 A/cm^2), suggesting that the band filling effect is quite weak for this device. The full-width at half-maximum of the optical spectrum was 5.6 nm, resulting in a time-bandwidth product of 1.33. Mode-locking was also observed for reverse bias between -2 V and -6 V.

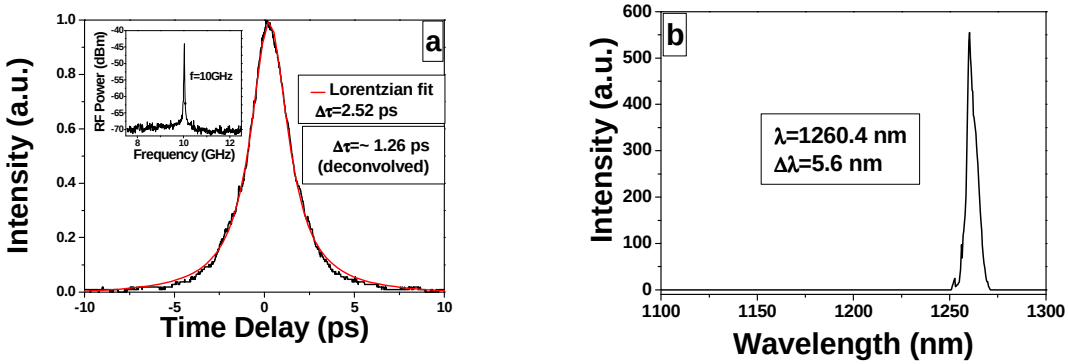

Fig.8.20 (a) Autocorrelation (Inset: RF spectrum); **(b)** optical spectrum for an injection current of 1.5 A and reverse bias of -4 V for a record-high peak power regime for quantum-dot tapered laser B.

Compared to the already significant peak power achieved by laser A, we have furthermore successfully improved the peak power by a factor of 3.8 to record values by a combined increase of the total laser length by a factor of 1.6 and the absorber-to-gain-ratio by a factor of 1.25.

Lorentzian-shaped autocorrelation for laser B compared to sech^2 autocorrelation for laser A were observed. It can be explained by different design and proportions of absorption and gain sections of the lasers which lead to different mode-locking

dynamics regions and generate pulses with different characteristics. Pulses generated by QD mode-locked lasers may display a slower falling edge that translates into a Lorentzian-shaped autocorrelation.

The far field pattern was also measured on device B at 1 A (the shortest pulse regime) and 1.5 A (the highest peak power regime) by III-V Lab. A single mode behaviour was exhibited at 1.5 A with very low full width of 2.2° at 1/e² of maximum. We also observed two lobes behaviour at 1 A and full width of 3.3° at 1/e² of maximum which corresponds to single high-order lateral mode (Fig.8.21). M² values are 2.9 and 2.1 at gain current of 1 A and 1.5 A at bias of -4 V respectively.

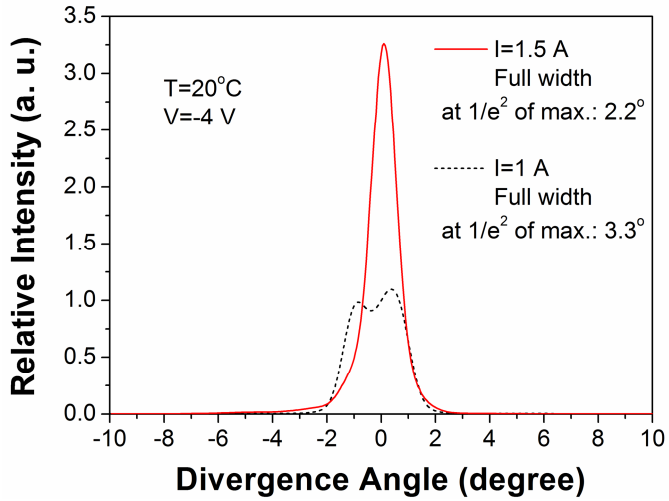

Fig. 8.21 Shows far field slow-axis pattern measured on device B at 1 A (shortest pulse width) and 1.5 A (highest peak power) with a very low full width of 3.3°and 2.2° at 1/e² of maximum, respectively (characterized by III-V Lab, France).

Phase noise measurements show that the integrated timing jitter for laser B can be as low as 2.6 ps (from 10 Hz to 50 MHz) at 14 °C (Fig. 8.22). This result shows that mode-locked QD two-section gain-guided tapered lasers are not only useful for the

generation of ultrashort pulses with high peak power, but they are also promising as sources for low noise applications.

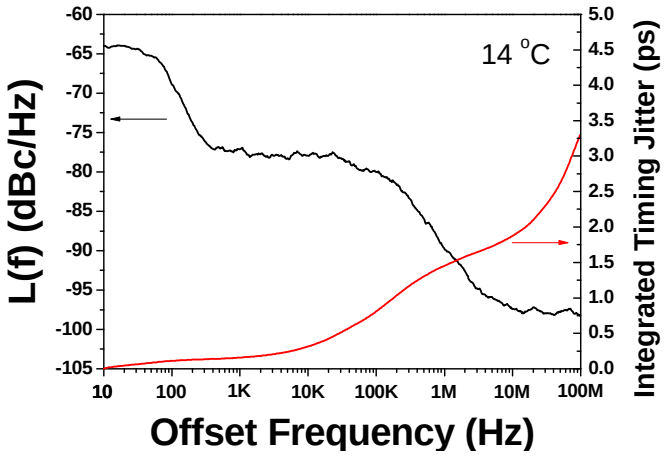

Fig. 8.22 A phase noise and integrated timing jitter for an injection current of 955 mA and reverse bias of -4.17 V at 14˚C for laser B.

8.3.5 Conclusion.

Passively mode-locked quantum-dot gain-guided tapered lasers with different structural parameters have been simulated, fabricated and investigated. Optimized structure designs were obtained by numerical simulations and the experimental findings fully confirm the trends identified by the modelling activity. Record high peak power and sub-picosecond Fourier-limited pulse generation has been demonstrated by two novel passively mode-locked fully gain-guided two-section quantum dot lasers with tapered gain sections. A peak power of 17.7 W with a pulse width of 1.26 ps and peak power of 3.8 W with a Fourier-limited pulse width of 672 fs is achieved by a proper choice of active region and laser structure geometry including absorber-to-gain ratio and total laser length. Quantum-dot tapered gain-guided lasers have therefore shown promising results as high power ultra-fast and ultra-compact semiconductor-based laser sources.

8.4 Multiphoton imaging using tapered lasers.

8.4.1 Introduction.

As described in section 1.3 multiphoton imaging is possible when the product of average power and peak power (see Eq.1.2) called the figure of merit (FOM) is high enough in order to produce high fluorescent intensity from the biological sample [1, 36-38]. QD based mode-locked tapered lasers have shown their potential producing high peak power and average power (see previous sections). In this context, tapered lasers are used for two-photon microscopy of biological sample – fluorescent beads.

8.4.2 Experimental setup.

Two experiments were performed using monolithic QD tapered lasers which were characterized prior to these experiments using the setup depicted in Fig. 8.11. The schematic for nonlinear imaging experiments is shown in Fig. 8.23 similar to the one in ref. [19] where there are not galvanometric mirrors and instead semiconductor disk laser tapered lasers are used which were mounted p-side up on the Peltier cooler to maintain operating temperature at 20 ^{o}C. The laser beam is coupled using aspheric lenses with NA of 0.55 and mirrors to the microscope. During the first experiment the microscope setup included the incorporation of a linear imaging system on the existing nonlinear microscope (NLM) platform (based on a continuous wave HeNe laser operating around 633 nm). This alternative system was mounted as this enabled excitation of different samples in a linear approach using the same samples to be tested with the QD laser diode described in 8.2. As tapered lasers exhibited higher peak power (described in 8.3) the second experiment was performed. In addition, several modifications were performed to the microscopy work station (i.e. beam path optimization).

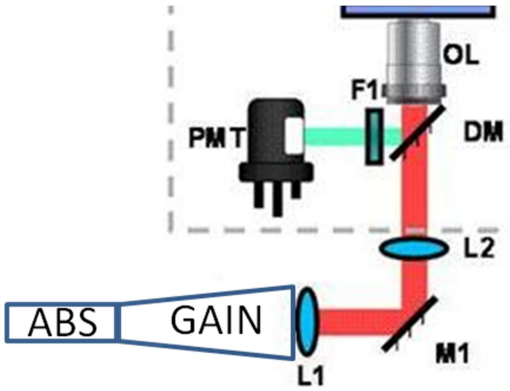

Fig. 8.23 Experimental setup using a tapered laser and nonlinear microscope.

As the major loss of power occurs in the microscope objective a new 60 x Nikon oil immersion Lambda-S microscope objective optimized for IR wavelengths with NA of 1.4 was used. This objective has a new coating design [39], allowing an increased transmission in for NIR wavelengths. This transmission goes from 15 % in the old objectives to 30 % in the Lambda-S series objectives. The sample was scanned in x-y directions using a translation stage (Tango, Marzhauser Wetzlar). To acquire the two photon excited fluorescence image a band pass filter (KG3, schott) was placed in front of a photomultiplier tube (Hamamatsu, H9305-03).

8.4.3 Experiments and Discussion.

The experiments were done in collaboration with The Institute of Photonic Sciences, Barcelona, Spain. The first tapered QD laser diode, operating at a central wavelength of 1260 nm, average output power of 200 mW, 3.6 W peak power and 14.6 GHz repetition and pulse duration of 3 ps was tested (described in section 8.2) . The recorded average power after such lens was 135 mW because the beam had a lot of astigmatism. However, the system was incorporated to our setup optimizing the path towards the microscope. For these tests we used 15 µm crimson fluorescent beads (designed to be excited using around 630 nm in linear fashion meaning that the sample is suitable for nonlinear excitation at 1260 nm), starch granules (as the laser has an increased repetition rate) and several laser bias conditions for the absorption and gain sections previously characterized at Dundee. During these tests the average power reaching the sample plane was 20 mW corresponding to a peak power of 0.48 W. In this case, we could not observe any nonlinear signal coming from the sample. At the Institute of Photonics sciences it was experimentally found that, if the maximum peak of two photon action cross section of any dye is well matched, the required threshold peak powers to excite such dyes in a nonlinear fashion would be around ten's of watts (peak power). Therefore we were not able to see any nonlinear signal emitted from the test sample.

For the next imaging trials after optimization of the nonlinear microscope system, the laser was similar to device B described in section 8.3 but with slightly lower average power of 100 mW. The pulse duration was about 1 ps and taking into account a repetition rate of 10 GHz, the peak power results in ~10 W. In this case the peak power of the laser system has been up scaled considerably, thus being able to deliver a

couple of watts into the sample plane. Based on previous experience such output power could be around the threshold value to start observing a NL emission. As before, fluorescent bead samples (suitable for NL excitation at 1260 nm) were used. Figure 8.24 shows the image obtained from the fluorescent beads sample. it is possible to observe the result from integrating 10 frames from the same sample region. This procedure was performed to increase the signal to noise ratio (SNR). However it can be clearly observed that individual spheres cannot be visualized correctly. In fact this effect can be attributed to the beam profile which suffers from astigmatism.

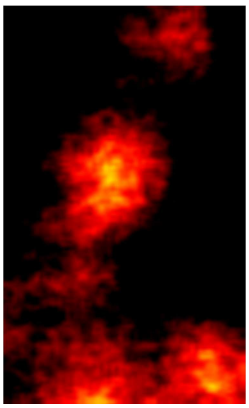

Fig. 8.24 A two-photon image of fluorescent beads using QD tapered laser B.

This was left without correcting the beam profile, as the lenses used to partially correct for this effect generate additional losses on our setup. Nevertheless, if higher peak power is available, such a correction would allow the concentration of light more efficiently before coupling the beam into the microscope objective. This is the scope of the future work.

8.4.4 Conclusion.

Thus it is for the first time QD based compact monolithic device enables the imaging of biological material using two-photon microscopy imaging technique. Successful demonstration of application of tapered QD based laser in biophotonics field was presented. It once again suggests that semiconductor lasers exhibit great potential in replacing bulk and expensive solid state systems which are used now for multi-photon imaging.

8.5 Summary.

QD based monolithic tapered laser was developed and investigated. A unique gain-guided design allows achieving picoseconds pulses with average power of more than 200 mW. For further improvement of the device, characteristics were obtained after second iteration of the tapered lasers with optimized structural characteristics based on simulation results. The record peak power of 17.7 W and transform limited pulses of 672 fs were achieved. Such phenomenal results enabled the use of tapered lasers for two-photon microscopy. The image of fluorescent beads was presented. Thus tapered QD lasers open new doors for next generation optical sources which can be effectively used in biophotonics area.

8.6 References.

[1] M. Kuramoto*, et al.*, "Two-photon fluorescence bioimaging with an all-semiconductor laser picosecond pulse source," *Opt. Lett.,* vol. 32, pp. 2726-2728, 2007.

[2] T. Shimada*, et al.*, "Intracellular disruption of mitochondria in a living HeLa cell with a 76-MHz femtosecond laser oscillator," *Opt. Express,* vol. 13, pp. 9869-9880, 2005.

[3] R. R. Gattass and E. Mazur, "Femtosecond laser micromachining in transparent materials," *Nat Photon,* vol. 2, pp. 219-225, 2008.

[4] G. Hollemann*, et al.*, "High-power laser projection displays," *Proceedings of SPIE,* vol. 4294, p. 36, 2001.

[5] M. Attygalle*, et al.*, "All-optical coding of mode-locked semiconductor laser pulse trains for high bit rate optical communications," *Optics Communications,* vol. 217, pp. 161-167, 2003.

[6] R. Diehl, *High-Power Diode Lasers: Fundamentals, Technology, Applications (Topics in applied physics 78)*. Berlin, Germany: Springer-Verlag, 2000.

[7] N. Michel*, et al.*, "Two-sections tapered diode lasers for 1 Gbps free-space optical communications with high modulation efficiency," San Francisco, California, USA, 2010, pp. 76161F-11.

[8] K. Paschke*, et al.*, "Nearly diffraction limited 980-nm tapered diode lasers with an output power of 7.7 W," *Selected Topics in Quantum Electronics, IEEE,* vol. 11, pp. 1223-1227, 2005.

[9] B. Sumpf*, et al.*, "High-Brightness Quantum Well Tapered Lasers," *Selected Topics in Quantum Electronics, IEEE,* vol. 15, pp. 1009-1020, 2009.

[10] M. T. Kelemen*, et al.*, "Tapered diode lasers at 976 nm with 8 W nearly diffraction limited output power," *Electronics Letters,* vol. 41, pp. 1011-1013, 2005.

[11] K. Kim*, et al.*, "1.4kW high peak power generation from an all semiconductor mode-locked master oscillator power amplifier system based on eXtreme Chirped Pulse Amplification(X-CPA)," *Opt. Express,* vol. 13, pp. 4600-4606, 2005.

[12] E. Innerhofer*, et al.*, "Mode-locked high-power lasers and nonlinear optics – a powerful combination," *Laser Physics Letters,* vol. 1, pp. 82-85, 2004.

[13] Y.-L. Cao*, et al.*, "High brightness InAs/GaAs quantum dot tapered laser at 1.3 μm with high temperature stability," in *Semiconductor Lasers and Applications IV*, Beijing, China, 2010, pp. 784404-9.

[14] K. A. Williams*, et al.*, "Monolithic passive mode-locking in single contact tapered lasers," in *Lasers and Electro-Optics Society Annual Meeting, 1995. 8th Annual Meeting Conference Proceedings, Volume 1., IEEE*, 1995, pp. 135-136 vol.2.

[15] A. Mar*, et al.*, "High-power mode-locked semiconductor lasers using flared waveguides," *Applied Physics Letters,* vol. 66, pp. 3558-3560, 1995.

[16] J. J. Plant*, et al.*, "250 mW, 1.5μm monolithic passively mode-locked slab-coupled optical waveguide laser," *Opt. Lett.,* vol. 31, pp. 223-225, 2006.

[17] F. R. Ahmad and F. Rana, "Passively Mode-Locked High-Power (210 mW) Semiconductor Lasers at 1.55 μm Wavelength," *Photonics Technology Letters, IEEE,* vol. 20, pp. 190-192, 2008.

[18] T. Schlauch*, et al.*, "High peak power femtosecond pulses from modelocked semiconductor laser in external cavity," *Electronics Letters,* vol. 44, pp. 678-679, 2008.

[19] R. Aviles-Espinosa*, et al.*, "Compact ultrafast semiconductor disk laser: targeting GFP based nonlinear applications in living organisms," *Biomed. Opt. Express,* vol. 2, pp. 739-747, 2011.

[20] E. U. Rafailov*, et al.*, "Mode-locked quantum-dot lasers," *Nat Photon,* vol. 1, pp. 395-401, 2007.

[21] W. Kaiser*, et al.*, "Theoretical and experimental investigations on temperature induced wavelength shift of tapered laser diodes based on InGaAs/GaAs quantum dots," *Applied Physics Letters,* vol. 91, pp. 051126-3, 2007.

[22] M. A. Cataluna*, et al.*, "High-Power Versatile Picosecond Pulse Generation from Mode-Locked Quantum-Dot Laser Diodes," *Selected Topics in Quantum Electronics, IEEE,* vol. PP, pp. 1-9, 2011.

[23] M. G. Thompson*, et al.*, "Subpicosecond high-power mode locking using flared waveguide monolithic quantum-dot lasers," *Applied Physics Letters,* vol. 88, pp. 133119-3, 2006.

[24] M. G. Thompson*, et al.*, "InGaAs Quantum-Dot Mode-Locked Laser Diodes," *Selected Topics in Quantum Electronics, IEEE,* vol. 15, pp. 661-672, 2009.

[25] D. Nikitichev*, et al.*, "High-power passively mode-locked tapered InAs/GaAs quantum-dot lasers," *Applied Physics B,* vol. 103, pp. 609-613, 2010.

[26] K. Petermann, "Calculated spontaneous emission factor for double-heterostructure injection lasers with gain-induced waveguiding," *Quantum Electronics, IEEE,* vol. 15, pp. 566-570, 1979.

[27] G. P. Agrawal, "Heuristic approach to spontaneous emission factor of gain-guided lasers," *J. Opt. Soc. Am. B,* vol. 1, pp. 406-408, 1984.

[28] M. Ruiz*, et al.*, "New tapered quantum-dot mode-locked laser diode with high peak power, low divergence and good beam quality," in *Semiconductor Laser Conference (ISLC), 2010 22nd IEEE International*, 2010, pp. 170-171.

[29] A. R. Rae*, et al.*, "InGaAs-GaAs Quantum-Dot Mode-Locked Laser Diodes: Optimization of the Laser Geometry for Subpicosecond Pulse Generation," *Photonics Technology Letters, IEEE,* vol. 21, pp. 307-309, 2009.

[30] D. Nikitichev*, et al.*, "High peak power and sub-picosecond Fourier-limited pulse generation from passively mode-locked monolitic two-section gain-guided tapered InGaAs quantum-dot lasers," *Optics Express,* 2011.

[31] M. Rossetti*, et al.*, "Modeling Passive Mode-Locking in Quantum Dot Lasers: A Comparison Between a Finite-Difference Traveling-Wave Model and a Delayed Differential Equation Approach," *Quantum Electronics, IEEE,* vol. 47, pp. 569-576, 2011.

[32] M. Rossetti*, et al.*, "Time-Domain Travelling-Wave Model for Quantum Dot Passively Mode-Locked Lasers," *Quantum Electronics, IEEE,* vol. 47, pp. 139-150, 2011.

[33] M. Rossetti*, et al.*, "Time domain travelling wave model for simulation of passive mode locking in semiconductor quantum dot lasers," presented at the European conference on Lasers and Electro-Optics 2009 and the European Quantum Electronics Conference. CLEO Europe - EQEC 2009., 2009.

[34] A. G. Vladimirov and e. al., "Model for passive mode-locking in semiconductor lasers," *Phys. Rev. A,* vol. 72, p. 033808, 2005.

[35] K. Merghem*, et al.*, "Short pulse generation using a passively mode locked single InGaAsP/InP quantum well laser," *Opt. Express,* vol. 16, pp. 10675-10683, 2008.

[36] M. Gu*, et al.*, *Femtosecond Biophotonics: Core Technology and Applications*. Cambridge: Cambridge University Press, 2010.

[37] H. Yokoyama*, et al.*, "Two-photon bioimaging with picosecond optical pulses from a semiconductor laser," *Opt. Express,* vol. 14, pp. 3467-3471, 2006.

[38] H. Yokoyama*, et al.*, "Nonlinear-microscopy optical-pulse sources based on mode-locked semiconductor lasers," *Opt. Express,* vol. 16, pp. 17752-17758, 2008.

[39] Nikoninstruments. Available: http://www.nikoninstruments.com/Products/Optics-Objectives/Apochromat-Objectives/Lambda-S-Objective-Series

Chapter 9. Conclusions.

9.1 Summary of the work.

In this thesis QD-based semiconductor lasers were studied with monolithic and external cavity configurations for generating ultrashort pulses. The influence of the cavity length and number of QD layers in the active region was analyzed. Two millimetre lasers with different numbers of QD layers in the active region were characterized thoroughly. It was found that QD based lasers with 10 layers of QD exhibit the most promising results: a 1 ps pulse duration and peak power of 600 mW. In this context, 5 layer QD lasers are more favourable for dual mode mode-locking. Simultaneous emission from ground and excited states with 83 nm spectral separation was shown which can be used for CARS and STED modalities [1]. As the cavity length decreased to 1.3 mm excited states emission takes place more easily due to the ground state saturation. Thus structural parameters of the laser enable the control of its optical characteristics and giving an extra flexibility in developing universal sources for time-domain spectroscopy, ultrafast optical processing and multi-photon imaging.

Bistable devices were developed using the advanced MBE growing technique. The highest spectral bistability range, 54 nm, was demonstrated generating picosecond pulses for gain currents between 260 mA to 330 mA. In addition, the wavelength tunability region of 45 nm was observed from 1245 nm to 1295 nm electronically controlled by reverse bias to the absorber [2]. These are very important results for optical communication applications as the spectral range is within the minimum fibre dispersion region.

External cavity QD lasers were investigated as well [3-6]. Peak power of up to 1.5 W with a repetition rate of 1.14 GHz, without the use of any pulse compression and

optical amplification, was achieved. Fundamental frequency tuning from 1 GHz to a record-low value of 191 MHz was demonstrated. Furthermore, a very broad harmonic repetition rate tunable range with picosecond pulses up to 6.8 GHz corresponding to 34^{th}order harmonic of 200 MHz fundamental frequency was shown. Moreover, a record-low -3dB RF linewidth of ~30 Hz from the QD-based external-cavity passively mode-locked laser was illustrated for a fundamental frequency of 281.3 MHz, which indicates the low noise and high stability operation of this device.

Novel gain-guided tapered lasers with 5 and 10 QD layers were realised and characterised. Two iterations of the devices were developed. In the first iteration, picosecond pulses with an average power of 209 mW were achieved giving the highest pulse energy of 14.2 pJ. This is more than one order of magnitude higher than previous results [7]. A second iteration of the devices was successfully realized with optimized structural characteristics, according to the simulations which were performed at Politecnico di Torino (see section 8.3.3).

The highest peak power ever reported from a monolithic mode-locked semiconductor laser of 17.7 W was achieved as well as ultrashort pulses in the range of 800 fs [8]. The improved optical parameters of the tapered laser enabled the achievement of nonlinear images of fluorescent beads (see Fig. 8.24). Thus one of the main goals of the thesis was accomplished. A new version of the semiconductor device was developed, that was used for multiphoton imaging. This is only the beginning of a new era of QD-based semiconductor lasers. In Fig. 9.1 the development of QD-based lasers presented in this thesis is shown. The product of the average power and the peak power was improved step by step, as can be seen in the table 9.1.

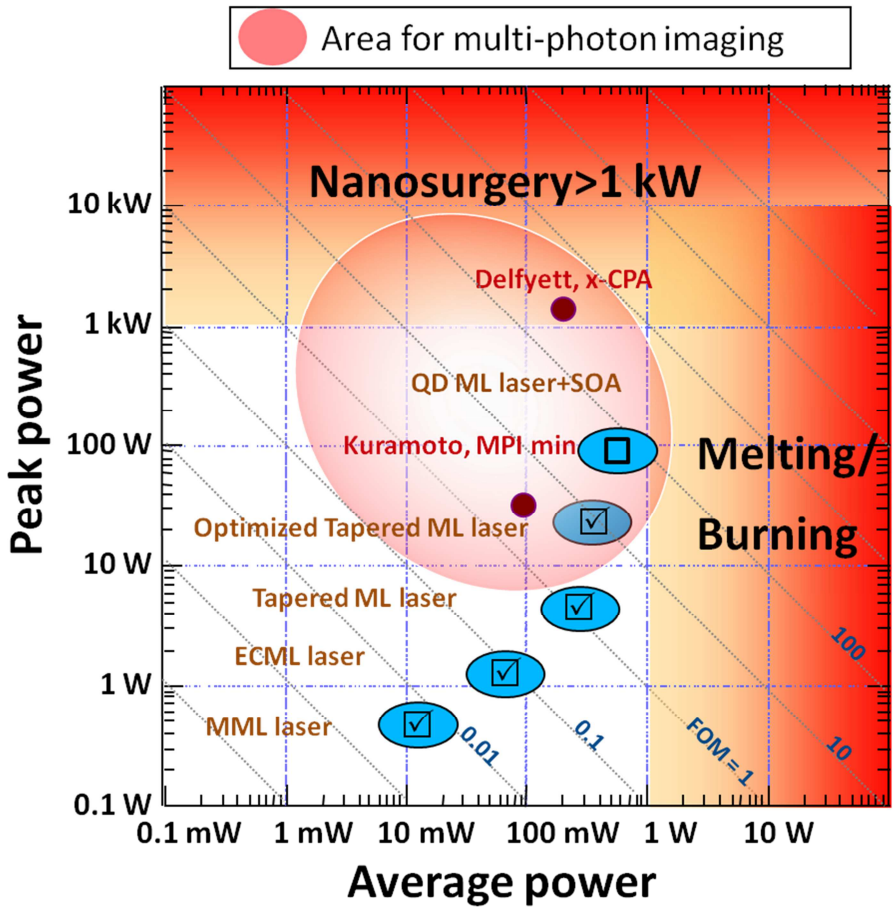

Fig. 9.1 A map for a progress of QD-based lasers: MML Laser- monolithic mode-locked laser, ECML- external cavity mode-locked laser, Tapered mode-locked (ML) laser toward biophotonics.

Table 9.1 Performance of QD-based devices presented in the thesis.

Laser	Pulse, ps	Rep. Rate, GHz	Configuration	Average Power, mW	Peak Power, W	Figure of Merit (FOM), W^2	Chapter/Reference
MML	2.5	20	Monolithic	30	0.6	0.018	5,6/[1-2, 9-10]
ECML	13.6	1.14	External	23.2	1.5	0.0348	7/[3-5]
Tapered ML 1	3.2	14.6	Monolithic	190	3.6	0.684	8/[11]
Tapered ML 2	1.26	10	Monolithic	223	17.7	3.941	8/[8]

9.2 Future work.

Progress in the development of QD-based lasers enabled the achievement of~ 18 W peak power with more than 200 mW average power. The next step is to exploit more complex systems with several stages of amplification, as was shown in previous reports [12-15], in order to satisfy the requirement for more peak power. For example, the investigation of the combination of a monolithic laser or an external cavity QD laser configuration in combination with a semiconductor optical amplifier (SOA).

Preliminary results show that a peak power of 32 W can be achieved from mode-locked external cavity lasers with tapered semiconductor optical amplifiers [16]. Another area of interest is THz frequency generation. QD based lasers with volume Bragg grating can be used as they have been demonstrated for developing the next-generation compact THz emission systems [17]. Moreover, dual-wavelength mode-locking regime needs to be investigated further in order to understand the mechanism underlying behind it. Another interesting area of research can be focused on QD lasers on different substrates rather than GaAs such as Si and Ge [18-19]. Short-wavelength QD lasers can be further investigated and developed, as a shorter wavelength is needed for imaging systems [20]. As autocorrelation doesn't provide information about the phase of the pulse, it would be very useful to perform frequency-resolved optical gating (FROG) measurements, such as reported in [21-23] for more insight understanding of the pulse in QD based lasers.

9.3 References.

1. Cataluna, M.A., et al., *Dual-wavelength mode-locked quantum-dot laser, via ground and excited state transitions: experimental and theoretical investigation.* Opt. Express, 2010. **18**(12): p. 12832-12838.

2. Nikitichev, D.I., et al., *Tunable quantum-dot mode-locked monolithic laser*, in *2nd EOS Topical Meeting on Lasers (ETML'11)*. 2011: Italy.

3. Ding, Y., et al., *Quantum-dot external-cavity passively modelocked laser with high peak power and pulse energy.* Electronics Letters, 2010. **46**(22): p. 1516-1518.

4. Ding, Y., et al. *Fundamental and harmonic mode-locking with pulse repetition rate between 200 MHz and 6.8 GHz in a quantum-dot external-cavity laser*. in *Lasers and Electro-Optics Europe (CLEO EUROPE/EQEC), 2011 Conference on and 12th European Quantum Electronics Conference*. 2011.

5. Cataluna, M.A., et al., *High-Power Versatile Picosecond Pulse Generation from Mode-Locked Quantum-Dot Laser Diodes.* Selected Topics in Quantum Electronics, IEEE, 2011. **PP**(99): p. 1-9.

6. Ding, Y., et al., *Broad Repetition-Rate Tunable Quantum-Dot External-Cavity Passively Mode-Locked Laser with Extremely Narrow Radio Frequency Linewidth.* Applied Physics Express, 2011. **4**(6).

7. Thompson, M.G., et al., *InGaAs Quantum-Dot Mode-Locked Laser Diodes.* Selected Topics in Quantum Electronics, IEEE, 2009. **15**(3): p. 661-672.

8. Nikitichev, D., et al., *High peak power and sub-picosecond Fourier-limited pulse generation from passively mode-locked monolitic two-section gain-guided tapered InGaAs quantum-dot lasers.* Journal of Laser Physics, 2011.

9. Nikitichev, D.I., et al., *Investigation of the pulse dynamics in a mode-locked quantum-dot laser, involving the ground/excited state transitions*, in *1st EOS Topical Meeting on Lasers 2009*. 2009: Capri, Italy. p. [2243].

10. Nikitichev, D.I., et al. *High-power spectral bistability in a multi-section quantum dot laser under continuous-wave or mode-locked operation*. in *CLEO 2011*. 2011. USA.

11. Nikitichev, D., et al., *High-power passively mode-locked tapered InAs/GaAs quantum-dot lasers.* Applied Physics B: Lasers and Optics, 2011. **103**(3): p. 609-613.

12. Kuramoto, M., et al., *Two-photon fluorescence bioimaging with an all-semiconductor laser picosecond pulse source.* Opt. Lett., 2007. **32**(18): p. 2726-2728.

13. Yokoyama, H., et al., *Nonlinear-microscopy optical-pulse sources based on mode-locked semiconductor lasers.* Opt. Express, 2008. **16**(22): p. 17752-17758.

14. Yokoyama, H., et al., *Two-photon bioimaging with picosecond optical pulses from a semiconductor laser.* Opt. Express, 2006. **14**(8): p. 3467-3471.

15. Kim, K., S. Lee, and P. Delfyett, *1.4kW high peak power generation from an all semiconductor mode-locked master oscillator power amplifier system based on eXtreme Chirped Pulse Amplification(X-CPA).* Opt. Express, 2005. **13**(12): p. 4600-4606.

16. Ding, Y., et al. *30-W peak power generated from all-quantum-dot master-oscillator power-amplifier system for nonlinear bioimaging applications*. in *CLEO 2012*. 2012. San-Jose, USA.

17. Leyman, R., et al., *Multimodal spectral control of a quantum-dot diode laser for THz difference frequency generation.* Applied Physics Letters, 2011. **99**(17): p. 171107-3.

18. Liu, H., et al., *Long-wavelength InAs/GaAs quantum-dot laser diode monolithically grown on Ge substrate.* Nat Photon, 2011. **5**(7): p. 416-419.

19. Wang, T., et al., *1.3 μm InAs/GaAs quantum-dot lasers monolithically grown on Si substrates.* Opt. Express, 2011. **19**(12): p. 11381-11386.

20. Schlereth, T.W., et al., *Short-Wavelength (760-920 nm) AlGaInAs Quantum Dot Lasers.* Selected Topics in Quantum Electronics, IEEE, 2009. **15**(3): p. 792-798.

21. Lester, L., et al., *Pulse characteristics of passively mode-locked quantum dot lasers.* Proceedings of SPIE, 2010. **7616**(1).

22. Xin, Y.C., L.F. Lester, and D. Kane, *Frequency-resolved optical gating characterisation of passively modelocked quantum-dot laser.* Electronics Letters, 2008. **44**(21): p. 1255-1257.

23. Schmeckebier, H., et al., *Complete pulse characterization of quantum dot mode-locked lasers suitable for optical communication up to 160 Gbit/s.* Opt. Express, 2010. **18**(4): p. 3415-3425.